TIME-RESOLVED PHOTOLUMINESCENCE STUDIES OF METAL ION TREATED n-GaAs IN ELECTROLYTES

Thesis by

Gail Naomi Ryba

In Partial Fulfillment of the Requirements

for the Degree of

Doctor of Philosophy

California Institute of Technology

Pasadena, California

1993

(Defended June 18, 1992)

Acknowledgements

I wish to thank the many teachers who listened to my questions and taught me what they knew. In particular, Jay Winkler at Caltech and Joe Perry at JPL were both great sources of information on the intricacies of picosecond lasers and I appreciate their willingness to take the time to teach me so much. Steve Feldberg at Brookhaven National Labs had boundless enthusiasm for teaching me computer modelling skills and hosted my two-week visit to BNL. Tom Dunn of Caltech is unsurpassed in patience and helpfulness for dealing with all things which fail to tick properly. The Fayer group at Stanford, especially Christine Petersen who talked p-chem with me *and* got me to play softball and flag football, was very helpful when I first ventured to learn about lasers. Finally, I wish to thank Nate Lewis, who took me on at Stanford, and both gave me freedom and pushed and prodded me through the challenges of doing picosecond spectroscopy and research in such an interdisciplinary field. The breadth of studies being pursued under his tutelage attracted me initially and has always made his lab an interesting and challenging place to be.

At Stanford, where the fun began, Hope Michelsen, Janine Bloomfield, Dave Nunn and my housemates at SKIL, especially, cultivated my love of bicycles and mountains and happily discussed lasers or African cooking with equal glee. At Caltech, Erika Harvey welcomed me to this place where, well, there aren't many women, and she remains an inspiration to me. The characters Donnie Cotter, LeRoy Whinnery, Gui Bazan, Richard Hartshorn and Dave Wheeler did the most to keep me from sitting around being lazy, and whether it was dragging me up a mountain or subjecting me to the Kronos Quartet, I'm glad they were here with me. I never thought the day would come when I'd be writing these lines, but everyone else in the Lewis group did -- or at least pretended to, -- and they all told me to keep at it. Mike Sailor's cheerful readiness to perform the task and Gordon Miskelly's cheerful readiness to question the task make them especially good scientific

colleagues, mentors and friends. Mary Rosenbluth, Bruce Tufts, and Amit Kumar are fantastic labmates and helped me learn to say "band-bending" with the best of them. I also wish to thank the former group members Lou Casagrande, Pat Santangelo, Sharon Lunt, Malcolm D. E. Forbes and Bao-Liang Tsai , with whom I have actually performed experiments, and who, in the sometimes stressful environment of shared labor, have all helped me to do research. The current crop is just as great and definitely has a new style. Nancy and Gary Shreve, Teri Longin, Ming Tan, Russ Pyllki and Tom Jozefiak have been wonderful this past couple of years. I thank both Son-Binh Nguyen and Nathan Frei for their inspiring attention to detail. Finally, I wish Chris Kenyon had arrived at Caltech sooner, because working with him has been productive, easy and fun - rare attributes for a lab partner.

I thank my parents most of all for the assurance that should I ever want to just catch the next plane, they'd be happy to pick me up at the airport. Their love and encouragement is impossible to repay, and I only hope they know how much it has meant to me. I would like to acknowledge by brother Dave for the loan of his Macintosh, without which this last document would have been slower in coming. I thank Dave, Diane and Eric, all, for both the rivalries and the sharing that siblings have and which helps a person keep her perspective when going through a tough experience like graduate school.

Abstract

Using the technique of time-correlated photon counting, the time-resolved photoluminescence response of n-type gallium arsenide (n-GaAs) in contact with aqueous KOH - Se^{2-} - Se_2^{2-} electrolytes was monitored before and after exposure to aqueous 0.010 **M** solutions of ruthenium, cobalt and osmium ions. Cobalt ions caused the rate of carrier loss from the GaAs to increase relative to that for untreated samples, as evidenced by faster decays. It was inferred that hole and/or electron transfer to the selenide redox species was catalyzed by the cobalt ions.

A model incorporating ambipolar diffusion, bulk trapping, radiative bimolecular recombination, surface trapping and surface charge transfer and employing a finite-difference algorithm was applied to the photoluminescence decays. Under high intensity illumination, the photoluminescence decays from the gallium arsenide samples with aluminum gallium arsenide overlayers could be fit using the expression for bimolecular kinetics, indicating that radiative recombination dominated the decays in these samples.

For the samples immersed in aqueous KOH - Se^{2-} - Se_2^{2-} solutions, with and without chemisorbed metal ions, a time-dependent increase in the GaAs photoluminescence indicated that changes occurred at the surface during the course of the experiment. Prior to metal ion treatment, the lifetime in KOH - Se^{2-} - Se_2^{2-} solutions stabilized at about 3.7 ns, which could be fit with an effective surface hole capture rate constant of 5.1×10^3 cm/sec. After cobalt ion treatment photoluminescence decays with 1/e lifetimes on the order of 0.6 ns were measured and, if it is assumed that surface hole capture dominated the decay, correspond to a surface hole capture rate constant of 1.7×10^5 cm/sec. The 1/e lifetimes for ruthenium and osmium treated surfaces were never observed to be less than 1.5 ns and quickly returned to the 3.7 ns lifetimes observed prior to metal ion treatment. It is inferred

that the cobalt treated surface is more chemically inert under illumination than either ruthenium or osmium treated surfaces.

Preliminary measurements for GaAs immersed in acetonitrile with and without dimethylferrocene and dimethylferrocenium indicated that the rates of carrier loss at the surface are much higher than they are for the aqueous selenide redox species, even in the absence of the redox species. However, small increases in rate of loss were discernible after addition of redox couple to the acetonitrile, and further work is warranted.

Table of Contents

List of Figures

List of Tables

Chapter 5

GENERAL INTRODUCTION

The aim of this thesis was to develop both an experimental technique and a quantitative model that would allow one to measure heterogeneous rate constants at the semiconductor/liquid junctions of photoelectrochemical cells. Justification for studies of semiconductor surfaces in general is readily found when one considers that all semiconductor based devices, whether they be transitors or solar cells, rely on the properties of junctions made between a semiconductor and another material (e.g., another semiconductor, a metal, a liquid, an insulator, or a polymer). Historically, the surfaces of semiconductors, and semiconductors in general, have been the purvey of solid-state physicists, materials scientists and semiconductor device engineers, who have developed most of the language and tools brought to bear in studying them. However, the possibility of tailoring the surface of a material by chemical synthesis and the study of chemical kinetics at semiconductor electrodes are highly appropriate subjects of study for chemists. The diminishing size of semiconductor devices and the consequent increase in surface-to-volume ratio only serve to further validate the importance of taking a molecular approach to the study of semiconductor surfaces.

Numerous semiconductors have been explored for use in photoelectrochemical cells as far back as 1839 when Becquerel observed a photovoltage at a AgCl electrode and Adams and Day in 1877 observed a similar effect at solid selenium.[1] The possibility of using photoelectrochemical cells to split water for fuels was stimulated by the report of K. Honda and A. Fujishima in 1972[2] that TiO_2 photoanodes could oxidize water in acidic aqueous electrolyte. A major drawback of the metal oxides in solar energy conversion is

that while they are relatively stable to corrosion, their bandgaps are so large that they can absorb only a small part of the solar spectrum. Smaller bandgap materials are not able to electrolyze water unassisted, and they produce smaller voltages, although they yield higher currents. The optimal band-gap for solar energy conversion to electricity is found to be 1.4 to 1.5 eV,[3] such as is found in indium phosphide (1.35 eV) and GaAs (1.42 eV).

Apart from solar energy considerations, GaAs deserves more study because it is potentially a better material for device applications. The speed of device operation is dependent on the mobility of the charge carriers; the mobility of electrons in GaAs is nearly six times that in silicon. Because of its optical properties, GaAs is also widely used in semiconductor diode lasers. A major limitation in its use, however, is that the rate of carrier loss at the surface is very high. Unlike silicon, which grows a thermal oxide that leaves a relatively defect-free surface, the oxide on GaAs does not terminate the surface in such a way as to maintain good electrical characteristics. To reduce surface defects, alternative cladding materials, such as AlGaAs, must be grown on the surfaces using elaborate crystal growth techniques.

Although rate constants for charge transfer at metal electrodes have been extensively studied, there have been very few corresponding measurements of the kinetics of interfacial charge transfer at semiconductor electrodes. Most often an overall charge capture velocity is reported, which does not elucidate the role of individual species in the mechanism of charge transfer. As discussed in a recent review article,[4] there are reports in the literature indicating that charge transfer at semiconductor/liquid interfaces occurs on timescales varying from picoseconds to milliseconds. Effects on the interfacial charge transfer at the GaAs/KOH - Se_2^{2-} - Se^{2-} interface investigated in this thesis were observable on the 0.5 to 5.0 ns timescale. To access this time regime a picosecond laser system and time-correlated photon counting apparatus were assembled in our laboratories.

The premise of the experiments performed is that changes in surface hole and electron transfer rates perturb the bulk radiative emission of the sample and can be measured by observing changes in the emission. Such measurements are analogous to time-resolved quenching experiments in homogeneous systems in that a laser pulse is used to initiate a charge transfer event that is then monitored by observing the luminescence of the excited system as it relaxes to the ground state. The excess holes and electrons which are created recombine via the various pathways, and a computer model incorporating all processes is used to extract values for the heterogeneous hole transfer rates as a function of the redox species in solution and surface preparation.

Chapter 1 of this thesis contains a discussion of charge transfer at semiconductor/liquid junctions and a brief history of the GaAs system studied in this work. Chapter 2 is a presentation of the relevant semiconductor physics and recombination processes which occur after photoexcitation, and Chapter 3 details the incorporation of these processes into the computer algorithm used to model the measured photoluminescence decays. Chapter 4 is a description of the experimental technique and the apparatus built to make these measurements, and Chapter 5 contains a discussion of the results and conclusions of this work.

CHAPTER 1

CHARGE TRANSFER AT THE SEMICONDUCTOR/ELECTROLYTE INTERFACE

The GaAs/KOH-Se_2^{2-}-Se^{2-} system studied in this work has previously been investigated in this laboratory and others, primarily using steady-state techniques. In this chapter an introduction to the relevant results from previous work will be presented, with particular attention to factors pertinent to the time-resolved experiments performed in this thesis.

A. Model for the Semiconductor/Liquid Interface

A diagram for describing the kinetics of photogenerated electrons and holes within a semiconductor/liquid junction, as considered in the present work, is shown in Figure 1-1. This figure shows a semiconductor and its valence and conduction band edges on the left in contact with a solution containing redox couple A and A^+ on the right; each of the arrows corresponds to a process with an associated rate constant described in the figure caption.

In Figure 1-1 the arrows which point along the direction of the abscissa are meant to indicate the fact that the carriers move through space and define the fluxes which are measured as currents in electrochemical cells or semiconductor devices. Because of the varying spatial, as well as temporal, properties involved, mathematical descriptions of flux take the form of partial differential equations which are detailed in Chapter 2.

Electric currents which flow across this interface are determined by the kinetics and thermodynamics of the reacting species and have been subjected to increasing scrutiny in

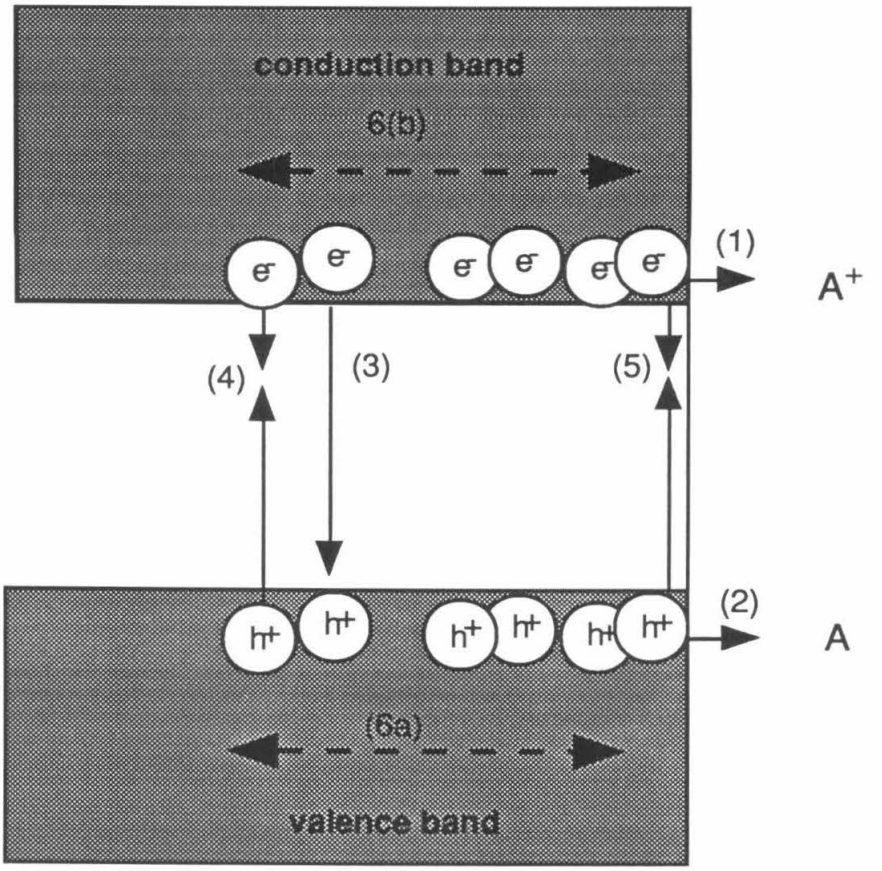

Figure 1-1. Semiconductor/liquid interface diagram depicting kinetics of photoexcited electrons and holes. The implicit ordinate in this figure is an energy scale, and the abscissa is distance. The rate constants corresponding to the processes numbered in the diagram are: (1) k_{et}, for reaction between a conduction band electron and an electron acceptor in solution; (2) k_{ht}, for reaction between a valence band hole and a hole acceptor in solution; (3) $k_{radiative}$ for the emission of a photon; (4) k_{nr}, for non-radiative processes in the bulk of the semiconductor, such as bulk trapping; (5) k_{ss}, for surface-state trapping, and (6) D_h, and D_e, the diffusion constants controlling hole and electron diffusion in the valence and conduction bands, respectively.

recent years. Electron transfer theories of semiconductor electrodes which take into account the distribution of charge carriers in the semiconductor and the reorganization energy of the redox species in solutions were first developed by Gerischer using a formalism parallel to that of Marcus.[5] Recently, Lewis has published an analysis of the semiconductor/liquid interface which details the theoretical framework of interfacial kinetics and clarifies the relations between heterogeneous rate constants measured at metal and semiconductor electrodes.[4] The flux of electrons at an electrode surface is the current density, J, divided by the charge on an electron, q, and has units of $cm^{-2}sec^{-1}$. It is most generally written

$$\frac{J}{q} = \text{flux} = k_{et}[A]n_s, \tag{1-1}$$

where [A] is the concentration of acceptor ion in solution, n_s is the concentration of electrons near the surface, both in units of cm^{-3}, and k_{et} is the heterogeneous rate constant, in units of cm^4s^{-1}. In a more detailed Marcus-type analysis, the rate constant is frequently broken down into a product of a nuclear frequency factor, ν_n, a nuclear term, κ_n, which takes into account the activation energies for reorganization around the ion in solution, and an electronic term, κ_{el}, which incorporates the matrix element for electronic coupling between the acceptor and donor. Each of these terms can be expressed differently, depending on the classical or quantum mechanical theories chosen to describe them. Adapting results from homogeneous kinetics, one such Marcus expression is

$$k_{et} = \nu_n[2\pi(r_A + r_e)\beta^{-3}]\{e^{-(\lambda_A' + \Delta G^{o'})^2/(4kT\lambda_A')}\} \tag{1-2}$$

where r_A is the effective radius of the acceptor ion, r_e, is the radius of the electron in the semiconductor, β is the attenuation of the electronic coupling in a direction perpendicular to the electrode surface, $\Delta G^{o'}$ contains the free energy for reaction and electrostatic work terms for assembling the reactants, and λ_A' is the reorganization energy near a material with a low dielectric constant, such as a semiconductor. For further details, the reader is

referred to the literature.[6] Applying several expressions, including eq. 1-2, to the ferrocene/ferrocenium redox system, Lewis estimated that the values of k_{et} should range from 10^{-16} to 10^{-17} cm^4 sec^{-1}.[4]

As carriers are lost at the surface, a concentration gradient develops which pulls charges from the bulk. The resulting flux is referred to as the *rate* of carrier loss at the surface, and, as for all fluxes, has units of $cm^{-2}sec^{-1}$, not cm^{-3} sec^{-1} as bulk loss rates do. The distinction of a flux from a bulk rate of loss must not be overlooked, particularly in actual numerical calculations of rates of electron and hole reactions in semiconductors, which are calculations of changes in concentration in units of cm^{-3}.

The simplest expression for the rate at which electrons are consumed at the surface is a rate constant times their concentration, or

$$\text{flux=rate at the surface}=S^*n_s, \qquad (1\text{-}3)$$

where the rate constant, S, has units of cm/sec and is most commonly referred to as the surface recombination velocity (SRV). For the case in which electrons actually cross the interface, the rate constant has been designated k_n, and the flux is referred to as the "semiconductor electrode charge-transfer collection rate" by Lewis, since it measures the capture of electrons by an acceptor in solution. Two parallel processes of interest can be described by a flux equation of this general form -- either the electron is captured at the electrode surface in a process known as trapping, or it can cross the interface and be captured by an acceptor ion in solution.

Because of the different nature of the charge capture processes, species relevant to the two pathways mentioned above are viewed in different terms. For trapping it is natural to think of the traps as species confined to a two-dimensional surface, and consequently, as existing in a concentration with units of cm^{-2}. It is then straightforward to apply the concepts of *bulk* trapping to the processes at the surface. The "rate constants" retain the

same units as for the capture of electrons by traps in the bulk, cm^3/sec, but instead of a bulk rate, a net flux is calculated.

For charge transfer to a solution acceptor, the species in solution is three-dimensional in nature, as with standard homogenous kinetics. It is the reaction between the semiconductor electron and the solution acceptor that is effectively confined to the two-dimensional interface, and so the units of the rate constant change to cm/sec for the unimolecular case, and cm^4/sec for the bimolecular case.

Recently, Gerischer has considered the nature of the reaction pair in greater detail.[7] At the interface between the semiconductor and the solution he envisions an electron at the surface in a region defined by ρ from a point at the interface opposite the acceptor species in solution a distance δ from the surface. If we adapt his model to the system in this thesis, one can consider the reaction pair shown in Figure 1-2, where a hole from the valence band interacts with the reduced selenide ion. A corresponding picture can be drawn for the electron in the conduction band interacting with the oxidized species in solution. The net reaction between these species represents the flux across the interface and the chemical reactions can be summarized,

$$2Se^{2-} + 2h^{+}\,(\text{valence band}) \underset{k_{-ht}}{\overset{k_{ht}}{\rightleftharpoons}} Se_2^{2-}$$

$$Se_2^{2-} + 2e^{-}\,(\text{conduction band}) \underset{k_{-et}}{\overset{k_{et}}{\rightleftharpoons}} 2Se^{2-}$$

Scheme I. Reactions at n-GaAs/KOH-Se_2^{2-}-Se^{2-} interface.

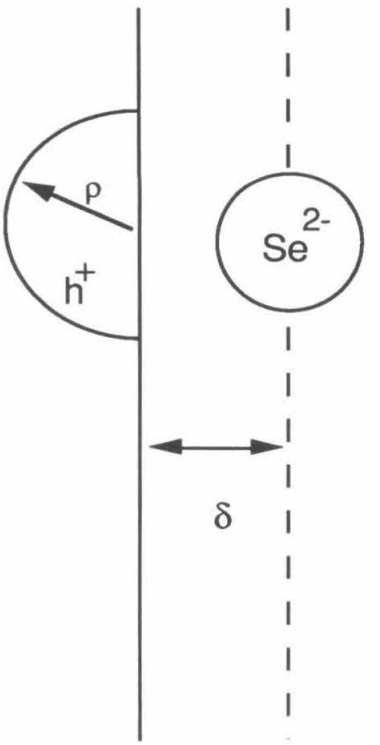

Figure 1-2. Modified Gerischer model for the interaction of a hole at the surface of a semiconductor with a hole acceptor in the electrolyte.

B. History of GaAs/KOH-Se^{2-}-Se_2^{2-} Studies

The system chosen for study in this work is that of GaAs immersed in KOH-Se_2^{2-}-Se^{2-} redox solution and continues a line of studies on this particular system begun in the 1980s in this lab[8] that followed initial explorations in other labs.[9] In 1965, Gerischer first investigated the photocorrosion of GaAs in aqueous systems.[10] In initial photoelectrochemical applications, GaAs was found to be unstable as a photoanode in aqueous electrolytes. However, in 1977, following their work on CdS, Chang *et al.*[9b] found that n-GaAs does not photocorrode in Se^{2-}/Se_2^{2-} solutions at sufficiently high concentrations of selenide. In 1978, Parkinson, Heller, and Miller reported that changes in the photoelectrochemical solar-energy conversion efficiency for GaAs/Se^{2-}/Se_2^{2-} could be affected by treating the surface with metal atoms or ions.[11] They observed that some metals, like Bi(III), caused a degradation in the current-voltage properties, while others such as Rh(III) and Ru(III) led to improvements, with Ru(III) showing the most long-lasting effects. These treatments led to the first report of a power conversion efficiency of 12% under ~100 mW/cm^2 sunlight, which passed the benchmark of 10% considered minimally necessary for commercial considerations.

For an n-type semiconductor, the yield of photoanodic current is determined by the partitioning of holes between the rates of surface trapping and transfer to an acceptor in solution, as depicted in Figure 1-1. That is, the yield of valence band holes (or minority carriers, in general) crossing to solution acceptors depends on the ratio $\frac{J_{ht}}{J_{ht}+J_{ss(h)}}$, where each J designates the flux (or rate at the surface) due to the corresponding processes in Figure 1-1. An increase in hole transfer current can, therefore, be attributed to either an increase in the rate of transfer across the interface or a decrease in the rate of loss to surface states.

The theory that Parkinson, Heller, and Miller proposed to explain the improvement after metal ion treatment was that, contrary to expectations that metal ions damaged the

surfaces and increased recombination losses, the binding of the metal ion to a surface state "shifts the position of the surface states closer to, or even into, the near band of the semiconductor,"[12] thereby reducing the surface recombination velocity. At this position, the probability of trapping both a hole and an electron would be greatly diminished over the mid-gap position, resulting in an overall decrease in carrier loss. They based their claim on the results of experiments in which chemisorption of Ru^{3+} caused both the intensity and the decay time of luminescence of a sample in air to increase.[13] Since this experiment was performed in air, they presumed that "the improvement upon Ru^{3+} chemisorption was not associated with any electrochemical reaction and could not be due to electrocatalysis. It could only be explained by the chemical redistribution of surface states."[12] In other words, they assumed that the loss of holes to surfaces states, $J_{ss(h)}$, had been decreased.

Subsequently Allongue *et al.*[14] used steady-state photocurrent and impedance techniques to measure the competition between photodissolution of n-GaAs and oxidation of Se^{2-}. Using a particular model for the interpretation of the impedance results, they suggested that in addition to reducing surface recombination, ruthenium ions bonded to the surface in such a way as to catalyze hole transfer to the selenide ion. In this laboratory, experiments that do not rely on impedance models were performed by Tufts *et al.*[15] on metal (In_2O_3), p-GaAs, and n^+-GaAs electrodes in which improvements in the current-voltage characteristics analogous to those on n-GaAs were observed after metal ion treatment. The fact that metal ions increased the anodic current for the p-type electrode in the dark could not be explained by a passivation of surface states, as proposed by Heller for the n-type systems originally studied, because for p-type materials, reduction of the flux of holes to the surface in the dark would be expected to reduce the overall anodic current. Moreover, the improvements on the metal-like surfaces, (In_2O_3 and n^+-GaAs) indicated that the result was general for the oxidation of Se^{2-} at various surfaces. It was concluded

that metal ion chemisorption acted by increasing the rate of charge transfer at the GaAs/KOH-Se^{2-} -Se_2^{2-} interface.

Although the evidence for catalysis is substantial, the measurements of steady-state currents do not permit an absolute measurement of the rate constant for the hole transfer. In any steady-state measurement, determination of a rate constant requires knowledge of the absolute values of the concentrations of electrons and acceptors, as indicated in eq. 1-1. A time-resolved measurement of the fluxes, however, offers the possibility of making these measurements.

More will be said in Chapter 4 on the time-correlated photon counting technique used in this work to measure the time-resolved photoluminescence. Other time-resolved techniques which have been used to monitor the decay of photoexcited carriers at semiconductor/liquid junctions include transient gratings,[16] microwave and rf (radio-frequency) conductivity[17] and transient currents.[18] Photoluminescence is unique in that it measures the recombination of an electron with a hole and is therefore sensitive to both populations, simultaneously. The microwave conductivity technique measures the intensity of the reflected microwave or rf power, which is proportional to the conductivity of the sample, which is a function of the mobilities of electrons and holes. Since the electron mobility in GaAs is 40 times greater than that of holes, rf and microwave conductivity are relatively insensitive to the hole concentration. Transient current measurements suffer from difficulties in resolving sub-nanosecond current transients due to RC constraints inherent to electrical measurements. Transient grating techniques utilize the field present at the surface to focus the holes in an n-type material towards the surface, potentially allowing selective study of hole dynamics.

Photoluminescence measurements are widespread in the study of semiconductors and can be made in a variety of ways. Using a streak camera, Evenor *et al.*[19] measured the photoluminescence from CdS in aqueous sulfide solutions and extracted a value for

surface recombination velocities. Correlation spectroscopy has been used by the McGill group at Caltech[20] and others[21] to measure time-resolved luminescence and thereby measure processes occurring in parallel with the luminescence, including bulk trapping and exciton recombination. The technique has a resolution limited only by the laser pulse width, which could be as short as 50 fs.

Time-correlated photon counting (TCPC) has been previously used in experiments that are similar to those in this thesis by Nelson *et al.*[13] and led to the results described above for initial reports on the effect of ruthenium ions on the GaAs/KOH-Se^{2-}-Se_2^{2-} system. TCPC has also been used to measure the time decay of room-temperature photoluminescence from GaAs layers less than 20 nm thick.[22]

---

[1] Fahrenbruch, A. L.; Bube, R. H. *Fundamentals of Solar Cells*; Academic Press: New York, 1983; p 9.

[2] Honda, K.; Fujishima, A. *Nature* **1972**, *238*, 37.

[3] Fahrenbruch, A. L.; Bube, R. H. *Fundamentals of Solar Cells*; Academic Press: New York, 1983; p 13.

[4] Lewis, N. S. *Annu. Rev. Phys. Chem.* **1991**, *42*, 543.

[5] (a) Gerischer, H. *Adv. Electrochem. Electrochem. Eng.* **1961**, *1*, 139. (b) Gerischer, H. in *Physical Chemistry: An Advanced Treatise* , Vol 9A; Eyring,H.; Henderson, D.; Jost, W. Eds.; Academic: New York, 1970; p 463. (c) Marcus, R. A. *J. Chem. Phys.* 1965, *43*, 679 and references therein.

[6] (a) Lewis, N. S. *Annu. Rev. Phys. Chem.* **1991**, *42*, 543. and references therein. (b) Marcus, R. A. *J. Phys. Chem.* **1990**, *94*, 1050 and references therein. (c) Gerischer, H. *J. Phys. Chem.* **1991**, *95*, 1356 and references therein.

[7] Gerischer, H. *J. Phys. Chem.* **1991**, *95*, 1356.

[8] (a) Casagrande, L. G. Ph.D. Thesis, Stanford University, 1988. (b) Tufts, B. J. Ph.D. Thesis, California Institute of Technology, 1991.

[9] (a) Ellis, A. B.; Bolts, J. M.; Kaiser, S. W.; Wrighton, M. S. *J.Am. Chem. Soc.* **1977**, *99*, 2848. (b) Chang, K. C.; Heller, A.; Schwartz, B.; Menezes, S.; Miller, B. *Science* (Washington, D.C.) **1977**, *196*, 1097. (c) Heller, A.; Chang, K. C.; Miller, B. *J. Am. Chem. Soc.* **1978**, *100*, 684.

[10] Gerischer, H. *Ber. Bunsenges. Phys. Chem.* **1965**, *69*, 578.

[11] Parkinson, B. A.; Heller, A.; Miller, B. *Appl. Phys. Lett.* **33**, 521 (1978).

[12] Heller, A. *Acc. Chem. Res.* **1981**, *14*, 154.

[13] Nelson, R. J.; Williams, J. S.; Leamy, H. J.; Miller, B.; Casey, H. C., Jr., Parkinson, B. A.; Heller, A. *Appl. Phys. Lett.* **1980**,*36*, 76.

[14] Allongue, P.; Cachet, H. *J. Electrochem. Soc.* **1984**, *131*, 2861.

[15] Tufts, B. J.; Abrahams, I. L.; Casagrande, L. G.; Lewis, N. S. *J. Phys. Chem.* **1989**, *93*, 3260.

[16] Gomez-Jahn, L. A.; Miller R. J. D. *J. Chem. Phys.* **1992**, *96*, 3981.

[17] Forbes, M. D. E.; Lewis, N. S. *J. Am. Chem. Soc.* **1990**, *112*, 3682. (b) Gmitter, T. J.; Yablonovitch, E.; Heller, A. *J. Electrochem. Soc.* **1988**, *135*, 2391.

[18] Willig, F. *Ber. Bunsenges. Phys. Chem.* **1988**, *92*, 1312.

[19] Evenor , M.; Gottesfeld, S.; Harzion, Z.; Huppert, D. *J. Phys. Chem.* **1984**, *88*, 6213.

[20] Johnson, M.; McGill, T.C. *J. Appl. Phys.* **1988**, *63*, 2077.

[21] Jorgensen, M.; Hvam, J. M. *Appl. Phys. Lett.* **1983**, *43*, 460.

[22] (a) Fouquet, J. E.; Siegman, A. E. *Appl. Phys. Lett.* **1985**, *46*, 280. (b) Fouquet, J. E.; Siegman, A. E.; Burnham, R. D.; Paoli, T. L. *Appl. Phys. Lett.*, **1985**, *46*, 374. (c) Fouquet, J. E.; Burnham, R. D. *IEEE J. Quantum Electron.* **1986**, *QE-22*, 1799.

CHAPTER 2

SEMICONDUCTOR ELECTRON-HOLE RECOMBINATION KINETICS

The reactive species in semiconductors are the electrons and holes, and they can be treated analogously to molecular species when writing rate equations. Moreover, as in electrochemical systems with metal electrodes, the concentrations of reactants (both the ions in solution and the free electrons and holes in the semiconductor bulk) are functions of space, as well as time. The rate of change of the semiconductor charge carrier concentrations can be expressed in what is known as a continuity equation, and it is the purpose of this chapter to explain the terms in this equation for the system studied in this thesis.

Throughout the description below, "n" will be used to designate the concentration of conduction band electrons, and "p", the concentration of valence band holes, both in units of particles·cm^{-3}, which will hereafter be abbreviated as cm^{-3}.

A. Basic Semiconductor Properties and Terms

The reactions of electrons and holes are generally depicted with reference to a semiconductor band diagram, such as was presented in Figure 1-1 of Chapter 1. The band diagrams arise from consideration of the electronic states arising from the very large number of atoms in a macroscopic solid. Just as Hückel-type molecular orbitals can be built up from symmetry-adapted linear combinations of atomic orbitals, so can wavefunctions which are eigenfunctions for the Hamiltonian of a periodic lattice be built up

from the atomic orbitals in each unit cell. For a solid, the standard procedure is to form a set of so-called Bloch functions, which have the symmetry of the lattice and are linear combinations of the atomic orbitals in each unit cell. Using Hückel theory in the molecular case, the wavefunctions of an N-atom chain can be expressed as[1]

$$\phi(k)= \sum_{p=1}^{N} c_{pk}\chi_p = \frac{1}{\sqrt{N}}\sum_{p=1}^{N}\left[\exp(ikR_p)\right]\chi(r-R_p), \qquad (2\text{-}1)$$

where $\chi(r-R_p)$ are the atomic orbitals and $R_p=(p-1)a$ gives the position of a unit cell, p , a is the width of the unit cell, and k runs from 0 to $2\pi/a$ in increments of $2\pi/Na$. For a set of atomic orbitals in the unit cell of a solid, $\{\chi_1, \chi_2,...,\chi_n\}$ one can form a set of Bloch functions $\{\phi_1, \phi_2,...,\phi_n\}$,

$$\phi_\mu(k)= \sum_{p=1}^{N} c_{pk}\chi_p = \frac{1}{\sqrt{N}}\sum_{p=1}^{N}\left[\exp(ikR_p)\right]\chi_\mu(r-R_p). \qquad (2\text{-}2)$$

Band orbitals which are eigenfunctions of the one-electron Hamiltonian of the entire periodic lattice are linear combinations of the Bloch functions,

$$\psi_j(k)= \sum_{\mu=1}^{n} c_{\mu j}(k)\phi_\mu(k). \qquad (2\text{-}3)$$

The number of band orbitals, N, is so large that they effectively merge and form the bands. Due to the periodic potential, a gap containing no allowed energies arises for certain values of k and two bands are formed. The quasi-continuous band below this gap is known as the valence band, the one above as the conduction band. The top valence band state and the lowest conduction band state correspond to the familiar HOMO and LUMO of chemistry. The point is that for small molecules, one typically presents an energy level diagram for the energy levels corresponding to these wavefunctions by stacking them in a vertical column, in order of energy. However, for large systems of atoms, the energy levels are presented as a function of the index k, in a diagram known as a dispersion curve.

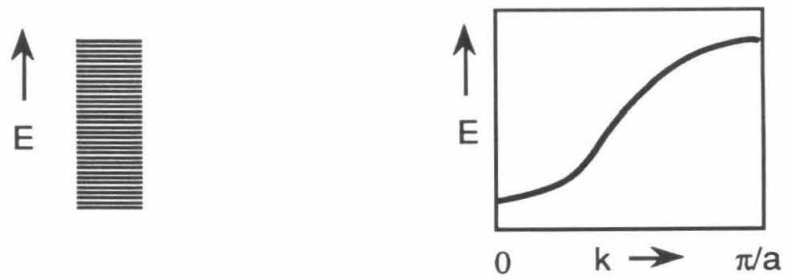

(a) (b)

Figure 2-1. Energy level diagrams. (a) Typical diagram for isotropic, molecular system. (b) Dispersion curve showing energy of levels as a function of *k*.

For a solid such as gallium arsenide, calculations of energies and wavefunctions vary along the crystal axes, due to the spatially varying nature of the potentials within the solid. Indexed by the wavevector, *k*, a complete band diagram is thus a function of direction. For gallium arsenide, this leads to the diagram partially depicted in Figure 2-2.

In zincblende structures such as GaAs, the valence band consists of four subbands which have maxima in energy at $k = 0$ while the conduction band has minima at several values of *k*. The minimum energy gap occurs at the point where $k = 0$ in both bands. Such a material is known as a direct gap material, and the probability for optical transitions in these materials is much higher than in materials where the valence band maxima and conduction band minima are at different *k* (which are referred to as indirect gap materials, and the most common of which is silicon).

As with molecules, it is the HOMO and LUMO which are generally the most important in understanding chemistry of semiconductors, so the complete energy level diagram is simplified to show only the $k = 0$ energies, and it is this pair of levels that is used in diagrams such as Figure 1-1. It is assumed that higher level states play a minimal role, even if photoexcitation populates them transiently, because more highly excited

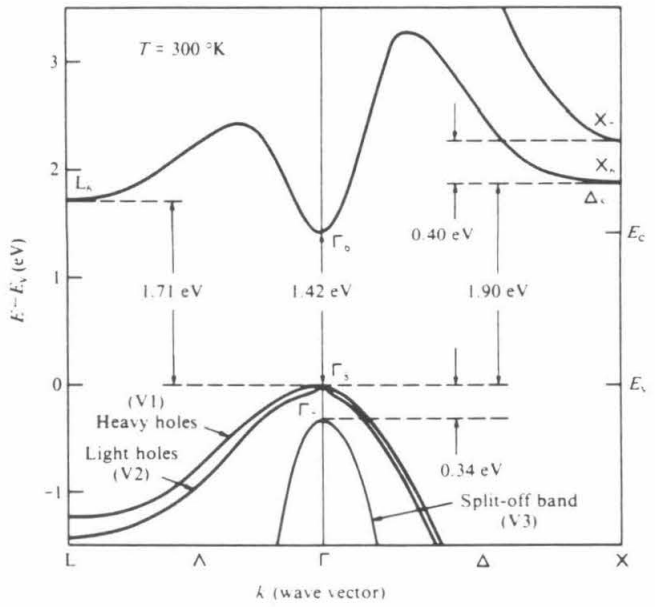

Figure 2-2. The energy band structure of GaAs showing upper valley at symmetry point L and lower valley at Γ. (Adapted from Pierret.[2])

electrons, so-called "hot electrons" relax to the band edges near $k = 0$ in approximately 4 ps via exchange of energy with the lattice.[3]

Additional energy levels due to impurities, including dopants, and defects also exist, and some of them lie in the bandgap, creating states where electrons and holes may reside. The dopant levels are near the band edges and are easily ionized to create a sea of free electrons that gives a semiconductor its conductivity. The thermal population of free electrons can be calculated based on application of Fermi-Dirac statistics to the appropriate set of one-electron levels.[2,4] Additional free electrons and holes may be introduced by a pulse of light which excites an electron from the valence band to the conduction band, and it is primarily these externally generated carriers which concern us below.

B. Equations for the Kinetics of Electrons and Holes - the Continuity Equations

Further details on the processes which will be summarized in this section can be found in numerous textbooks on semiconductor physics.[5] Equilibrium values of electron and hole species will be designated with a subscript 0, while net excesses injected by a light pulse, for example, will be designated by Δn or Δp, so that total electron and hole concentrations at or away from equilibrium are

$$n=n_0+\Delta n \tag{2-4a}$$

and

$$p=p_0+\Delta p. \tag{2-4b}$$

For an n-type material in which the equilibrium number of carriers, n_0, is equal to the dopant density, N_D, the introduction of excess carriers at low levels, Δn, $\Delta p << n_0$, is referred to as low-level injection, and the introduction of large numbers of excess carriers where $\Delta n = \Delta p >> n_0$, p_0, as high-level injection.

The presence of excess free carriers and the existence of non-equilibrium conditions, in general, affects semiconductor properties in numerous ways. Usually there is net excess charge present at the surface of a semiconductor which creates an electric field in the near-surface region (known as band-bending). At sufficiently high injection, the surface charges are screened by the sea of excess carriers and no electric field arises in the surface region. For this reason, high-injection experiments are considered to take place at "flatband." The important consequence of this is that fluxes due to drift can be neglected, which markedly simplifies the equations describing the electron and hole concentrations.

High concentrations of free charges can have effects on other electronic properties, including absorption and mobility, but these will be neglected, since they are expected to be secondary effects.

Just as for standard chemical kinetics, each of the reactions involving electrons or holes can be thought of as having a forward and backward direction. However, for semiconductors, it is conventional to refer to *recombination* and *generation* processes, since one is interested in the rates of release and capture of electrons and holes by various sites in the semiconductor. The terminology describes both the steady-state condition in which only thermal processes are occurring, as well as the non-equilibrium condition resulting from application of external stimuli such as light or applied fields which create additional free carriers. The general rate expression for a recombination-generation process is

$$\frac{dn}{dt} = g\text{-}r \qquad (2\text{-}5)$$

where g is the rate of electron generation and r is the rate of recombination due to that process.

The population densities also change because the carriers move in response to the gradients of electric field and concentration. It is this motion which leads to the measured current fluxes.

A partial differential equation which completely describes the kinetics of electrons and holes is thus a sum of terms due to individual processes and should include drift, diffusion, bulk trapping, surface trapping, electron and hole transfer, radiative recombination and external generation. The processes at the surface define boundary conditions for the partial differential equation, and, strictly speaking, are not terms in the sum. However, in modelling the equations with a finite-difference computer algorithm as is done in this work, their effects are considered as losses to the concentrations of electrons and holes in the surface region. The continuity equation for electrons can most generally be written

$$\frac{\partial n(x,t)}{\partial t} = \frac{\partial n(x,t)}{\partial t}\Big|_{\text{drift}} + \frac{\partial n(x,t)}{\partial t}\Big|_{\text{diffusion}} + \frac{\partial n(x,t)}{\partial t}\Big|_{\substack{\text{bulk}\\ \text{trapping}\\ \text{(R-G)}}} + \frac{\partial n(x,t)}{\partial t}\Big|_{\substack{\text{surface}\\ \text{trapping}\\ \text{(R-G)}}}$$

$$+ \frac{\partial n(x,t)}{\partial t}\Big|_{\substack{\text{electron}\\ \text{transfer}}} + \frac{\partial n(x,t)}{\partial t}\Big|_{\substack{\text{radiative}\\ \text{recombination}\\ \text{(R-G)}}} + g_E, \qquad (2\text{-}6)$$

where (R-G) designates the occurrence of both a recombination and a generation process. An analogous equation for holes is written by substituting p for n. Each of the terms in these sums will be discussed in turn.

1. Drift and Diffusion Terms

The first two terms of drift and diffusion describe spatial motion, or fluxes, of carriers in the bulk of the semiconductor. The equations describing these fluxes in terms of

current are referred to as the transport or current density equations. These take the standard form for charged particles moving in an electric field and concentration gradient, namely,

$$J_n = q\,\mu_n\,nE_x + qD_n\frac{dn}{dx} \tag{2-7a}$$

$$J_p = q\,\mu_p\,pE_x - qD_p\frac{dp}{dx} \tag{2-7b}$$

where q is the quantity of charge on an electron, $\mu_{n(p)}$, is the mobility of an electron (hole), and E_x is the electric field in the x direction. For completeness, it is noted that the drift terms depend on the electric field, and can be described by solving Poisson's equation. However, as indicated above, the use of high injection leads to a reduction of the electric field in our systems, and so this term is not considered further.

Differential expressions of the form required in the continuity equation are obtained by applying Fick's second law which states that the time rate of change of concentrations is given by the spatial derivative of the fluxes, or

$$\frac{\partial n}{\partial t} = \frac{1}{q}\frac{\partial J_n}{\partial x} = D_n\frac{\partial^2 n}{\partial x^2} \tag{2-8a}$$

$$\frac{\partial p}{\partial t} = -\frac{1}{q}\frac{\partial J_p}{\partial x} = D_p\frac{\partial^2 p}{\partial x^2}\,. \tag{2-8b}$$

This form can be readily incorporated into the calculations, as discussed below.

2. Bulk Recombination-Generation Processes

The recombination-generation processes comprise all of the processes by which free electrons and holes in the material are either created or destroyed and can be separated into bulk and surface types.

The five most common bulk processes are band-to-band, radiative recombination; trapping of electrons at midgap levels associated with impurities or defects; trapping in levels near the bandedges at sites created by dopant ions; Auger recombination; and

recombination via excitons.[6] The first four of these processes are commonly depicted as in Figure 2-3.

a. Band-to-Band, Radiative Recombination

In general, for very pure direct gap semiconductors having bandgaps in the 1 to 1.5 eV range, radiative recombination is a dominant bulk recombination pathway after photoexcitation. Since it is the observable in these experiments, it will be described in some detail.

Luminescence results from the recombination of an electron from the conduction band with a hole in the valence band and represents the release of their energy. Both the loss of electrons from the conduction band and the loss of holes from the valence band can be written

$$\frac{dn}{dt} = \frac{dp}{dt} = - k_{radiative} np. \qquad (2\text{-}9)$$

The net rate of change due to radiative recombination can be obtained by considering the process at equilibrium, where no net loss of electrons from the conduction band or holes from the valence band occurs. This statement of equilibrium is referred to as the Principle of Detailed Balance in semiconductor recombination-generation analysis and is simply a definition of equilibrium. As noted by Blakemore,[7] it is related to the principle of microscopic reversibility, except that microscopic reversibility refers to transition probabilities, not rates. Moreover, microscopic reversibility is quantum-mechanical rather than statistical in nature, so that it applies to both equilibrium and non-equilibrium cases.

Application of detailed balance tells us that at equilibrium the rate of radiative recombination must be balanced by an inverse generation process. Thus, if $G_{radiative}$ is the equilibrium generation rate, and $R_{radiative}$ the corresponding equilibrium recombination rate, we can write

$$G_{radiative} = R_{radiative} = k_{radiative} n_0 p_0 = k_{radiative} n_i^2 \qquad (2\text{-}10)$$

Figure 2-3. Recombination-generation processes in semiconductors. ● designates an electron, ○ designates a hole, CB designates the conduction band, and VB, the valence band. (a) A free electron and hole move to the same position in space and recombine, giving off a photon at the energy of the bandgap. (b) Electrons from the conduction band are trapped and released in unoccupied states near the middle of the bandgap. Similarly, holes from the valence band move into mid-gap states which are occupied by electrons. (c) Shallow level traps due to dopant atoms in the semiconductor can also trap electrons and holes, and recombination of electrons or holes in these states can lead to sub-bandgap emission at the transition energies indicated by (1), (2) and (3). (d) Auger recombination involves three carriers, and involves the transfer of energy from one carrier to another. (Adapted from Pierret .[8])

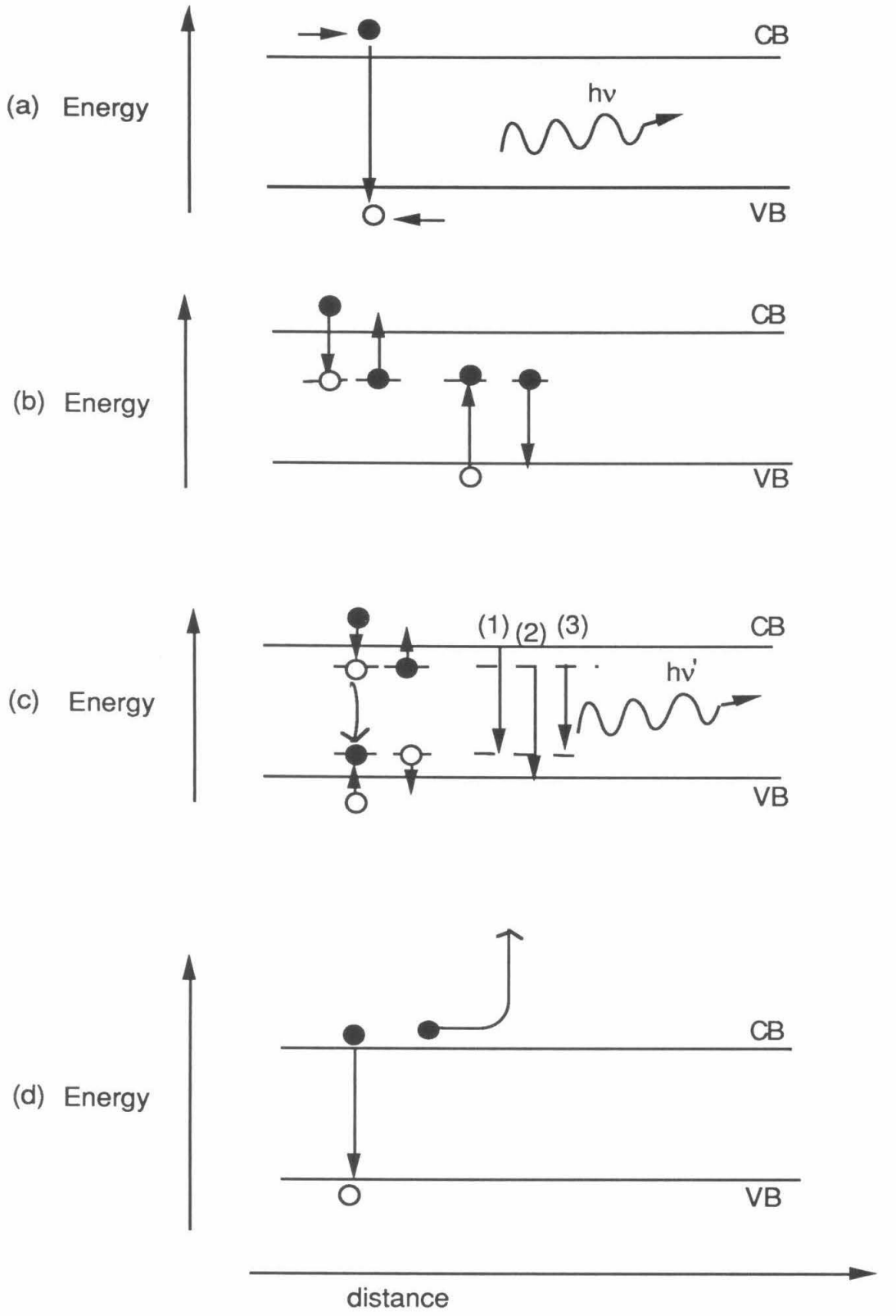
(a) Energy
CB
hν
VB
(b) Energy
CB
VB
(c) Energy
(1)
(2)
(3)
CB
hν'
VB
(d) Energy
CB
VB
distance

where we have used the fact that $n_0 p_0 = n_i^2$, and where n_i is the density of electrons in the undoped material.

If we assume that the thermal generation rate is relatively unperturbed by the high intensity light injection, then the net radiative recombination-generation term is the thermal generation rate minus the non-equilibrium radiative rate, i.e.,

$$\left.\frac{\partial n}{\partial t}\right|_{radiative} = G_{radiative} - r_{radiative}$$

$$= k_{radiative}\, n_i^2 - k_{radiative}\, np$$

$$= k_{radiative}\,(n_i^2 - np)$$

$$= k_{radiative}\,(n_i^2 - (n_0+\Delta n)(p_0+\Delta p)). \qquad (2\text{-}11)$$

For the case in which a large injection of excess charge is created by a light pulse, $\Delta n >> n_0$, and $\Delta p >> p_0$, so this simplifies to

$$\frac{d(\Delta n)}{dt} = -k_{radiative}(\Delta n \Delta p - n_i^2). \qquad (2\text{-}12)$$

Additionally, equal numbers of electrons and holes are created for each absorbed photon, so

$$\Delta n = \Delta p$$

and we can write

$$\frac{d(\Delta n)}{dt} = -k_{radiative}\,\Delta n^2. \qquad (2\text{-}13)$$

Luminescence, L, is the manifestation of this process, and can thus be written

$$L(t) = \frac{dP}{dt} = k_{radiative}\,\Delta n^2 \qquad (2\text{-}14)$$

where P is the total time integrated emission of photons.[9] When no other recombination pathways contribute significantly to the overall kinetics, the continuity equation can be

simplified to this expression which can be solved to yield the familiar result of bimolecular kinetics. Namely, the solution for the electron concentration, Δn, is

$$\Delta n(t) = \frac{\Delta n(t=0)}{1+\Delta n(t=0)k_{radiative}t} . \tag{2-15}$$

The expression for $\Delta n(t)$ can be rearranged to obtain

$$\Delta n(t) = \sqrt{\frac{L}{k_{radiative}}}$$

which leads to

$$L(t) = \frac{L_0}{(1+ t \sqrt{k_{radiative}L_0})^2} \tag{2-16}$$

where $L_0 \equiv L(t=0) = k_{radiative}\Delta n(t=0)^2$.

Rearranging, it is found that

$$\frac{1}{\sqrt{L}} = \frac{1}{\sqrt{L_0}} + \sqrt{k_{radiative}}\, t \tag{2-17}$$

from which it can be seen that a plot of $\frac{1}{\sqrt{L}}$ vs. t should give a linear plot with a slope of $\sqrt{k_{radiative}}$ and an intercept of $\frac{1}{\sqrt{L_0}}$.

This only differs from a standard bimolecular kinetics analysis in that usually it is the actual concentration of a reactant, A, which is measured, not the rate of change, and one generally plots $\frac{1}{[A]}$ vs. t to obtain the rate constant.

Unfortunately, in photon counting, the signal measured is a number of counts, N, which is merely proportional to the total number of photons being emitted, and without information on the absolute value of L, only one of the unknowns, L_0 or $k_{radiative}$, can be determined, and the other must be assumed. This can be seen by choosing a constant of proportionality, c^2, so that we can write $L = c^2N$, and then eq. 2-17 is

$$\frac{1}{c\sqrt{N}} = \frac{1}{c\sqrt{N_0}} + \sqrt{k_{radiative}}\, t$$

or

$$\frac{1}{\sqrt{N}} = \frac{1}{\sqrt{N_0}} + c\sqrt{k_{radiative}}\, t \qquad (2\text{-}18)$$

and a plot of the observables, $\frac{1}{\sqrt{N}}$ vs. t, yields a slope that is only proportional to $\sqrt{k_{radiative}}$.

At low injection, $\Delta p > p_0$, but $n \approx n_0$, so the decay follows the minority carrier decay, and luminescence can be simplified to

$$L(t) = \frac{dp}{dt} = k_{radiative}\, np = k_{radiative}\, (n_0+\Delta n)(p_0+\Delta p)$$

$$= k_{radiative}\, n_0 \Delta p \qquad (2\text{-}19)$$

or

$$\frac{d(p_0+\Delta p)}{dt} = \frac{d\Delta p}{dt} = -\, k_{radiative}\, n\, \Delta p \qquad (2\text{-}20)$$

and one should observe a single exponential decay with a lifetime given by $\frac{1}{k_{radiative}\, n}$.

b. Bulk trapping

Bulk trapping is not expected to be the dominant recombination-generation process for the material used in this thesis, because the GaAs samples are very pure, and band-to-band recombination proceeds very fast in direct band gap materials. However, the rates of midgap trapping may contribute to the overall carrier kinetics, particularly at low injection. Moreover, the form of the kinetics of bulk trapping is paralleled by that at the surface, and since the kinetics describing the bulk reaction are conceptually closer to traditional isotropic chemical kinetics, the equations for the bulk case will be discussed first, and the extension to the surface trapping rates will be made below.

The form of these kinetics was first modeled by W. Shockley and W.R. Read[10] and independently by R.N. Hall,[11] and is frequently referred to as SRH recombination-

generation. The equations are confined to the trapping of electrons, but analogous equations can be written for holes.

In what is presented below, I have chosen to use the letter "k" for rate constants, but for comparison with the literature, it should be noted that the bulk trapping rate constant, designated $k_{n(\text{bulk tr})}$, is commonly written as c_n and referred to as the electron capture coefficient. Likewise, $k_{p(\text{bulk tr})}$ is commonly written as c_p and referred to as the hole capture coefficient.

A trap site is an energy level in the bandgap created by impurities or defects in the semiconductor, and electron trapping is the term designating the capture of a free electron by an unoccupied trap level. The reaction between these two species (free electron and empty trap site) can be written as a bimolecular reaction, with the concentrations of reactants expressed as densities in units of cm^{-3}. The rate of electron capture from the conduction band is

$$\left.\frac{\partial n}{\partial t}\right|_{\substack{\text{bulk}\\ \text{electron}\\ \text{capture}}} = -k_{n(\text{bulk tr})} n(1-f_T)N_T \qquad (2\text{-}21)$$

where $k_{n(\text{bulk tr})}$ is the rate constant in units of cm^3sec^{-1}, f_T is the fraction of occupied traps in the material at one energy level, and N_T is the density of traps, also in units of cm^{--3}.

A corresponding reverse rate is written as emission from the trap, so

$$\left.\frac{\partial n}{\partial t}\right|_{\substack{\text{bulk}\\ \text{electron}\\ \text{emission}}} = k'_{n(\text{bulk tr})} n' f_T N_T \qquad (2\text{-}22)$$

where $k'_{n(\text{bulk tr})}$ is the trap emission rate constant, and n' is the density of empty conduction band states. In a semiconductor, only a small fraction of the conduction band

states are occupied, so that the process is pseudo-first-order, and a rate constant which incorporates the concentration of empty conduction band states can be written, so that

$$\left.\frac{\partial n}{\partial t}\right|_{\substack{\text{bulk}\\ \text{electron}\\ \text{emission}}} = k''_{n(\text{bulk tr})} f_T N_T \tag{2-23}$$

where now $k''_{n(\text{bulk tr})}$ has units of sec^{-1}.

The *net* rate of conduction band electron trapping is thus

$$\left.\frac{\partial n}{\partial t}\right|_{\substack{\textit{net}\\ \text{bulk}\\ \text{electron}\\ \text{trapping}}} = -k_{n(\text{bulk tr})} n(1-f_T) N_T + k''_{n(\text{bulk tr})} f_T N_T. \tag{2-24}$$

Applying the Principle of Detailed Balance again and setting the net rate equal to zero and rearranging yields

$$-k_{n(\text{bulk tr})} n_0 (1-f_{T0}) N_T = k''_{n(\text{bulk tr})} f_{T0} N_T, \tag{2-25}$$

or

$$k''_{n(\text{bulk tr})} = -k_{n(\text{bulk tr})} \frac{n_0(1-f_{T0})}{f_{T0}}. \tag{2-26}$$

The expression $\frac{n_0(1-f_{T0})}{f_{T0}}$, designated n_1, is made up of the known Fermi distributions for the populations of the traps and conduction band levels. Given the density of states at each level and their energies, the concentrations n_0, n_{T0} and n_i can be calculated.[12] For trap levels significantly far from midgap, where $E_T - E_i > 0$, the rates of capture fall off rapidly, because a trap near the conduction band edge efficiently traps electrons, but not holes. A trap in the center of the gap does not collect electrons as well, but the product of collecting both electrons and holes is higher. It can be shown that for

energies far from the center of the gap, trapping probabilities are low, and an overall surface recombination velocity is weighted by rates near the center of the gap.[13] The simplification that trapping occurs only via midgap traps leads to the equality $n_1 = n_i$; this assumption is utilized for the calculations in this thesis.

Hence, the bulk trapping term in the continuity equation can be written

$$\left.\frac{\partial n}{\partial t}\right|_{\substack{\text{net}\\ \text{bulk}\\ \text{electron}\\ \text{trapping}}} = -k_{n(\text{bulk tr})}(n(1-f_T)N_T - n_i f_T N_T). \tag{2-27}$$

If, instead of considering this process as a loss of electrons from the conduction band, one casts it in terms of the change of occupancy of the traps, then the net change of occupied traps is the negative of eq. 2-28 or

$$\frac{dn_T}{dt} = k_{n(\text{bulk tr})}(n(1-f_T)N_T - n_1 f_T N_T). \tag{2-28}$$

A completely analogous derivation for capture of valence band holes by the same traps leads to

$$\frac{dp_T}{dt} = k_{p(\text{bulk tr})}(p f_T N_T - p_1(1-f_T)N_T). \tag{2-29}$$

Given these equations which reflect electron capture and emission and hole capture and emission, a net trapping rate can be obtained by setting them equal, solving for n_T, and reexpressing the rates in terms of the concentrations of electrons and holes and the constants $k_{n(\text{bulk tr})}$, $k_{p(\text{bulk tr})}$, n_i, n_1,p_1 and N_T.

The steady-state recombination rate expression which results is

$$R = \frac{np - n_i^2}{\frac{1}{k_{p(\text{bulk tr})}N_T}(n+n_1) + \frac{1}{k_{n(\text{bulk tr})}N_T}(p+p_1)}. \tag{2-30}$$

Under low-level injection the equation can be simplified to

$$R = k_{p(\text{bulk tr})} N_T \Delta p. \tag{2-31}$$

The product $k_{p(\text{bulk tr})}N_T$ has the units of a first order rate constant (sec^{-1}). Its inverse has the units of time and defines the excess carrier lifetime for holes, i.e.,

$$\tau_p = \frac{1}{k_{p(\text{bulk tr})} N_T}. \tag{2-32}$$

For the high level injection, where $\Delta n = \Delta p >> n_0$ or p_0, R simplifies to

$$R = \frac{\Delta p}{\frac{1}{k_{p(\text{bulk tr})} N_T} + \frac{1}{k_{n(\text{bulk tr})} N_T}} = \frac{\Delta n}{\frac{1}{k_{p(\text{bulk tr})} N_T} + \frac{1}{k_{n(\text{bulk tr})} N_T}} \tag{2-33}$$

so the carrier lifetime is described by

$$\frac{\Delta n}{R} = \frac{\Delta p}{R} = \frac{1}{k_{p(\text{bulk tr})} N_T} + \frac{1}{k_{n(\text{bulk tr})} N_T} = \tau_p + \tau_n. \tag{2-34}$$

It can be seen that the lifetime due to this process is dominated by the smaller of the two trapping rate constants. The two main assumptions used in deriving this expression are that the material is non-degenerate, which yielded the expression for the concentration of conduction band electrons, and that the emission and capture coefficients remain fixed at their equilibrium values in non-equilibrium situations such as those investigated in this thesis.

c. Excitonic and shallow donors recombination

Exciton recombination between an electron-hole pair bound by Coulombic forces is similar to band-to-band recombination between free carriers, but at room temperature, relatively few of the carriers are bound, and their contribution to the bandgap luminescence is negligible. The recombination of donor-bound electrons recombining with holes, electrons recombining with neutral acceptors, or electrons bound to donors recombining

with holes bound to nearby electrons is thought to be negligible.[14] Also, at room temperature, donors will be ionized, which eliminates optical transitions in which donors play a role.

d. Auger recombination

Auger recombination involves three particles. It describes the direct recombination between an electron and a hole, accompanied by the transfer of energy to another free hole or electron. In general, the Auger recombination rate increases with decreasing bandgap energy, so it is most important for small band-gap semiconductors. It is believed that it is only important for GaAs for carrier densities greater than 10^{19} cm^{-3}.[15]

3. Surface Processes

The surface processes define the boundary conditions of the differential equation describing the kinetics in the slab of semiconductor. Were the differential equation to be solved analytically, integration would yield constants of integration, whose values would be determined by the boundary conditions. To obtain a complete solution for the concentrations, n(x,t) or p(x,t), requires two integrations over x and one over t, necessitating three boundary conditions to uniquely define all constants of integration. In general, these constraints are values for the fluxes at the front and back surfaces of the sample, and an initial condition at $t = 0$. Given that an analytic solution is not used, let us consider further how the boundary conditions are incorporated into a calculation of $\frac{\partial n(x,t)}{\partial t}$. The two surface processes which determine these conditions are surface trapping and surface charge transfer.

a. Surface trapping

Surface trapping takes an analogous form to that in the bulk except with regard to features particular to the two-dimensional nature of the surface. The rate of loss is

effectively being evaluated *at* a plane (defined by x=0), and is, therefore, a flux. As noted above, application of Fick's second law, the law of diffusion, permits conversion of a flux into a bulk rate, via calculation of the spatial derivative of the flux.

$$\frac{\partial n(x,t)}{\partial t} = -\frac{1}{q}\frac{\partial J(x,t)}{\partial x} = D\frac{\partial^2 n(x,t)}{\partial x^2} \tag{2-35}$$

Previewing the description of the finite difference calculation, let us consider a small box at the surface, with dimensions $\Delta x \Delta y \Delta z$, with the interface at x=0. The loss of carriers from that box can either be expressed as a change in concentration, n, or a change in the total number of carriers, N_n. Considering only the flux process at the surface, the loss of total carriers from the box due to this process will be the flux in from one side minus flux out from the other side multiplied by the area of the wall of the box. Flux is defined per unit area, so we write that

$$\frac{dN_n(\Delta x,t)}{dt} = (J(0+\Delta x,t) - J(0,t))A. \tag{2-36}$$

For convenience, we can chose the box to have unit area, A, and a width, Δx. Dividing through by the volume will yield the expression for rate of change in concentration on the left, and flux divided by Δx on the right, since the area terms will cancel. Thus,

$$\frac{\partial n(\Delta x,t)}{\partial t} = \frac{J(0+\Delta x,t) - J(0,t)}{\Delta x}. \tag{2-37}$$

We recognize that in the limit as Δx goes to 0 (from x less than 0, if we describe the x axis increasing from left to right as shown for the semiconductor half of Figure 1-1), this is almost the derivative of the flux with respect to x. (We can actually only consider the left hand derivative, i.e., $\lim_{\Delta x \to 0^-}$, since the function is not defined to the right of zero, and is, therefore, not strictly differentiable at the surface.) I have chosen to designate this limit as the gradient of the flux, evaluated at x=0.

$$\left.\frac{\partial n(x,t)}{\partial t}\right|_{\substack{\text{surface}\\ \text{trapping}}} = \frac{1}{q}\lim_{\Delta x \to 0^-}\frac{J(0+\Delta x,t) - J(0,t)}{\Delta x} = \frac{1}{q}\left.\frac{\partial J(x,t)}{\partial x}\right|_{x=0} \qquad (2\text{-}38)$$

The method above for converting an absolute number of carriers lost in a surface region to concentration loss assumes that the number lost at the surface is lost from the whole box evenly. In the limit of an infinitely small box, this is a reasonable approximation, and as a practical matter one can check the calculations by making boxes smaller, to determine whether any inaccuracies have been introduced.

By substituting surface trap concentrations in cm^{-2} in place of the bulk trap concentrations one obtains surface trapping rates that have units of $cm^{-2}\ s^{-1}$, which are the units of flux. The result which is evaluated explicitly in the textbook by Pierret,[5a] for example, parallels the expression for the bulk recombination rate, eq. 2-30; the subscript "s" is used to designate the species at the surface, and the surface flux due to trapping is

$$R_S = \frac{n_S p_S - n_i^2}{\frac{1}{k_{p\ surface} N_{TS}}(n_S + n_{1S}) + \frac{1}{k_{n\ surface} N_{TS}}(p_S + p_{1S})} \qquad (2\text{-}39)$$

where n_S, p_S, n_{1S} and p_{1S} are concentrations in the surface region and, so, retain the units of cm^{-3}, and $k_{p\ surface}$ and $k_{n\ surface}$ are still $cm^3 sec^{-1}$, but N_{TS} has units of cm^{-2}. Expressions for n_S, p_S, n_{1S} and p_{1S} which assume that the carrier distributions remain Maxwellian (i.e., proportional to $\exp(E_t - E_i/kT)$) under non-equilibrium conditions can be substituted into this expression to obtain a calculation of the rate in terms of the trap energies and potential at the surface.[16] Again, however, it is assumed that the trap energies are at midgap, so that n_{1S} is equal to n_i.

The products corresponding to the bulk trapping lifetimes of eq. 2-34 now have units of cm/sec and are referred to as the surface recombination velocities of electrons and holes, denoted s_n and s_p, respectively. They can be written

$$s_n = k_{n\ surface} N_{Ts} = \frac{R_s}{\Delta n_s} \tag{2-40a}$$

and

$$s_p = k_{p\ surface} N_{Ts} = \frac{R_s}{\Delta p_s}. \tag{2-40b}$$

For the high injection case eq. 2-39 simplifies just as the parallel equation for the bulk rate did, to

$$R_s = \frac{\Delta p_s}{\frac{1}{k_{p\ surface} N_{Ts}} + \frac{1}{k_{n\ surface} N_{Ts}}} . \tag{2-41}$$

An expression corresponding to the high injection surface recombination velocities is thus

$$\frac{\Delta p_s}{R_s} = \frac{1}{S} = \frac{1}{s_p} + \frac{1}{s_n} \tag{2-42}$$

where it is assumed that the equilibrium condition that $\Delta n_s = \Delta p_s$ still holds. This may not be true at a surface in which electrons and holes are being captured at widely different rates. It can be seen that the measured S is dominated by the smaller of the two trapping rate constants, s_p or s_n.

In the case where only bulk and surface trapping occur, it was shown originally by Shockley[17] that at low injection the rate equation for the loss of excess carriers in a slab is a function of a bulk and a surface term and can be written

$$\frac{dp}{dt} = - \left[\frac{1}{\tau_p} + \frac{s_p + s_{p(h)}}{L} \right] p \tag{2-43}$$

where s_p is the surface recombination velocity for holes at the front of the slab, $s_{p(h)}$ is the surface recombination at the back of the slab, and L is the thickness of the slab. The solution of this equation is readily seen to be single exponential in form.

$$p(t) = p(0) e^{- k_{fil}\, t} \tag{2-44}$$

where $k_{fil} = \left[\frac{1}{\tau_p} + \frac{s_p + s_{p(h)}}{L} \right]$ is the so-called filament lifetime.

At low injection, as noted above, the radiative recombination is also monomolecular in form, so if we include the radiative recombination term, the decay for this filament can be written as being due to a linear sum of monomolecular processes, with the largest rate constant dominating. An effective rate constant is thus,

$$k_{effective} = k_{fil} + k_{radiative}\, p,$$

$$= \left[\frac{1}{\tau_p} + \frac{s_p + s_{p(h)}}{L} \right] + k_{radiative}\, p. \qquad (2\text{-}45)$$

In other words, eq. 2-43 can be written as the first-order equation,

$$\frac{dp}{dt} = -k_{effective}\, p = -\frac{p}{\tau_{low\ injection}}$$

and there would be a single-exponential lifetime, $\tau_{low\ injection}$, where

$$\frac{1}{\tau_{low\ injection}} = \left[\frac{1}{\tau_p} + \frac{s_p + s_{p(h)}}{L} \right] + k_{radiative}\, p. \qquad (2\text{-}46)$$

As discussed further in Chapter 3, $k_{radiative}$ is on the order of 2×10^{-10} $cm^3 sec^{-1}$ for GaAs, and the equilibrium carrier density is 10^{15} cm^{-3}, so that the low-injection radiative lifetime is expected to be on the order of 6 μs. Experimentally, the longest lifetime observed is 80 ns, which we attribute to the filament lifetime. Since the material used in this experiment is of such high quality, we can assume that the bulk trapping lifetime, τ_p, is long, and therefore negligible. Thus, the single exponential lifetime at low injection is attributed to the front and back surface recombinations, s_p and $s_{p(h)}$. For the heterostructures used in these experiments, the interface at both sides of the GaAs active layer is equivalent, so $s_p = s_{p(h)}$. Quantitatively, then, the measured lifetime is expected to be

$$\frac{1}{\tau_{low\ injection}} = \frac{2s_p}{L} \qquad (2\text{-}47)$$

so that from a measured lifetime, a value of s_p can be determined, i.e.,

$$s_p = \frac{L}{2\tau_{\text{low injection}}}. \qquad (2\text{-}48)$$

From the equations for s_p and s_n in eq. 2-40a and b and S in eq. 2-42, it can be seen that S at high injection can be approximated by s_p obtained at low injection in this fashion if it is smaller than s_n, which requires that $k_{p\ \text{surface}}$ be less than $k_{n\ \text{surface}}$. In the literature, these values are frequently reported in terms of a capture cross section, σ_p or σ_n, that reflects the effectiveness of the traps in capturing holes and electrons, and the rate constants are identified with the product σv where v is the thermal velocity of the carrier. Thus, if the cross sections for trapping holes is the same or smaller than that for electrons, the term $\frac{1}{s_p}$ dominates in the expression for S (assuming their thermal velocities are equivalent). Literature values for bulk electron and hole traps show that the opposite is generally the case, that σ_n ranges from 10^{-20} to 10^{-16} cm^2, while σ_p ranges from 10^{-17} to 10^{-14} cm^2.[18] If s_n dominates the sum in eq. 2-42, the lifetime at high injection may be significantly longer than the one determined at low injection. It is possible that immersing semiconductors in solution changes the trap cross sections, as well. The important point to note is that caution must be used in applying the value of S obtained from experiments such as the one described for low-injection luminescence measurements, to the high injection results.

b. Surface electron and hole transfer

A discussion of the rates of surface electron and hole transfer was presented in Chapter 1. Using kinetic expressions of the form of eq. 1-1, the fluxes of electrons into and out of the conduction band and of holes into and out of the valence band can be derived, and rates of carrier loss at the surface due to these fluxes can be evaluated using Fick's second law.

At equilibrium, the net flux from valence band to solution species, f_{ht}, is equal is zero, and the exchange currents, or fluxes out and in, can be written

$$F_{out} = F_{in} = k_{ht} p_{s0} C_D = k_{-ht} N_V C_A \qquad (2\text{-}49)$$

where C_D is the concentration of hole acceptors, C_A is the concentration of hole donors, and N_V is the effective density of states in the valence band.

Away from equilibrium, net flux for both valence and conduction bands can be written as the difference between the fluxes in and out. Experimentally, an external light pulse is expected to introduce a large increase in electrons and holes in the semiconductor, and thereby perturb the equilibrium fluxes of holes and electrons out of the semiconductor, while not dramatically changing the reverse reaction. Therefore,

$$\begin{aligned} f_{net(vb)} &= f_{out} - F_{in} \\ &= k_{ht} p_s C_D - k_{ht} p_{s0} C_D \\ &= k_{ht} C_D (p_s - p_{s0}) \\ &= k_{ht} C_D \Delta p_s \end{aligned} \qquad (2\text{-}50a)$$

where f_{out} is the non-equilibrium flux. An analogous equation holds for the conduction band,

$$\begin{aligned} f_{net(cb)} &= k_{et} C_A (n_s - n_{s0}) \\ &= k_{et} C_A \Delta n_s. \end{aligned} \qquad (2\text{-}50b)$$

Given these flux equations, the loss of electrons and holes with time due to electron transfer can now be determined in the same manner as was done for surface trapping, by applying Fick's second law in the limit as we approach the surface,

$$\left.\frac{\partial n(x,t)}{\partial t}\right|_{\substack{\text{electron} \\ \text{transfer}}} = - \left.\frac{\partial f_{et}(x,t)}{\partial x}\right|_{x=0} \qquad (2\text{-}51a)$$

$$\left.\frac{\partial p(x,t)}{\partial t}\right|_{\substack{\text{hole} \\ \text{transfer}}} = - \left.\frac{\partial f_{ht}(x,t)}{\partial x}\right|_{x=0} . \qquad (2\text{-}51b)$$

It should be noted that the fluxes for charge transfer to solution operate in parallel with the fluxes expressed by the surface trapping rate of eq. 2-39 and a surface

recombination velocity attributable to the charge transfer fluxes, f_{et} and f_{ht}, can also be written. That is, parallel to eq. 2-40,

$$s_{n(et)} = \frac{f_{et}}{\Delta n_s}$$

and

$$s_{p(ht)} = \frac{f_{ht}}{\Delta p_s} .$$

Although this formalism does not make explicit the charge transfer nature of the flux it reflects the fact that without an independent measure of the acceptor concentration in solution, the flux at the surface due to charge transfer can be parameterized as an overall hole capture velocity just as surface trapping is.

Thus, expressions for each of the terms in the continuity equation, eq. 2-6, have been written in terms of the concentrations of electrons and holes in the semiconductor. In Chapter 3 the calculations made using these expressions will be discussed.

---

[1]Albright, T. A.; Burdett, J. K.; Whangbo, M. H. *Orbital Interactions in Chemistry*; Wiley-Interscience: New York, 1985. p 215. (b) For a very readable account of bands and orbitals, see Hoffmann, R. *Angew. Chem.* **1987**, *26*, 846.

[2] Pierret, R. F. *Advanced Semiconductor Fundamentals*, Vol VI in the Modular Series on Solid State Devices, Pierret, R. F.; Neudeck, G. W. Eds. Addison-Wesley: Reading, Massachusetts, 1987: p 75.

[3]Shank, C. V.; Fork, R. L.; Leheny, R. F.; Shah, J.; *Phys. Rev. Lett.* 1979, **42**, 112.

[4] (a) Sze, S. M. *Physics of Semiconductor Devices*; Wiley-Interscience: New York, 1981. (b)Wang, S. *Fundamentals of Semiconductor Theory and Device Physics*; Prentice Hall: Englewood Cliffs, NJ, 1989.

[5]Pierret, R. F. *Advanced Semiconductor Fundamentals*, Vol VI in the Modular Series on Solid State Devices, Pierret, R. F.; Neudeck, G. W. Eds. Addison-Wesley: Reading, Massachusetts, 1987. (b) Sze, S. M. *Physics of Semiconductor Devices*; Wiley-Interscience: New York, 1981. (c) Wang, S. *Fundamentals of Semiconductor Theory and Device Physics*; Prentice Hall: Englewood Cliffs, NJ, 1989.

[6] Pierret, R. F.*op. cit.*, p. 140.

[7] Blakemore, J. S. *Semiconductor Statistics*; Dover: New York, 1987.

[8] Pierret, R. F. *op. cit.,* p 141.

[9] J. E. Fouquet, Ph.D. Thesis, Stanford University, 1986.

[10] Shockley, W.; Read, W. T.,Jr. *Phys. Rev.* **1952**, *87*, 835.

[11] Hall, R. N. *Phys. Rev.* **1952**, *87*, 387.

[12] Pierret, R. F. *op. cit.*,.p. 152.

[13] Pierret, R. F. *op. cit.*, p. 166.

[14] Pankove, J. I. *Optical Processes in Semiconductors*; Dover: New York, 1975: p 180.

---

15 (a) Fahrenbruch, A. L.; Bube, R. H. *Fundamentals of Solar Cells*; Academic Press: New York, 1983: p. 58 (b) Fouquet, J. E. Ph.D. Thesis, Stanford University, 1986. (c) McLean, D. G.; Roe, M. G.; D'Souza, A. I.; Wigen, P. E. *Appl. Phys. Lett.* **1986**, *48*, 992.

16Many, A.; Goldstein, Y.; Grover, N. B. *Semiconductor Surfaces*; North -Holland: Amsterdam, 1965: Chpt. 5.

17Shockley, W. *Electrons and Holes in Semiconductors*; Van Nostrand: New York, 1950: p. 318.

18*Impurities and Defects in Group IV Elements and III-V Compounds*; Madelung, O., Ed.; Landoldt-Börnstein Numerical Data and Functional Relationships in Science and Technology, New Series III/22b; Springer-Verlag, Berlin, 1987; p. 597.

CHAPTER 3

SOLUTIONS FOR THE CONTINUITY EQUATION: Finite Difference Calculations and Computer Algorithm.

A. Introduction

Having written expressions for each of the terms in the complete continuity equations, the rate equations governing electron-hole kinetics for the system of interest can be reexpressed for electrons as

$$\frac{\partial n(x,t)}{\partial t} = D_n \frac{\partial^2 n}{\partial x^2} - \frac{\partial}{\partial x}(k_{n\ surface} N_{Ts}\, \Delta n_s(t))\Big|_{x=0} - \frac{\partial}{\partial x}(k_{et} C_A \Delta n_s(t))\Big|_{x=0}$$

$$- k_{radiative}(\Delta n \Delta p - n_i^2) - k_{n\ bulk}(n p_T - n_1 n_T) + g_E \qquad (3\text{-}1a)$$

and analogously for holes,

$$\frac{\partial p(x,t)}{\partial t} = D_p \frac{\partial^2 p}{\partial x^2} - \frac{\partial}{\partial x}(k_{p\ surface} N_{Ts}\, \Delta p_s(t))\Big|_{x=0} - \frac{\partial}{\partial x}(k_{ht} C_A \Delta p_s(t))\Big|_{x=0}$$

$$- k_{radiative}(\Delta n \Delta p - n_i^2) - k_{n\ bulk}(n p_T - n_1 n_T) + g_E \qquad (3\text{-}1b)$$

where the terms marked by $\Big|_{x=0}$ denote that the flux terms are evaluated at the surface and are used to include the boundary conditions in the total continuity equation. In order to relate the rate constants for hole and electron transfer to the experimental observable, the luminescence, which we have noted takes the form $L=k_{radiative}np$, a solution must be obtained for the concentration of electrons, n(x,t), and holes, p(x,t), in the semiconductor/liquid system.

Equation 3-1 is a second-order, inhomogeneous, partial differential equation. It is similar to the diffusion equations used in many situations, except that it includes a bimolecular term for radiative recombination.

Solutions for the continuity equations have been developed for numerous cases since the development of the p-n junction and relevant semiconductor statistics in the 1950s. Of particular relevance is the solution for eq. 3-1 when all terms except the bimolecular radiative term are included. As a practical matter, neglect of this term is justifiable in materials where bimolecular recombination is believed to be small relative to monomolecular processes such as bulk trapping. In this case, an analytic solution, attributed to Vaitkus,[1] and requiring several lines of text to state, can be written for specific generation functions, g_E, given in an analytic form, such as a δ-function, or a Gaussian pulse. Agmon[2] utilized this equation in describing the photoconductivity decays observed in Cr-doped GaAs samples. Evenor and co-workers[3] describe the same approach for analysis of photoluminescence decays of CdS, in which the bimolecular recombination is relatively small, but chose to utilize a numerical solution for their calculations in order to address the non-linearity of the photoluminescence. Agmon chose a generation function given by a δ-function. Both Agmon and Evenor and co-workers employed semiconductor samples that were thick enough (1-2 mm in the work of Evenor *et al.*) that the bulk of the material was assumed to be unaffected by the excitation during the course of the experiment. This permits use of the boundary conditions

$\frac{\partial n(x,t)}{\partial x}\Big\vert_{x=0} = \frac{S}{D^*}\Delta n(x=0,t)$	boundary condition on the front surface
$\Delta n(x=\infty,t) = 0$	semi-infinite condition
$\Delta n(x,t=0) = 0$	initial value condition

where S is the surface recombination velocity.

Alternative approaches to obtaining an analytic solution are also in the literature. For example, Luke and Cheng[4] solved the continuity equation subject to an initial condition that incorporates the initial impulse laser pulse. In both the work of Evenor *et al.* and of Luke and Cheng, the simulations use convolution to incorporate the effect of the system response.

The calculations in this thesis utilize the numerical simulation technique of finite-difference used by Evenor *et al.* in the cited work , which was developed for use in electrochemical simulations by S. Feldberg[5] of Brookhaven National Labs. The diffusion, drift and kinetic expressions used to describe the fluxes of charged particles (*i.e.*, ions) in electrochemical solutions are equally applicable to the charged particles (*i.e.*,electrons and holes) in semiconductors. Finite-difference methods are one of the more straightforward techniques used by semiconductor device physicists for modelling electron and hole transport in semiconductor devices, and numerous more elaborate schemes which include the effects of electric fields, but not surface charge transfer, exist in the semiconductor literature.[6,7] The finite-difference method is described in the next section.

B. Finite-Difference Calculations

1. Discretization

The finite-difference method requires simply that the differential equation be discretized. That is, the differential terms are converted from expressions evaluated in the limit of infinitely small time and space increments to expressions written in terms of finite sized time and space increments. To begin, it is noted that the equation for flux in the derivative form can be reexpressed as the limit in the calculus as

$$f(x,t) = -D \frac{\partial n(x,t)}{\partial x} = -D \lim_{\Delta x \to 0} \frac{n(x+\Delta x,t) - n(x,t)}{\Delta x} \qquad (3\text{-}2)$$

where f denotes flux. It is reasonable, therefore, to write flux as

$$f(x,t) = -D\frac{\Delta n(x,t)}{\Delta x} = -D\frac{n(x+\Delta x,t) - n(x,t)}{\Delta x} = -D\frac{n(x+\Delta x/2,t) - n(x-\Delta x/2,t)}{\Delta x} \qquad (3\text{-}3)$$

for chosen Δx.

The time derivatives undergo the same conversion so the expression for changes due to fluxes are

$$\left.\frac{\partial n(x,t)}{\partial t}\right|_{\text{diffusion}} = \frac{\Delta n(x,t)}{\Delta t} = -\frac{\Delta f(x,t)}{\Delta x} = \frac{-f(x+\Delta x/2,t) + f(x-\Delta x/2,t)}{\Delta x} \qquad (3\text{-}4)$$

which by substitution leads to

$$\left.\frac{\Delta n(x,t)}{\Delta t}\right|_{\text{diffusion}} = D\frac{\frac{n(x+\Delta x,t) - n(x,t)}{\Delta x} - \frac{n(x,t) - n(x-\Delta x,t)}{\Delta x}}{\Delta x}$$

$$= D\frac{n(x+\Delta x,t) - 2n(x,t) + n(x-\Delta x,t)}{\Delta x^2} \qquad (3\text{-}5)$$

The expression for the radiative recombination is

$$\frac{\Delta n(x,t)}{\Delta t} = k_r n(x,t)p(x,t). \qquad (3\text{-}6)$$

A closer approximation to the differential equation is achieved for smaller Δx and Δt, although the higher resolution results in longer computation times. In practice, a minimum number of boxes is specified (generally 5 for the work in this thesis), and the width of a box, Δx, is defined by dividing the width of the sample by the number of boxes. As shown in work by Feldberg,[8] a criterion for the selection of Δt is the constraint that $\frac{D\Delta t}{\Delta x^2} \leq 0.5$, where D is the relevant diffusion coefficient, so that the simulation does not become unstable. Following the practice of Feldberg, it is set to 0.4 in this work. The effect of this constraint is that in the time, Δt, the reactants do not diffuse much beyond Δx so that changes in concentration are accurately tracked by the calculations, and species are not allowed to move a distance greater than one box per iteration. Two other constraints

are that the diffusion layer span several space elements and the time elements be smaller than the half life of any reactions.[9] As a practical matter, calculating the simulation using Δt equal to the time increment in the experimental data, or some multiple thereof, simplifies comparison of the data with the simulation.

Calculations for the individual time and space increments require that they be indexed, as is diagrammed in the following.

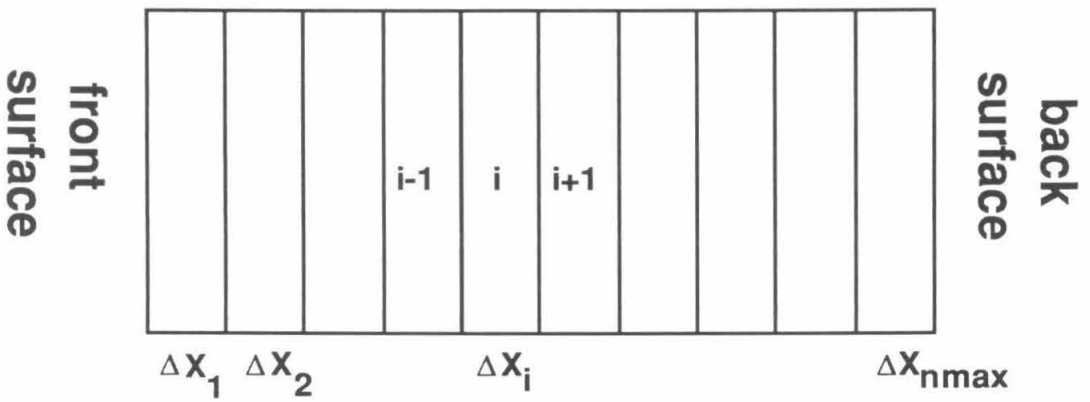

Figure 3-1. Diagram of indexing used for Δx in the finite difference calculations.

The increments of time are indexed by k.

As drawn, x increases from left to right , and so fluxes are defined as negative when flowing towards the front surface. In the work of Feldberg, flux at the left interface of box i is designated by a single prime, f'_i, while that at the right of box is f''_i so that the expression $\frac{df}{dx}$ is discretized as $\frac{f''_i - f'_i}{\Delta x}$. The equivalent notation in this thesis is $\frac{f_{i+1} - f_i}{\Delta x}$ indicating that flux in from the right side of box i is f_{i+1}, and that out the left side is f_i.

Concentrations are calculated for x at the right hand side of the boxes as diagrammed in Figure 3-1. Then, the following identities are made for use in the computer calculation

$$n(x) \text{ --> } n(i), \tag{3-7a}$$

$$n(x+\Delta x) \text{ --> } n(i+1) \tag{3-7b}$$

$$n(x-\Delta x) \text{ --> } n(i-1). \tag{3-7c}$$

Thus, the expression for the flux (eq. 3-3) becomes

$$f(i,k) = - D\frac{n(i+1,k) - n(i,k)}{\Delta x} \tag{3-8}$$

and eq. 3-5 becomes

$$\frac{\Delta n(i,k)}{\Delta t} = D\,\frac{n(i+1,k) - 2n(i,k) + n(i-1,k)}{\Delta x^2} \tag{3-9}$$

or, rearranging, the change in a concentration in a box, i, can be written

$$\Delta n(i,k) = \frac{D\Delta t}{\Delta x^2}\,(n(i+1,k) - 2n(i,k) + n(i-1,k)). \tag{3-10}$$

The dimensionless term $\frac{D\Delta t}{\Delta x^2}$ is set at 0.4 due and is designated as D* in the work of Feldberg.

2. Boundary Conditions

The boundary conditions from the differential equation are incorporated by making special provisions for the fluxes in the first and last box. For the first box,

$$\frac{\Delta n(1,k)}{\Delta t} = - \frac{f(1,k)-f(0,k)}{\Delta x} = \frac{D}{\Delta x}\left(\frac{n(2,k)-n(1,k)}{\Delta x} - \frac{f(0,k)}{\Delta x}\right), \tag{3-11}$$

and for the last box,

$$\frac{\Delta n(nmax,k)}{\Delta t} = - \frac{f(b,k)-f(nmax,k)}{\Delta x} = \frac{D}{\Delta x}\left(\frac{f(b,k)}{\Delta x} - \frac{n(nmax,k)-n(nmax-1,k)}{\Delta x}\right), \tag{3-12}$$

where f(1,k) and f(nmax,k) have been replaced with an expression like that defined in eq. 3-8. f(0,k) is the flux calculated for the front surface process and f(b,k) is that for the back. The values for the surface terms are calculated in a separate section of the computer program and subtracted from the concentration in the first box. As a point of consistency it should be noted that the terms containing f(b,k) and f(0,k) are of opposite sign using the notation above, from which one might conclude that losses at one surface are added, while

at the other they are subtracted. As discussed in Chapter 2, these surface terms actually reflect limits as Δx approaches zero, but for the front the limit is approaching from the right, while at the back it is approaching from the left, so in fact Δx is of opposite sign, and so the loss terms $\frac{f(0,k)}{\Delta x}$ and $\frac{f(b,k)}{\Delta x}$ both lead to reduction of the concentrations in the boxes.

Since the differential formalism at the surface is not strictly valid other workers have suggested alternative formulations for incorporating the surface flux term that use other polynomial expansions to increase precision of the approximated derivative at the surface, such as Newton's derivative approximation.[6b]

$$\left.\frac{df}{dx}\right|_{x=0} = \frac{-3f(0,k)+ 4f(1,k) -f(2,k)}{2\Delta x} + \text{terms of the order of } \Delta x^2. \qquad (3\text{-}13)$$

However, no need was found to use a higher precision expression for this work.

3. Luminescence

When all of the differential terms from Eq. 3-1 are written in discrete form, the computer is able to calculate the changes, Δn and Δp, given initial concentration n(i,0) and p(i,0) which are determined by the laser pulse. The Δn and Δp terms for each process in each box are added to the starting values of n and p for those boxes, to yield an updated n_{new} and p_{new}, which form the starting point for the next iteration. The end result is a value for n and p at each time t (or index k) of the calculation. These functions, n(x,t) and p(x,t) with values at discrete points, x_i, permit calculation of the decay curve, $L(x,t)=k_{radiative}[n(x,t)p(x,t)-n_i^2]$. The total luminescence from the sample is the sum of the luminescence from each box. That is,

$$L(t) = k_r \int_0^d [n(x,t)p(x,t)-n_i^2]\, dx \qquad (3\text{-}14)$$

or in discrete units,

$$L(k) = \sum_{i=1}^{nmax} [n(i,k)p(i,k)-n_i^2] \quad . \tag{3-15}$$

A diagram of the calculated concentrations vs. distance and a flow chart for the calculation appear in Figures 3-2 and 3-3, respectively.

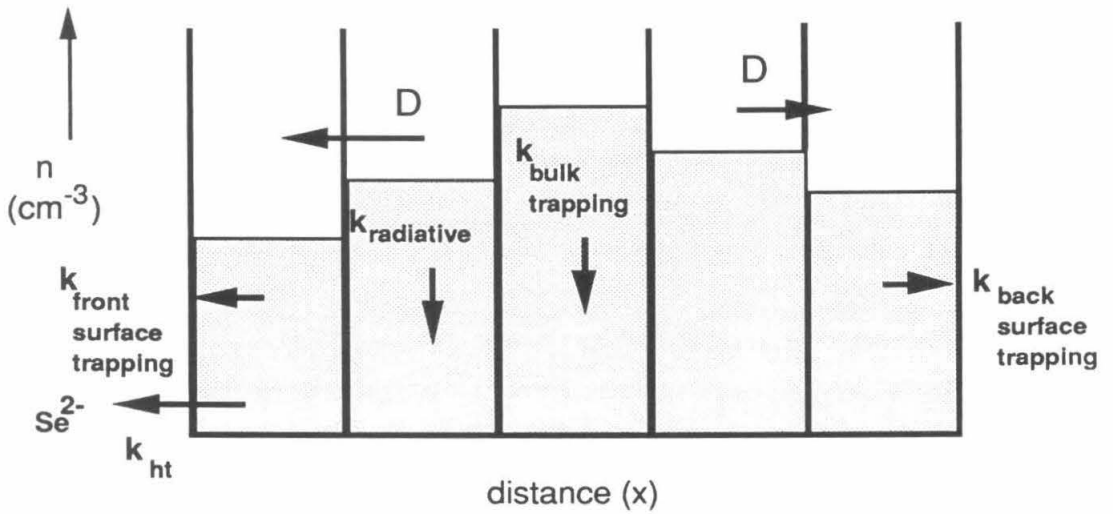

Figure 3-2. Diagram of concentration profiles generated by finite difference computer algorithm. The arrows indicate the terms incorporated in the calculation that are described in the text.

The concentration profiles calculated according to this scheme are most readily grasped in the graphs in Figures 3-4 and 3-5, showing the evolution of the concentration profiles for two limiting values of a surface rate measured for the system in this thesis. Figure 3-4 shows the concentration profiles derived for the case when there is no electron transfer and only a small surface recombination loss due to surface trapping which has been determined to be S = 625 cm/sec as discussed in Chapter 5. Figure 3-5 shows the change resulting when an additional surface rate corresponding to surface electron and hole transfer is included. The effective surface recombination velocity in this calculation is 10^5 cm/s.

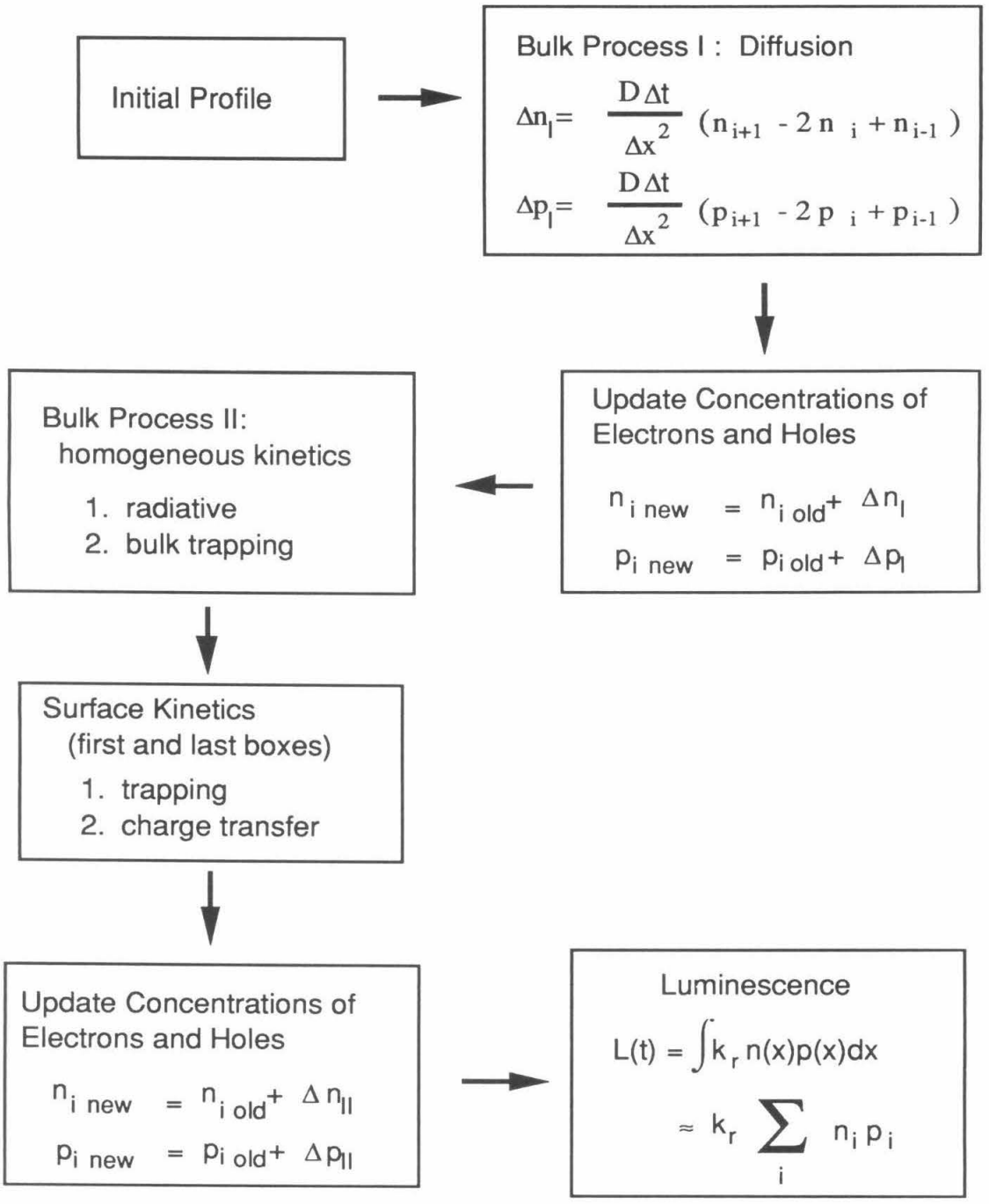

Figure 3-3. Flow chart for computer algorithm of finite-difference calculation.

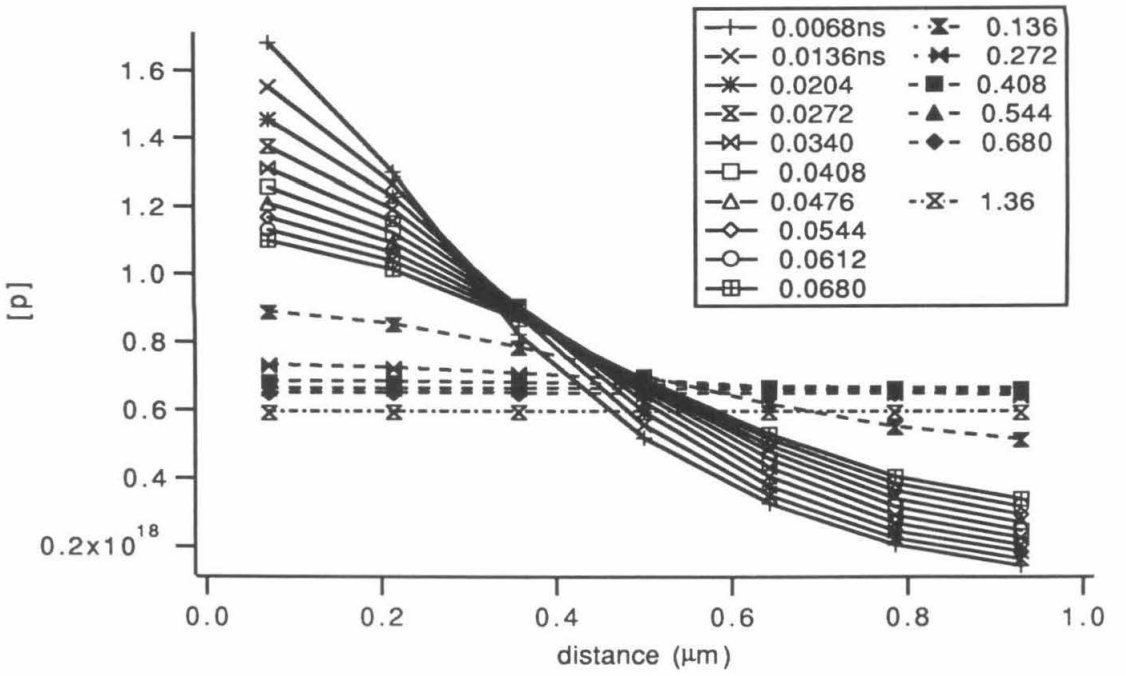

Figure 3-4(a) Concentration profiles for early times; k_{ht}=0

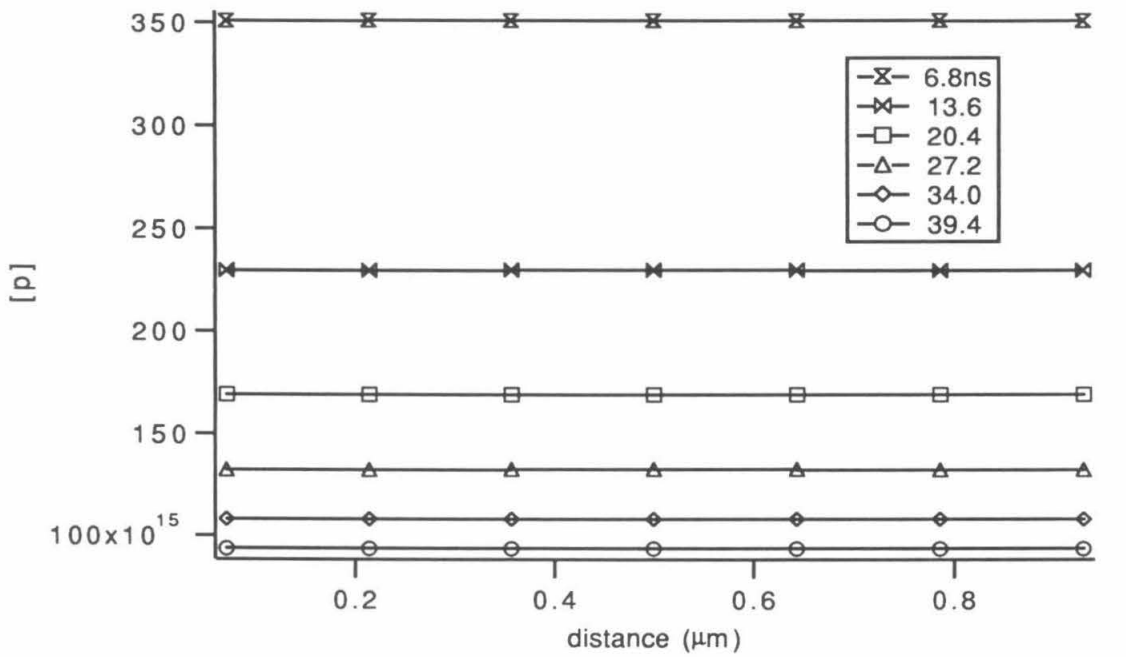

Figure 3-4(b) Concentration profiles for later times; k_{ht}=0

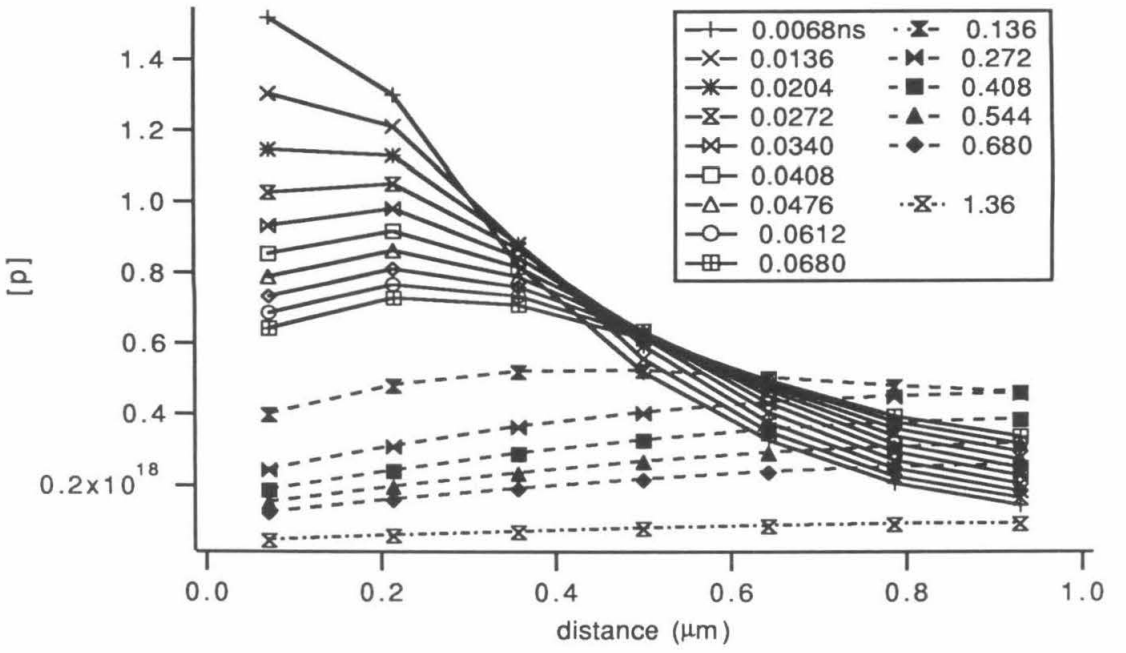

Figure 3-5(a) Concentration profiles for early times; $k_{ht}=2x10^{-15}$

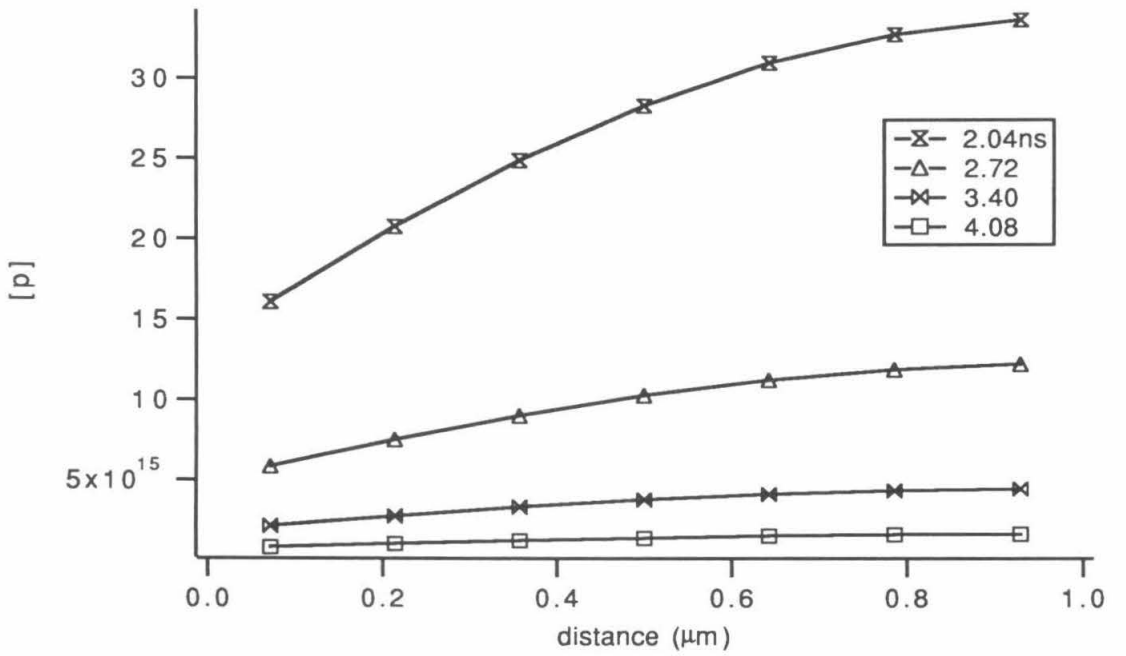

Figure 3-5(b) Concentration profiles for later times; $k_{ht}=2x10^{-15}$

4. Convolution

In order to account for the shaping of the signal introduced by the finite bandwidth of the electronics and the finite width of the laser pulse, the simulated luminescence decay curve is convoluted with the instrument response function. Convolution is a well-established procedure, discussed in textbooks,[10] and available in commercial software packages. The electronics involved in collecting the photons and transmitting the signal to the collection computer introduce uncertainties, collectively described in the system response, which is determined by measuring the TCPC signal when a laser pulse is directly input to the collection system. This measurement also incorporates the finite width of the laser pulse itself and the fact that not all molecules start their decay together, because some are excited by the tail of the excitation pulse, while others are excited by the initial edge.

Conceptually, the instrumentation broadens each individual point in the ideal, but unrealizable, decay, and so the observed value of the decay at some time t is the superposition of all the individual broadened pulses that have occurred prior to t. Mathematically, this is written as

$$\begin{aligned} L(t) &= \text{InstrumentResponse}(t) \otimes \text{Simulation}(t) \\ &= \int_0^t \text{InstrumentResponse}(t')\,\text{Simulation}(t-t')\,dt' \,. \end{aligned} \tag{3-16}$$

For the data presented in this thesis, an algorithm in the MATLAB software package (The MathWorks, Inc., Natick MA) performs the sum

$$c(n+1) = \sum_{k=0}^{N-1} a(k+1)b(n-k) \tag{3-17}$$

where N is the length of the simulated data set or of the instrument response function, whichever has more points.

5. Model Parameters

a. Diffusion Constant, D

The diffusion coefficients are derived from the literature values for the mobility

constants using the Einstein relationship[11] $D_e = (kT/q)\,\mu_e = .026\mu_e$, and $D_h = .026\mu_h$, where μ_e, the mobility for electrons is 8500 $cm^2/V\text{-}s$, and μ_h, the mobility of holes, is 200 $cm^2/V\text{-}s$,[12] k is the Boltzmann constant, q is the charge on an electron, and T is the temperature, taken to be 300 K. The unequal mobilities of electrons and holes might be expected to lead to charge separation as the electrons and holes diffuse into the bulk of the semiconductor. The voltage which arises in this case is known as the Dember potential and is due to the Dember or photo-diffusion effect.[13] However, incipient charge separation creates a field that retards further separation, and the electrons and holes appear to diffuse with an effective diffusion constant, the so-called ambipolar diffusion constant, $\bar{D} = \frac{2D_hD_e}{D_h+D_e}$, referred to as "Dbar" in the computer program.

Feldberg *et al.*[14] investigated the possibility of significant charge separation due to the unequal mobilities and showed that electroneutrality can be assumed if certain criteria are met. These criteria, developed for typical semiconductor parameters, include that initial surface concentrations are greater than $1x10^{17}$ cm^{-3} for a surface recombination velocity of 0 cm/sec and greater than $5x10^{17}$ cm^{-3} in the limit of infinite surface recombination velocity. Kinetics which deplete one of the carriers faster than diffusional flattening of the profiles might also change the conditions for electroneutrality. Feldberg demonstrated that this deviation will be minimal as long as $k\delta^2/\bar{D} < 0.055$, where k is the first-order kinetic rate constant, δ is the penetration depth of the light, which reflects the width of the exponential profile created by the absorption of the light, and $\bar{D}$ is the ambipolar diffusion constant. For the experimental conditions herein, δ is $3x10^{-5}$ cm, and $\bar{D}$ is 10 cm^2/Vs, so this requires that $k < 6x10^8$ s^{-1}, or alternatively, that the lifetime corresponding to the first-order process be greater than 1.6 ns. Finally, Feldberg found that the surface recombination is not expected to lead to significant charge separation, when it is assumed

that e^- - h^+ pairs are consumed at the surface, rather than just one charge or the other. If electrons reach the surface more quickly than holes and holes are consumed more quickly, it is plausible that some excess negative charge might build up on the surface. Nonetheless, even at the slower rate of hole diffusion, the original absorption profile flattens quickly, and, in this work, the condition of electroneutrality was presumed.

b. Absorption Coefficient, α

In the calculations for this thesis, the generation function, g_E, is taken to be the simplest case, a delta function. This is reasonable, given that the pulse width from the laser is less than 10 ps, while the time scale of events being measured is several hundred picoseconds or more. Moreover, the maximum time resolution of the instrumentation is 13 ps, and the overall system response shape is accounted for by convolution described above. As a result of the delta pulse input the simulation starts with a distribution of carriers reflecting an exponential Beer's Law absorption profile from the front into a depth determined by the absorption coefficient.

The absorption coefficients have been tabulated by Aspnes.[15] From Table II in the Aspnes work, the absorption coefficient in the range of laser excitation accessible with the apparatus used in this thesis has been converted to penetration depth as a function of wavelength and is plotted in Figure 3-6.

For GaAs structures similar to the samples used in these experiments, except grown by liquid phase epitaxy (LPE) instead of organometallic chemical vapor deposition (OMCVD), Sell and Casey[16] report a value of $\alpha = 0.99 \times 10^4$ cm^{-1} at 1.96 eV (penetration depth of 1.0 μm at 633 nm). In the calculations made in this work, α for the incident 660 nm light was taken to be 3.2×10^4 cm^{-1}, while the absorption coefficient used for reabsorption of emitted bandgap light at 880 nm was taken to be 1×10^4 cm^{-1}.

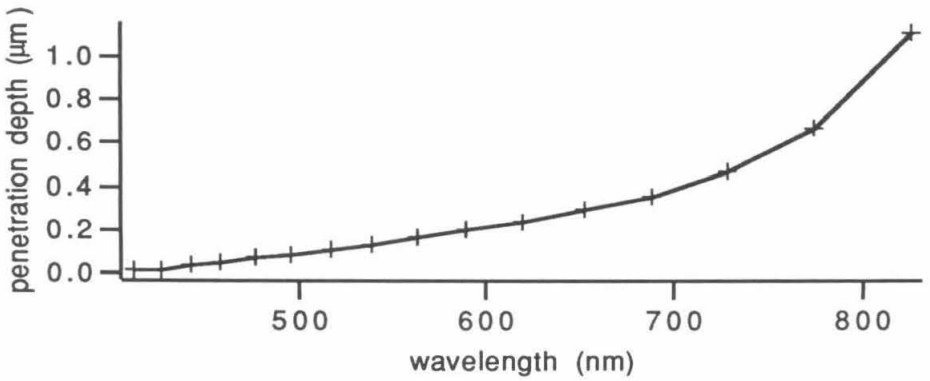

Figure 3-6. Penetration depth as a function of wavelength for GaAs.

c. Radiative Recombination Coefficient, $k_{radiative}$

Numerous factors affect the importance and value of the radiative recombination rate constant, including dopant density, temperature and injection level. Since the value was not measured in the experiments performed in this thesis, it was necessary to rely on a value from the literature, but because of the high injection conditions used in the experiment, there is some uncertainty in its actual experimental value. A brief discussion of some of the issues determining a radiative recombination rate are given here. The letter "B" is used to designate $k_{radiative}$ in the literature, and that notation is followed in this section.

The quantum efficiency of radiative recombination has been calculated by Hwang[17] for highly doped materials, and is seen to peak at dopant densities of $2x10^{18}$ cm^{-3}, where the internal quantum efficiency measures 40%. However, it falls rapidly for lower donor concentrations.

Theoretical calculations of the rate of emission are described in various physics texts and lead to some insight into factors determining the efficiency of radiative recombination.[18] It is a term of particular importance to the field of light-emitting semiconductor devices such as diodes and lasers in which stimulated radiative emission is produced by current injection. The net radiative recombination rate is determined by the probability for a carrier to make a transition from a filled state to an empty state times the

number of filled states, times the number of empty states. From a classical perspective, the rate is calculated by describing the number of filled (or empty) states as being proportional to the number of photons in a material. This in turn is determined by the probability of absorbing a photon per unit time and the density of photons, which can be expressed as functions of the absorption coefficient and the refractive index, to yield the expression for thermal generation which is equal to recombination at equilibrium. Fonash[19] states it as

$$g_{th}^{R} = \frac{8\pi c^2 k^4 T^4}{h^4} \int_0^{\infty} \frac{\alpha(x)[\eta(x)]^2 \, x^3 \, dx}{e^x - 1} \tag{3-18}$$

where $x=h\nu/kT$, c is the speed of light and η is the refractive index.

Using arguments similar to those made in Chapter 2 for bulk recombination, a thermal equilibrium rate is

$$R_{eq} = g_{th}^{R} = Bn_0p_0.$$

Therefore,

$$B = g_{th}^{R}/ n_0p_0 = g_{th}^{R}/ n_i^2,$$

where B is described as the probability for recombination,[20] and has been completely expanded in the terms of eq. 3-18 and expressions for n_i^2 as functions of the intrinsic properties of the semiconductor have been written out by Hall and Varshni.[20a ,21] Quantum mechanical calculations of the transition matrix elements and densities of states have also been made. Stern[22] has performed semiempirical calculations, and for GaAs he reports $B \approx 2\times10^{-10}$ cm^3/sec. The strong temperature dependence is noted in his Figure 6, where it is seen that B increases by a factor of 5 upon changing the temperature from 297 K to 77 K. Specifically for calculations of GaAs lasers, a value of $B = 9.5\times10^{-11}$ cm^3/sec was calculated for undoped GaAs.[23]

For multiple quantum wells grown using molecular beam epitaxy (MBE) long decay times of 45 ns were observed at high excitation, and this led to determinations that

the value of B was on the order of $2x10^{-11}$ cm^3/sec.[24] Work on lightly doped thin GaAs layers in GaAs-$Al_xGa_{1-x}As$ double heterostructures, similar to those used in this work were reported to have $B=1.4x10^{-9}$ cm^3/sec.[16]

Nelson and Sobers[25] have experimentally determined B over a wide range of p-doping (germanium doped) for LPE-grown GaAs samples and find close agreement with Sterns theory. Their experimentally determined value for a dopant density of $p_0=2x10^{15}$ cm^{-3} is $B=3.7x10^{-10}$ cm^3/sec. For unintentionally doped GaAs heterostructure lasers, 't Hooft determined B to be $1.3x10^{-10}$ cm^3/sec.[26]

The work of Stern[22] is cited by several authors,[27] and Stern's value of $B=2x10^{-10}$ cm^3/sec was used in this work.

Affects of photon reabsorption may also affect the measured external efficiency. They are considered by Hwang,[17] but inclusion of reabsorption of the bandgap emission had no effect on the calculated decays in this thesis.

6. Computer Software

The program itself is run using the minimization function based on the Simplex algorithm in the MATLAB software package (The MathWorks, Inc., Natick MA). The minimization is with respect to the sum of the differences between point in the simulated and experimental decays on a linear scale. Hence, it effectively weights earlier times, where the magnitude of the difference is larger due to the fact that the absolute value of the points are larger. The C version used in the fitting procedure was compiled on an IBM 6000/520. The original program for these calculations was nllum12.bas, written by N.S. Lewis. The C Version of the algorithm and the MATLAB macros along with nllum12.bas are presented in the appendix to the thesis.

---

[1] Vaitkus, J. *Phys. Status Solidi A* **1976**, 34, 769.

[2] P. Agmon, Ph. D. Thesis, California Institute of Technology, 1979.

[3] Evenor , M.; Gottesfeld, S.; Harzion, Z.; Huppert, D. *J. Phys. Chem.* **1984**, *88*, 6213.

[4] Luke, K. L.; Cheng, L. -J. *J. Appl. Phys.* **1987**, *61*, 2282.

[5] (a) Feldberg, S. W. *Electroanal. Chem.* **1969**, *3*, 199. (b) A concise summary of the method is given in Bard, A. J.; Faulkner, L. R. *Electrochemical Methods*; John Wiley & Sons: New York; 1980. Appendix B.

[6] While not exhaustive, two texts of relevance which provide numerous references are (a) Carroll, J. E. *Rate Equations in Semiconductor Electronics;* Cambridge University Press: Cambridge, 1985 (b) Snowden, C. M. *Introduction to Semiconductor Device Modelling*; World Scientific Publishing Co.: Singapore, 1986.

[7] Complete computer program code has been published by Stanford university for at least two programs: (a)Pinto, M. R.; Rafferty, C. S.; Dutton, R. W. *PISCES II: Poisson and Continuity Equation Solver*; Stanford Univeristy, Stanford, CA 94305; 1984. (b) D'Avanzo, D. C.; Vanzi, M.; Dutton, R. W.; *One-Dimensional Semiconductor Device Analysis (SEDAN)*; Technical Report No. G-201-5; Stanford University, Stanford, CA 94305; 1979.

[8] Feldberg, S. W. in A. J. Bard (Ed.), *Electroanalytical Chemistry*, Vol. 3; Marcel Dekker: New York, 1969: p 199.

[9] Joslin, R.; Pletcher, D. *J. Electroanal. Chem.* **1974**, *49*, 171.

[10] O'Connor, D. V.; Phillips, D. *Time-correlated Single Photon Counting*; Academic Press: London; 1984: Chpt. 2.

[11] Pierret, R. F. *Advanced Semiconductor Fundamentals*, Vol VI in the Modular Series on Solid State Devices, Pierret, R. F.; Neudeck, G. W. Eds. Addison-Wesley: Reading, Massachusetts, 1987.

[12] Sze, S. M. *Physics of Semiconductor Devices*; Wiley-Interscience: New York, 1981.

[13] Moss, T. S. *Optical Properties of Semiconductors*; Butterworths: London; 1961: p 61.

[14] Feldberg, S. W.; Evenor, M.; Huppert, D.; Gottesfeld, S.; *J. Electroanal. Chem.* **1985**, *185*, 209.

[15] Aspnes, D. E.; Kelson, S. M.; Logan, R. A.; Bhat, R. *J. Appl. Phys.* **1986**, *60*, 754.

[16] Sell, D. D.; Casey, H. C., Jr. *J. Appl. Phys.* **1974**, *45*, 800.

[17] Hwang, C. J. *Phys. Rev. B.* **1972**, *6*, 1355.

[18] (a) Pankove, J. I. *Optical Processes in Semiconductors*; Dover Publications, Inc.: New York, 1971: p 108. (b) Casey, Jr., H. C.; Panish, M. B. *Heterostructure Lasers*; Academic Press: New York, 1978: Chpt. 3, (c) Blakemore, J. S. *Semiconductor Statistics*; Dover Publications, Inc.: New York, 1987: Chpt. 5.

[19] Fonash, S. J. *Solar Cell Device Physics*; Academic Press: NewYork, 1981: p 31.

[20] (a) Varshni, Y. P. *Physic. Stat. Sol.* **1967**, *19*, 459. (b) Pankove, J. I. , *op. cit.*, p. 111.

[21] Hall, R. N. *Proc. Inst. Elec. Eng.* **1959**, *B106*, 923.

[22] Stern, F. *J. Appl. Phys.* **1976**, *47*, 5382.

[23] Stern, F. *IEEE J. Quant. Elec.* **1973**, *QE-9*, 290.

[24] Fouquet, J. Ph.D. Thesis, Stanford University, 1986.

[25] Nelson, R. J.; Sobers, R. G. *J. Appl. Phys.* **1978**, *49*, 6103.

[26] 't Hooft, G. W. *Appl. Phys. Lett.* **1981**, *39*, 389.

[27] van Opdorp, C.; 't Hooft, G. W. J. *Appl. Phys.* **1981**, *52*, 3827. (2) Von Lehmen, A.; Ballantyne, J. M. *J. Appl. Phys.* **1985**, 58, 958.

CHAPTER 4

EXPERIMENTAL TECHNIQUE AND SAMPLES

A. Time-Correlated Photon Counting

The experimental technique used to measure the time-resolved photoluminescence decay from semiconductor samples immersed in electrolyte solutions was time-correlated photon counting (TCPC). The theory behind the technique of TCPC is well documented, and the reader is referred to the commonly cited text, *Time-correlated Single Photon Counting*, by D. V. O'Connor and D. Phillips,[1] for further details. The technique was chosen primarily because it satisfied two major criteria. The first requirement was that the technique have subnanosecond time resolution so that it would be sensitive to the very fast electron and hole transfer rates at the semiconductor-electrolyte interface. The second was that the photoexcitation source be sufficiently powerful to introduce $> 10^{17}$ photons cm^{-3} in order that enough excess charge would be introduced to screen the charges in the semiconductor so that there would be no electric field in the interfacial region. Use of a dye laser also permits variation of the excitation wavelength. Finally, the timing electronics used in TCPC are less expensive, more durable and have a greater dynamic range than streak cameras which can record the entire decay curve after one excitation pulse and have comparable time resolution. The main disadvantage of TCPC is the need to excite the sample repeatedly (on the order of 10^{10} times) to collect a single decay curve.

Time-correlated single photon counting requires measuring the time between the excitation pulse and the detection of a single photon emitted by the excited sample. By performing this measurement a statistically significant number of times, one obtains a

histogram of counts versus time, with more counts being recorded at early times in the decay when there is more emission, and fewer counts at later times. Based on arguments using Poisson statistics which are applicable to the independent events being recorded, the histogram can be shown to accurately represent the true decay of the sample. As the counts are recorded, the decay is thus built up until one has counts per unit time as shown in Figure 4-1.

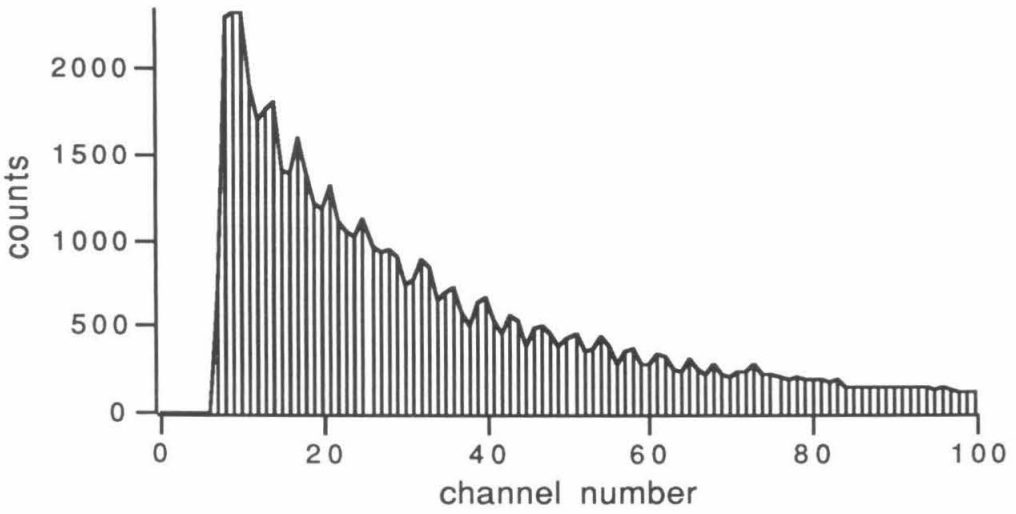

Figure 4-1. Histogram display of counts recorded per channel in the multichannel analyzer. Solid curve overlaid along the top of the histogram is taken to be luminescence decay curve.

There are two experimentally relevant consequences of the statistics governing the method. First, it is generally recommended that to obtain a precision of 5% one acquire 40,000 counts in the channel of maximum counts. Second, because the electronics detect only the first photon in a given time interval for a given excitation cycle, it is necessary to make sure that the number of photons being detected is small enough that they can be shown to come from early and late times in the decay in correct proportion to their true distribution. Mathematically it can be shown that this condition will be met if the number

of detections is kept at 5% or less of the excitations. It is standard practice to keep it at about 1%, which was the nominal choice for the experiments reported in this thesis. The use of a 152 kHz laser repetition rate also ensures that the electronics are easily able to resolve individual signals. By integrating the area under an exponential decay which falls from its maximum to the e^{-2} point over a range of 1000 channels, it can be seen that merely to collect 10,000 counts in the main channel requires almost an hour.

B. Apparatus

1. Laser

Initial experiments performed for this thesis between September 1989 and November 6, 1990 were performed while the laser apparatus was located on the second floor of the Noyes laboratories. After January 1991, the laser was located in the Beckman Institute Laser Resource Center, where improvements in the instrument calibration were made. The differences are apparent in comparison of data recorded for the same experiment before and after the move.

The time correlated photon counting apparatus used in these experiments is drawn in Figures 4-2(a) and (b). It consisted of a Coherent Model 76-S Antares Nd:YAG laser, equipped with a Model 7600 Mode Locker. The infrared output at 1.06 microns was nominally 100 ps FWHM and the CW power was 22 W. The IR was passed through a Model 7900 second harmonic generation (SHG) assembly consisting of a KTP crystal in which type II phase matching occured to double the frequency of the laser. The output 532 nm pulses were nominally 70 ps in width and the CW power was about 1.5 W. The p-polarized light pumped a Model 701 Dye Laser equipped with a Model 7200 Cavity Dumper and Model 7200-38 Cavity Dumper Driver. The dye used in the dye laser was DCM manufactured by Kodak. The wavelength was measured by optimizing the throughput of a 0.22 meter monochromator (SPEX Minimate, Edison, NJ).

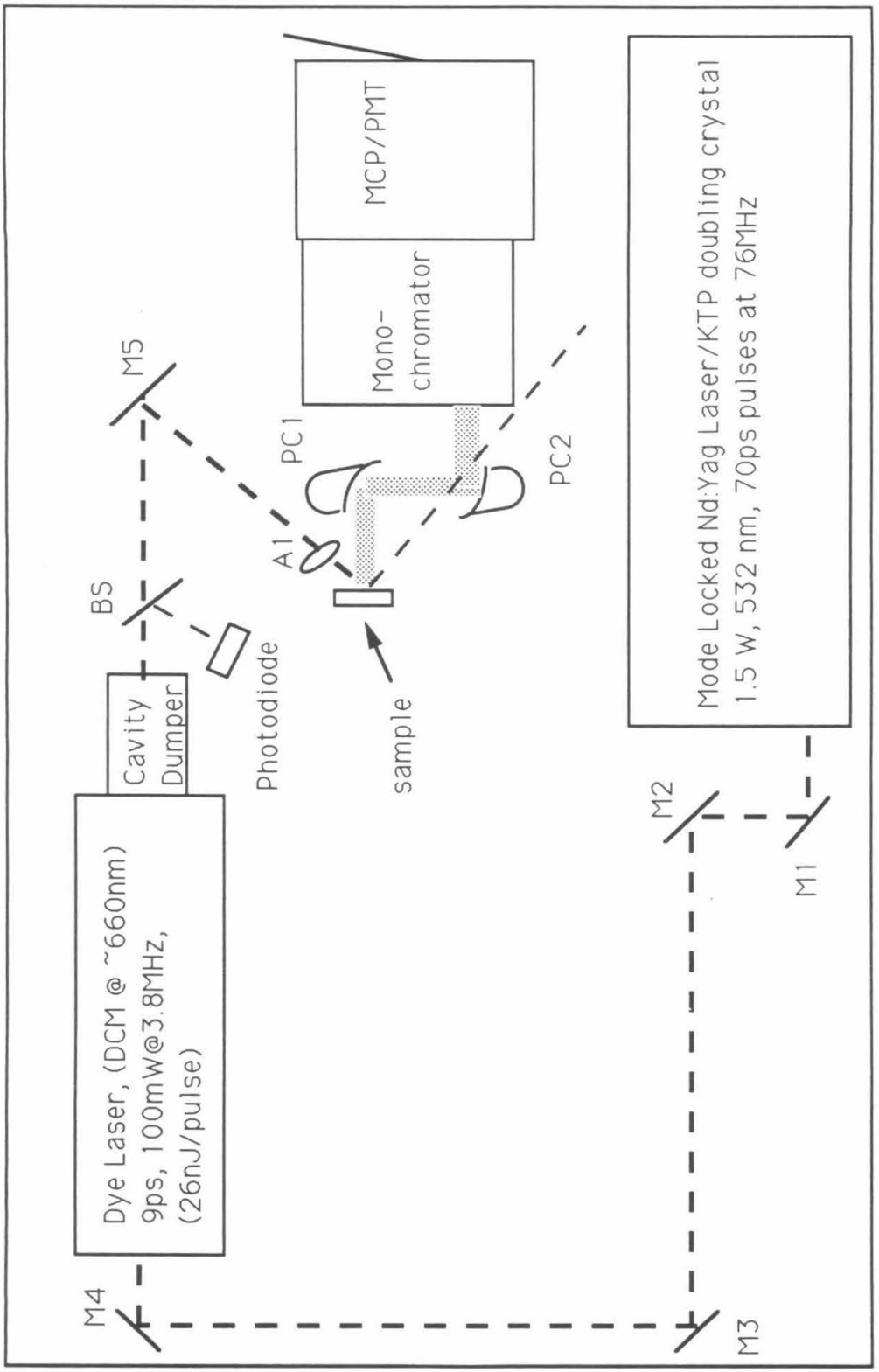

Figure 4-2(a). Laser Table Setup. M1 - M5: Broadband dielectric coated mirrors; BS: Beam splitter; PC1, PC2 Parabaloidal mirrors; A1: Focussing lens; ▒▒ GaAs emission — — laser beam

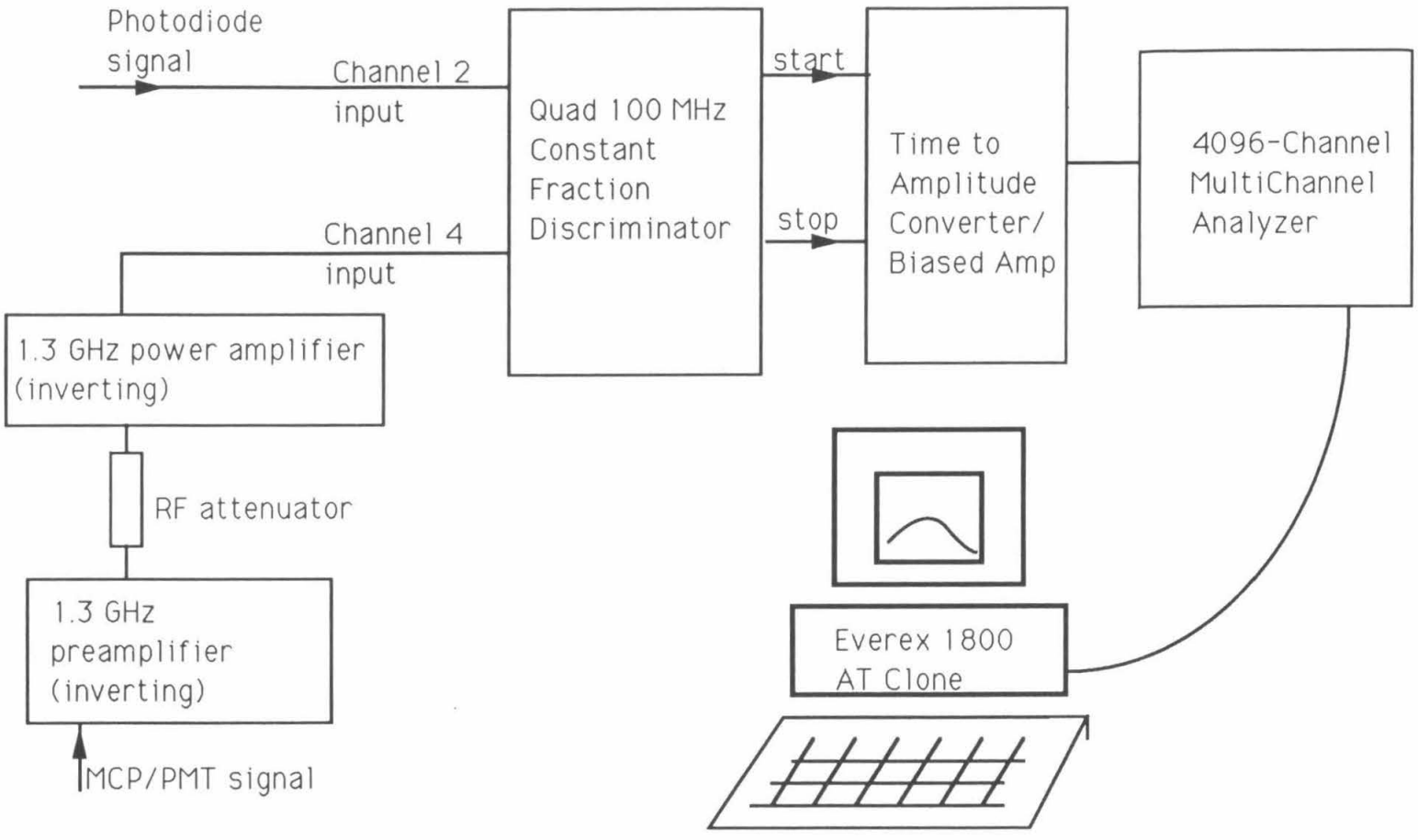

Figure 4-2(b). Time-correlated photon counting electronics

The pulse width and power of the output dye laser pulses were extremely sensitive to cavity-dumping conditions. The procedure for maximizing power for these experiments was as follows. First, if two diffraction spots were output from the dye laser, the Bragg crystal in the cavity dumper was tuned until one peak of maximum intensity was obtained. As stated in the cavity dumper manual, there is no systematic procedure for this; rather, it was a matter of trial and error. Once a single well defined spot was obtained, power was optimized using all dye laser controls and monitoring power on the Coherent Labmaster LM-10 power meter. For this optimization, the cavity dumper was set to divide down the mode-locker frequency by 10 to yield pulses at 3.8 MHz. Powers on the order of 100 mW were readily measured, and a calculation of the power per pulse was made by dividing the power by 3.8 $x10^6$ pulses per second. No autocorrelation measurement was made of the dye laser pulses, but variations in pulse width were detectable in the system response measurements.

For TCPC experiments, the cavity dumper was run on the divide-by-250 setting resulting in a repetition rate of 152 kHz. Since the power meter was unable to accurately measure power at the low repetition rate, it was assumed that the powers measured at the higher repetition rate held. Unfortunately, it appears that the pulse power and shape did not remain exactly constant as the repetition rate was changed to permit 500 round trips instead of 20, even though the laser gain saturates at about 10 cavity round trips. The process by which the cavity dumper selects and outputs optical pulses from the dye laser cavity is based on the Bragg diffraction of the optical pulse off of a traveling acoustic wave in a quartz slab in the dye laser cavity. The electronics which control the acoustic wave did not appear to produce the same diffraction characteristics at all repetition rates. Adjustments of the phase controls on these electronics after changing the pulse selection rate often increased the brightness of the emitted spots, from which it can be inferred that the optimization performed at the divide-by-10 setting was not perfectly transferrable to the

divide-by-250 setting. For this reason, power measurements were assumed to have an uncertainty of a factor of two.

2. Optical Path

The remainder of the optical path is as follows. About 5% of the dye laser pulse was split off using an achromatic beam sampler (Model 10B20NC.1, Newport Corporation, Fountain Valley, CA) into an ultrafast photodiode (EG&G Electrooptics, Salem, MA, Model No. FND-100). The percentage of light reflected by the achromat is dependent on the angle of incidence; therefore, it is important to maintain it in a fixed position, so that both the power transmitted and the power reflected onto the photodiode remain constant. In early work in this lab, the photodiode was packaged in the same manner used by many other groups, such as that of A. Zewail at Caltech and that of M. Fayer at Stanford, and reported in the literature.[2]

Construction of the mount for these plates when used as a source of positive pulses was as follows. Two plates of aluminum were used to encase the photodiode. The front plate was drilled out just large enough to allow a press fit of the photodiode can into it (21/64" for the FND-100). The back plate was drilled for a BNC connector (thread for BNC bulkhead receptacle is 3/8-32), and plates were held apart by Mylar sheet. Nylon screws were used to bolt the two plates around the photodiode, and a Plexiglass rod was mounted on the plate edge as a handle. A 90 V Eveready Radio "B" battery was used to reverse bias the diode, and the anode lead was soldered to the BNC pin. The cathode and the common leads were soldered to each other, and held at the +90 V applied to the front plate of the holder.

After the microchannel plate (MCP) was installed, the photodiode was used in the reverse configuration, because it was possible to use the negative pulse directly from the cathode of the photodiode, making a GHz-bandwidth inverting amplifier unnecessary. For the FND-100, this required that signal was taken from the cathode pin (pin 2) and the

anode and case pins were not soldered together, because the photodiode case was left floating with no applied voltage. The +90 V side of the battery was tied to the BNC case, so that ground was effectively floated at +90 V, and a 50 nF capacitor and a 10^4 ohm resistor were connected from the +90 V lead to the anode. It was found that such a configuration shortened the lifetime of the diodes relative to that in which the anode was biased at +90 V.

The remainder of the laser pulse was directed at the sample using broad-band Pyrex mirrors with MaxBrite coatings (Melles Griot). The cell geometry and incident light beams are discussed below.

3. Light Intensity

In order to maximize the incident photon density, the sample was placed as close to the focal point of a lens as possible. Initially, a 100 mm focal length (f.l.) lens was used, but most of the data reported in this thesis were taken using a 25.4 mm f. l. diffraction limited achromatic lens (Newport PAC022). Both the sample and the lens were mounted on x-y-z translation stages, and at the beginning of the experiments they were adjusted to maximize the signal. The diffraction limited spot diameter can be calculated as[3]

$$D=2.44\ \lambda\ f/d$$

where f is the lens focal length, λ is the wavelength of light, and d is the laser beam diameter. Thus at 670 nm, assuming the diameter of the laser beam to be 1.3 mm, which is specified by the laser manufacturer, the diameter of the point at the focus of the 25.4 mm lens is

$$D=2.44 * 670\times10^{-6}\ \text{mm} * 25.4\ \text{mm}/1.3\ \text{mm}=31.9\ \mu\text{m}. \qquad (4\text{-}1)$$

(It is 126 μm for the 100 mm focal length lens.) At short focal lengths one must consider the effects of spherical aberration, which vary as a function of beam diameter. Assuming that the beam diameter was 1.3 mm, the spherical aberration and diffraction limited focal spot diameters were calculated and are displayed in Figure 4-3.

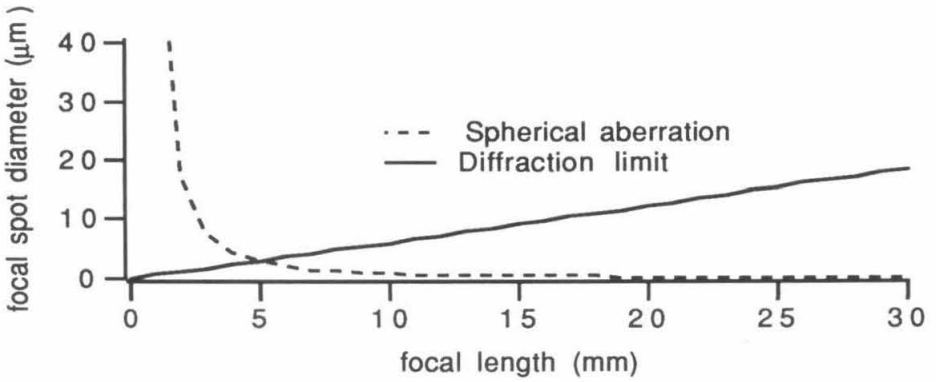

Figure 4-3. Effects of diffraction and third-order spherical aberration from a singlet lens on a 1.3 mm beam at 670 nm.

It might be possible to tighten the focus by decreasing the f-number (focal length/beam diameter) by increasing the beam diameter, but this would also increase the third-order spherical aberration.

Finally, the approximately 45° angle of incidence of the beam onto the sample resulted in an elliptical spot, which is estimated from simple geometry to have a major axis diameter of D' = 32 μm/sin 45 = 45 μm. The area of the ellipse was thus

$$A = \pi * \frac{1}{2}(32\text{x}10^{-4}\text{cm}) * \frac{1}{2}(45\text{x}10^{-4}\text{ cm}) = 1.1\text{x}10^{-5}\text{ cm}^2 . \quad (4\text{-}2)$$

($18\text{x}10^{-5}$ cm^2 for the 100 mm focal length lens.) Thus, for a typical laser power of 100 mW measured at a laser repetition rate of 3.8 MHz (the cavity dumper set to divide the mode-locker frequency by 10), the incident photon flux can be calculated.

The energy per pulse is

$$\frac{100\text{mW}}{3.8\text{x}106\text{ pulses/sec}} = \frac{0.10\text{J/s}}{3.8\text{x}106\text{ pulses/sec}} = 26.3\text{ nJ/pulse.} \quad (4\text{-}3)$$

The energy per photon at 670 nm is

$$E = h\nu = hc/\lambda = \frac{6.654\text{x}10^{-34}\text{ Js} \cdot 3.0\text{x}10^{8}\text{m/s}}{670\text{ x }10^{-9}\text{m}} = 3.0\text{x}10^{-19}\text{ J/photon.} \quad (4\text{-}4)$$

The number of photons per pulse is thus,

$$\frac{26.3 \times 10^{-9} \text{ J/pulse}}{3.0\text{x}10^{-19} \text{ J/photon}} = 8.8\text{x}10^{10} \text{ photons/pulse.} \quad (4\text{-}5)$$

Reflectivity measurements in the literature suggest that about 35% of the power is reflected.[4] Additionally, the laser was reflected twice from high quality MAXBrite coated mirrors, and passed through a glass cuvette before reaching the sample, all of which caused additional losses. The net number of photons hitting the sample is probably on the order of one half of the above number, i.e., $4.4\text{x}10^{10}$ photons/pulse. The photon flux is obtained by dividing this number by the area of illumination,

$$\text{Incident flux} = \frac{4.4\text{x}10^{10} \text{ photons/pulse}}{1.1\text{x}10^{-5} \text{ cm}^2} = 4.0\text{x}10^{15} \text{ photons/cm}^2. \quad (4\text{-}6)$$

($2.4\text{x}10^{14}$ photons/cm^2 for the 100 mm focal length lens). The absorption depth at 670 nm is about 0.3 μm, meaning that nearly 100% of the photons are absorbed in the 1 μm thick samples, so that the average density of carriers created (where one electron and one hole are created per photon) is expected to be on the order of $4\text{x}10^{19}$ cm^{-3}. Modelling results discussed later indicate that, in practice, incident fluxes of only 7.5×10^{13} photons/cm^2 are actually achieved. Moreover, decays measured using the 25.4 mm f.l. lens were not significantly different from those measured with the 100 mm f.l. lens, suggesting that a focal spot of roughly equal sizes was achieved with both lenses.

4. Collection Optics

Emission from the gallium arsenide samples was collected using a pair of off-axis paraboloidal concave mirrors (Janos Technology, Part No. A8037-205), the first of which collected the light at approximately f/4, and collimated it, and the second of which focussed it onto the slit of a 0.35 meter monochromator (McPherson, Model 270). Entrance and exit slit widths were set at 0.75 mm. Stray light was rejected using two long-pass cutoff filters (Hoya Optics, Fremont, CA) at 740 and 810 nm.

The monochromator was set to pass the wavelength at which the greatest number of counts from emitted light was measured, usually 874 nm. In the initial experiments before January 1990, the output of the monochromator was aligned with the input of a photomultiplier housing holding a Hamamatsu Model R928HA Photomultiplier which was biased at -1600 V. The current output of the photomultiplier tube (PMT) was fed directly into the discriminator in the set of timing electronics. For experiments performed after March 1990, the monochromator was bolted directly to the front of a liquid nitrogen cooled microchannel plate housing (Products for Research Liquid Nitrogen Refrigerated Housing Model TE 335) which held the 2-stage proximity-focussed microchannel plate/photomultiplier tube (MCP/PMT) (Hamamatsu, Model R1564U-05).

5. Electronics

The negative current pulse output of the MCP/PMT was fed into the preamplifier input of the DC-1.3 GHz amplifier (Hewlett Packard, Model HP8447F). A 0-1800 MHz RF limiter (Hewlett Packard, Model 11867A) was installed on the front of this amplifier (to prevent recurrence of the unexplained blowout of the amplifier, which may have come from a static shock. It was, however, rigorous practice to ground all cables and hands before touching the amplifier in order to discharge any accumulated static charge). The output of the preamplifer was fed into the input of the second stage power amplifier. In experiments after April 1991, the signal from the first stage of the amplifier was put through a 0-2 GHz attenuator (Kay Elemetrics, Model 839, Pine Brook, NJ) before being input to the second stage in order to prevent the signal from saturating the second stage which was used to reinvert the pulse, not amplify the signal.

Electronically, the timing measurement is made by measuring the difference between a start pulse generated by the photodiode detecting the pulse picked off at the output of the laser and a stop pulse from the MCP/PMT occurring in some finite time interval thereafter. The negative current pulse from the photodiode described above was

fed into the input of the Quad Constant Fraction 100-MHz Discriminator (CFD) (EG&G Ortec, Model 934). On the initial installation, the zero crossing and threshold settings on the CFD were optimized by monitoring the zero-crossing and output pulses on a 500 MHz oscilloscope. The amplitude of the negative current pulse varied with light intensity, but was always sufficient to trigger the CFD. No reoptimization of the discriminator settings was made for the daily power variations of the laser pulses, since the photodiode amplitude was always greater than the set threshold and it was assumed that the constant fraction discrimination could adequately compensate for input pulse height fluctuations. The negative-going output pulse from the amplifiers connected to the MCP/PMT was fed into a second channel of the CFD. In April 1991, the external shaping delay cable for the channel used to detect the MCP/PMT channel was replaced with an internal short between the delay pins. The output pulses from the discriminator were fed into the start and stop inputs of the Time-to-Amplitude Converter (TAC)/Biased Amplifier (Tennelec, Model TC 864), and its output was fed into the input of the MultiChannel Analyzer (MCA) (EG&G Ortec, Model 916 Spectrum Ace-4k) which was installed inside the acquisition computer (Everex, Model 1800B IBM-AT clone). The NIM electronics were mounted in an EG&G Ortec Model 40001A/402D NIM bin and power supply. All of the LEMO connectors used for connections to the NIM electronics were assembled from LEMO plugs and RG 174/U 50Ω coaxial cable. The TAC settings were not varied except to change the timescale, which for most experiments was set to be 50 ns.

The MCA was calibrated by putting a delay box (EG&G Ortec, Model 425A) in-line with the input signal and introducing known delays of 2, 4, 6 and 8 ns to the system response signal. The number of channels between the delays was observed on the MCA display. Thus, it was found that the calibration was 13.58 ps/channel. Previously, a pulse generator (Stanford Research Systems, Model DG535, Four Channel Digital Delay/Pulse Generator) had been used to introduce start and stop pulses to the CFD and it

was found that this method yielded a calibration of 13.75 ps/channel . For all subsequent data analysis, the MCA calibration is taken to be 13.6 ps/channel. It is of note that this number is significantly different from the number anticipated for a 50 ns timescale nominally selected on the TAC spread across the 4096 channels of the MCA (which predicts 12.2 ps/channel). After October 1990, this calibration was checked periodically and found to be invariant. On the 100 ns and 500 ns TAC timescale settings, at which data was also taken, the pulse generator calibration yielded 26.9 ps/channel, and 136 ps/channel respectively. The 2 ns increments of the delay box could not be resolved on the 100 ns and 500 ns timescales, so these numbers are not reported.

6. Microchannel Plate Calibration

As per the manual and accompanying literature,[5] an optimization of the MCP/PMT performance requires that the pulse height distribution be measured. Prior to March 1991, the proper amplifiers neededto observe the pulse height distribution were not available. Therefore, the settings on the timing electronics were optimized by adjusting them and monitoring the system response as a function of applied MCP/PMT bias until the most symmetrical and narrowest system response were obtained, with the weight being toward narrowness. In the spring of 1990 this resulted in setting the MCP voltage at -2850 V. In March 1991, a complete pulse height analysis was done, and a voltage of -3025 V was found to produce a pulse height distribution with the best resolved single photon peak. The schematics of the measurement circuit are shown in Figure 4-4.

The pulse height distribution as a function of voltage applied to the MCP/PMT is shown in Figure 4-5. Although the nature of the tube aging was unknown, the pulse height analysis at -2800 volts suggested that a well resolved single photon peak may not have been obtained at the -2850 V setting used in early experiments.

Since single photon counting is, as its name suggests, very sensitive to low levels of light, it was necessary to filter out most of the radiation emitted from capped GaAs

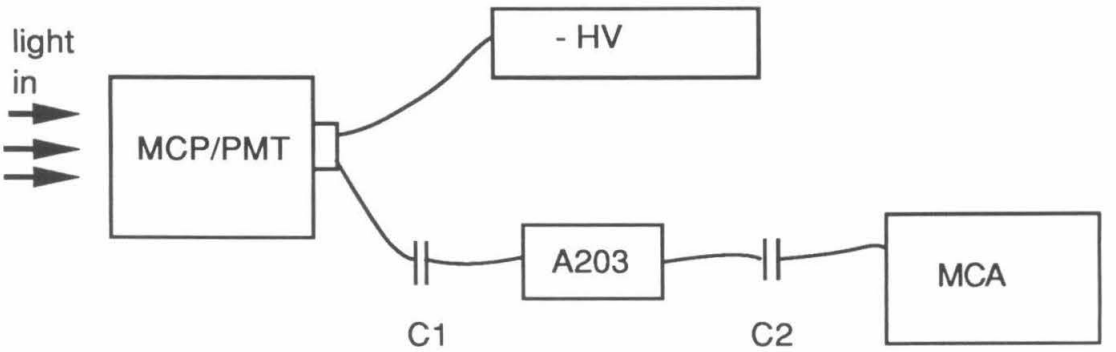

Figure 4-4. Test circuit to measure single photon pulse height distribution. (HV) High voltage supplied by Bertran Model 205A-05R High Voltage Power supply. (A203) Charge Sensitive Preamplifier/Shaping Amplifier Model A203 (Amptek, Bedford, MA) (C1) 0.001 μF capacitor, (C2) 0.01 μF capacitor; the MCP/PMT and MCA are described in the text. The A203 shaping amplifier was adequate to shape and amplify the sub-nanosecond output pulses from the MCP/PMT for detection by the MCA input without further amplification by the A206 voltage amplifier commonly employed in tandem with the A203.

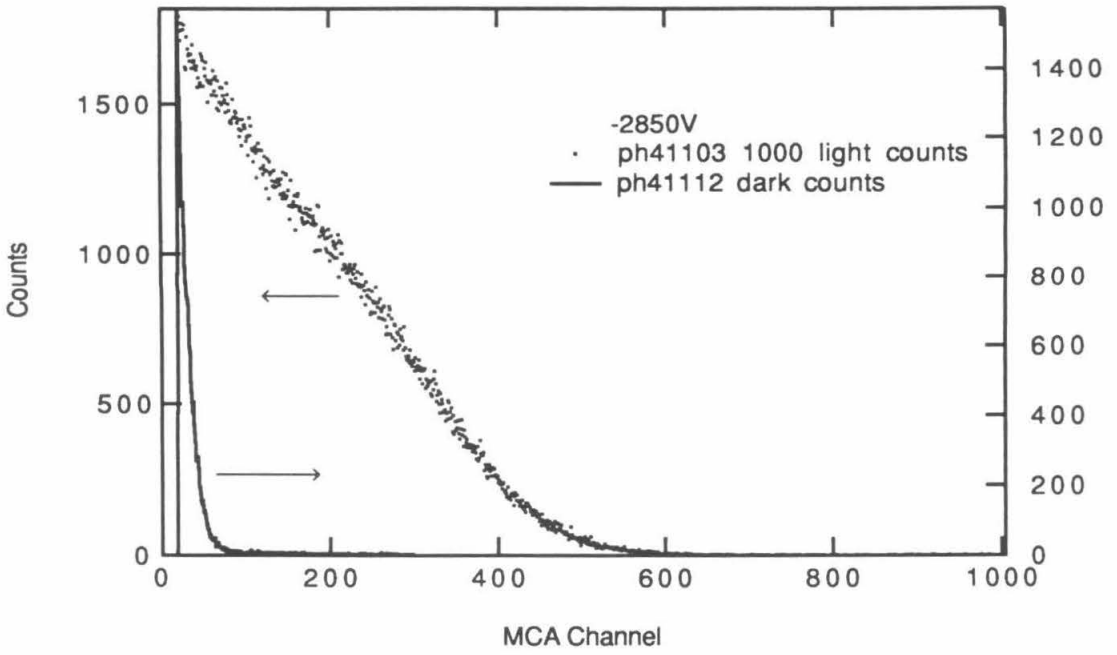

Figure 4-5a. Pulse Height Distribution for MCP/PMT bias of -2850V.

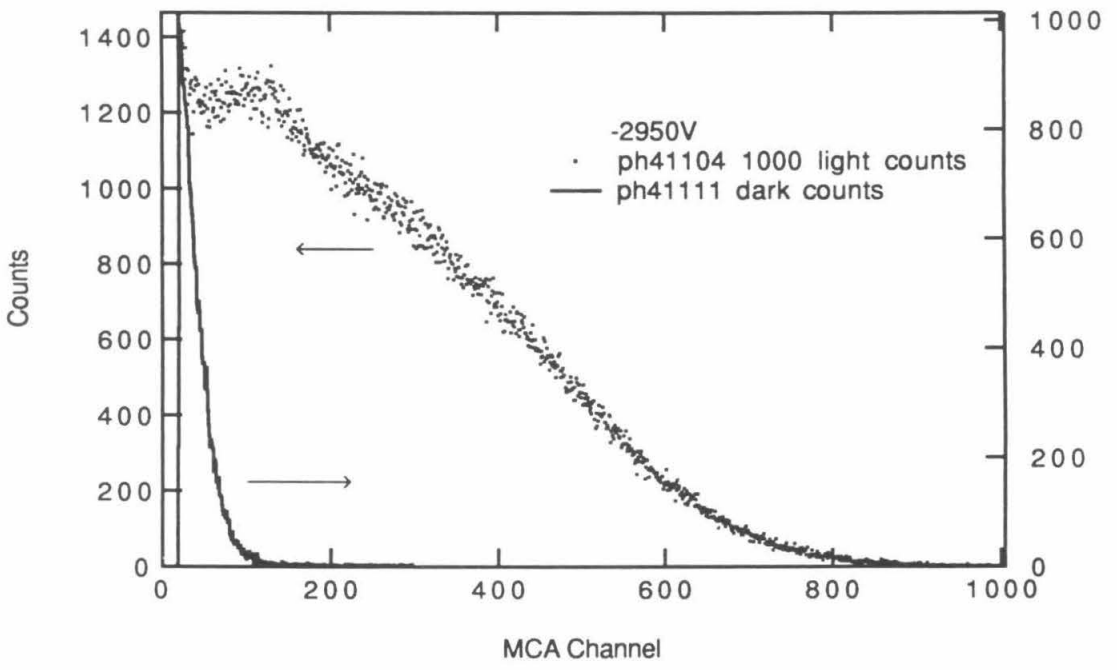

Figure 4-5b. Pulse Height Distribution for MCP/PMT bias of -2950V.

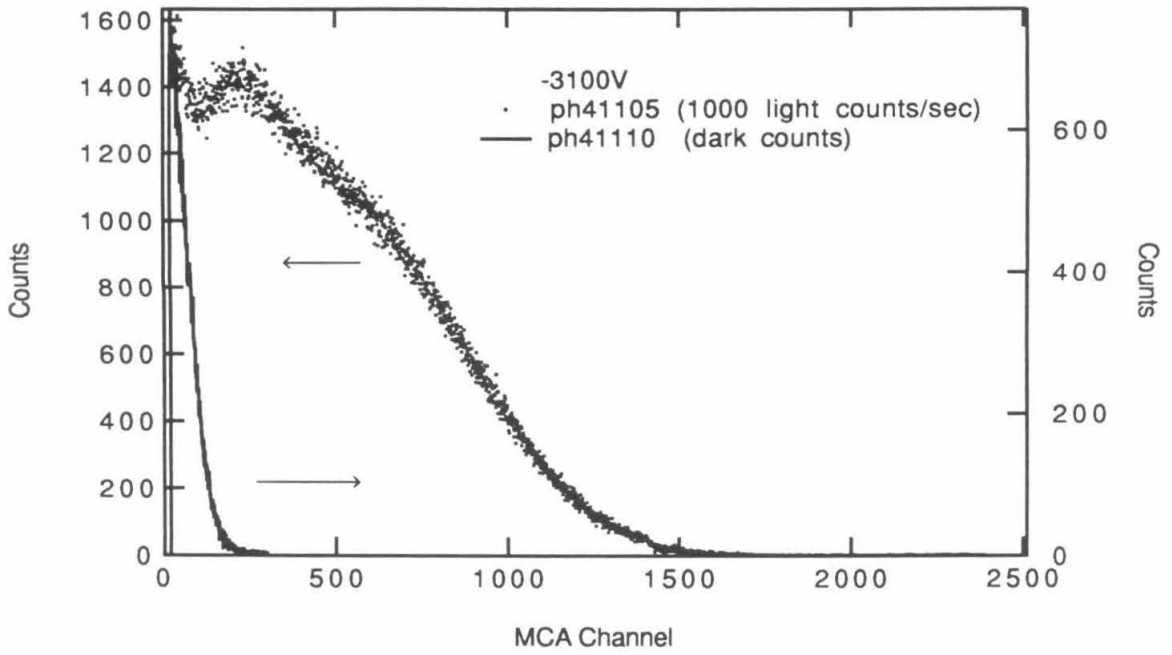

Figure 4-5c. Pulse Height Distribution for MCP/PMT bias of -3100V.

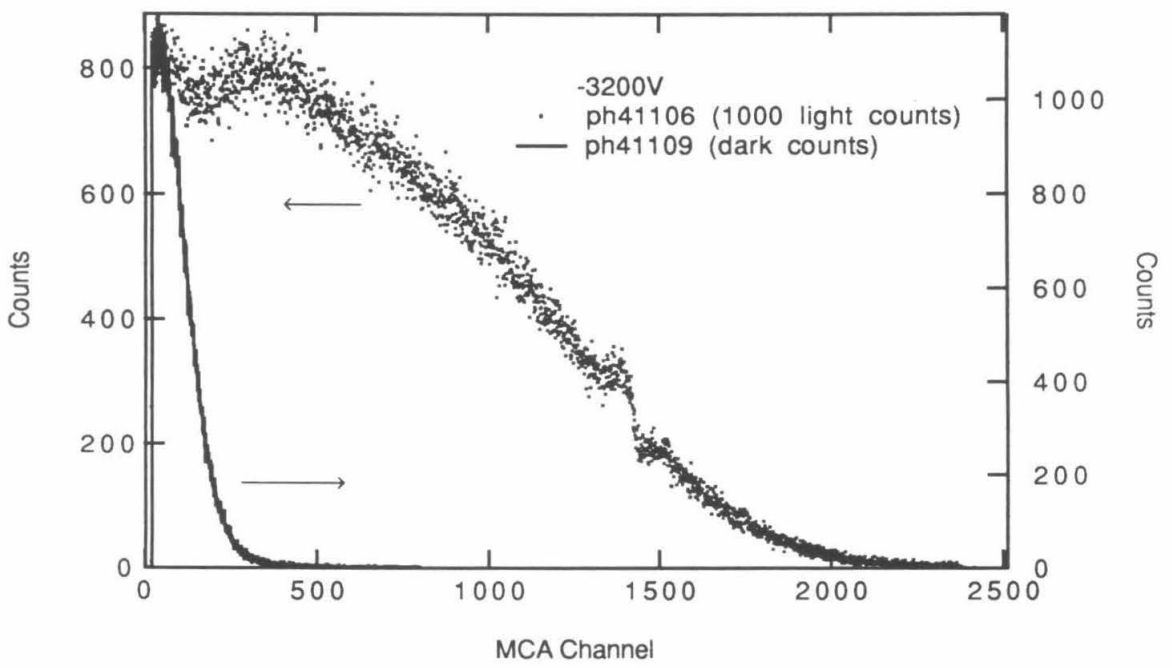

Figure 4-5d. Pulse Height Distribution for MCP/PMT bias of -3200V.

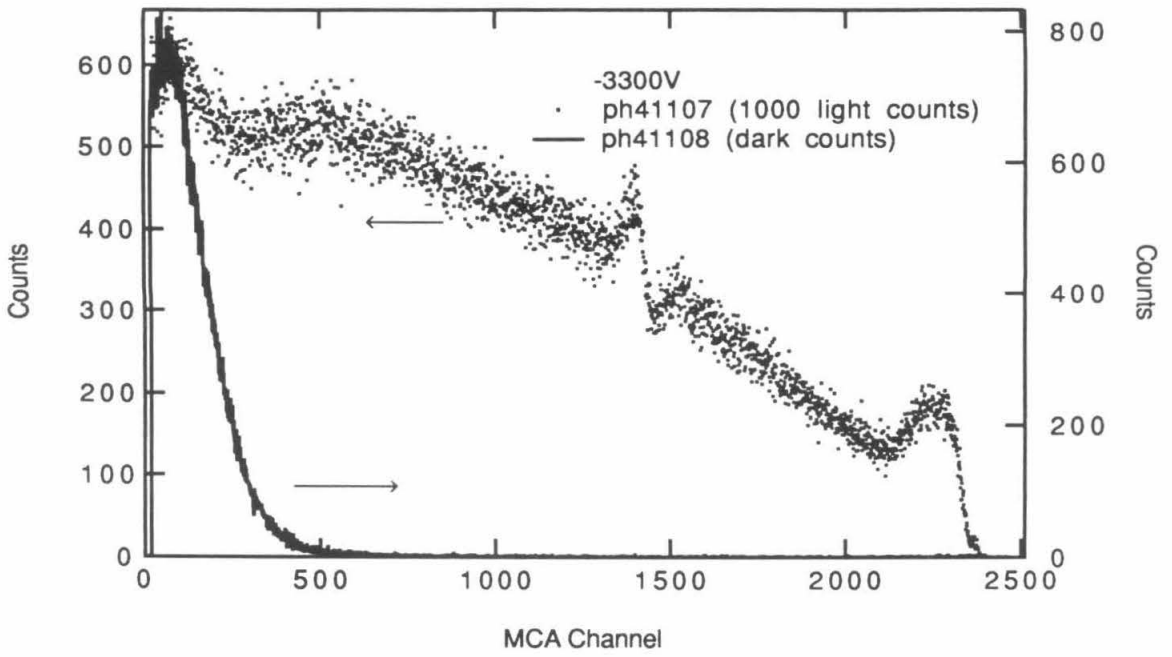

Figure 4-5e. Pulse Height Distribution for MCP/PMT bias of -3300V.

samples in order to remain below the 1000 counts/sec limit on count rate. Typically this required inserting at least two neutral density filters (Hoya Optics, Fremont, CA) which transmitted only 3% of the incident light each when observing the luminescence from unetched GaAs samples, and replacing neutral density filters as required to detect the lower light levels which were generated by etched and metal ion treated samples.

As a final check that the timing electronics were measuring correlated counts, and not scattered room light, a visible LED on the front panel of the TAC was visually monitored.

Prior to and at the end of most sets of experiments, a measure of the system response was made by scattering dye laser light off a piece of white teflon, with the monochromator set to pass the laser wavelength. The system responses taken on two days that are representative of most of the data presented in this thesis are shown in Figure 4-6. Most of the data reported for GaAs in KOH -Se^{2-} - Se_2^{2-} solutions and treated with metal ions were taken with a system response similar to the one in Figure 4-6(a). Most of the data reported for the intensity dependences were taken with a system response similar to the one in Figure 4-6(b).

Finally, two checks of the system were made to see that all things were operational. Firstly, lifetimes similar to those measured in the laboratories of Joe Perry at Jet Propulsion Labs were obtained with the apparatus built at Caltech. Second, lifetimes of ruthenium coordination complexes made by Alan Friedman from the J. Barton lab were measured in June 1990, and found to be within 5% of those obtained in the laboratories of N. Turro at Columbia University.

7. Sample Cell

Figure 4-7 shows a drawing of the cell. A Kontes valve attached to a glass cuvette with an o-ring joint at the top allowed electrodes to be removed from the cell for etching and metal ion treatment while maintaining an inert gas purge over the selenide solution.

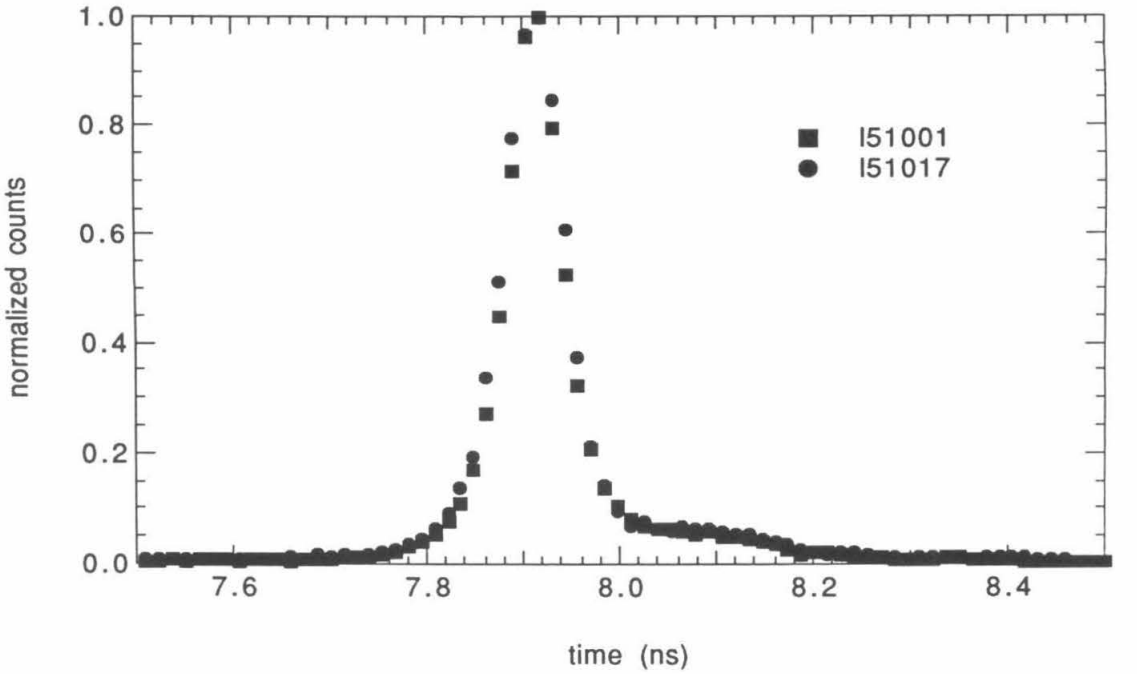

Figure 4-6(a). System responses taken May 10, 1991. The full width at half the maximum height (FWHM) is 68ps.

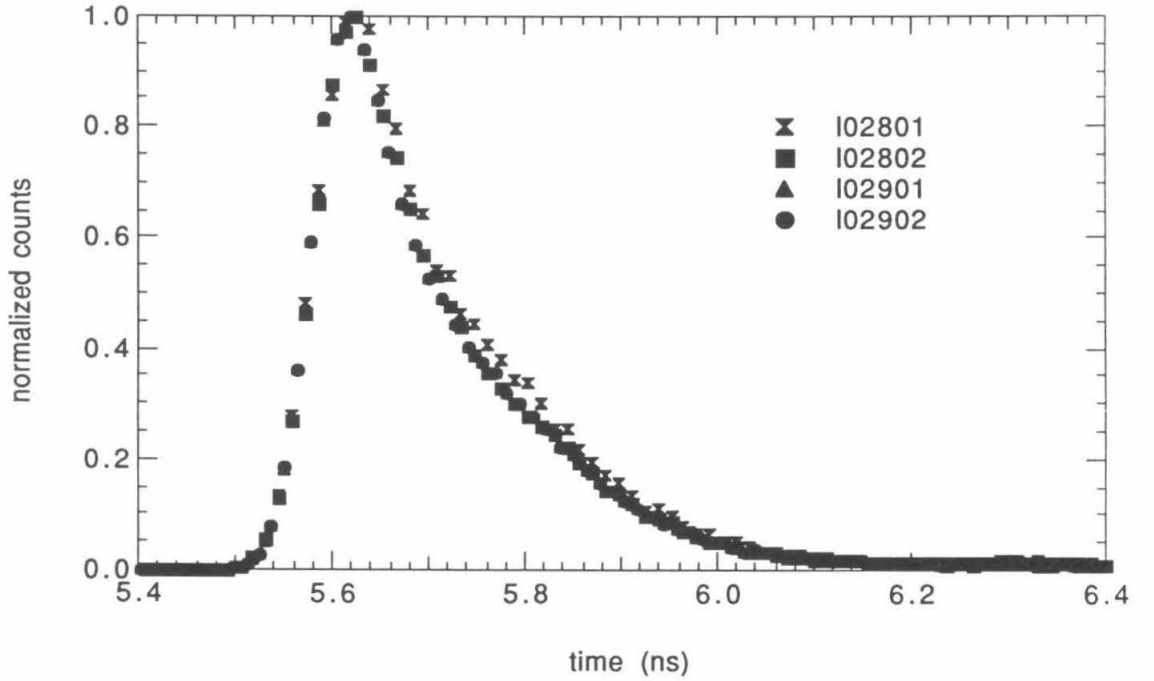

Figure 4-6(b). System responses taken October 28th and October 29th, 1990.

The top half of the o-ring joint terminated in an 8 mm o.d. tube that fit the Lewis Lab standard Teflon holder (Plasma Tech). The 1 cm face of the cuvette generally allowed the incident and reflected laser beam to exit through the front face of the cell if the electrode was positioned in the center of the cell. The sample was placed at the focal point of the collection optics and luminescence was collected normal to the sample surface.

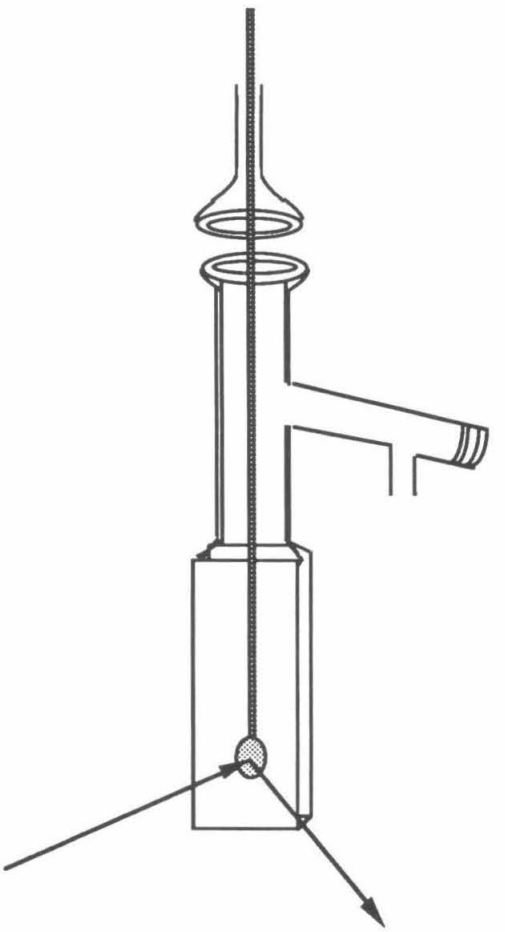

Figure 4-7. Glass cell for photoluminescence experiments on GaAs samples immersed in electrolyte. Arrows represent incident and reflected laser beams.

A visual alignment of the sample was made by observing the scattered light from the surface on the entrance slit to the monochromator. Fine adjustments were made using x-y-z translation stages to position the sample and the focus of the laser beam on the sample while maximizing the number of counts being detected by the MCP/PMT.

C. Chemicals and GaAs samples

1. Metal Ion Solutions

Metal ion solutions were made according to procedures previously reported by Lewis and coworkers.[6] Deionized water (18 MΩ-cm) was obtained from a Barnstead NANOpure water purifier and was used for all etches and metal ion solutions. Aqueous solutions of pH 2.0 were made from HCl (Fischer) and of pH 11 from KOH (Mallinckrodt). pH was determined using an electronic pH meter. Metal complexes were dissolved to make 0.010 **M** solutions of metal ions. Osmium ions were obtained from $K_2[Os(IV)Cl_6]$ (Engelhard), cobalt ions from $Co(NH_3)_6Cl$ (Strem) and ruthenium ions from $RuCl_3 \cdot xH_2O$ (Alfa).

All solvents and acids used for etches were either J.T. Baker MOS grade or Mallinckrodt Transistar stock. For the Aspnes etch, the bromine/methanol solution consisted of 0.05% by volume Br_2 (Mallinckrodt) dissolved in methanol. The KOH solution was 1.0 **M**. Ferrocene was obtained from Aldrich and purified by vacuum sublimation prior to use. Acetonitrile was purified by distillation by other members of the research group and stored over molecular sieves.

2. Selenide Solution

The 1.0 **M** KOH-1.0 **M** K_2Se electrolyte was prepared by adding HCl to solid Al_2Se_3 and bubbling the resulting H_2Se through 3.0 **M** KOH. A complete description of the procedure used in this laboratory and vehement warnings about the danger of H_2Se are presented in the Ph.D. thesis of B. J. Tufts.[7] Both at the time of making the selenide ion

solutions and near the end of the experiments, the molarity of this solution was assayed to be 1.0 **M** by oxidizing a measured amount of solution to selenium metal and weighing the precipitate.

3. GaAs Samples

GaAs was obtained from several sources. The samples used were all of the so-called heterostructure form, in which an epitaxially grown layer (epilayer) of the material of interest (known as active layer in diode lasers) is sandwiched between two thinner epilayers of $Al_xGa_{1-x}As$ which serve to terminate the GaAs surfaces with minimal strain. The three epilayers are grown onto a bulk, conducting or semi-insulating substrate which is about 300 μm thick. The samples for most of the data presented in this thesis were grown by organometallic chemical vapor deposition (OMCVD) by Hugh MacMillan of Varian, Inc.. The wafers consisted of a 300 μm undoped substrate, 1.0 μm epilayer $Al_{.40}Ga_{.60}As$, 1.0 μm GaAs, and 0.10 μm epilayer $Al_{.40}Ga_{.60}As$. Since the active layer was nominally undoped, it is expected that typical impurity concentrations of 10^{15} cm^{-3} comprise the effective dopant density. The sample structure is depicted in Figure 4-8.

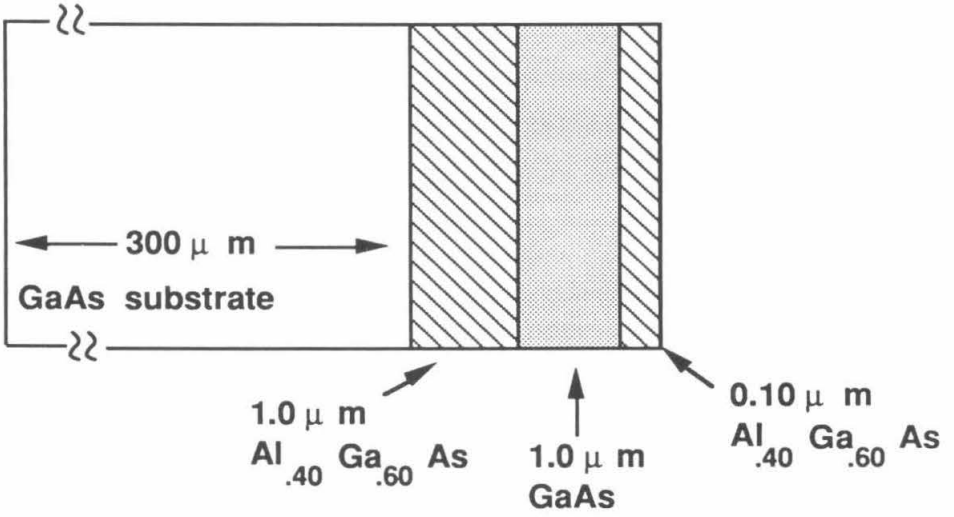

Figure 4-8. AlGaAs capped GaAs heterostructures for photoluminescence. measurements grown by Hugh MacMillan, Varian Laboratories.

Thicker, more highly doped samples were grown by OMCVD in the same reactors by Carol Lewis at Varian Laboratories with both GaAs and AlGaAs active layers. The structure charts for the OMCVD materials are reproduced in Figure 4-9.

A sample was also grown by Lars Eng of the A. Yariv group at Caltech using molecular beam epitaxy (MBE) (Sample #909A). Its structure consisted of a conducting GaAs substrate, 1.0 μm $Al_{.50}Ga_{.50}As$, 1.0 μm GaAs, and a 0.20 μm $Al_{.70}Ga_{.30}As$ cap. It was nominally undoped.

To prepare samples for use in the experiments, the original D-shaped wafers were carefully scribed on their backs with a diamond scribe and cracked into roughly square pieces by rolling a wooden dowel across their front, which was protected by a layer of Kodak high quality optical lens paper. Six-millimeter glass rods were flattened on one end, and the GaAs pieces were attached to the glass using epoxy (Epoxi-Patch, Dexter Corp., Pittsburg, CA) which completely covered the cleaved edges. (Experimental note: The epoxy itself luminesces at the excitation wavelengths used in these experiments, so care must be taken to center the laser beam away from the epoxy. It has a 1/e lifetime of 1.3 ns.)

D. Experimental Procedure

Typical sample preparation was as follows. Time-resolved PL from the GaAs sample was measured just before the sample was etched to enable a measure of the power. Next, three chemical steps were performed. First the AlGaAs cap was etched off using Br_2/CH_3OH. Prior to the last batch of MacMillan samples, the GaAs samples had AlGaAs caps with higher aluminum content, and HF (48% solution, used as purchased, or in a 4:1 ratio of H_20:HF) was found to selectively etch the AlGaAs layer and leave GaAs.[8,9,10] To remove the $Al_{.40}Ga_{.60}As$ cap on the MacMillan samples it was necessary to etch the sample in 0.05% Br_2 in CH_3OH, because the HF etches were not effective on the materials with

'Nate Lewis Heterostruc' (not stored: began as #9 on 'May 89' disc.) OM3-4256
V/III=60, 700C 11May90
Substrate:Sumi 2"rd SI undoped Goodies:coil 39 Mo 2 Run time is 1:04:00.
J.O.#10250-150

FLOW_TABLE

	Chem:	TMAl	TMGa	AsH3	H2Se	Group		Other Sources		
	T/c:	18 C	7 C	100	55/M	III				
	Flux:	.832	5.36	4	.002	Flux	Time	3inj	5Ain	5Bin
1)	*					0	0:10	3	3	6
2)						0	2:00	3	3	6
3)	*			.203		0	3:00	3	3	6
4)		(27)	(19)	.203	(200	0	2:00	3	3	6
5)		(27)	(19)	.203	(20)	0	0:30	3	3	6
6)	*	(24)	(5.)	.203	(5)	0	2:00	3	3	6
7)	*	24	5.59	.203	5	50	4:00	3	3	6
8)	*	(24)	(9.)	.203	(5)	0	1:00	3	3	6
9)			9.5	.203	(5)	51	20:00	3	3	6
10)	*		(5.)	.203	5	0	1:00	3	3	6
11)	*	24	5.59	.203	5	50	4:00	3	3	6
12)	*			.203		0	2:00	3	3	6
13)	L			.203		0	2:00	5	4	7
14)						0	20:00	5	4	7
15)	*					0	0:20	1	1	1

705598-035
D077
GaAs:Φ 77

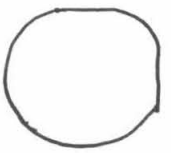

3/4 ⇐

std. 4:1:1 prep

3-C STRUCTURE CHART

step		layer	vapor phase composition	t um	H2	T C	time
11)	*	5:	Al(.4)Ga(.6)As:Se(5) 1.3×10^{17} n	.199	12	700	4:00
10)	*	4:	As:Se(5)	0	12	700	1:00
9)		3:	GaAs ~ 10^{15} n	1.01	12	700	20:00
8)	*	2:	As	0	12	700	1:00
7)	*	1:	Al(.4)Ga(.6)As:Se(5) 1.3×10^{17} n	.199	12	700	4:00

Figure 4-9(a). Structure charts for GaAs heterostructures grown by Hugh MacMillan. Active layers are 1.0 μm thick and nominally undoped.

STRUCTURE CHART

step	layer	vapor phase composition	t um	H2	T C	time
10) *	3:	!Al(.62)Ga(.38)As:Se(200)	0.76	9	780	39:23 / 15
9) *	2:	!Al(.23)Ga(.77)As:Se(1)	9	9	780	176:45
8) *	1:	!Al(.62)Ga(.38)As:Se(200)	2	9	780	39:15

Sample 60M 1063.

STRUCTURE CHART

step	layer	vapor phase composition	t um	H2	T C	time
13)	6:	!Al(.62)Ga(.38)As:Se(200)	1.9	9	780	37:17
12) *	5:	!Al(.62)Ga(.38)As:Se(200)	.102	9	780	2:00
11) *	4:	!GaAs:Se(8)	.122	9	730	2:00
10) *	3:	!GaAs:Se(9)	8.88	9	730	145:08
9)	2:	!Al(.62)Ga(.38)As:Se(200)	.101	9	730	2:00
8) *	1:	!Al(.62)Ga(.38)As:Se(200)	1.9	9	780	37:17

60M 1062

Sample 60M 1062.

Figure 4-9(b). Structure charts showing vapor phase composition, layer thicknesses, and temperature of reactor for GaAs heterostructures, samples 60M 1062 and 60M 1063, grown by Carol Lewis, Varian Laboratories. All layers are doped at 1.0×10^{17} cm^{-3}. Active layers are 9.0 μm thick. For sample 60M 1063, the growth run was aborted under AsH_3 after 15 minutes of step 10, so that only 0.76 μm of capping layer were grown.

40% aluminum. The samples were etched in Br_2/CH_3OH for 4 - 5 minutes, depending on the strength of the solution, which lost significant quantities of bromine during the half hour required to prepare the samples and laser system. It was then etched using the procedure of Aspnes *et al.*[11] which has been determined to leave a clean, abrupt surface and produces a mirror finish (by visual inspection). This procedure will hereafter be referred to as the Aspnes etch; it consists of 4 cycles of exposing the surface in consecutive order to 1.0 **M** KOH for 15 seconds, a water rinse, a stream of nitrogen to dry the surface, 0.05% Br_2/CH_3OH for 15 seconds, a methanol rinse, and a nitrogen dry, with a final 15 seconds in KOH, a water rinse, and a nitrogen drying. During the course of the etching, the time-resolved PL was measured to determine if the lifetime had gotten shorter due to the increase in surface recombination which occurs when the AlGaAs cap is removed. Typically the lifetime and number of photons emitted by the sample remained constant for the first 4 to 4.5 minutes and then dropped rapidly in the next 30 seconds to a new constant value. The photon count rate dropped by over one hundredfold even accounting for the reduced number of filters in front of the monochromator, and the lifetime dropped to the shortest values recorded under any circumstances for these samples. This transition was taken to mark the removal of the $Al_{.40}Ga_{.60}As$ layer as discussed in Chapter 5. At this point, the photoluminescence decay of the GaAs was then measured under argon.

Next, the selenide-KOH solution was injected into the cell. A syringe with a metal needle was purged in the flow of nitrogen from an N_2 cylinder and 1 ml of selenide solution was taken through the septum of the 1.0 **M** $Se^{2-/-}$/KOH solution stored under N_2 and squirted into the cell at the joint between the top and bottom (see Figure 4-6) as it sat in its position. The cell was purged continuously with argon, and then clamped shut when the selenide solution was inside. One or more luminescence decays were then recorded.

Finally, a metal ion treatment was performed. The selenide solution in the cell was kept under argon, while the electrode top was taken to the etching hood and treated with

one of the metal ions. First the electrode was rinsed, blown dry with N_2, and then held in the metal solution for 30 seconds. After treatment it was rinsed with deionized water, blown dry and returned to the selenide cell, and the decay of the final metal ion treated electrode was measured. Because the cell was held fixed, the electrode was returned to very nearly the same position each time it was treated.

In each experiment new etching and metal ion solutions were poured into the plastic cups where the electrode was treated.

---

[1] O'Connor, D. V.; Phillips, D. *Time-correlated Single Photon Counting*, Academic Press: London, 1984.

[2] (a) Bebelar, D. *Rev. Sci. Instrum.* **1979**, *50*, 1629. (b) McCall, G. H. *Rev. Sci. Instrum.* **1972**, *43*, 865. (c) Tom Dunn of the Caltech Chemistry Department Electronics Shop provided specifications for the particular mounts used in these experiments.

[3] CVI Laser Corporation, 1990 CVI Laser Optics Catalog, C VI Laser Corporation, P.O. Box 11308, Albuquerque, NM 87192. p 100.

[4] Blakemore, J. S. *J. Appl. Phys.* **1982**, *53*, R123.

[5] Koyama, K.; Kume, H.; Fatlowitz, D. *Application of MCP-PMTs to Time Correlated Single Photon Counting and Related Procedures*, Technical Information Bulletin, No. ET-03/Oct 1987, Hamamatsu Corporation, Bridgewater, NJ, 1987.

[6] Tufts, B. J.; Abrahams, I. L.; Casagrande, L. G.; Lewis, N. S. *J. Phys. Chem.* **1989**, *93*, 3260.

[7] Tufts, B. J. Ph.D. Thesis, California Institute of Technology, 1991.

[8] Lewis, C. R., Jet Propulsion Laboratories, personal communication, 1988. C. R. Lewis suggested that $Al_xGa_{1-x}As$ would be selectively etched by a 10:1:1 ratio of H_2O:HF:H_2O_2, although such etches are more selective for aluminum fractions greater than 0.6. A second suggested etch is a 5:4:1 ratio of H_2O to H_2NO_3 to HF, in which the AlGaAs is dipped until it bubbles.

[9] (a) Sell, D. D.; Casey, Jr., H. C. *J.Appl. Phys.*, **1974**, *45*, 800.(b) Wu, X. S.; Coldren, L. A.; Merz, J. L. *Electronics Letters*, **1985**, *21*, 558.

[10] van der Ziel, J., Bell Laboratories, personal communication, 1986. J. van der Ziel recommended the following etches when I was etching holes through GaAs: 1. A non-selective fast etch is 1:8:10 H_2SO_4:H_2O_2:H_2O. When the mixture is still hot from reaction

it etches at 5 μm/minute. Cooled to 24 °C it etches at 3 μm/min. 2. A second non-selective fast etch is a mixture of (A) 3 parts methanol and 1 part phosphoric acid and (B) 30% H_2O_2. Four parts of (A) and one part (B) etches GaAs at 2 μm/min. Once the bulk of the GaAs substrate has been removed, a slow, selective etch should be used to etch off the final few microns of GaAs. J. van der Ziel uses a solution of 30% H_2O_2, to which drops of NH_4OH are added to adjust the pH to 7.05-7.1. He reported that this solution etches GaAs at 6 μm/hour,while it etches $Al_{0.2}Ga_{0.8}As$ at 0.6 μm/hour. See also Logan, R. A.; Reinhart, F. K. *J. Appl. Phys.* **1973**, *44*, 4172

[11] Aspnes, D. E.; Studna, A. A. *Appl. Phys. Lett.* **1981**, *39*, 316.

CHAPTER 5

RESULTS AND DISCUSSION

The first section of this chapter presents results obtained from samples that had been capped, etched and immersed in redox solution, in that order. For the capped samples the expected low injection behavior was observed, and it was found that the decays at high injection could be fit with the model in which the decay is predominantly due to bimolecular, radiative recombination. The behavior of etched samples prior to immersion in solution is presented and a comparison of samples etched with HF and samples etched using the Br_2/CH_3OH and KOH solution of the Aspnes process is made. The nature of decays in samples immersed in selenide ion solutions before and after metal ion treatment, and the overall conclusion that metal ions on the surface caused the carriers to be lost faster than they were without metal ions, is detailed. Preliminary results for GaAs in ferrocene/acetonitrile solutions are then presented. Finally, attempts to model the decays and values for a hole capture velocity are discussed. However, primarily due to changes in the surface caused by long term illumination during data collection, an accurate determination of the surface charge-transfer rate constants was not possible.

A. Capped GaAs Samples

As discussed in Chapter 2, there are two limiting cases in considering the recombination kinetics in semiconductors. At low injection, the number of excess majority carriers (electrons for the n-type samples in this work) created by the light pulse is negligible, and relaxation of the excess excited carriers to the equilibrium state is

determined by the minority carriers (holes). It is reasonable to expect that in the low injection regime, once diffusion has flattened the initial carrier profile, the expression derived in Chapter 2 should apply, *i.e.*,

$$s_p = \frac{L}{2\tau_{\text{low injection}}} \quad . \tag{5-1}$$

At high injection, the radiative decay term should dominate. Therefore, as incident light intensity is varied from low to high power, one expects to observe a transition from a limiting single-exponential decay at low injection to a radiatively-controlled decay at high injection.

In the experiments performed on the 1 μm samples, the longest lifetime was observed at an intermediate level of injection, and shorter decays were observed at high injection and very low injection. The results of the experiments in which lifetimes were measured as the incident power was varied with neutral density (ND) filters are summarized in Tables 5-I(a) and(b). The first column on the left contains the time at which the decay had fallen to 1/e of its highest value, which I refer to as the 1/e lifetime. Also in the first column of Table 5-1(b), in parenthesis, is the slope obtained from a linear least squares fit to the natural log of the data between 6.5 and 160 ns. The second column contains the number of ND filters placed in the beam, with their nominal transmissions (*e.g.*, ND25 for a neutral density filter transmitting 25% of the incident light). The third column contains the total transmittance and was calculated by multiplying together the transmission values of all the ND filters in column two. The fourth and fifth columns record the filters used to attenuate the light into the monochromator and the count rate measured by the TCPC system. The sixth column is a measure of the counts reported by the detector multiplied by the values of the attenuation filters in front of the detection and provides a measure of how strong the signal was. The seventh column is the file name and comments relevant to the experiment. Note that the two sets of experiments recorded in

Tables 5-I(a) and (b) are not directly comparable, because changes were made in the experimental configuration between the times they were obtained.

Power measurements made with and without the filters suggest that more laser light was passed by the filters than indicated by their nominal optical transmission values. For example, an ND40 was found to transmit 47% of the incident 660 nm light. Using the available power meter, it was not possible to determine powers accurately below 10 mW; since the output of the laser was about 100 mW, only transmission of the ND40 and ND25 could be checked. For the experiments in Section 2 of Table 5-I(b), the incident intensity was increased by moving the focus of the laser, not by inserting or removing neutral density filters, and the number of counts detected per second is the only measure of comparative intensities. There are several sources of uncertainty in making this comparison. The efficiency with which light is collected varies with the position of the beam on the sample relative to the input of the monochromator. Additionally, there are background counts which must be subtracted from the observed value, although the number is usually constant at approximately 100-200 counts/sec. Finally, the recorded count rate is only an observers rough average of a number appearing on the electronic counter which has a gating time of one second, and fluctuates by at least ±100 counts/sec.

Based on a comparison of counts from the experiments of Table 5-I(a) and Section one of Table 5-I(b), a scaling factor for the intensities of Table 5-I(a) to those in Table 5-I(b) was determined by interleaving the two sets of lifetimes. From a comparison of the counts in the first and second sections of Table 5-I(b) it was also estimated that the 1/e lifetimes for data sets in Section 2 correspond to transmission values of 100%, 150%, 1080% and 1150% in order that comparison could be made between the two sections.

Figures 5-1(a) and (b) summarize the data in this table, by plotting the measured 1/e lifetime vs. the relative incident power as measured by the scale of 10/29/90 along the bottom x axis and by the scale of 10/28/90 along the top axis.

Table 5-I(a). Record of experiments performed 28 November 1990 on 1.0 μm GaAs to measure carrier lifetime as a function of light intensity. Details about the table headings are provided in the text.

1/e lifetime (ns)	ND filters in Beam	% of Full Power Incident on Sample	ND filters in Front of MC	Count Rate (counts•sec^{-1})	Relative Light into MCP/PMT	File (comments)
indeterminate	ND13+13 +25	.42	none	500[a]	500	h1928u04
9.8	ND25+13 +40	1.3	none	400-500	450	h1928u07
15.0	ND13+13	1.7	none	500	500	h1928u05
35	ND25+13	3.25	none	980	980	h1928u06
22.0	none	100	ND03 +03	1200	1.33×10^6	h1928u01
24.6	none	100	same	1300	1.44×10^6	h1928u02
28.5	none	100	same			h1928u03
Beam widened at this point, during realignment.						
34.4	ND13 +25	3.2	none	150[a]	150	h1928u10
83	ND13	13	none	150	150	h1928u08[b]
78.7	ND13	13	none	1200	1200	h1928u09[c]
60.4	ND13	13	ND13	300	2.3×10^3	h1928u14
Laser power at end of experiment was 33 mW.						

a) Signal not well correlated.
b) Beam expanded again.
c) Detector and sample were moved.

Table 5-I(b). Record of experiments performed 29 November 1990 to measure carrier lifetime as a function of light intensity. Details about the table headings are provided in the text.

1/e time lifetime (ns) [linear plot (ln slope)]	ND filters in Beam	% of Full Power Incident on Sample	ND filters in Front of MC	Count Rate (counts·sec^{-1})	Relative Light into MCP/PMT	File (comments)
SECTION 1						
29-34 (44)	ND25+40 +40	4	none	750		h1929u06
25.9 (41)	ND25+40 +40	4	none	500-600		h1929u08
25.9 (43.4)	ND 25+40+40	4	none	550		h1929u11
24 (41)	ND 25+40+50	5	none	500		h1929u07[a]
35 (47)	ND13 +40	5.2	none			h1929u02
34.8 (46)	ND13+40	5.2	none	700-900		h1929u03
45	ND13 +40	5.2	none	900		h1929u01
48.1 (59.3)	ND 40+40+40	6.4	none	1100		h1929u09
46.3 (58)	ND 40+40+40	6.4	none	1100		h1929u10
72 (98)	ND 25+40	10	ND 40	1900[b]	4750[c]	h1929u05
67 (86)	ND25 +40	10	none	2400		h1929u12
82.6 (111.6)	ND40+40	16	ND13	750		h1929u14
74.8 (101)	ND25	25	ND25 (ND40)	1700 (2400)		h1929u13
83.1 (110.4)	ND40	40	ND03	2200		h1929u15
90.0 (112.6)	ND40	40	ND03+40	850		h1929u16
69.15 (92)	none	100	ND03+13	1000	256210 (1)	h1929u17
SECTION 2. Higher flux was achieved by moving sample to obtain tighter focus.						
63 (89)	none	100	ND03+13	1000	256210 (1)	h1929u19[d]
29.1 (52.3)	none	100+	ND03+13	1500	384415 (1.5)	h1929u18

7.95 (13 ns)	none	100+	ND03 +03	2500	2.78×10^6 (10.8)	h1929u20[e]
7.6 (13)	none	100++	ND03 +03	2650	2.94×10^6 (11.5)	h1929u21
11/1/90 New dye, 140 mW, continued study.						
7.16	none	100++	ND03+03 +40	2300	6.39×10^6	h1901u01
7.1	none	100++	ND03+03 +25	700	3.11×10^6	h1901u02
5.87	none	100++	ND03+25 +slits	800		h1901u05[f]
6.75	none			850		h2201u01[g]
6.52				900		h2101u01[g]
6.31				800		h2001u01[g]

a) Oscillations in data interfere with exact determination of lifetime.
b) Count rate was 4200 without the ND40.
c) If 200 background counts are subtracted off the 1900 counts recorded, the value is 4250.
d) Sample was moved away from lens.
e) Laser was adjusted to 85 mW.
f) Laser power measured to be 80 mW.
g) New sample.

Representative curves from the series of experiments are presented in the cycle of Figures 5-2(a)-(d), which, if followed in a clockwise manner up the page on which Figures 5-2(a) and (b) appear and back down the page which Figures 5-2(c) and (d) appear, show the longer lifetime growing in, plateauing in the ND40 range, and then dropping off as high injection is reached. Within this set of experiments, the single exponential lifetimes are measured at an intensity that is just under two orders of magnitude less than that for the highest injection experiments.

1. Low Injection Results

The longest lifetime measured at any time for the 1 μm OMCVD samples was 80-90 ns. One possible explanation for why the lifetime did not plateau as the intensity was lowered is that in spite of the high quality GaAs/AlGaAs interface, some charge is trapped at the interface and creates an electric field which separates the electrons and holes. As the light level is lowered, fewer and fewer excess charges are available to screen the charge, and the electric field increases, resulting in shorter and shorter lifetimes.

If it is assumed that the longest lifetime, 80 ns, corresponds to the filament lifetime of eq. 5-1, the low-injection surface recombination velocity for holes is 625 cm/sec. This is the value used in the model for subsequent calculations on measurements made in the high injection experiments.

Low-injection lifetimes from OMCVD-grown 9 μm thick, GaAs and AlGaAs doped at 10^{17} cm^{-3}, and MBE-grown, nominally undoped 1 μm GaAs were also measured and provide a consistent picture of low-injection behavior, although limiting lifetimes were observed for these materials.

In Figure 5-3(a) and (b), the data for a 9 μm GaAs active layer (sample 60M 1062) for which light intensity was varied by an ND13 and an ND40, respectively, are shown along with linear fits to the regions indicated in parenthesis following the fit information in the graph legends. Using an ND13, the slope of the natural log plot between 100 and 200

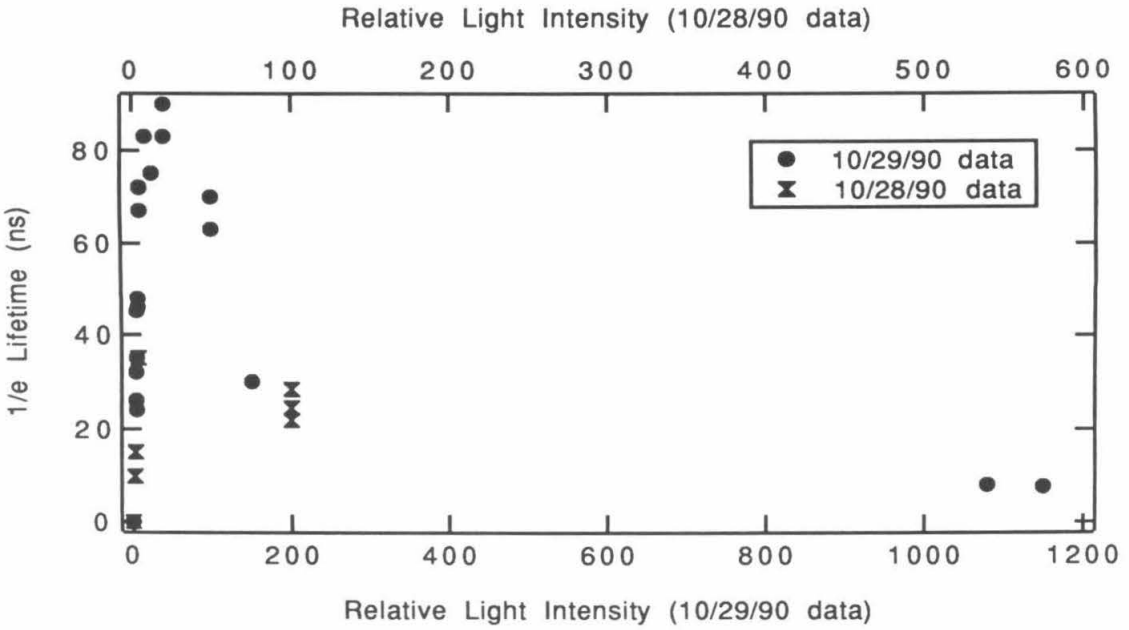

Figure 5-1(a). 1/e lifetime vs. incident light intensity. Data from Table 5-I(a) is plotted against top axis. Data from Table 5-I(b) is plotted against bottom axis.

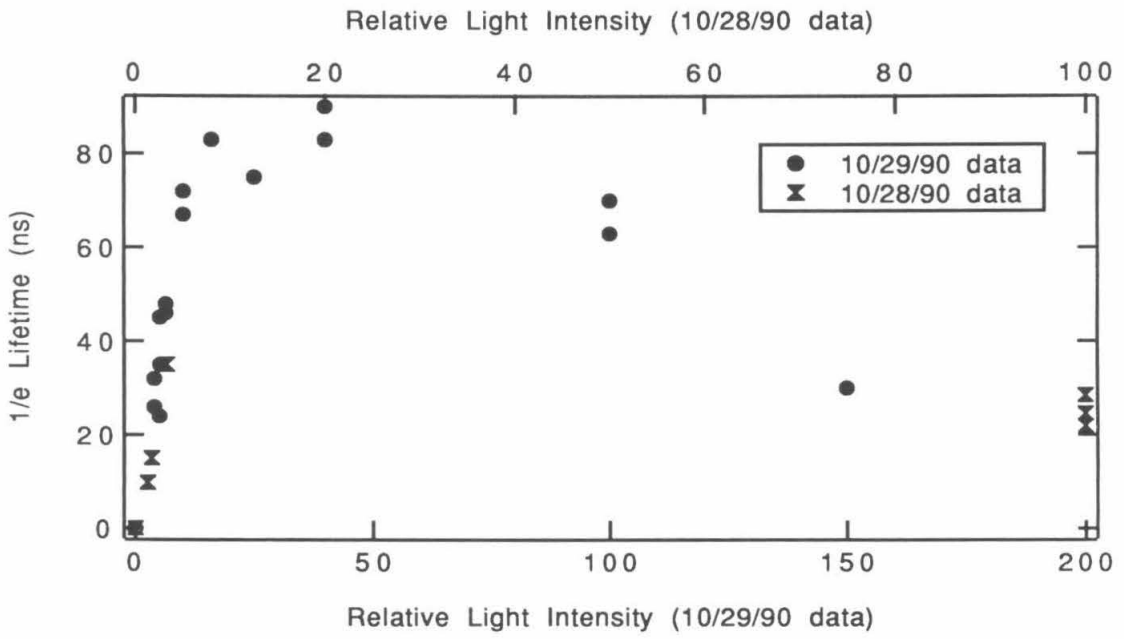

Figure 5-1(b). Expanded view of Figure 5-1(a). Data from Table 5-I(a) is plotted against top axis. Data from Table 5-I(b) is plotted against bottom axis.

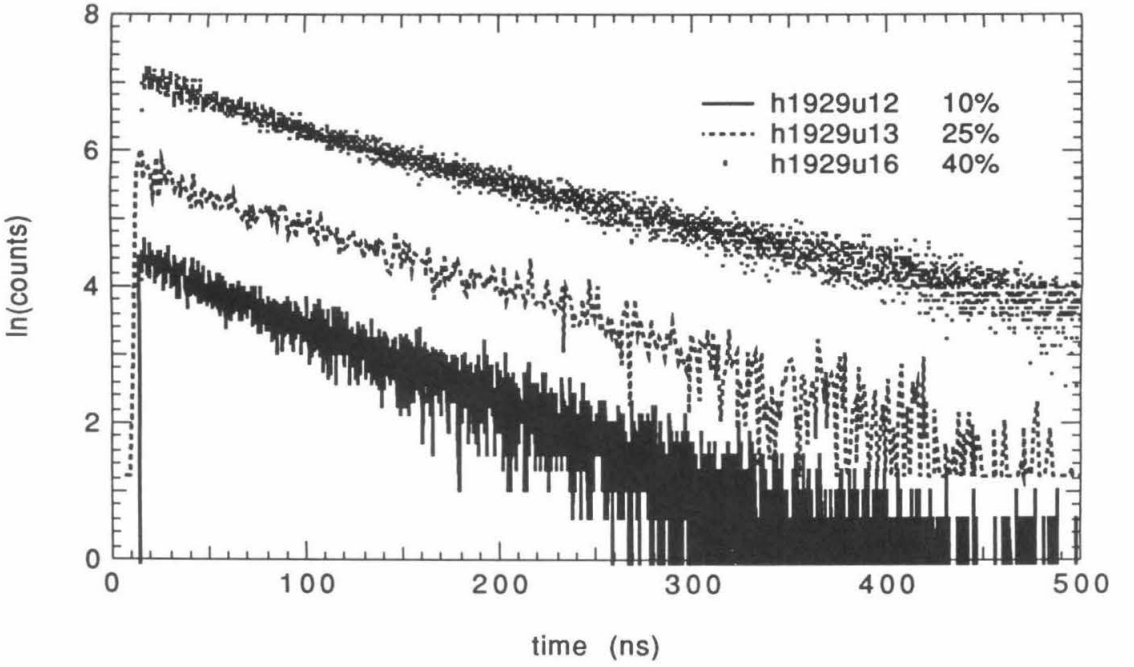

Figure 5-2(b). PL decays as a function of light intensity. Percent of total laser power is designated in legend.

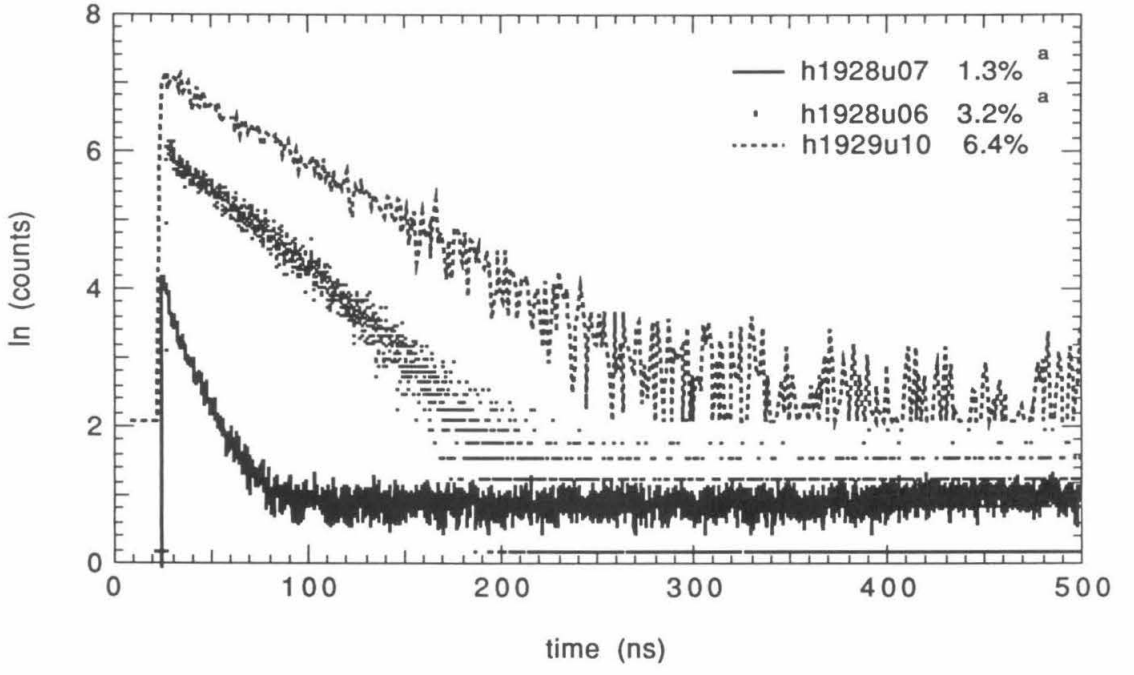

Figure 5-2(a). PL decays as a function of light intensity. Percent of total laser power is designated in legend. [a] % scale for 10/28/90. See text.

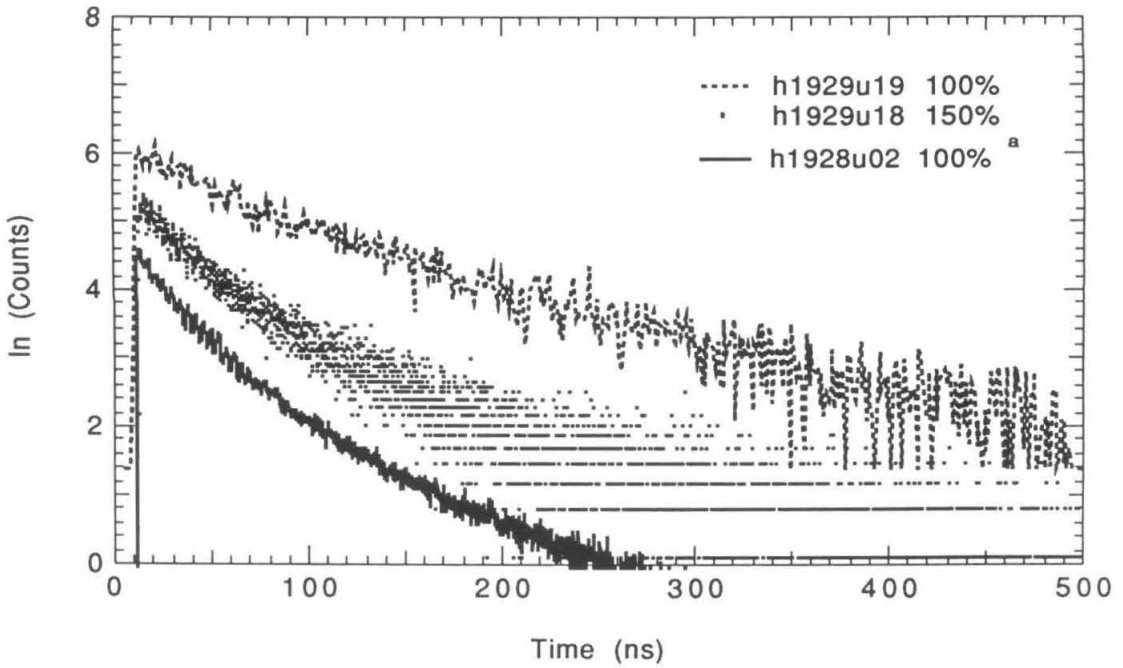

Figure 5-2(c). PL decays as a function of light intensity. Percent of total laser power is designated in legend. [a] % scale for 10/28/90. See text.

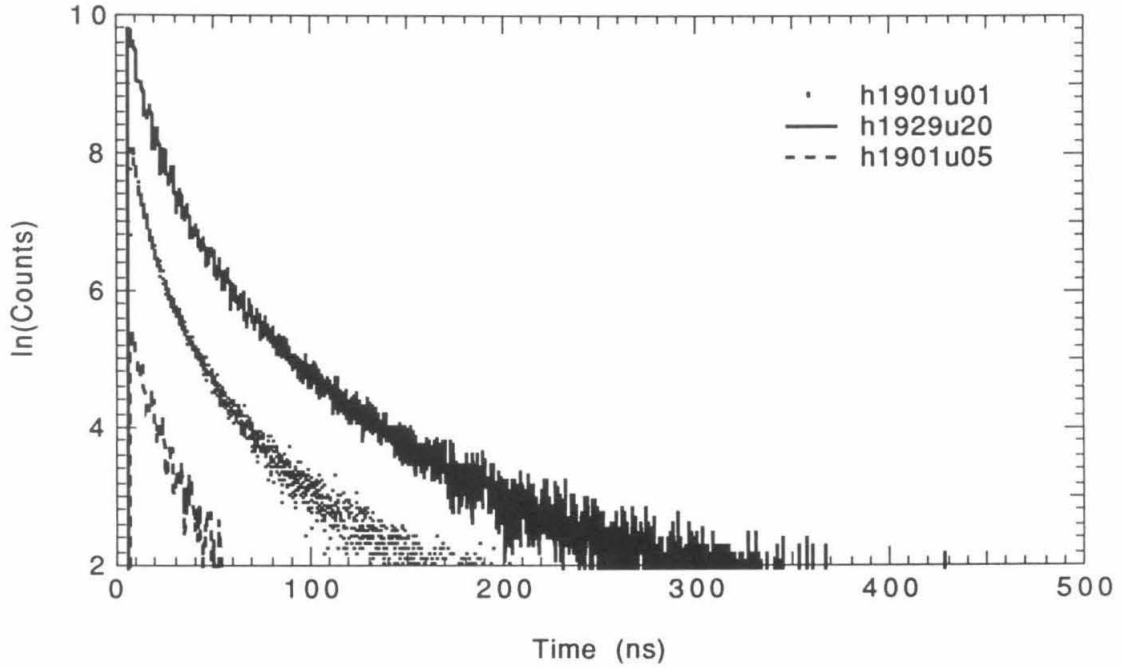

Figure 5-2(d). PL decays as a function of light intensity which was increased using beam focus. See text.

ns changed from 118 ns to 98 ns, and using an ND40, the slope measured between the 20 and 400 ns points changed from 110 ns to 105 ns. In both cases, lower intensities yielded shorter lifetimes. In spite of the scatter in the data and seemingly small magnitude of change in the lifetimes, this trend was consistently observed in these experiments. At even later times in the decay, however, the rate of decay begins to decrease, as can be seen for the curve labelled g6m30n07 in Figure 5-3(b). This change in the rate can also be seen in the decays taken for a 9 μm $Al_{.23}Ga_{.77}As$ sample (Sample 60M 1063) taken with a TCPC apparatus at Jet Propulsion Laboratories, Pasadena, CA, and shown in Figure 5-3(c). Moreover, the lifetime of the $Al_{.23}Ga_{.77}As$ in the 30-200 ns range was similar to that of the GaAs samples, roughly 110 ns. Interestingly, however, the decays for the thicker samples appear to finally evolve into a decay that is very linear on a ln scale, with a slope corresponding to a lifetime of about 600 ns. As with the 1 μm samples described above, the lifetimes of the 9 μm samples appear to be limited by surface recombination. Again assuming that bulk trapping is negligible and using eq. 5-1, the 600 ns lifetime corresponds to a value of s_p of 750 cm/sec, which is similar to the value of s_p obtained for the 1 μm samples above. The fact that the lifetimes measured for the two OMCVD-grown samples yielded capture velocities of similar magnitude supports the hypothesis that their decays are dominated by surface recombination and not by bulk trapping. Given that a limiting lifetime was observed for the 9 μm samples, it is not clear why such was not the case for the 1 μm samples.

The luminescence decay was also measured for a sample grown using molecular beam epitaxy (MBE), for which the interface characteristics are expected to be different from OMCVD-grown material. The lifetime for a 1 μm, nominally undoped sample MBE sample was found to be almost invariant under all low injection conditions. Moreover, there was not as much deviation from linearity in the ln plot at the early times as for the OMCVD material. Figure 5-4(a) shows decay curves for the MBE samples irradiated

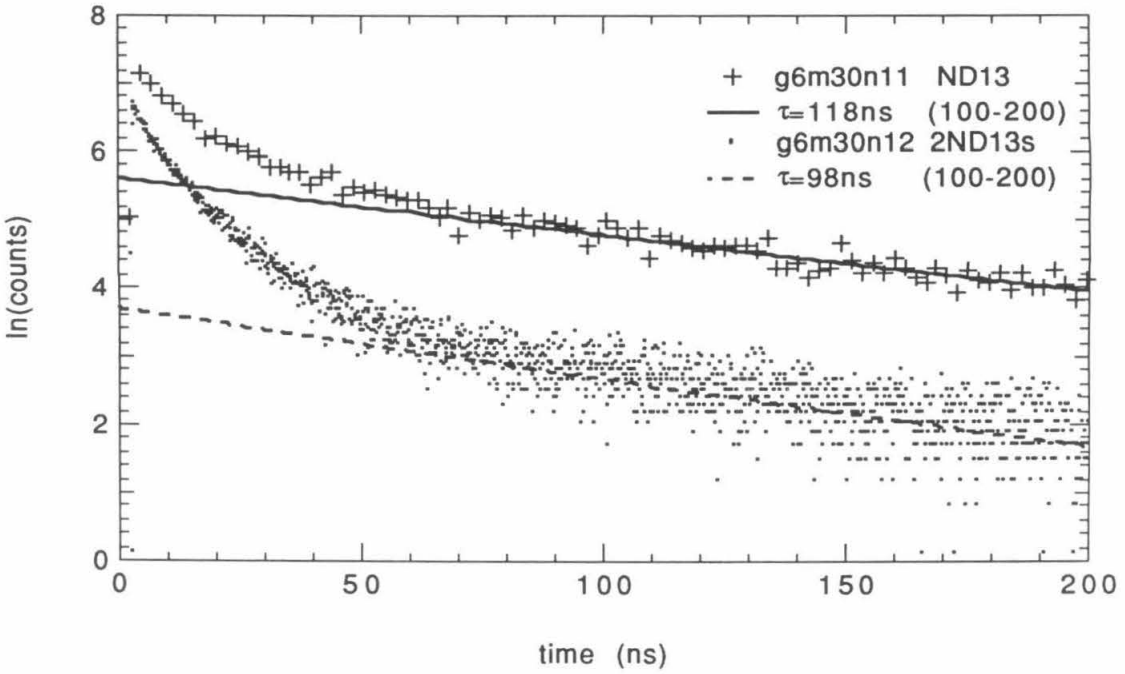

Figure 5-3(a). Low-injection PL decays for 9 μm GaAs, with one and two ND13s.

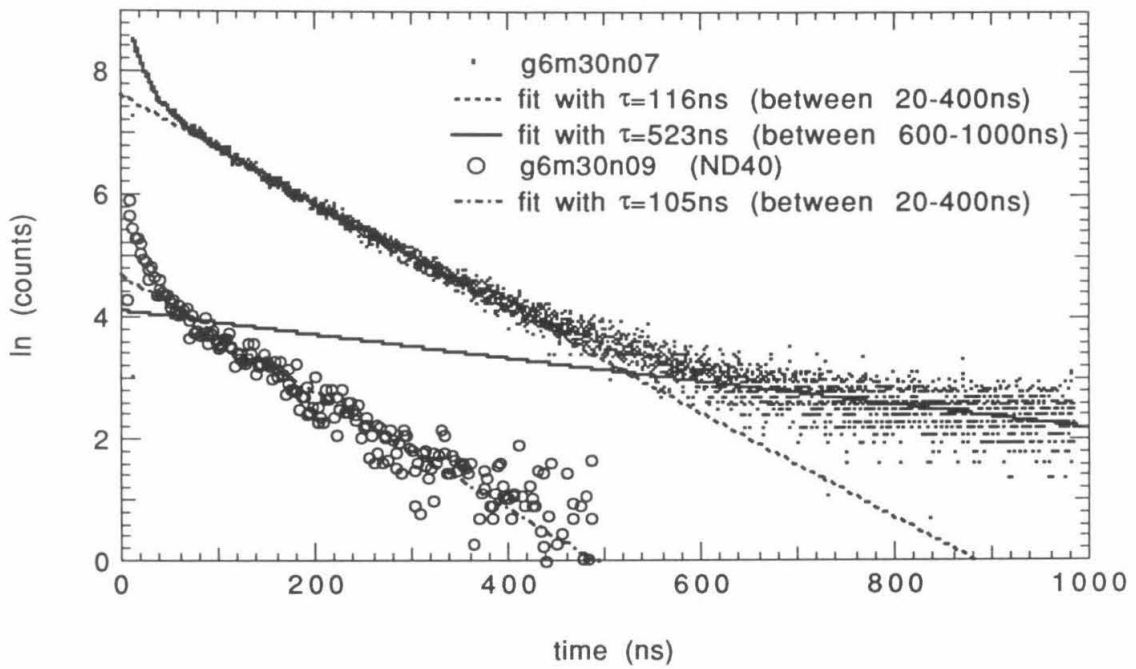

Figure 5-3(b). Low-injection PL decays for 9 μm GaAs, with and without ND40.

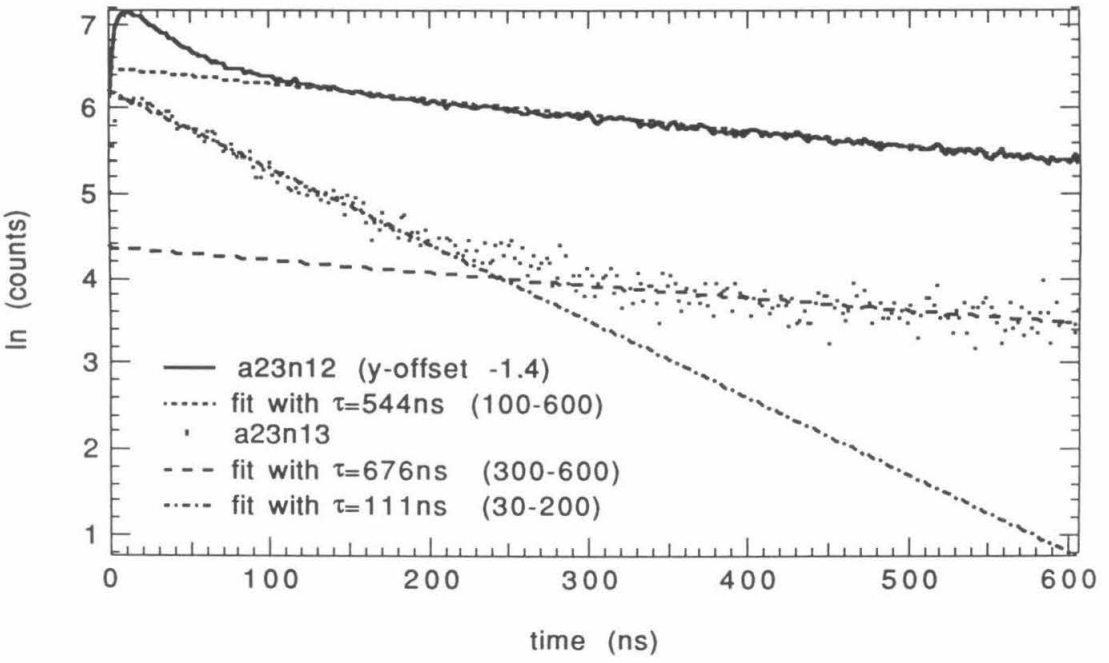

Figure 5-3(c). Low injection PL decays for 9 μm $Al_{.23}Ga_{.77}As$, measured at JPL.

through the 0.2 μm $Al_{.7}Ga_{.3}As$ cap using both 440 nm and 630 nm light at low injection. (It was noted that the 0.2 μm $Al_{.7}Ga_{.3}As$ cap absorbs 80% of the incident 440 nm light.[1]) Figure 5-4(b) is the difference in decay curves with and without an ND40 filter in the incident beam, while Figure 5-4(c) demonstrates the difference for incident beams with and without an ND13. In Figure 5-4(c), the decay at the early times is steeper for the sample at lower light levels, just as it was for OMCVD material. Overall, the MBE material appears to have a limiting low injection lifetime of about 15-20 ns, which is significantly shorter than the OMCVD material. This material either has a higher surface recombination velocity of 2500 cm/sec, or the bulk trapping mechanism dominates the recombination.

2. High Injection Results

At high injection, the decays are distinctly not single exponential. As discussed in Chapter 2, the formalism of bimolecular kinetics dictates that a plot of the observables, $\frac{1}{\sqrt{N}}$ vs. t, where N is the number of counts, should yield a straight line with a slope that is proportional to $\sqrt{k_{radiative}}$. In Figure 5-5, four decays illustrating this point are presented. Figures 5-5(a) and (b) show decays h691930 and h1929u18 used in computer fits to determine the incident intensity (vide infra). Figure 5-5(c) illustrates a typical decay taken prior to etching and metal ion treatments performed in May 1991. Figure 5-5(d) is an example of a decay from a capped sample described above for the low injection case, showing that the $\frac{1}{\sqrt{N}}$ vs. t plot is not linear at low injection.

As discussed in Chapter 2, the bimolecular fits can either yield the intensity or the radiative recombination rate constant, and the other must be assumed. As discussed in Chapter 3, the value of $k_{radiative}$ was taken from the literature to be $2x10^{-10}$ cm^3/sec, and an attempt was made to fit a series of high-injection decay curves in which intensity was controlled by the use of neutral density filters, so that known relative intensities were measured. In Figure 5-6 the series h691930-h691932 is shown with the corresponding fits obtained by the computer. Two other values of $k_{radiative}$ were also tested, to see if the

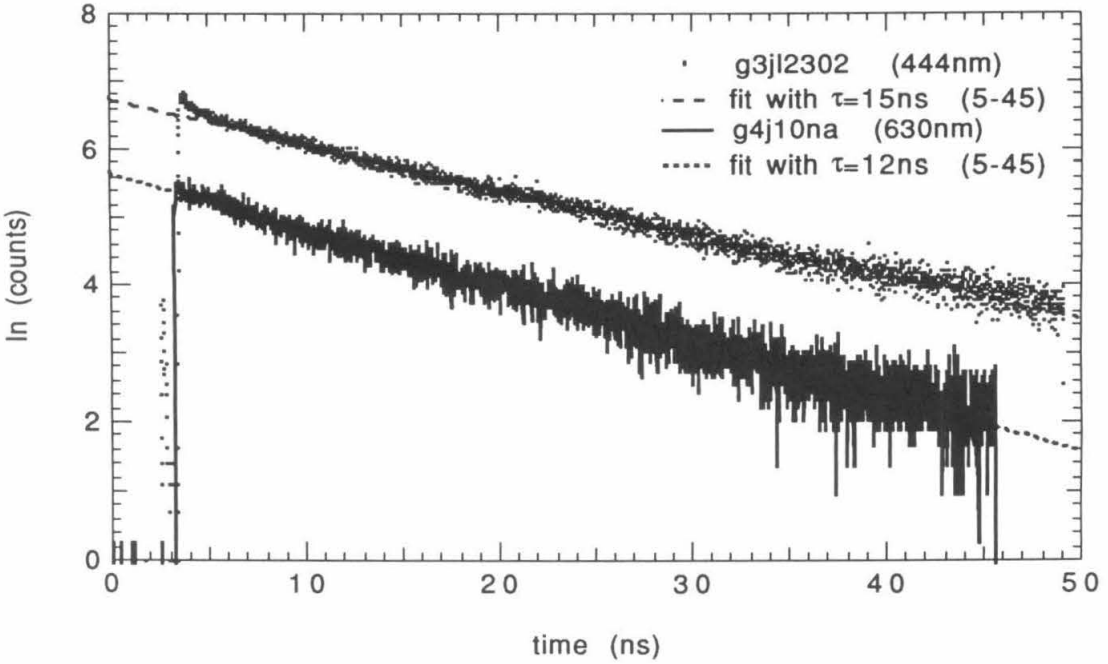

Figure 5-4(a). Low injection PL decays for 1 μm MBE-grown GaAs using 444 and 630 nm light.

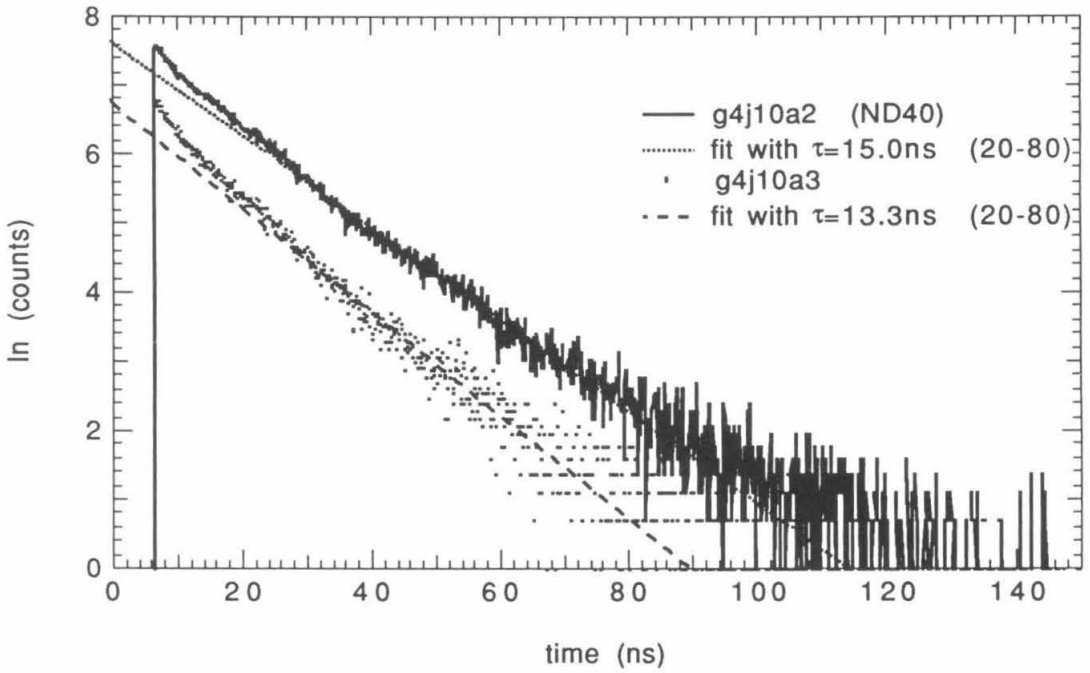

Figure 5-4(b). Low injection PL decays for 1 μm MBE-grown GaAs . Intensity was varied using an ND40.

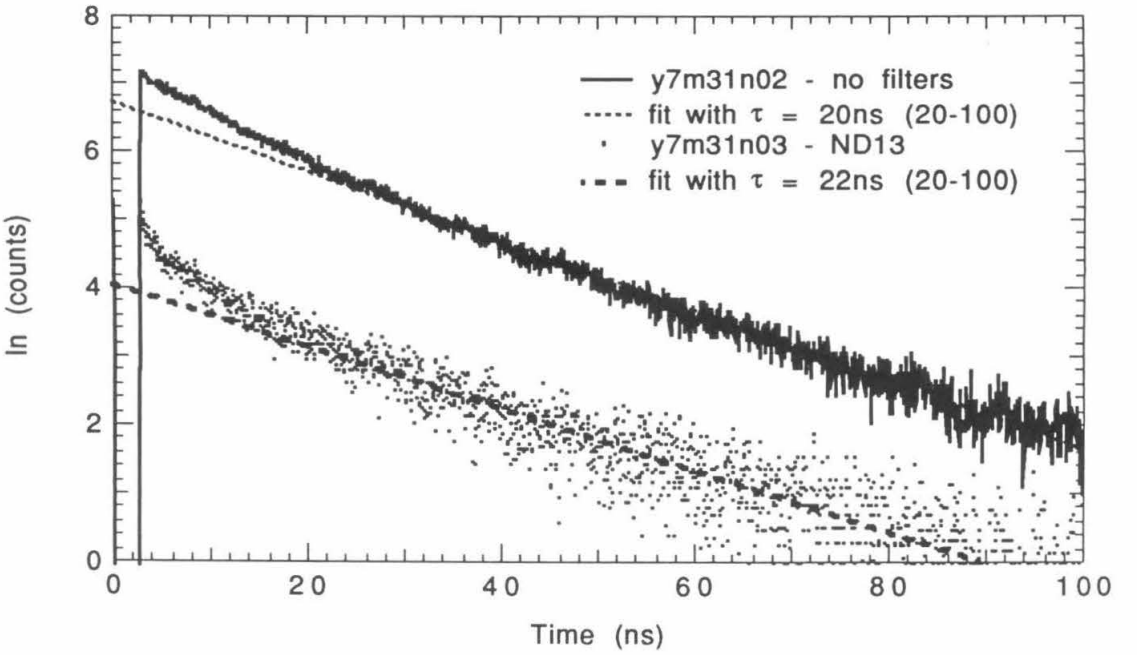

Figure 5-4(c). PL decays for 1 μm MBE sample. Intensity varied using ND13.

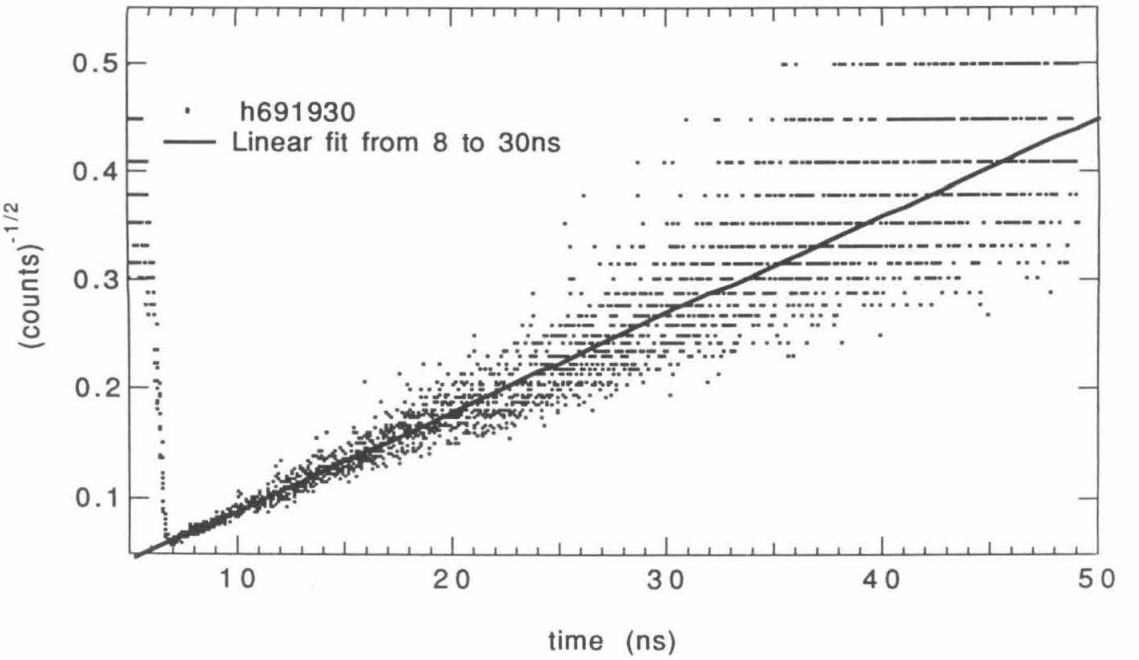

Figure 5-5(a). Inverse square root of PL decay for high injection illumination of capped sample h691930.

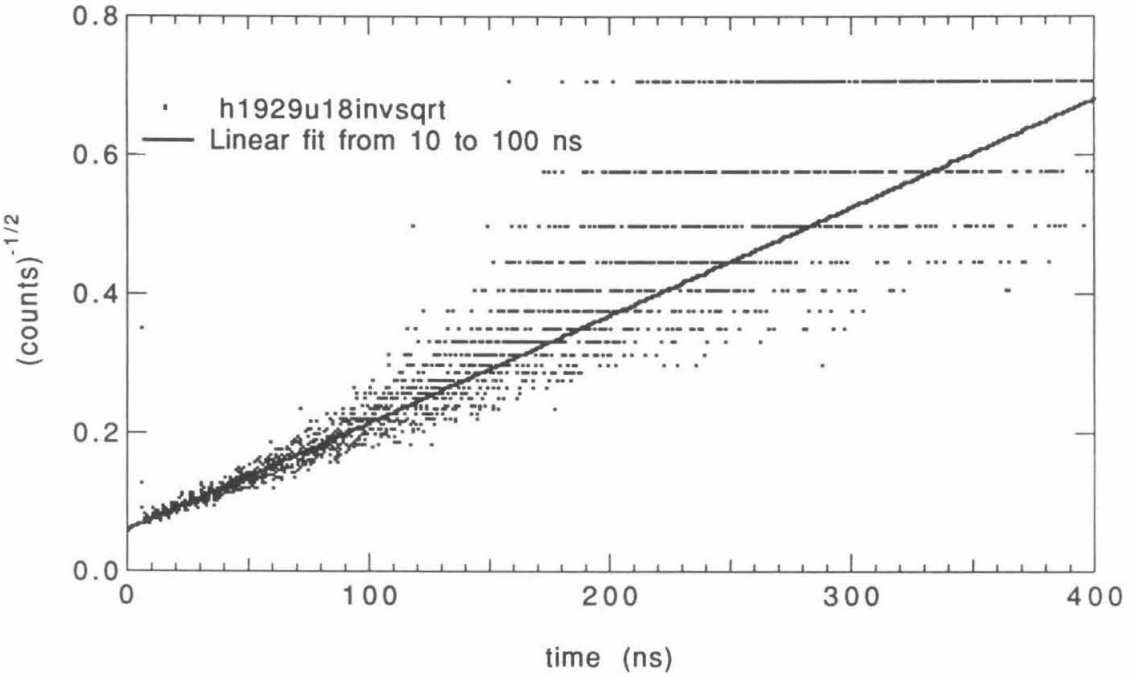

Figure 5-5(b). Inverse square root of PL decay for high intensity illumination of capped sample h1929u18.

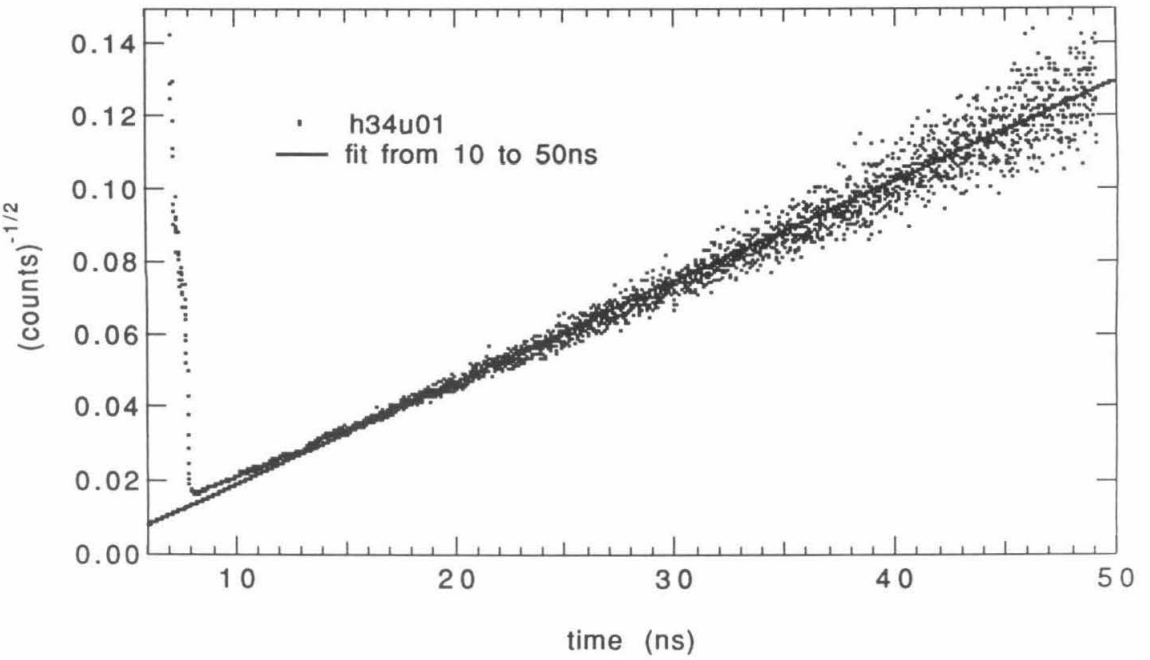

Figure 5-5(c). Inverse square root of high-injection PL decay prior to removal of AlGaAs cap. This sample was subsequently immersed in selenide solution.

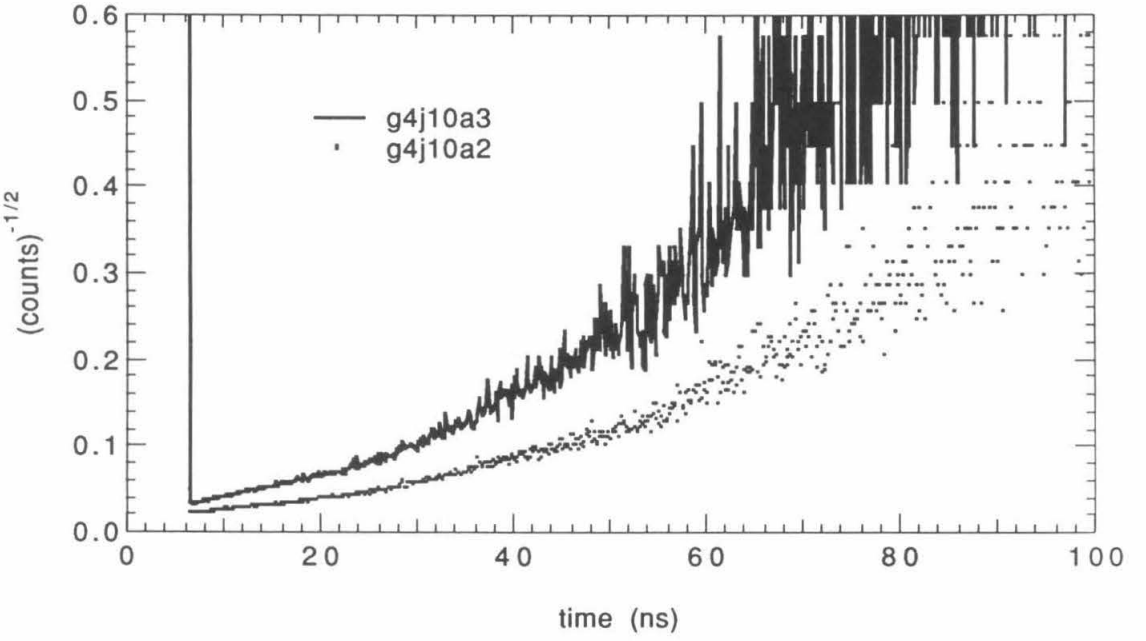

Figure 5-5(d). Inverse square root of low-injection PL decay prior to removal of AlGaAs cap.

Figure 5-6 Computer fits to series of high-injection decays for which light intensity was varied using neutral density filters. Model parameters are displayed along right side of graph. Fit was made varying the incident light intensity, x-offset, and amplitude. $k_{radiative}$ was set at $2x10^{-10}$ cm^3/sec. The experimentally measured laser power was 70 mW with no neutral density filters in-line, and 33 mW for the nominally 40% transmitting filter. The beam was focussed onto the sample using a 100 mm focal length lens. The linear and residuals plots are presented as (I) and (II), respectively, for each experiment.

(a) Fit and data for sample h691930. 100% of laser beam was incident on sample. Incident light intensity was fit to $7.2x10^{13}$ photons·cm^{-2}.

(b) Fit and data for sample h691931. 40% of laser beam was incident on sample. Incident light intensity was fit to $5.0x10^{13}$ photons·cm^{-2}.

(c) Fit and data for sample h691933. 13% of laser beam was incident on sample. Incident light intensity was fit to $5.0x10^{13}$ photons·cm^{-2}.

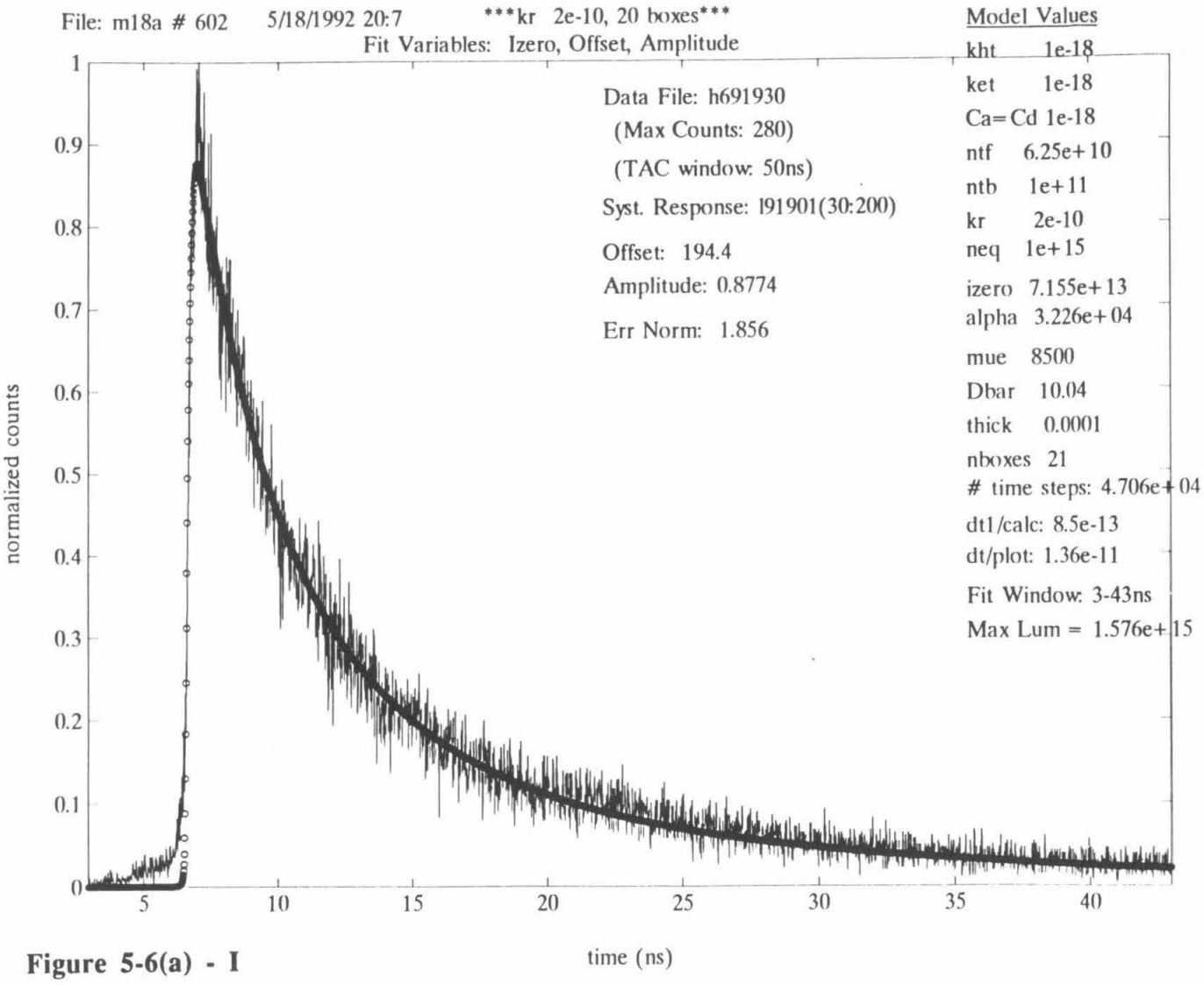
File: m18a # 602 5/18/1992 20:7 ***kr 2e-10, 20 boxes***
Fit Variables: Izero, Offset, Amplitude
Data File: h691930
(Max Counts: 280)
(TAC window: 50ns)
Syst. Response: l91901(30:200)
Offset: 194.4
Amplitude: 0.8774
Err Norm: 1.856
Model Values
kht 1e-18
ket 1e-18
Ca=Cd 1e-18
ntf 6.25e+10
ntb 1e+11
kr 2e-10
neq 1e+15
izero 7.155e+13
alpha 3.226e+04
mue 8500
Dbar 10.04
thick 0.0001
nboxes 21
time steps: 4.706e+04
dt1/calc: 8.5e-13
dt/plot: 1.36e-11
Fit Window: 3-43ns
Max Lum = 1.576e+15
normalized counts
time (ns)
0
0.1
0.2
0.3
0.4
0.5
0.6
0.7
0.8
0.9
1
5
10
15
20
25
30
35
40

Figure 5-6(a) - I

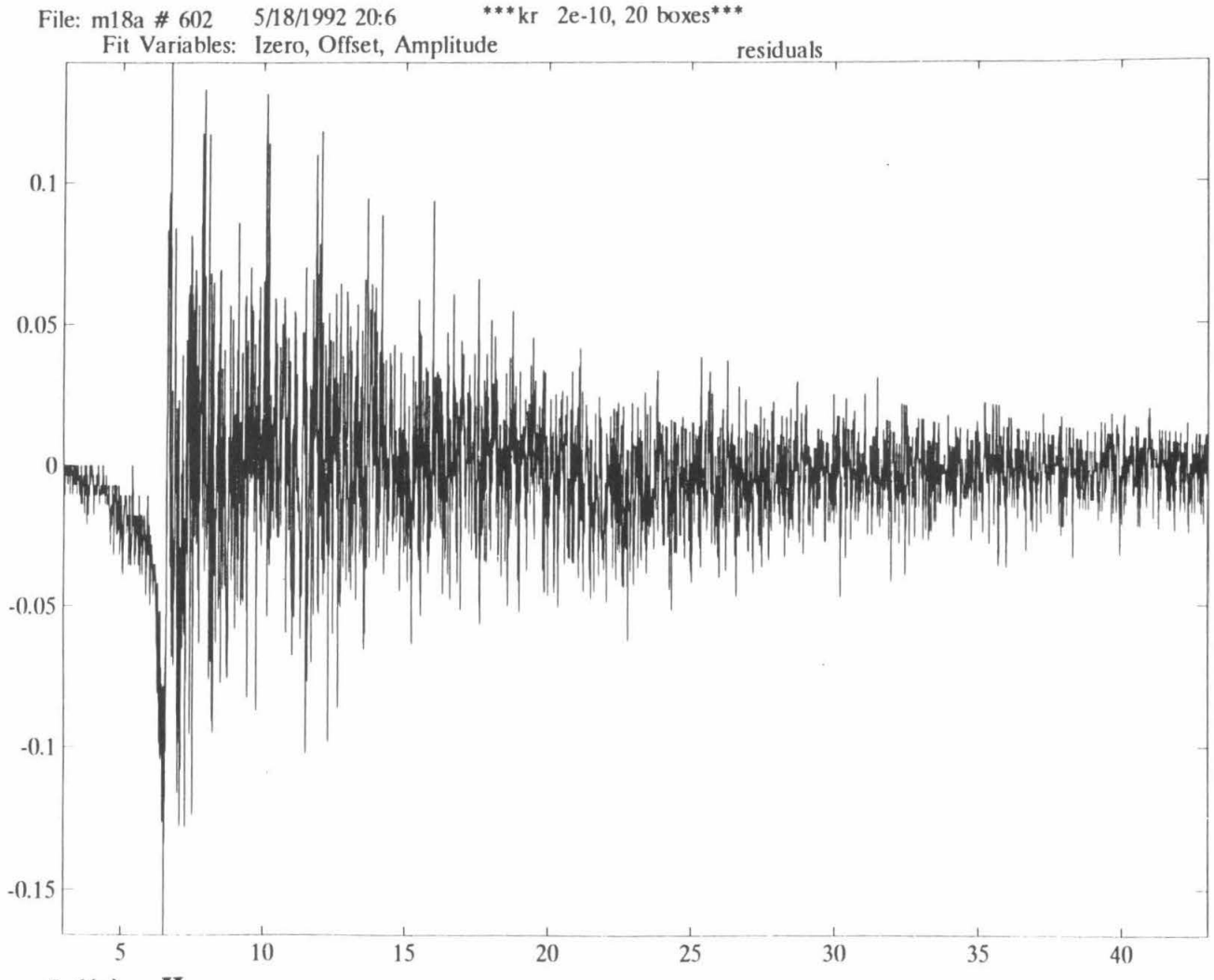

Figure 5-6(a) - II

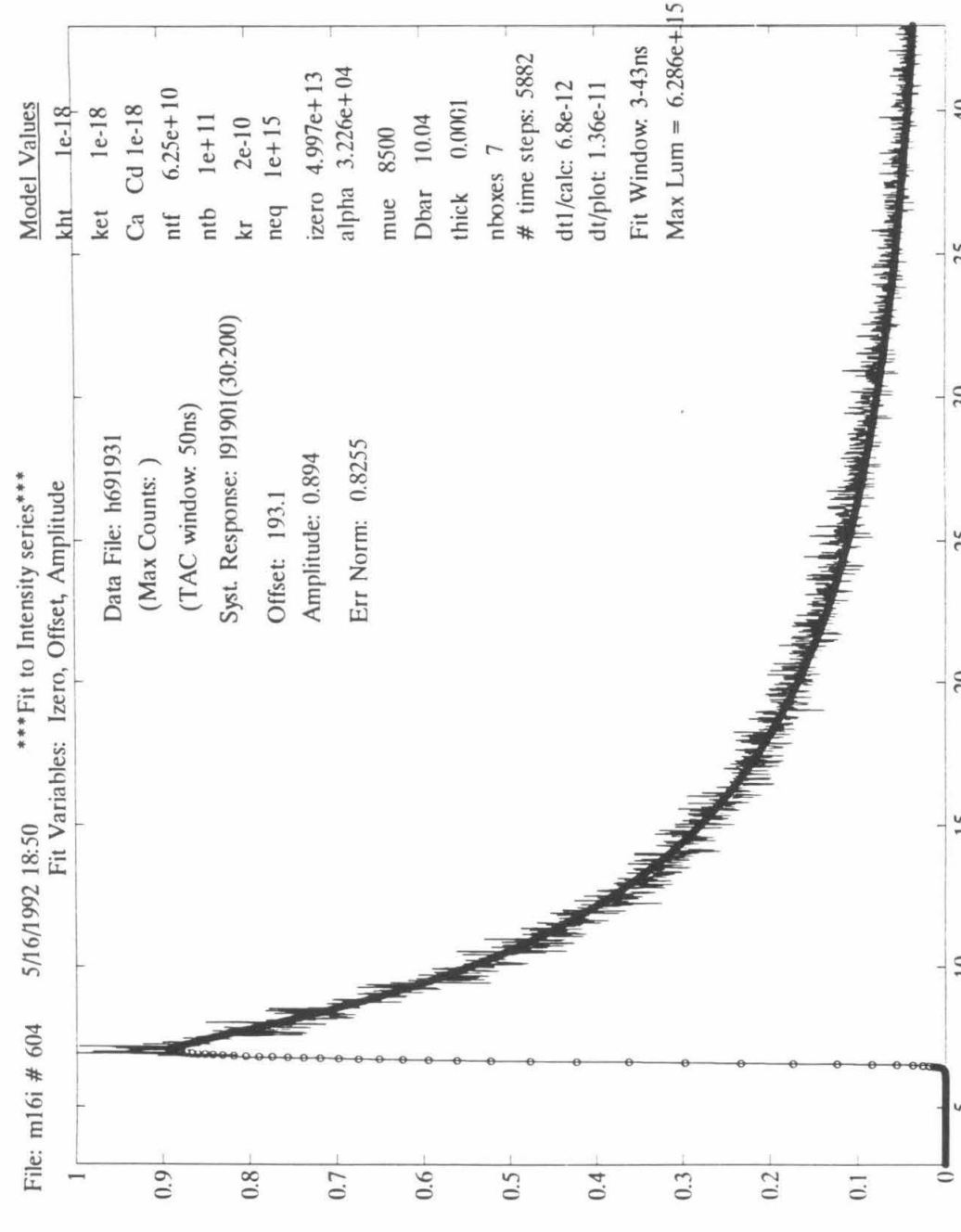
File: m16i # 604 5/16/1992 18:50 ***Fit to Intensity series***
Fit Variables: Izero, Offset, Amplitude
Data File: h691931
(Max Counts:)
(TAC window: 50ns)
Syst. Response: I91901(30:200)
Offset: 193.1
Amplitude: 0.894
Err Norm: 0.8255
Model Values
kht 1e-18
ket 1e-18
Ca Cd 1e-18
ntf 6.25e+10
ntb 1e+11
kr 2e-10
neq 1e+15
izero 4.997e+13
alpha 3.226e+04
mue 8500
Dbar 10.04
thick 0.0061
nboxes 7
time steps: 5882
dt1/calc: 6.8e-12
dt/plot: 1.36e-11
Fit Window: 3-43ns
Max Lum = 6.286e+15
normalized counts
time (ns)

Figure 5-6(b) - I

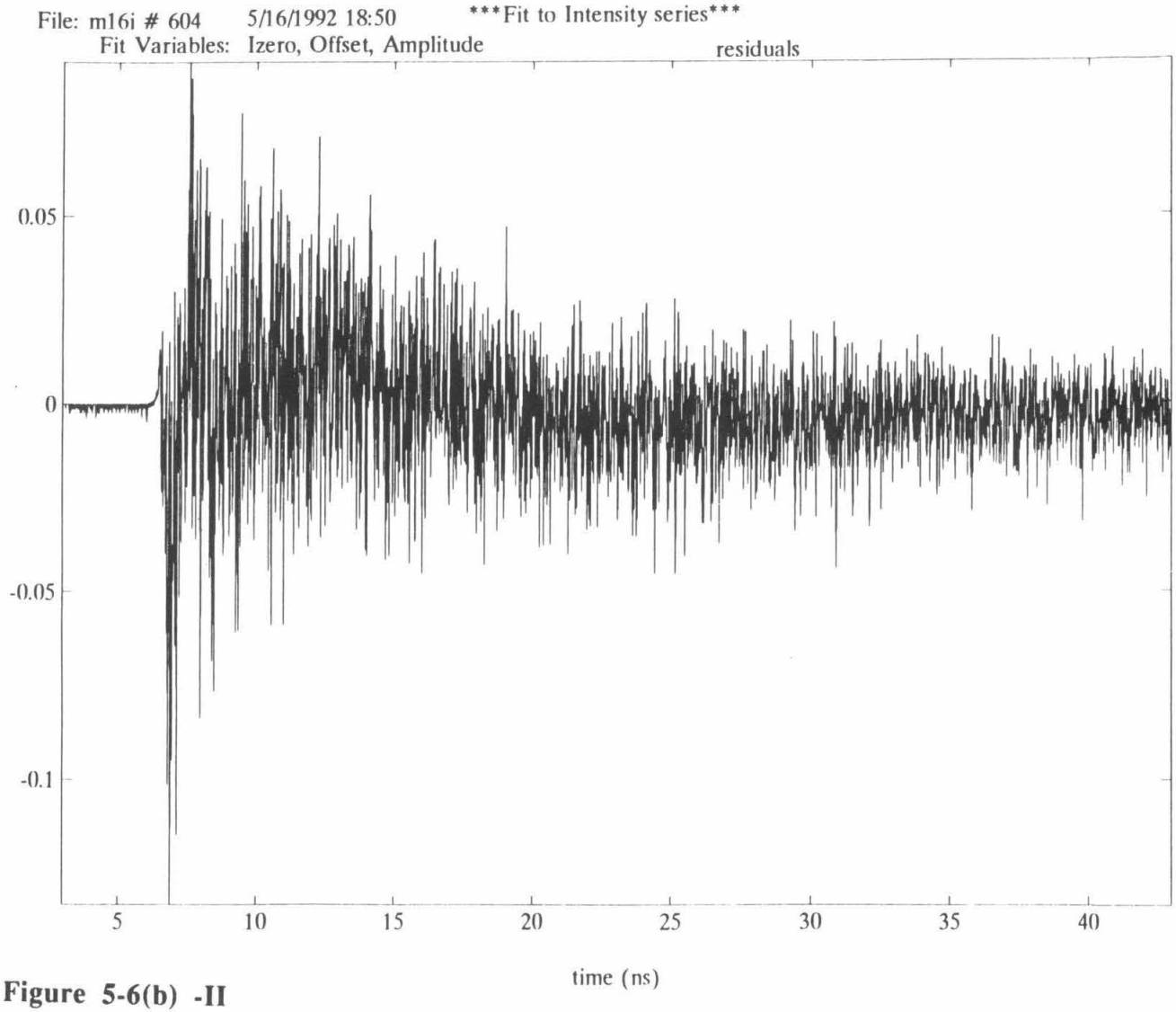

Figure 5-6(b) -II

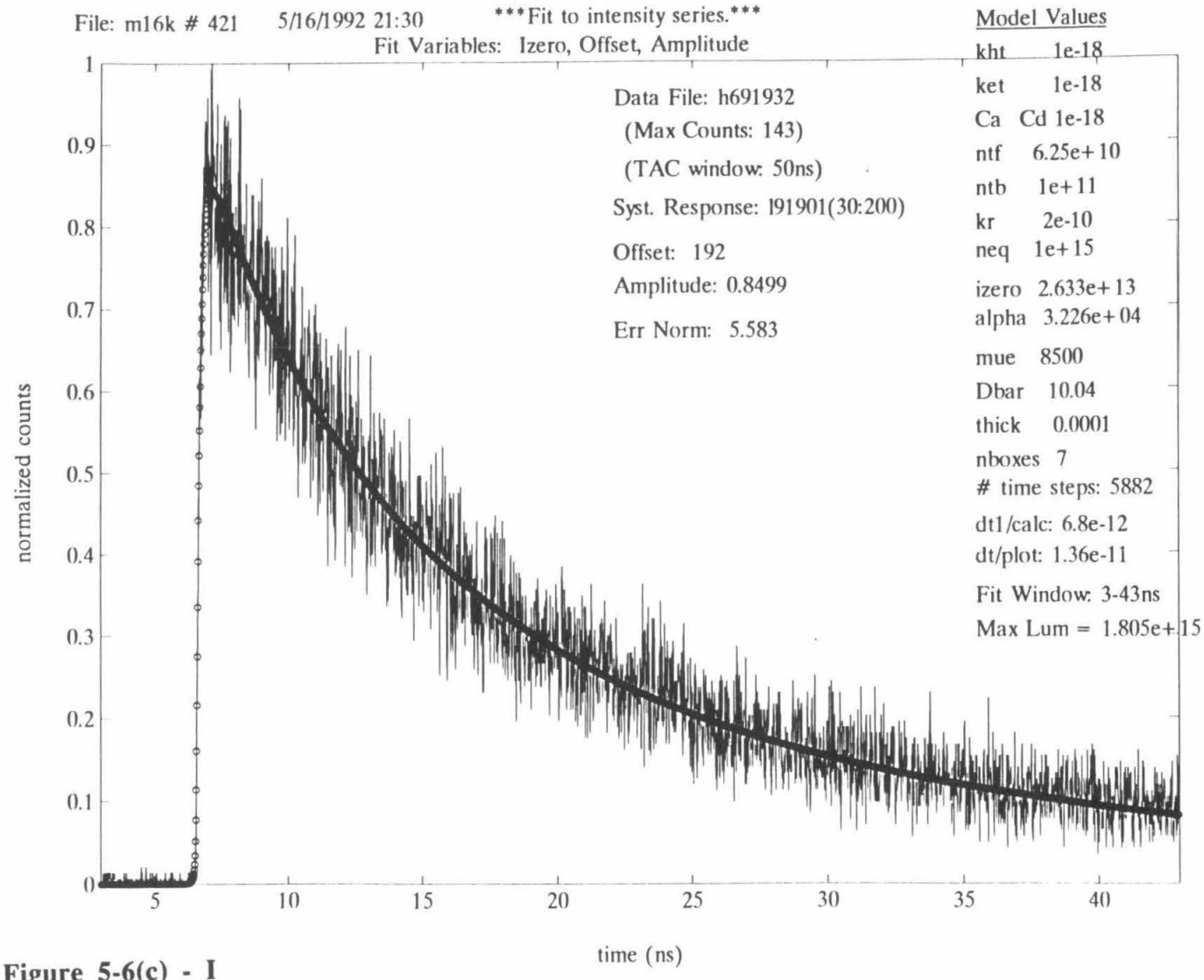
File: m16k # 421 5/16/1992 21:30
Fit to intensity series.
Fit Variables: Izero, Offset, Amplitude
Data File: h691932
(Max Counts: 143)
(TAC window: 50ns)
Syst. Response: I91901(30:200)
Offset: 192
Amplitude: 0.8499
Err Norm: 5.583
Model Values
kht 1e-18
ket 1e-18
Ca Cd 1e-18
ntf 6.25e+10
ntb 1e+11
kr 2e-10
neq 1e+15
izero 2.633e+13
alpha 3.226e+04
mue 8500
Dbar 10.04
thick 0.0001
nboxes 7
time steps: 5882
dt1/calc: 6.8e-12
dt/plot: 1.36e-11
Fit Window: 3-43ns
Max Lum = 1.805e+15
normalized counts
time (ns)
0
0.1
0.2
0.3
0.4
0.5
0.6
0.7
0.8
0.9
1
5
10
15
20
25
30
35
40

Figure 5-6(c) - I

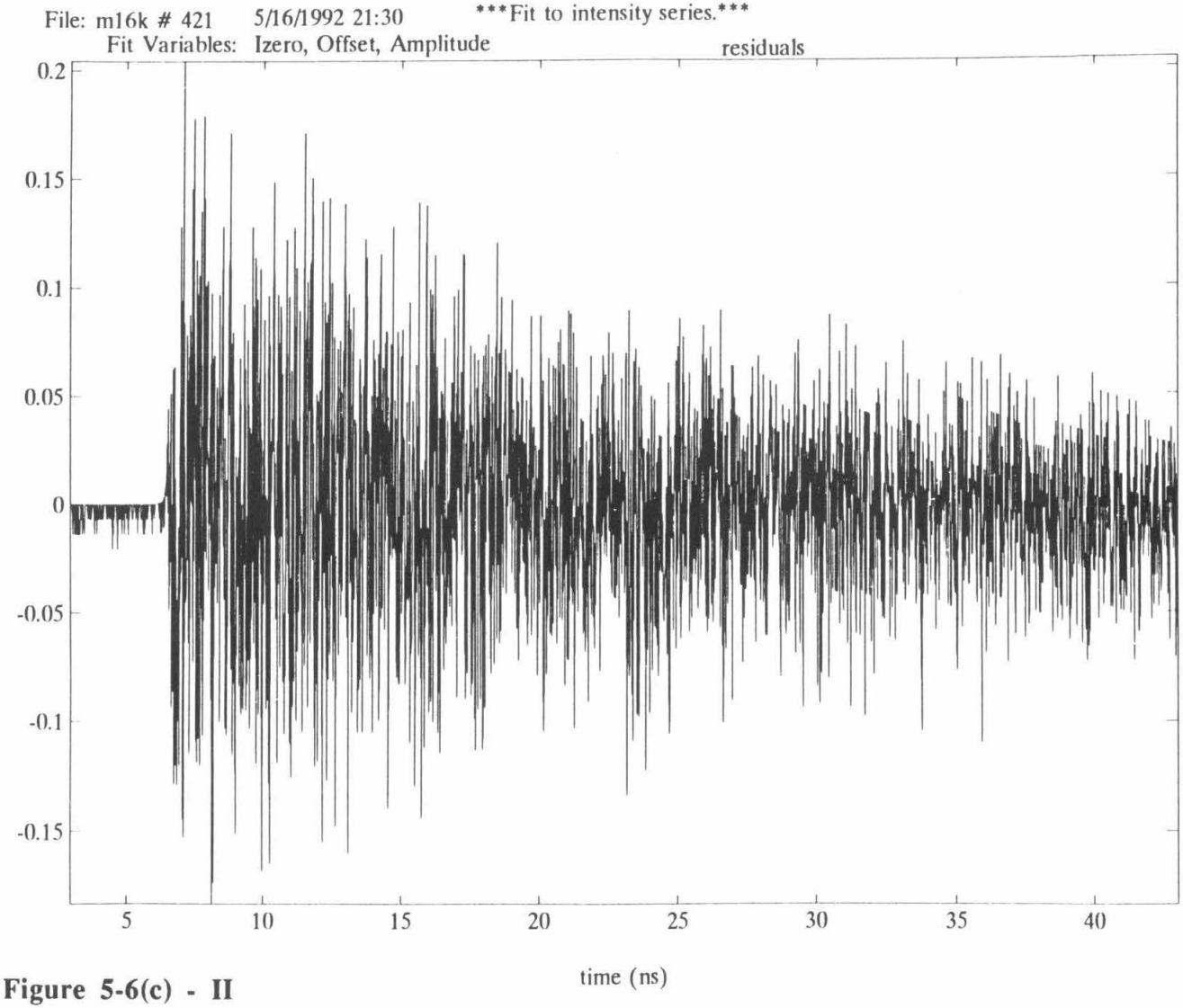

Figure 5-6(c) - II

intensities obtained from the fits would be closer to the ratio predicted by the ratio of ND filters used. Table 5-II compares the known ND filter values to the computer-generated intensity values for three values of $k_{radiative}$.

Table 5-II. Comparison of experimental and predicted intensity variations.

Sample	% Transmission nominal (experimental)	Calculated Relative Intensity (absolute Izero, in photons·cm^{-2})		
		k_{rad}=2x10^{-10}	k_{rad}=7x10^{-11}	k_{rad}=1x10^{-10}
h691930	100	100 (7.2x10^{13})	100 (2.1x10^{14})	100 (1.4x10^{14})
h691931	40 (47)	69 (5.0x10^{13})	66 (1.4x10^{14})	71 (1.0x10^{14})
h691932	13	39 (2.6x10^{13})	36 (7.5x10^{13})	37 (5.2x10^{13})

This ratio of fit intensities is the same for both $k_{radiative}$ = 2x10^{-9} and 3x10^{-10} cm^3/sec. It can be seen that the predicted relative values significantly overestimate the experimentally set intensities. Due to the limitations of the power meters, it was not possible to accurately measure lower laser powers, but at the high fluxes present in laser beams, the neutral density filters may behave non-linearly, and, as suggested by the higher than expected transmission observed for the ND40, may transmit more light than specified. This effect partially accounts for the error in the fitted intensities. Following the calculations in eqs. 4-2 to 4-6, 70 mW is expected to yield 1.7x10^{13} photons·cm^{-2} when focussed to the diffraction limited spot of a 100 mm f.l. lens, which is a factor of four lower than the value obtained from the fit for $k_{radiative}$ equal to 2x10^{-10} cm^3/sec.

Different intensities were achieved in a second experiment by changing the focus of the beam on the sample. The count rate decreased by a factor of 7.2, and it was assumed that the collection efficiency was the same in both cases, and, therefore, that the incident photon flux decreased by an equivalent amount. The data and fits for this pair of decays are shown in Figure 5-7. The best fit from the computer was for intensities which varied by a factor of 9.6. Basing the intensity value on the measured count rate relies on the

Figure 5-7. Computer fits to series of high-injection decays for which light intensity was varied by changing the beam focus. Model parameters are displayed along right side of graph. Fit was made varying values for the incident light intensity, x-offset, and amplitude. $k_{radiative}$ was set at $2x10^{-10}$ cm^3/sec. The measured laser power was 50 mW with no neutral density filters in-line, and it dropped slightly during the course of the experiment. The beam was focussed onto the sample using a 100 mm focal length lens. The linear and residuals plots are presented as (I) and (II), respectively, for each experiment.

(a) Fit and data for sample h1929u18. Approximately 150% on the ND scale of Figure 5-1. Incident light intensity was fit to $4.5x10^{12}$ photons·cm^{-2}.

(b) Fit and data for sample h1929u21. 7.2 times more intense than h1929u18, based on count rate. Incident light intensity was fit to $4.3x10^{13}$ photons·cm^{-2}.

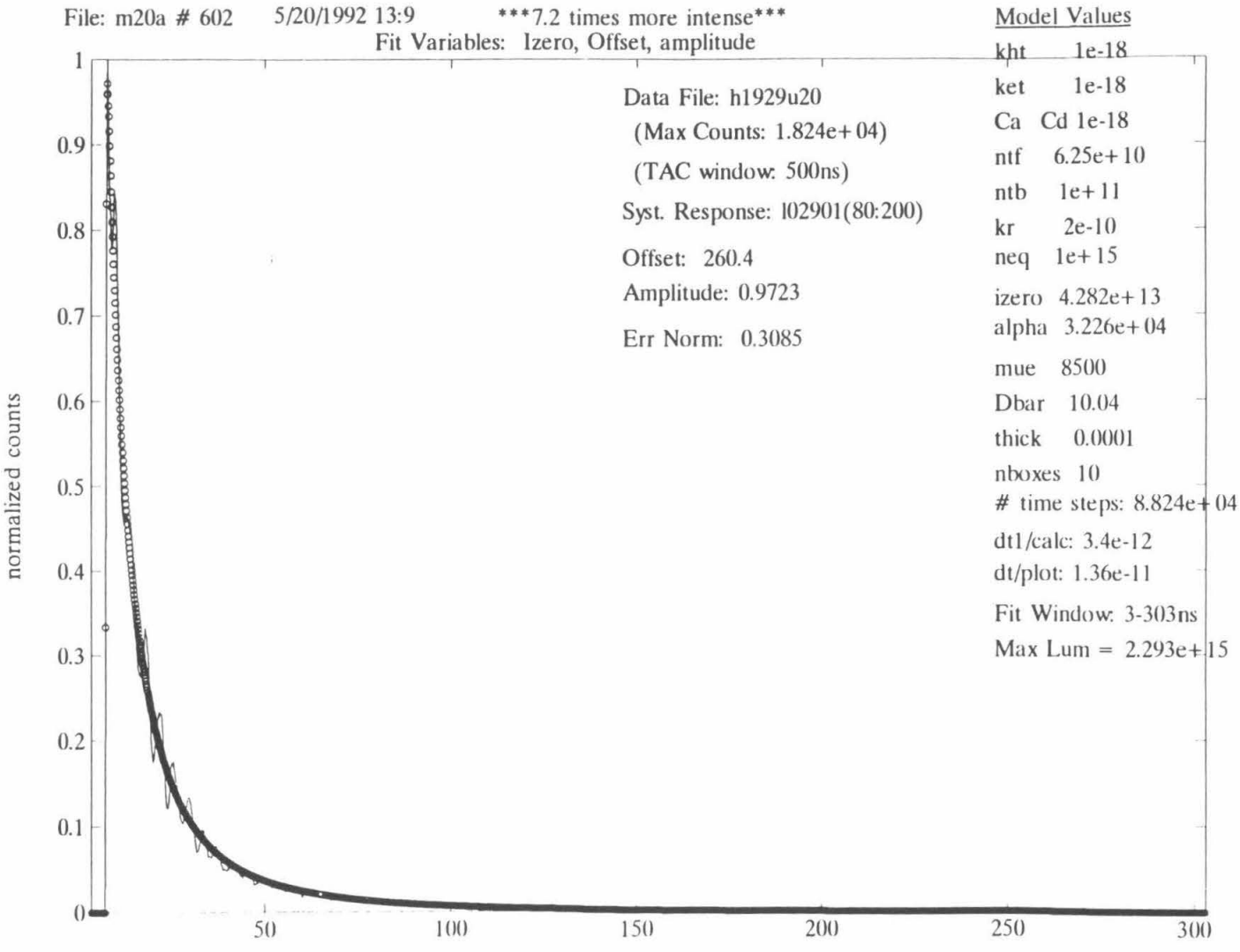
File: m20a # 602 5/20/1992 13:9 ***7.2 times more intense***
Fit Variables: Izero, Offset, amplitude
Data File: h1929u20
(Max Counts: 1.824e+04)
(TAC window: 500ns)
Syst. Response: l02901(80:200)
Offset: 260.4
Amplitude: 0.9723
Err Norm: 0.3085
Model Values
kht 1e-18
ket 1e-18
Ca Cd 1e-18
ntf 6.25e+10
ntb 1e+11
kr 2e-10
neq 1e+15
izero 4.282e+13
alpha 3.226e+04
mue 8500
Dbar 10.04
thick 0.0001
nboxes 10
time steps: 8.824e+04
dt1/calc: 3.4e-12
dt/plot: 1.36e-11
Fit Window: 3-303ns
Max Lum = 2.293e+15
normalized counts
time (ns)
0
0.1
0.2
0.3
0.4
0.5
0.6
0.7
0.8
0.9
1
50
100
150
200
250
300

Figure 5-7(a) - I

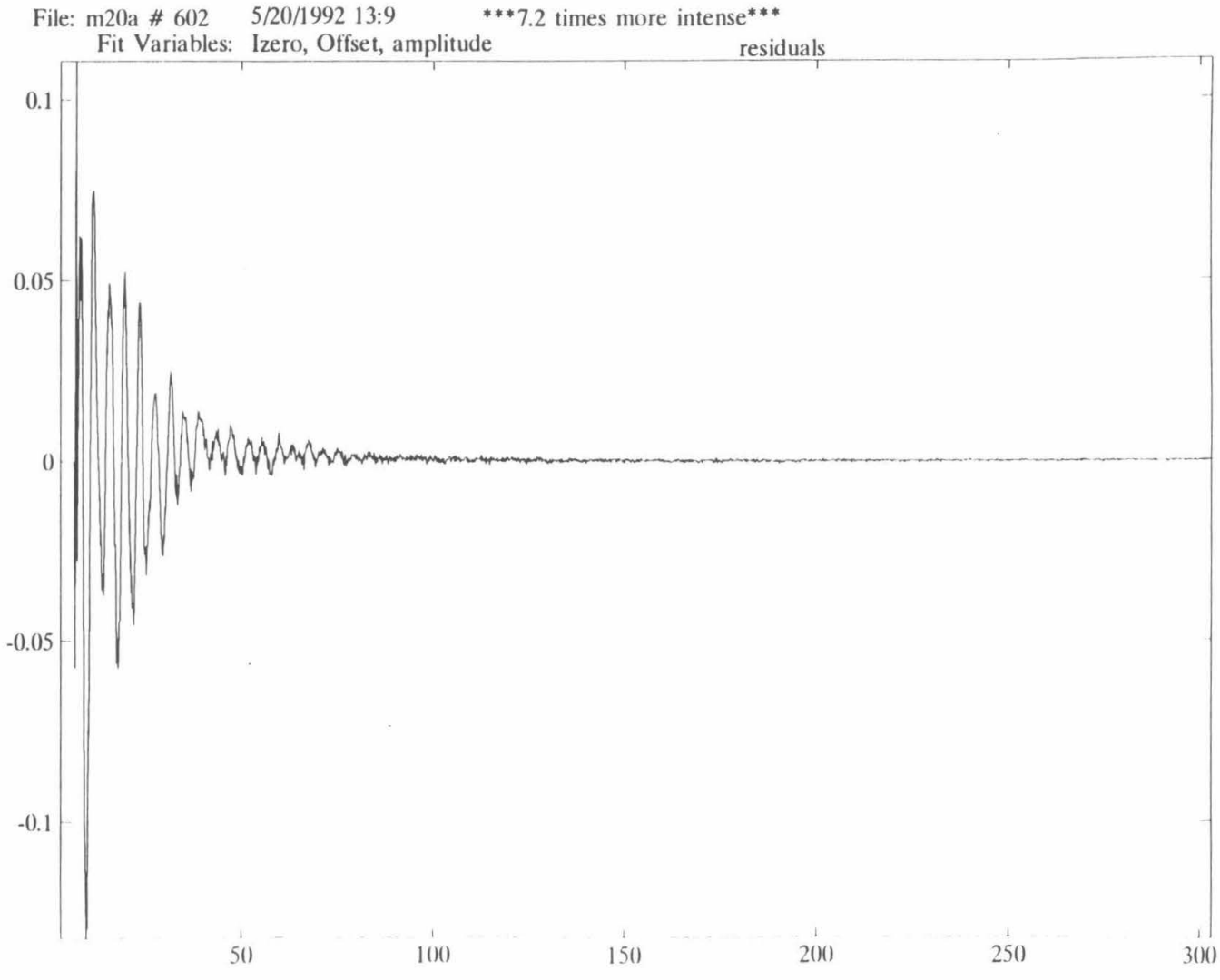

Figure 5-7(a) - II

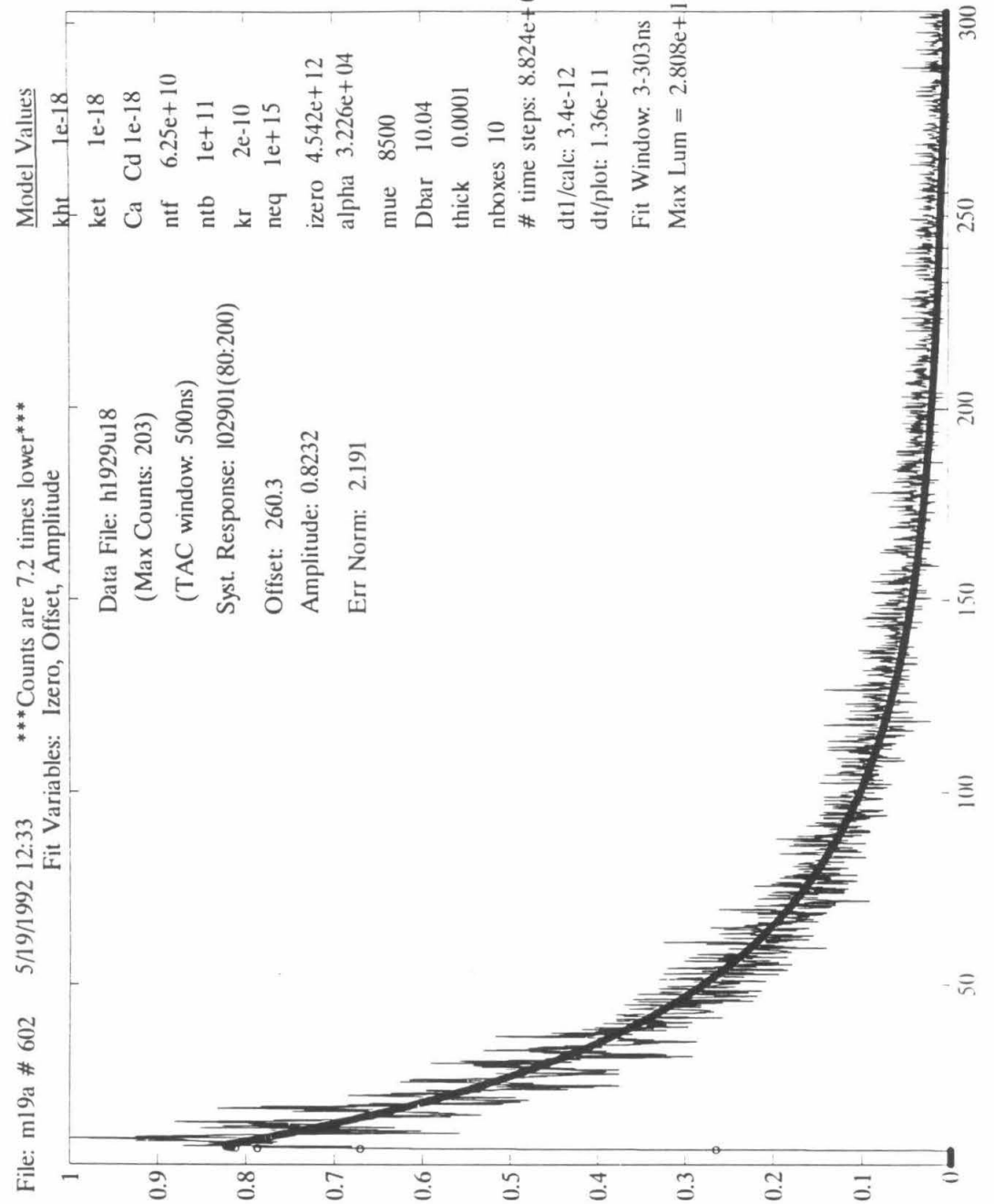
File: m19a # 602 5/19/1992 12:33 ***Counts are 7.2 times lower***
Fit Variables: Izero, Offset, Amplitude
Data File: h1929u18
(Max Counts: 203)
(TAC window: 500ns)
Syst. Response: 102901(80:200)
Offset: 260.3
Amplitude: 0.8232
Err Norm: 2.191
Model Values
kht 1e-18
ket 1e-18
Ca Cd 1e-18
ntf 6.25e+10
ntb 1e+11
kr 2e-10
neq 1e+15
izero 4.542e+12
alpha 3.226e+04
mue 8500
Dbar 10.04
thick 0.0001
nboxes 10
time steps: 8.824e+04
dt1/calc: 3.4e-12
dt/plot: 1.36e-11
Fit Window: 3-303ns
Max Lum = 2.808e+13
normalized counts
time (ns)

Figure 5-7(b) - I

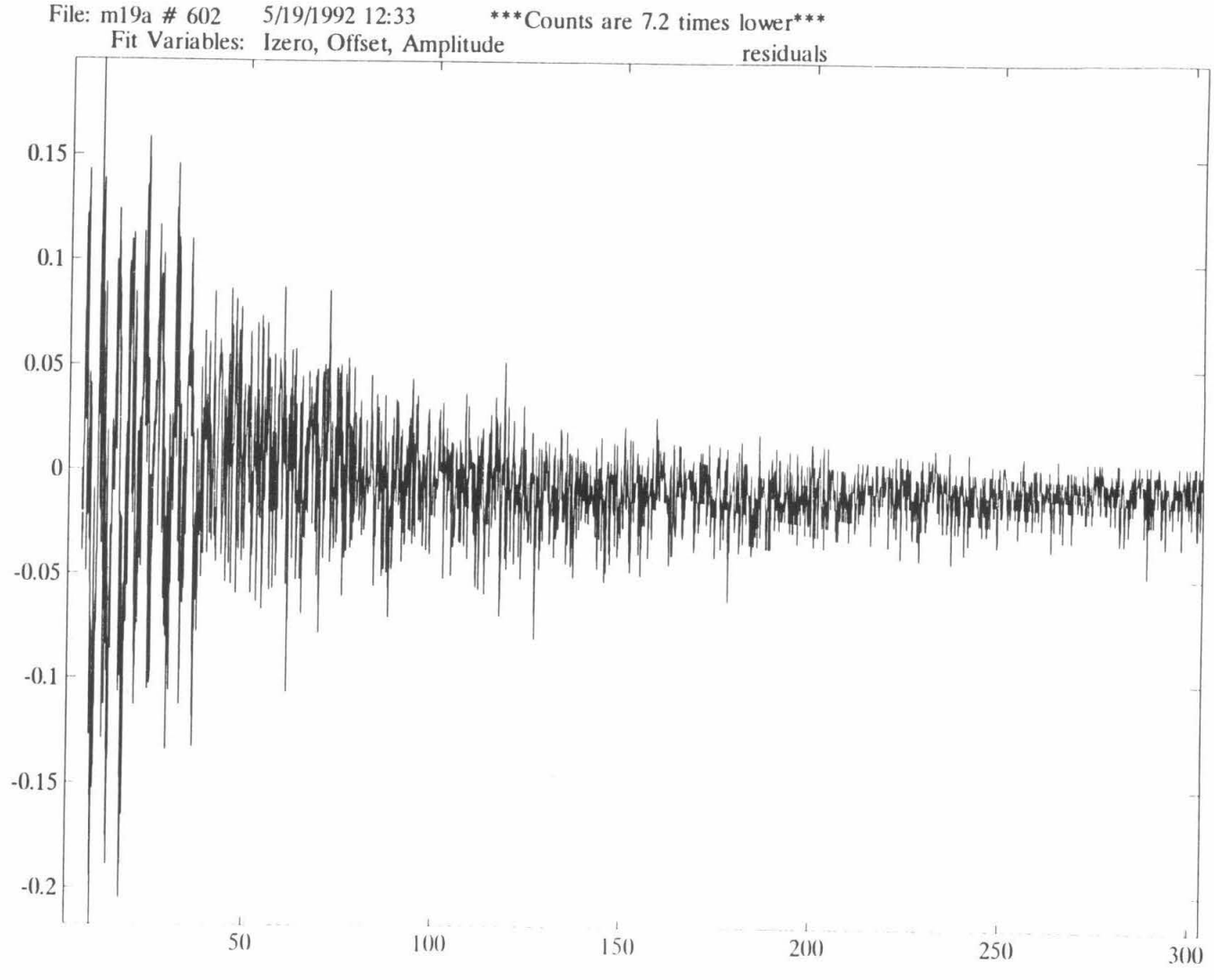

Figure 5-7(b) - II

assumption that the counts collected are directly proportional to the incident laser intensity. The collection efficiency alone varies greatly as a function of sample and beam position, and so this computer fit is probably accurate within the uncertainty of the measurement.

The incident photon fluxes for all subsequent experiments were determined by analogous fits to the decays for the unetched samples. Once this number was obtained, it was used in the fits to subsequent samples which had increased surface recombination due to etching the cap and placing the sample in redox couple.

B. Etched Samples

For all runs, the removal of the cap via etching was verified by the sharp drop in PL lifetime which occurred. XPS studies of the surface were performed by Sharon Lunt in March 1988, to correlate this drop in lifetime with removal of the cap for one of the $Al_{.62}Ga_{.38}As/Al_{.23}Ga_{.77}As/Al_{.62}Ga_{.38}As$ heterostructures (Sample 60M 1063) used in initial experiments at JPL. After a 5 second etch in pure HF, XPS results showed the sample surface to be $Al_{.22}Ga_{.70}As$.[2] Using 4:1 H_2O to HF, four samples were etched for different times (3,15, 40, or 53 seconds) and surface compositions of $Al_{.60}Ga_{.40}As$, $Al_{.42}Ga_{.58}As$,$Al_{.47}Ga_{.53}As$, and $Al_{.34}Ga_{.66}As$, respectively, were measured. The value for the sample etched for 15 seconds was deemed invalid, because the sample was too small and too much of the sample edge was visible to the XPS beam. A plot of the aluminum content vs. etch time is shown in Figure 5-8.

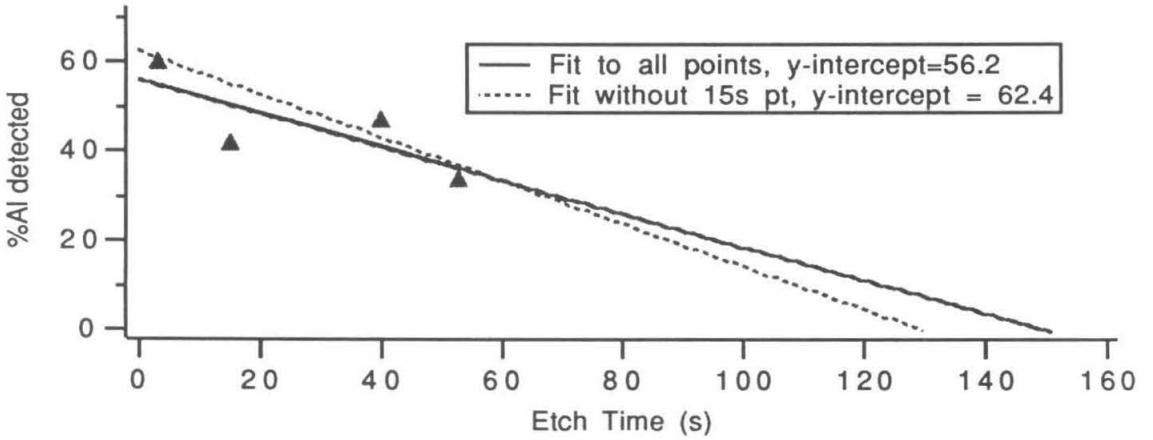

Figure 5-8. %Al detected on surface as a function of etch time in 4:1 H_20:HF.

The HF etch leaves a visibly pockmarked surface, indicating that the etching rate is not uniform across the surface. Moreover, the higher content aluminum material is etched at least 10 times faster than that with the lower aluminum content. The XPS measurement is sensitive to only the top 50 angstroms or less of the near-surface region, but averages regions in the sampling area that are etched to different extents. Figure 5-8 suggests that the cap comes off completely during the first 80 - 100 seconds. In the photoluminescence measurements it was generally found that about 100 seconds of etch were needed before the long lifetime of the AlGaAs samples changed to an abruptly short one due to the unprotected surface. No corresponding measurement was made for the caps that were etched off GaAs with Br_2/CH_3OH. However, a marked transition from a long PL lifetime to a short one came consistently after about 4.5 minutes of etching in Br_2/CH_3OH. It is concluded that this transition corresponded to the removal of the cap layer.

It was also noted that the PL lifetimes for samples subjected to two very different etches was markedly different and reproducible. The mirror finish of the Aspnes-etched surface yielded a longer lifetime than the pockmarked finish of the HF etch did. It was possible to alternate between the two reproducible surfaces and lifetimes. Figure 5-9 shows four curves for a sample that was HF etched, then Aspnes etched, then HF etched, and then Aspnes etched.

The etched surfaces under argon also increased in lifetime in some cases, so no lifetime for an invariant surface was measurable. However, the count rates for the etched samples under argon did not increase as quickly as samples in selenide solutions did. To estimate the rate of surface loss at high injection for these samples, a fit for an etched sample measured prior to immersion in KOH - Se^{2-} - Se_2^{2-} solutions is presented in Figure 5-10. The fit was made by determining an incident intensity from the unetched sample shown in Figure 5-10(a), and then varying only the density of traps on the surface (ntf) for the etched sample. The value of ntf obtained corresponds to an effective surface

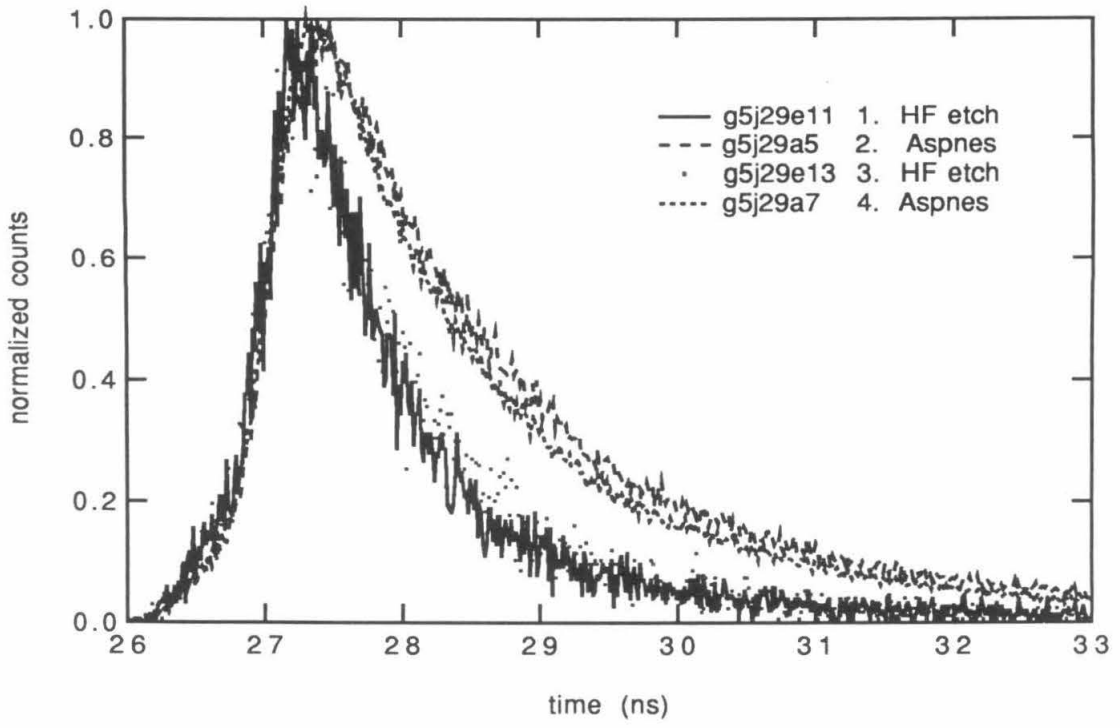

Figure 5-9. Comparison of PL decays after HF and Aspnes etches.

Figure 5-10. Fit to Aspnes-etched surface under argon at high injection for sample h41. 1/e lifetime was about 0.70 ns. The linear and residuals plots are presented as (I) and (II), respectively, for each experiment.

(a) The fit for the unetched sample prior yielded an incident intensity of 7.5×10^{13} photons/cm^2.

(b) The fit for the etched sample yielded a surface trap density (ntf) of 1.8×10^{13} cm^{-2}. The surface trapping rate constant was fixed at 1×10^{-8} cm^3/sec, and the surface recombination velocity is the product of these values, 1.8×10^5 cm/sec.

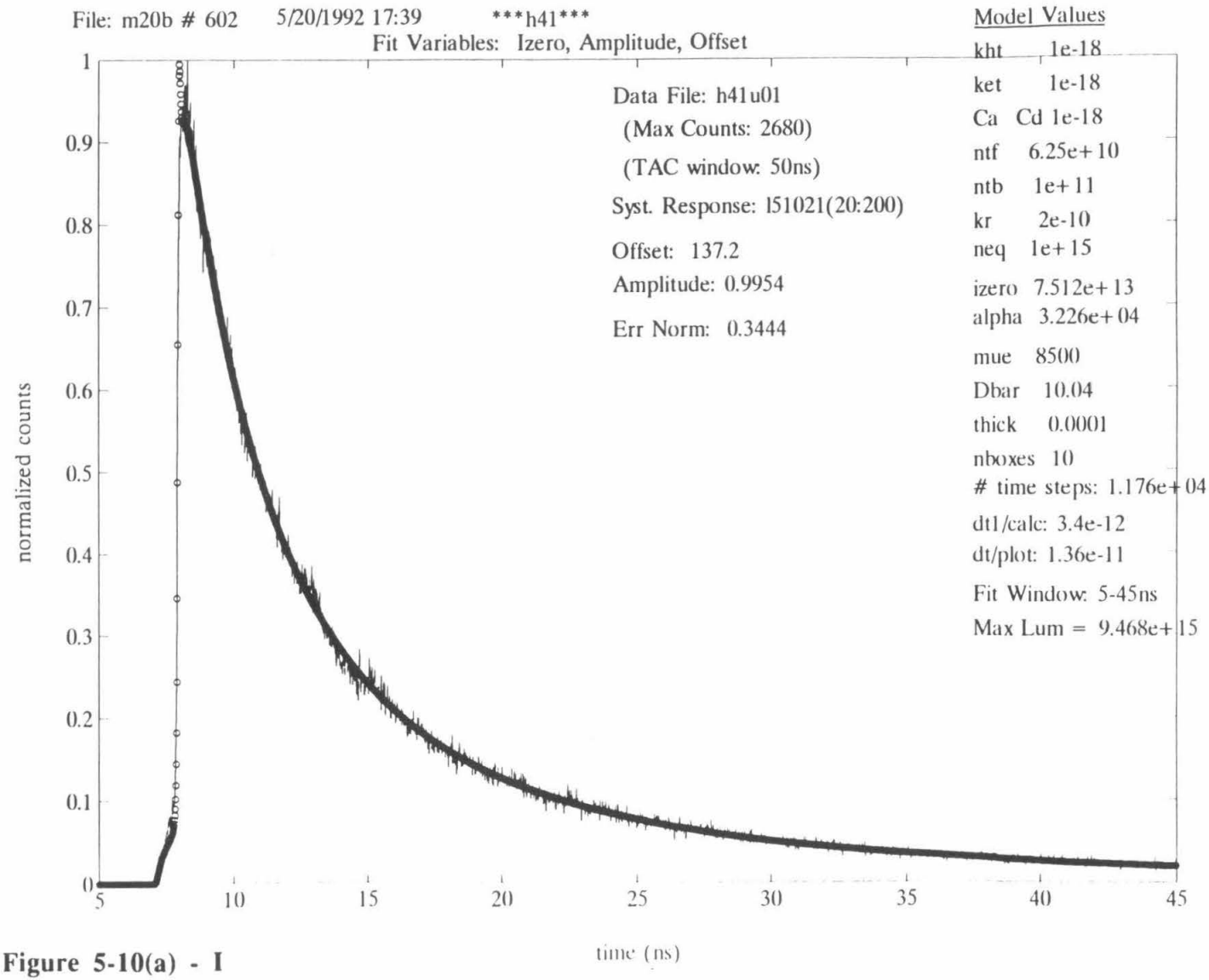

Figure 5-10(a) - I

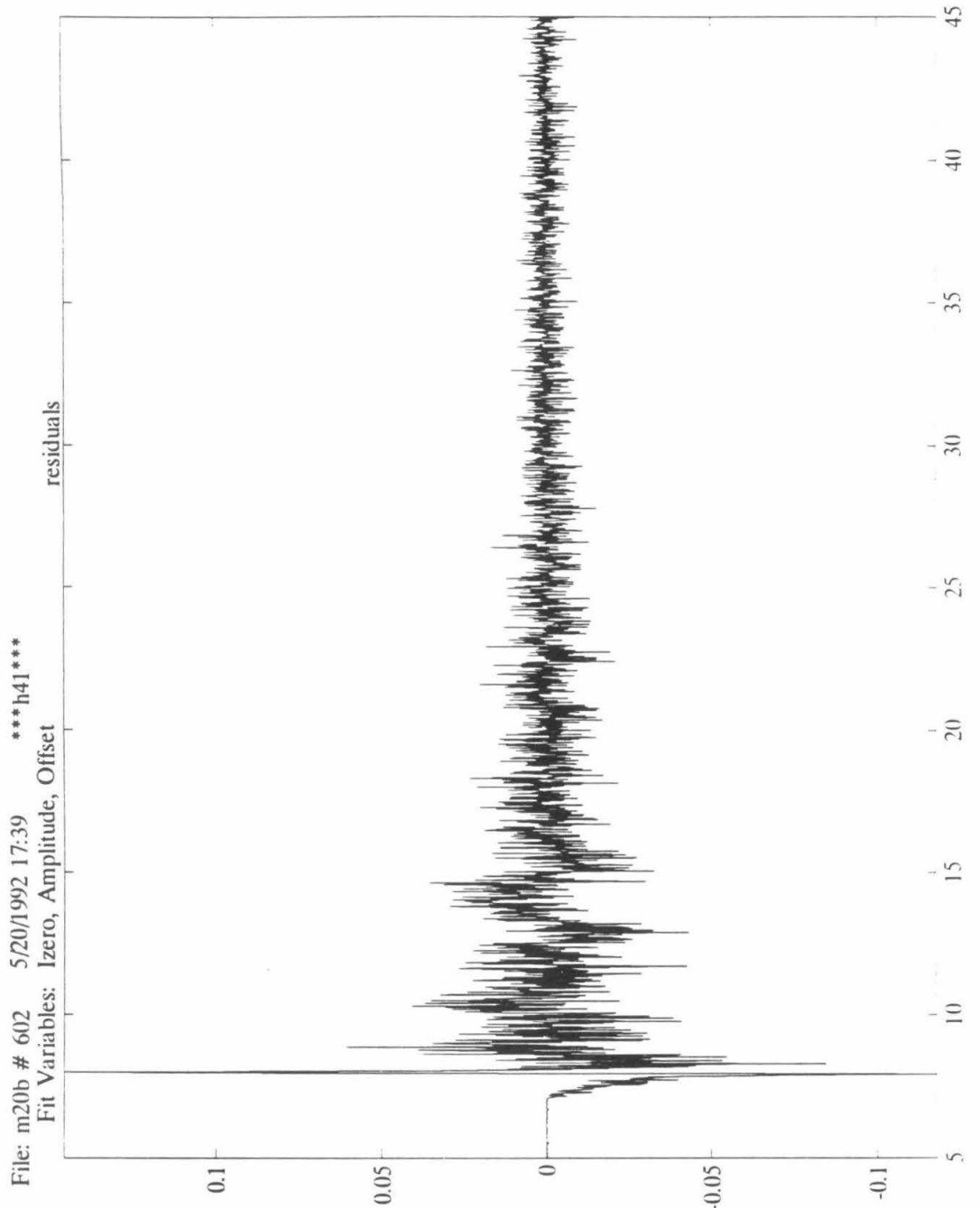

Figure 5-10(a) - II

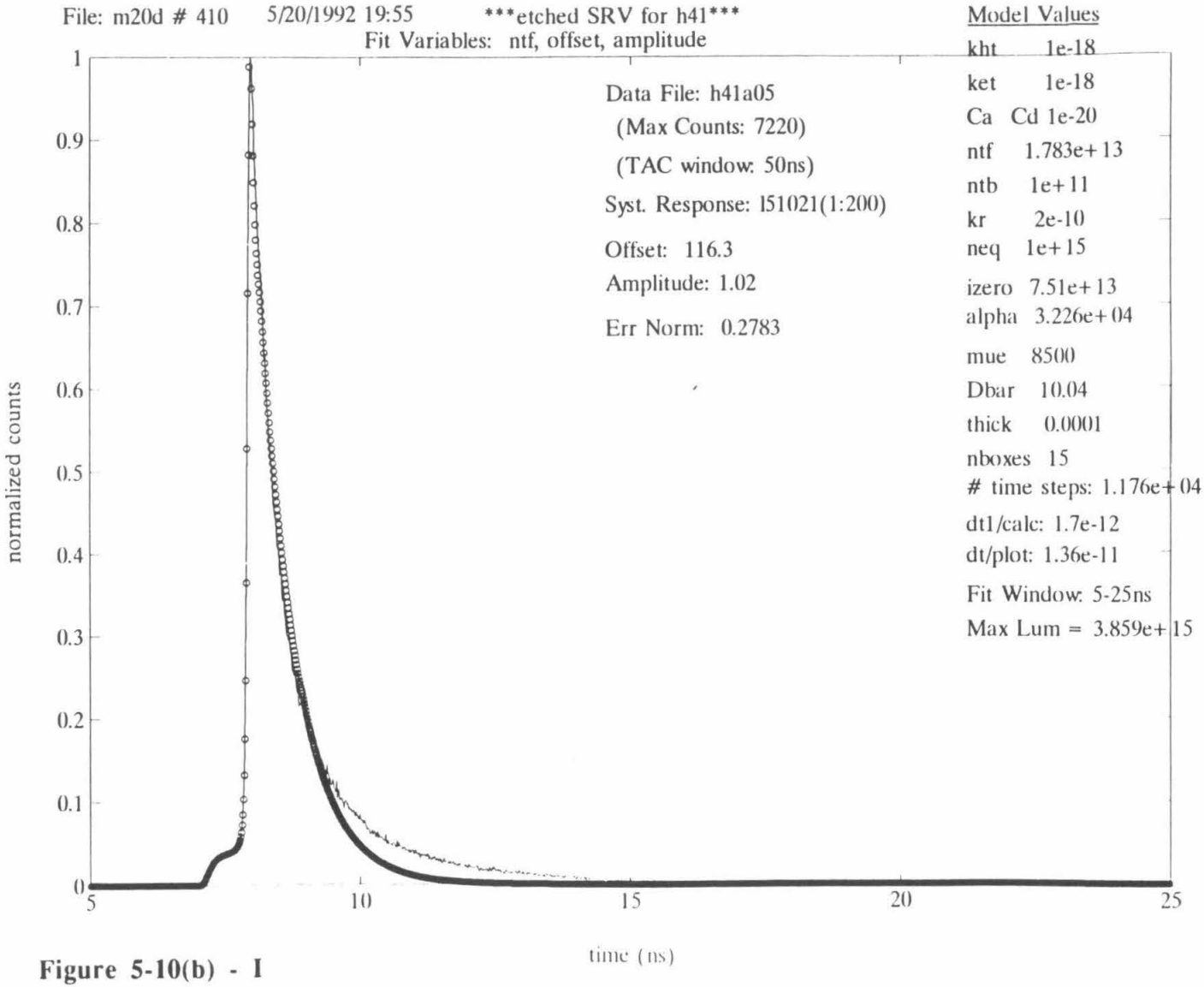

Figure 5-10(b) - I

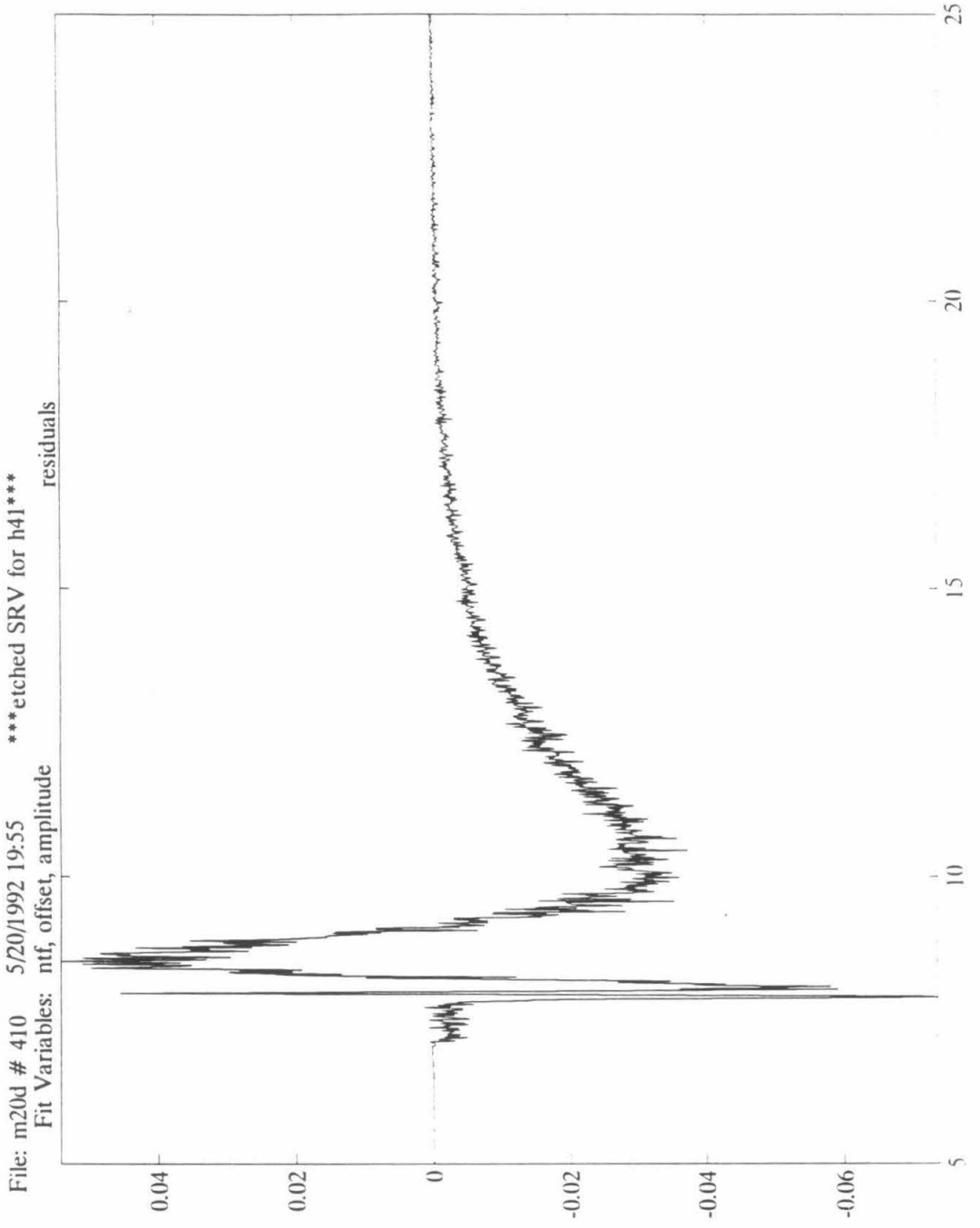

Figure 5-10(b) - II

recombination velocity of $1.8x10^5$ cm/sec. The fit for the Aspnes etched surface just prior to immersion in KOH - Se^{2-} - Se_2^{2-} solutions is shown in Figure 5-10(b).

C. Photoluminescence Decays for GaAs Immersed in Redox Solutions

The remainder of this thesis discusses the decays measured in the presence of redox couple and the attempts to model the results. The bulk of the measurements were made in solutions of the selenide ion redox couple, and these are presented first. Particular detail is given for the first sample discussed under the cobalt heading, since it was felt that this experiment was prototypical of all results obtained. Rather than detailing each of the data sets presented with their individual variations, the results are tabulated by metal, and trends are highlighted.

The results of a cursory examination of GaAs in an acetonitrile/ferrocene solution are also presented. The lifetimes that were measured in solvent alone were very short, and the effects of the redox couple were indeterminate.

Finally, modelling results for selected experiments are presented along with ideas on how the models can be used to explain the data for which no good fits were obtained.

1. Metal Ions on GaAs in Aqueous KOH - Se^{2-} - Se_2^{2-} Solutions

To evaluate the effects of each of the three metals, ruthenium, cobalt and osmium, luminescence decays were measured for freshly etched samples that were immersed in aqueous KOH - Se^{2-} - Se_2^{2-} solutions, both before and after metal ion treatment. In all cases, it was observed that the immersion in KOH - Se^{2-} - Se_2^{2-} solutions resulted in a decay that was longer than that for etched samples in air, while treatment with metals ions caused the decays to get significantly shorter than they were in KOH - Se^{2-} - Se_2^{2-} solutions prior to metal ion treatment.

The primary difficulty in assigning absolute values to the lifetimes is that during data collection the PL lifetimes in KOH - Se^{2-} - Se_2^{2-} solutions, both before and after metal

ion treatment, became longer during data collection and the amount of light emitted increased. It was concluded that photochemistry occurred at the surface, causing a continuous change in the surface being measured. Moving the beam to a fresh point on the surface yielded a decay and count rate identical to the original one, followed by a similar subsequent climb to a higher count rate and a longer lifetime. Moreover, illuminating different spots for the same amount of time resulted in very similar decays and count rates, indicating that the rate of the photochemical change was reproducible. Consequently, the evaluation of lifetimes requires consideration of the length of time over which the data was collected.

To represent the uncertainty in the results, data for several samples are presented in tabular form for each of the metals examined. In these tables, the 1/e lifetimes measured from a graph of the data are reported as a function of the sample treatment. As taken from the graph, they represent the decay time for the counts accumulated during the period of data collection, and are only directly comparable with other decays taken for the same amount of time at the same light intensity. That caveat notwithstanding, these values serve to characterize the decays and are used throughout the discussion.

The data presented was collected both before and after the final optimization of the apparatus in March 1991. While the trends are invariant, the actual lifetimes recorded in the tables partially reflect the difference in time resolution as represented by the different system responses presented in Chapter 4 (Figure 4-6). Three examples of the raw data are presented in graphs for each of the metals studied in order to show the changes that occurred on going from etched to immersion in selenide solutions to metal ion treatment. The reported illumination times were calculated by adding the amount of time it took to collect the decay to the amount of time since the start of the first data set taken at the same point of illumination.

Although the decays for etched samples in air represent a completely different experiment than the decays measured in solutions of the selenide redox couple, they are presented here to provide a further point of comparison between samples, since, all things being equal, an Aspnes etch should leave the surfaces in equivalent starting conditions. In general, a short, 0.50 ns, lifetime is typical of the starting sample under argon, but it was not always fixed at precisely this value. The metal ion treated samples often yielded a lifetime very close to that obtained for the etched sample under argon. It is also of interest to note that in KOH - Se^{2-} - Se_2^{2-} solutions, losses at the surface decrease relative to the sample under argon. Thus, while the presence of the selenide ion acceptor provides a pathway for the consumption of holes, and electrons, it simultaneously reduces the loss of one or the other via surface trapping which occurs outside of KOH - Se^{2-} - Se_2^{2-} solutions.

As noted in the discussion of intensity dependences above, effects of band bending may affect the results for decays measured at low injection. In order to ascertain whether different results would be obtained, one ruthenium experiment at low injection is also presented.

In the figures for the metal ion section which follows, the scheme for symbols is presented in Table 5-III. The data file names recorded in the figure captions and legends identify the experiments in two ways. The first three letters refer to the GaAs sample used. The last three differentiate the experiment; the letter "u" indicates an unetched sample, the letter "a" or "e" means etched, the letter "s" means selenide ion solution, prior to metal ion treatment, and the letters "c", "r" and "o" mean cobalt-treated, ruthenium-treated and osmium-treated, respectively. Additional numbers refer to dates and data set numbers.

Table 5-III. Scheme for symbols used in graphs of metal ion data.

Sample	Graph symbol
unetched samples	solid lines ——
etched samples, under argon	crosses, plusses × +

samples in KOH - Se^{2-} - Se_2^{2-} solutions, no metal ion	lines, dots, open symbols — ·· △ ○ □
samples in KOH - Se^{2-} - Se_2^{2-} solutions, after metal ions	solid symbols ● ■ ▲ ⧗

a. Cobalt

Of the three types of metal ion treatments, cobalt caused the shortest decays and showed the smallest increases in lifetime during data collection. The 1/e lifetimes for each sample are recorded in Table 5-IV.

Prototypical Case, Sample h34

Figures 5-11(a), (b) and (c) serve to illustrate the series of measurements made on all samples to be discussed in this section and also exemplify the photoeffects discussed above. Figure 5-11(a) shows a decay curve from each phase of the experiment. In the order presented in the figure legend they are the first unetched, the final etched, the final KOH - Se^{2-} - Se_2^{2-} solutions, and initial cobalt treated decay curves from the experiment performed on sample h34. Figure 5-11(b) contrasts decays in selenide solutions collected during sequential periods with the last decays for the Aspnes-etched surface under argon. Figure 5-11(c) compares the two traces for the cobalt-treated sample in selenide solutions to the two traces for the final Aspnes-etched surface in air.

In the experiments recorded in Figure 5-11, an initial decay for the unetched GaAs sample was recorded to ascertain the high injection lifetime for the capped sample. (Figure 5-11(a), curve h34u01). The power measured from the dye laser just prior to colletion of this data set was 95 mW, and an optimal system response was recorded (identical to those shown in Figure 4-6(a)). The 1/e lifetime for h34u01 was measured in two separate experiments to be 4.91 ns and the count rate did not vary with time, even after 22 minutes of illumination. The sample was then etched for four minutes in the 0.05% Br_2/CH_3OH

solution; a decay collected for 51 seconds yielded a 1/e lifetime of 4.79 ns. After a fifth minute of bromine/methanol etching there was still no change. After a sixth minute the lifetime dropped to 0.70 ns. After one Aspnes etch, the decay was measured under argon purge and the counts were observed to increase from 800 counts/sec to 1400 counts/sec during the 93 seconds of data collection. The 1/e time for the recorded decay was 0.64 ns. A second decay trace was recorded while illuminating the same spot , and the count rate was found to hold nearly steady at 1600 counts/sec during the 203 seconds of data collection, except that they dropped to about 1100 counts/sec just at the end. The 1/e lifetime was determined to be 0.87 ns, and the data is shown as curve h34a02 in Figure 5-11(a). Selenide solution was then injected into the cuvette from the syringe used to extract it from the storage flask, and the decay was recorded for 15 seconds, during which the count rate increased from 2500 counts/sec to 3000 counts/sec. A second data collection file was started after storing the first as quickly as possible, and the count rate continued to rise from 3000 to 3900 counts/sec. Finally, a third decay was recorded and the count rate continued to climb. An additional neutral density filter was inserted in front of the monochromator, so the absolute value of the count rate is not comparable, but during the collection of the third decay, the count rate climbed from 800 to 1400 counts/sec. The 1/e time taken from each of these curves was 1.70, 2.20, and 3.70 ns respectively. These curves are labelled h34s01, h34s02, and h34s03, respectively, and are shown in Figures 5-11(a) and (b). Under argon purge, the cell was opened, and the sample was removed and soaked in the pH 11 cobalt solution for 60 seconds, rinsed with deionized water, blown dry with nitrogen gas, and reinserted into the selenide solution. The trace labelled h34c01 in Figures 5-11(a) and (c) was collected during 51 seconds of illumination, during which the count rate rose from 2000 to 2800 counts/sec. A repeat data set is shown as h34c02, which was collected for 232 seconds, and during which the count rate rose from 2500 to 3100 counts/sec. The 1/e times for these curves are 0.70 and 0.82 ns, respectively.

Samples h39 and h31

A second and third experiment for the cobalt treated samples are depicted in Figures 5-12 and 5-13, for samples h39 and h31, respectively, and parallel histories are provided in Table 5-IV.

As with h34 described above, the lifetimes for h39 and h31 increased under illumination both before and after metal ion treatment. The two data sets recorded after 30 and 290 seconds of illumination are h39s01 and h39s02 shown in Figure 5-12(a), where it can be seen that the lifetime increases from 1.8 ns to 3.44 ns. After cobalt treatment a decay collected for 1150 seconds shows a lifetime of 0.41 ns, and during the collection, the count rate climbed from 1000 to only 1400 counts/sec.

The results for sample h31 are shown in Figure 5-14(a) and (b). In KOH - Se^{2-} - Se_2^{2-} solutions the curves lengthened from 1.18 ns taken in 16 seconds, to 2.63 ns after collecting for 1031 seconds. The cobalt treatment caused a drop to a lifetime of 0.72 ns, which grew to 0.84 ns after 42 and 232 seconds of collection, respectively.

The cobalt curves h39c02 in Figure 5-12(b) and h3107c03 in Figure 5-13(a) were recorded at different spots on the samples than the the decays recorded before them (h39c01 and h3107c02, respectively) and show that the lifetime collected in a new spot for the same time is reproducible.

As can be seen from the numbers recorded in Table 5-IV, the selenide solution lifetimes all started at about 1.7-1.8 ns as recorded after 15-30 seconds of illumination, and rose to 2.6 to 3.5 ns after more than 10 minutes of illumination. Cobalt ions caused them to drop to lifetimes on the order of 0.70 ns or less and to become very similar to the decays recorded for the Aspnes etched surfaces under argon.

Other data recorded in Table 5-IV, taken in October and November 1990, also had lifetimes of less than 0.8 ns after cobalt treatment, except for sample h22.

Table 5-IV. Summary of experiments for cobalt surface treatment.

Sample	h31	h34	h39	h22	h14	h6
Date	5/7/91	5/10/91	5/13/91	11/6/90	10/23/90	10/14/90
Initial Power	45 mW	95 mW	<80 mW	150 mW	100 mW	100 mW
Comments				Sample previously treated with Os		Sample previously treated with Ru
	Lifetimes	in ns				
Unetched	4.46	4.91	5.26	6.09 (before Os)		
	5.22	4.92				
Bromine (#min etched)	(4 min, new Br)	(4 min, old Br)	(5.5 min new)		(5 min)	
	.85	4.79	.46		.70	
		(2 min more)				
		.70				
Aspnes (cumulative #sec collected)	.75 (465)	.64 (90)	.48 (173)[b]	2.24 (8)	1.46 (41)	
		.87 (301)		2.42 (51)	30 secs more Br_2 1.19	
				1.83 (109) 1.44 (232) 1.11 (305)	1.58 (131)[d]	
Bromine					30 sec more Br_2 1.18	
					1.87 (13)[d]	
					1.38 (117)	
Aspnes						.65
Se (1)	1.81 (16)	1.70 (15)	1.70 (29)	2.27 (9)	1.78 (19)	~.7
(2)	2.63 (1031)	2.20 (96)	3.45 (789)	2.57 (35)	2.54 (193)	
(3)		3.70 (1108)		2.57 (64)		

				3.20 (143) 3.20 (206)		
Co	.72 (42)	.70 (51)	.41 (1150)	.68 (20)	.39 (51)	.48 (34)[c]
	.84 (232)	.82 (292)	.40 (21)[a]	.76 (76)	.43 (834)	.65 (513) 1.24 (2200) .49 (64)[a] .49 (290) .84 (1400)
	.72 (55)[a]					
Aspnes				1.41 (14?)	1.42 (45)[e]	

a) moved spot of illumination.
b) constant count rate.
c) $Co(NH_3)_6$ pH 11 prepared by M. Tan. Surface turned black.
d) Aspnes etched.
e) 82 mW measured at end of experiment.

Figure 5-11(a). PL decays for a prototypical set of experiments on sample h34. Cumulative illumination time given in parenthesis.

h34u01: (912 sec) AlGaAs-capped GaAs. 1/e lifetime is 4.91 ns.

h34a02: (301 sec) Aspnes-etched GaAs under argon. 1/e lifetime is 0.87 ns.

h34s03: (1108 sec) GaAs in KOH - Se_2^{2-} - Se^{2-}, third data set. 1/e lifetime is 3.7 ns.

h34c01: (51 sec) First data set after cobalt ion treatment for GaAs in KOH - Se_2^{2-} - Se^{2-}. 1/e lifetime is 0.70 ns.

Figure 5-11(b). A short PL lifetime measured under argon after etching is compared to the increasingly long decays in KOH - Se_2^{2-} - Se^{2-}.

h34a02: (301 sec) Aspnes-etched GaAs under argon. 1/e lifetime is 0.87 ns.

h34s01: (15 sec) GaAs in KOH - Se_2^{2-} - Se^{2-}, first data set. 1/e lifetime is 1.70 ns.

h34s02: (96 sec) GaAs in KOH - Se_2^{2-} - Se^{2-}, second data set. 1/e lifetime is 2.20 ns.

h34s03. (1108 sec) GaAs in KOH - Se_2^{2-} - Se^{2-}, third data set. 1/e lifetime is 3.7 ns.

Figure 5-11(c). PL decays demonstrating that even after illumination, the cobalt-treated GaAs surface in KOH - Se_2^{2-} - Se^{2-} at a rate similar to that of Aspnes-etched surface under argon.

h34a01: (93 sec) Aspnes-etched GaAs under argon, first data set.

h34a02: (301 sec) Aspnes-etched GaAs under argon, second data set. 1/e lifetime is 0.87 ns.

h34c01: (51 sec) First data set after cobalt ion treatment for GaAs in KOH - Se_2^{2-} - Se^{2-}. 1/e lifetime is 0.70 ns.

h34c02: (292 sec) Second data set after cobalt ion treatment for GaAs in KOH - Se_2^{2-} - Se^{2-}. 1/e lifetime is 0.82 ns.

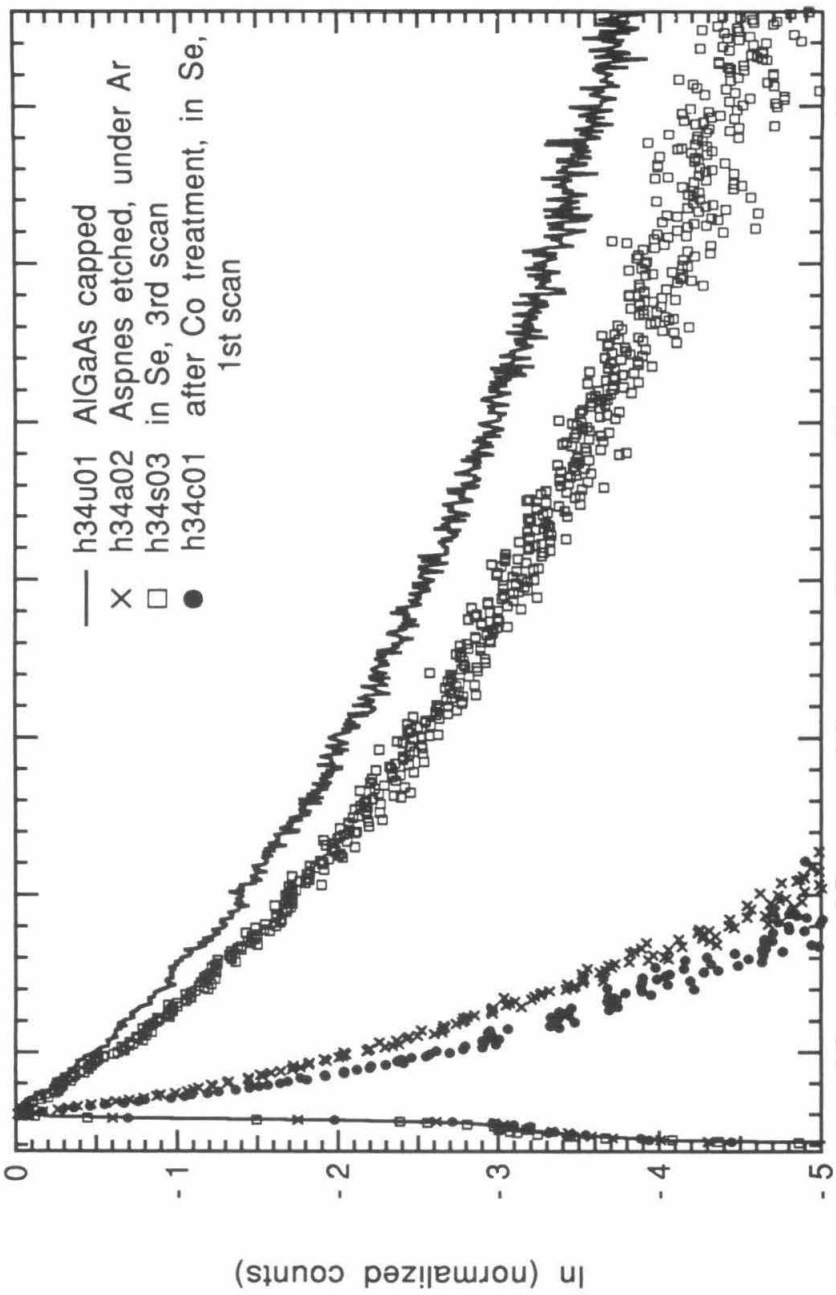
h34u01 AlGaAs capped
h34a02 Aspnes etched, under Ar
h34s03 in Se, 3rd scan
h34c01 after Co treatment, in Se, 1st scan
ln (normalized counts)
time (ns)
0
-1
-2
-3
-4
-5
10
15
20
25
30
35
40

Figure 5-11(a).

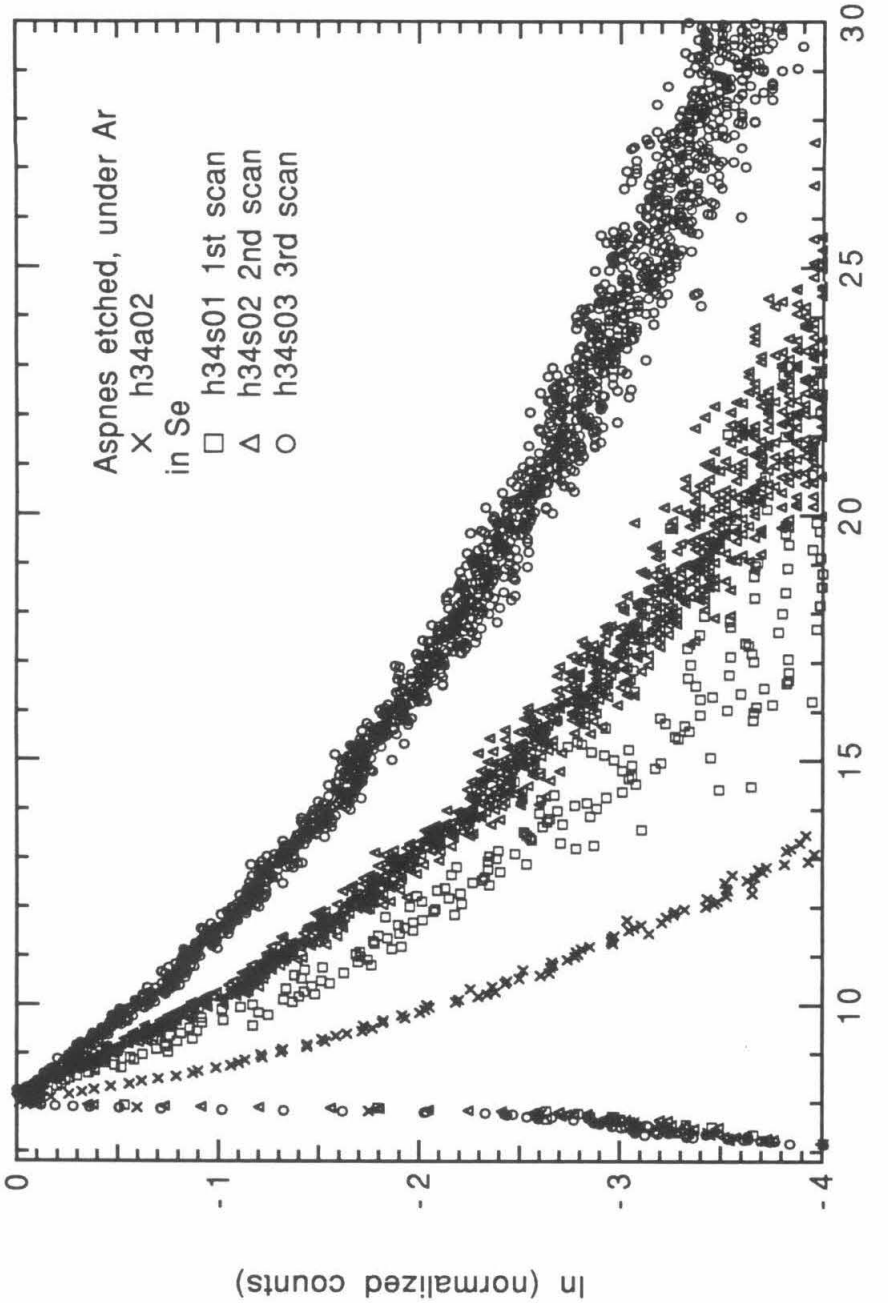
Aspnes etched, under Ar
X h34a02
in Se
□ h34s01 1st scan
Δ h34s02 2nd scan
○ h34s03 3rd scan
ln (normalized counts)
0
-1
-2
-3
-4
10
15
20
25
30
time (ns)

Figure 5-11(b)

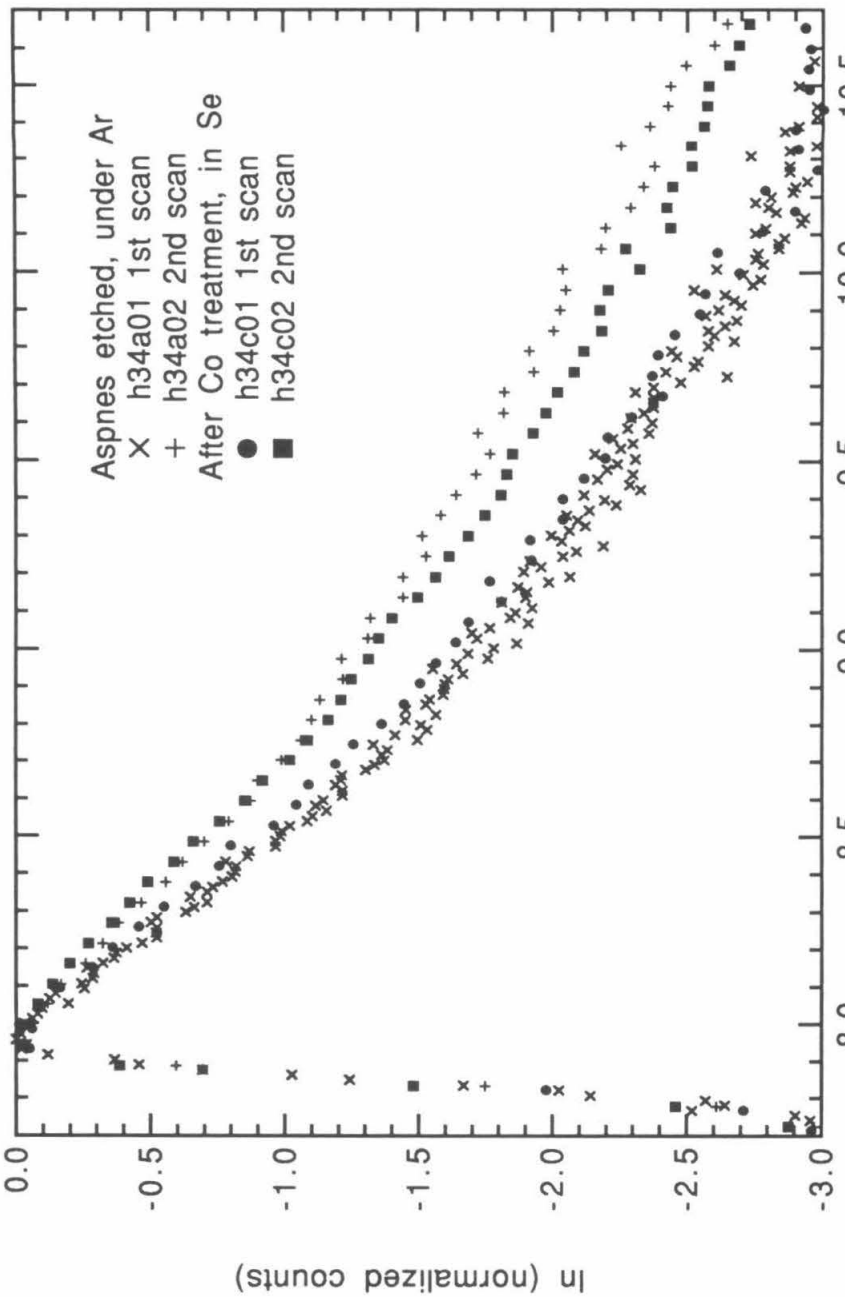
Aspnes etched, under Ar
X h34a01 1st scan
+ h34a02 2nd scan
After Co treatment, in Se
● h34c01 1st scan
■ h34c02 2nd scan
ln (normalized counts)
time (ns)
0.0
-0.5
-1.0
-1.5
-2.0
-2.5
-3.0
8.0
8.5
9.0
9.5
10.0
10.5

Figure 5-11(c).

Figure 5-12(a). PL decays for sample h39. As for sample h34, the lifetime increased in KOH - Se_2^{2-} - Se^{2-}, but dropped to a relatively invariant lifetime after metal ion treatment.

h39s01: (29 sec) GaAs in KOH - Se_2^{2-} - Se^{2-}, first data set. 1/e lifetime 1.78 ns.

h39s02: (789 sec) GaAs in KOH - Se_2^{2-} - Se^{2-}, second data set. 1/e lifetime is now 3.44 ns.

h39c01: (1150 sec) After cobalt ion treatment, first data set. 1/e lifetime 0.41 ns.

h39c02: (21 sec) After cobalt ion treatment, second data set. 1/e lifetime 0.40 ns.

Figure 5-12(b). Cobalt-treated sample in KOH - Se_2^{2-} - Se^{2-} was found to have a slightly shorter lifetime than the etched sample under argon had.

h39a01: (173 sec) Etched sample under argon. 1/e lifetime is 0.48 ns.

h39c01: (1150 sec) After cobalt ion treatment, first data set. 1/e lifetime is 0.41 ns.

h39c02: (21 sec) After cobalt ion treatment, second data set. 1/e lifetime is 0.40 ns.

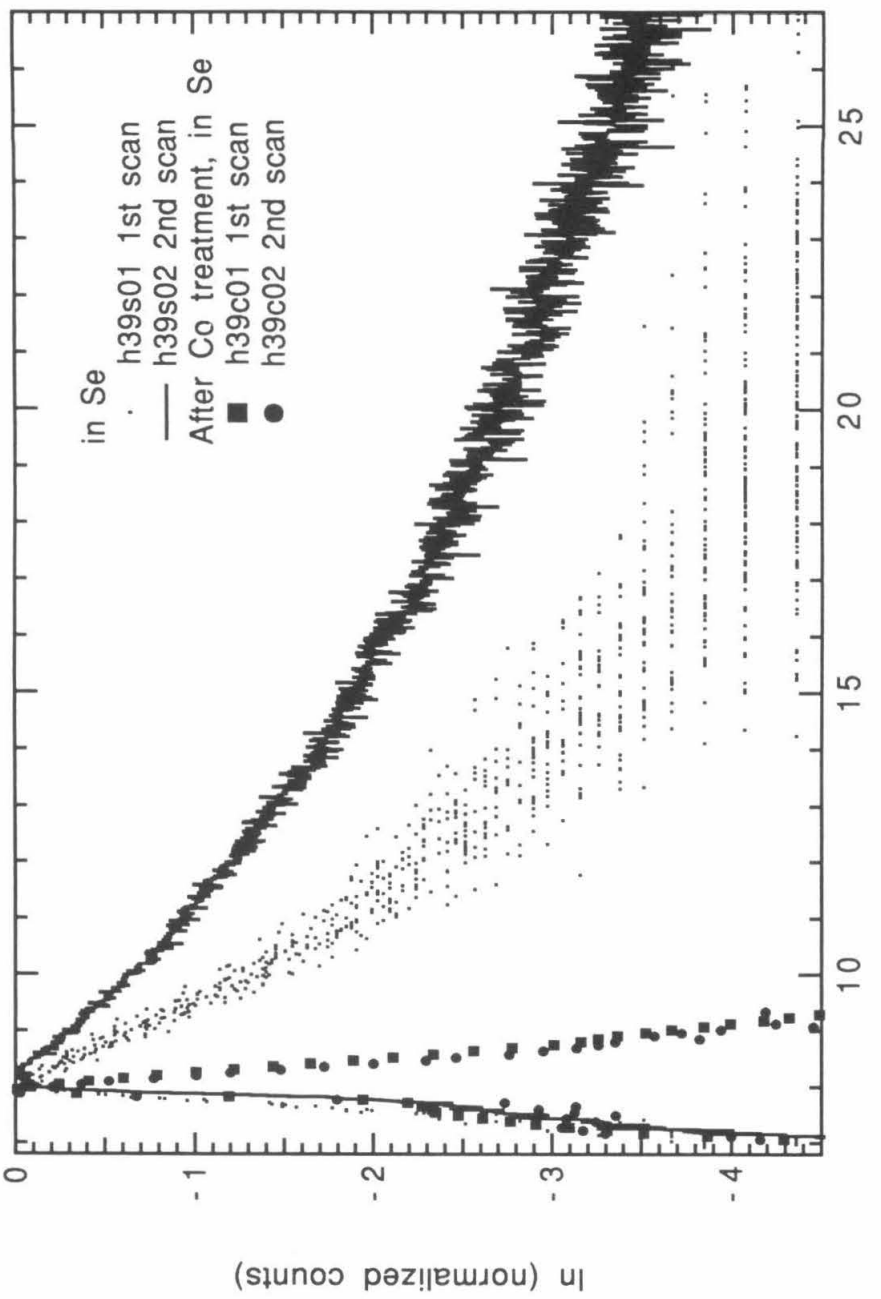
in Se
h39s01 1st scan
h39s02 2nd scan
After Co treatment, in Se
h39c01 1st scan
h39c02 2nd scan
0
-1
-2
-3
-4
10
15
20
25
time (ns)
ln (normalized counts)

Figure 5-12(a).

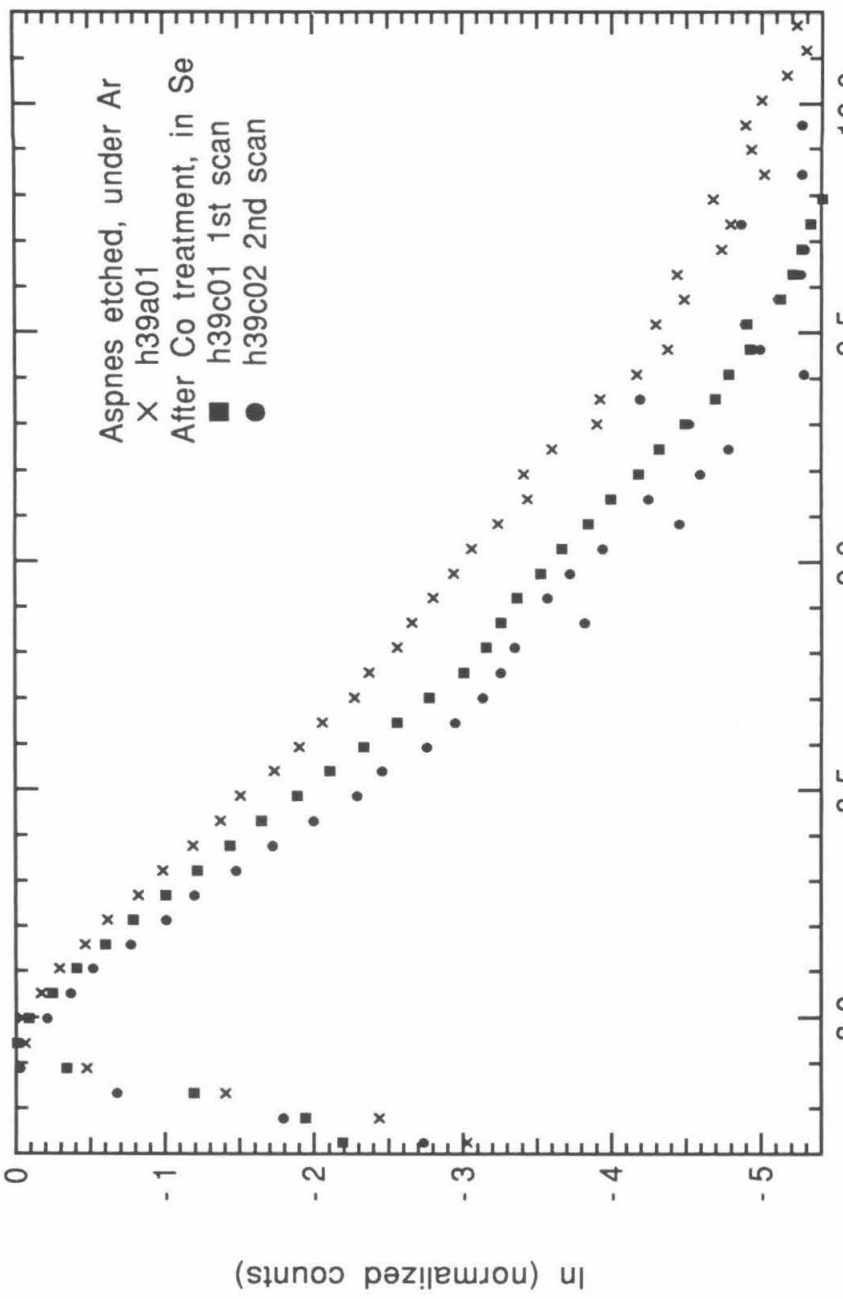
Aspnes etched, under Ar
X h39a01
After Co treatment, in Se
h39c01 1st scan
h39c02 2nd scan
ln (normalized counts)
time (ns)
0
-1
-2
-3
-4
-5
8.0
8.5
9.0
9.5
10.0

Figure 5-12(b).

Figure 5-13(a). PL decays for cobalt-treated sample h31. While in KOH - Se_2^{2-} - Se^{2-} the lifetime increased, but after cobalt treatment, the lifetime is about the same as that for the etched sample under argon.

h3107a01: (465 sec) After Aspnes etch, under argon. 1/e lifetime is 0.75 ns.

h3107s01: (16 sec) GaAs in KOH - Se_2^{2-} - Se^{2-}, first data set.

h3107s02: (1031 sec) GaAs in KOH - Se_2^{2-} - Se^{2-}, second data set.. 1/e lifetime is 2.63 ns.

h3107c03: (55 sec). After cobalt treatment, first data set on a fresh spot of illumination. 1/e lifetime is 0.72 ns.

Figure 5-13(b). The lifetime increases slowly after cobalt treatment and changes from being a slightly faster decay than the etched surface in air to a slightly slower one.

h3107c01: (42 sec) After cobalt treatment, first data set. 1/e lifetime is 0.72 ns.

h3107c02: (232 sec) After cobalt treatment, second data set. 1/e lifetime is 0.84 ns.

h3107c03: (55 sec) After cobalt treatment, first data set for a fresh spot of illumination. 1/e lifetime is 0.72 ns.

h3107a01: (465 sec) After Aspnes etch, under argon. 1/e lifetime is 0.75 ns.

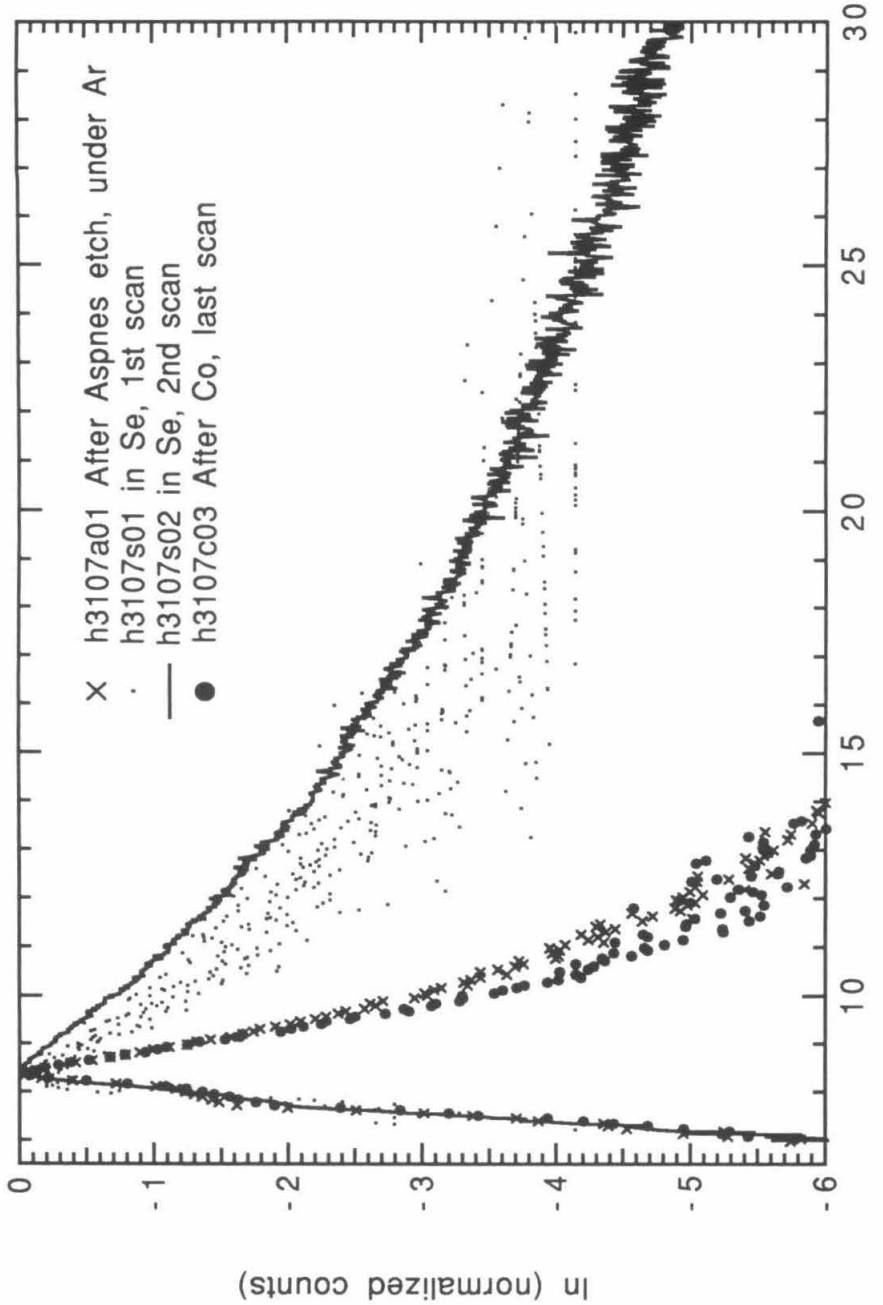
h3107a01 After Aspnes etch, under Ar
h3107s01 in Se, 1st scan
h3107s02 in Se, 2nd scan
h3107c03 After Co, last scan
ln (normalized counts)
time (ns)
0
-1
-2
-3
-4
-5
-6
10
15
20
25
30

Figure 5-13(a).

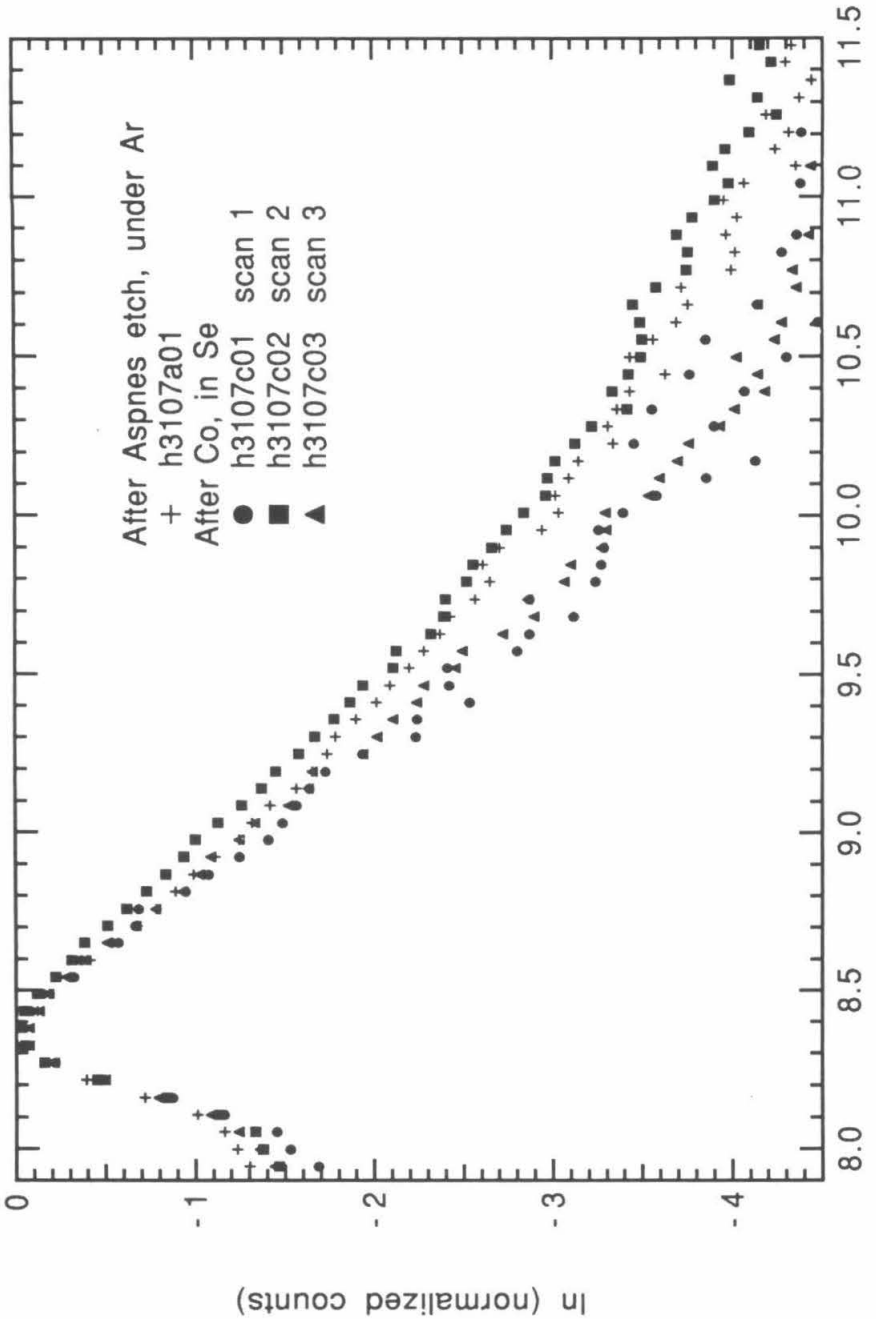
After Aspnes etch, under Ar
+ h3107a01
After Co, in Se
h3107c01 scan 1
h3107c02 scan 2
h3107c03 scan 3
ln (normalized counts)
time (ns)
0
-1
-2
-3
-4
8.0
8.5
9.0
9.5
10.0
10.5
11.0
11.5

Figure 5-13(b).

b. Ruthenium

The lifetimes measured after treatment with ruthenium ion were all longer than those measured for cobalt. The lifetimes also increased during illumination, a greater change in lifetime was observed, which can be attributed to the fact that the lifetimes were originally longer to start with (*i.e.*, they had fewer surface losses).

Sample h38 - High injection

The increases observed for before and after ruthenium treatment for sample h38 are shown in Figure 5-14(a) and the comparison with the etched sample is shown in Figure 5-14(b). A very short lifetime in KOH - Se^{2-} - Se_2^{2-} solution of 0.96 ns was observed in the trace recorded in 14 seconds of data collection as h38s01. After 974 seconds of illumination time, the 1/e time of the final decay was 2.83 ns, and the count rate had risen from 600 counts/sec to 1800 counts/sec. After treatment with ruthenium ion, the decay recorded after 36 ns appears very similar in shape to that recorded after 2044 seconds of illumination for which the 1/e time is 2.29 ns. The count rate during the collection of h38r01 and h38r02 rose only a small amount from 1100 to 1200 counts/sec.

Sample h33 - High Injection

In Figure 5-15(a), the lifetime for sample h33 after etching, and under argon, is seen to increase dramatically from 0.98 to 1.65 ns after 152 and 257 seconds of illumination, respectively. In order to determine whether a limiting lifetime would be reached after long enough illumination, the data was collected on a single spot for almost 4000 seconds. After 28 seconds a 1/e time of 2.23 ns was measured, after 1700 seconds, the lifetime was 5.33, after 2692 it was 5.65, and after 2773, it was still 5.65 ns. As shown in Figure 5-15(b), the limiting lifetime is nearly the lifetime of the unetched sample. The fact that the decay time for the curve shown for the last trace in KOH - Se^{2-} - Se_2^{2-} solution, h33s06, is slightly longer than that of the initial trace for the unetched sample, h33u02, taken two hours previously, may be due to a decrease in incident light due to a

decline over time of the dye laser power, as well as absorption by the selenide solution. The series of decays recorded after ruthenium treatment are shown in Figure 5-15(c). Ruthenium ion shortened the lifetime to 1.95 ns, but the decay again increased to 2.29 ns after 58 seconds of illumination. It plateaued at about 3 ns after 1300 seconds, and a further 2600 seconds of illumination led to an insignificantly longer final lifetime. The laser beam was then moved to a new spot, and after 1543 seconds of illumination, a lifetime of 3.05 ns was again measured, confirming the observation that after 1300 seconds, the limiting lifetime is reached. Thus, it appears that the photomodified surface in selenide solution has a lifetime of 3 ns.

It was observed in several other experiments that the same amount of illumination led to the same lifetimes. Thus, it also appears that the rate of photochemical change causing the increase in lifetime is constant from sample to sample.

Sample h13 - Low injection

Because reports in the literature for the system of interest in this thesis were originally reported for ruthenium treatment, but the opposite results was observed, namely, that metal ions caused a lengthening of the lifetime,[3] these experiments were repeated for light intensities kept in the low-level injection regime. These data were taken using sample h13 and are shown in Figure 5-16. The decay measured in selenide was longer than the decay measured for the etched sample in air and fell to 1/e in 1.44 ns. After ruthenium treatment, the lifetime shortened to 0.67 ns and remained roughly constant under illumination, although it should be noted that the count rate was very low, and changes would have been more difficult to detect than when the level of emitted light was higher. A final Aspnes etch caused the lifetime to return to a longer 1.84 ns lifetime for a decay measured in air. Thus, in the experiment performed here, the effect of the metal ion was found to be same at low-level injection as at high-level injection.

Table 5-V. Summary of experiments for ruthenium surface treatment, Part 1.

Sample	h38	h33	h32	h23		
Date	5/13/91	5/13/91	5/11/91	11/6/90		
Initial Power		80 mW		150 mW		
Comments			Os run first, not rinsed			
Unetched	5.22	5.22	5.09		continued from previous column	continued from previous column
		5.91				
Bromine (#min etched)	5:00	4:00	3:30 0.59	6:20		
Aspnes (cumulative #sec collected)	1.61 (48)	1.40 (110)	.38 (701)	4.04 (78)	1.07 (11)	
Bromine				0:30 0.94		
				0.94		
Aspnes	0.46 (44)	0.98 (152)		0.94 (35)	3.22 (357)	
Aspnes	.53 (114)	1.65 (257)			1.85 (>9)	
	.53 (43)				2.83 (44)	
					3.44 (118)	
					2.78- 3.04? (144)	
Se (1)	.96 (14)	2.23 (28)	2.84 (2187)[c]	1.57 (9)	1.85 (5)	1.57 (12)[b]
(2)	2.83 (974)	5.33 (1700)	3.0 (3056)	1.74 (34)	2.13 (38)	1.57 (52)
(3)		5.65 (2692)	3.39 (1750)	1.94 (181)	~2. (74)	2.89 (323)
		5.65 (2773)				2.89 (349)
Ru	1.46 (36)	1.96 (13)	2.78 (44)	3.09 (14)	2.02 (11)	1.5 (10)
	2.29 (2044)	2.29 (58)	3.68 (390)	3.09 (54)	2.28 (44)	1.72 (43)

		2.39 (101)			2.94 (196)	2.10 (113)
		2.96 (1351)			2.13 (6)	2.10 (174)
		3.05 (4176)			2.22 (36)	
		3.05 (1543)[a]				
		50 mW at end				

a) Moved illumination spot.
b) Aspnes, fresh KOH - Se^{2-} - Se_2^{2-} solution
c) 92 mW, laser unstable

Table 5-V. Summary of experiments for ruthenium surface treatment, Part 2.

Sample	h20	h15	h13	h12	h11	h5
Date	11/1/90	10/24/90	10/23/90	10/18/90	10/18/90	8/3/90
Initial Power	140 mW			93 mW		
Comments			"low injection study"			440 nm excitation
Unetched	6.63	25-28 ns			7.83	59.15
Bromine (#min etched)	(4:00) 6.19	(5:00) 10.64	much etching	(5:00)	(6:30) 1.02	(70)[b] 49.58
			(5:30)			
Aspnes (cumulative #sec collected)		7.83 (21)	1.35 (11)	not recorded		42[c]
			.64 (69)			
Bromine	(10:45) 2.20	(1:30)[d] 7.83		(:30) 1.07		
				.88[e]		
Aspnes	1.60 (276)	1.94 (44)				1.13 (2955)
	1.13 (43)	2.0 (143)	.90[f]			
	.97 (99)	1.8 (499)	.43			
	1.20 (8)[a]	1.81 (222)[g]				
	1.17 (75)[h]					
Se (1)	1.63 (11)	1.46 (24)	1.44 (768)	2.4 (624)[i]	1.49 (54)	1.09 (57)

(2)	1.63 (55)	2.08 (527)				27.6
(3)	2.00 (411)					1.2
						3.3
Ru	1.59 (8)	1.21 (27)	.67 (99)	.84 (14)	.94 (94)	
	2.04 (56)		.7 (1182)	.97 (184)	1.37 (812)	
	2.59 (454)	1.69 (446)	.7 (203)			
					.94 (18)[j]	
					.14 (478)	
Aspnes		1.6? (23)	1.04 (124)	2.09 (59)[k]	.76 (234)[l]	
		find longest spot 2.33	1.12 (912)			
Se					2.26 (7)[m]	
					2.26 (155)	
					2.24	

a) Moved point of illumination.
b) Broken into 5 etches: 12, 10, 10, 10, and 20 sec each.
c) Used HF, also
d) Broken into 2 etches: 1:00 min aged solution, 30 sec fresh solutions
e) Value measured 3 hours later.
f) 85 mW
g) Only used one KOH/Br/KOH cycle
h) 11/6/90 laser power ~100 mW
i) Selenide solution was old.
j) Retreated with ruthenium ion after rinse and dry.
k) Measured in air the following day.
l) Rinsed, dried, and measured in air.
m) Returned to original KOH - Se^{2-} - Se_2^{2-} solution.

Figure 5-14(a). PL decays for ruthenium-treated sample h38. Under illumination both the Se and Ru curves are seen to rise during data collection.

h38s01: (14 sec) GaAs in KOH - Se_2^{2-} - Se^{2-}, first data set. 1/e lifetime is 0.96 ns.

h38s02: (974 sec) GaAs in KOH - Se_2^{2-} - Se^{2-}, second data set. 1/e lifetime is 1.46 ns.

h38r01: (36 sec) After two minutes soak in ruthenium solution, first data set. 1/e lifetime is 1.46 ns.

h38r02: (2044 sec) After ruthenium treatment, second data set. 1/e lifetime is 2.29 ns.

Figure 5-14(b). The decays recorded for the etched samples under argon are shorter than those for ruthenium-treated samples in KOH - Se_2^{2-} - Se^{2-}, both of which are shorter than untreated samples in KOH - Se_2^{2-} - Se^{2-}.

h38s01: (14 sec) GaAs in KOH - Se_2^{2-} - Se^{2-}, first data set. 1/e lifetime is 0.96 ns.

h38s02: (974 sec) GaAs in KOH - Se_2^{2-} - Se^{2-}, second data set. 1/e lifetime is 1.46 ns.

h38a04: (43 sec) After 5 minutes of etching in 0.05% Br_2/CH_3OH, and three Aspnes etches. Showed no increase in count rate or change in lifetime as compared to previous data set. 1/e lifetime is 0.53 ns.

h38r01: (36 sec) After two minutes soak in ruthenium solution, first data set. 1/e lifetime is 1.46 ns.

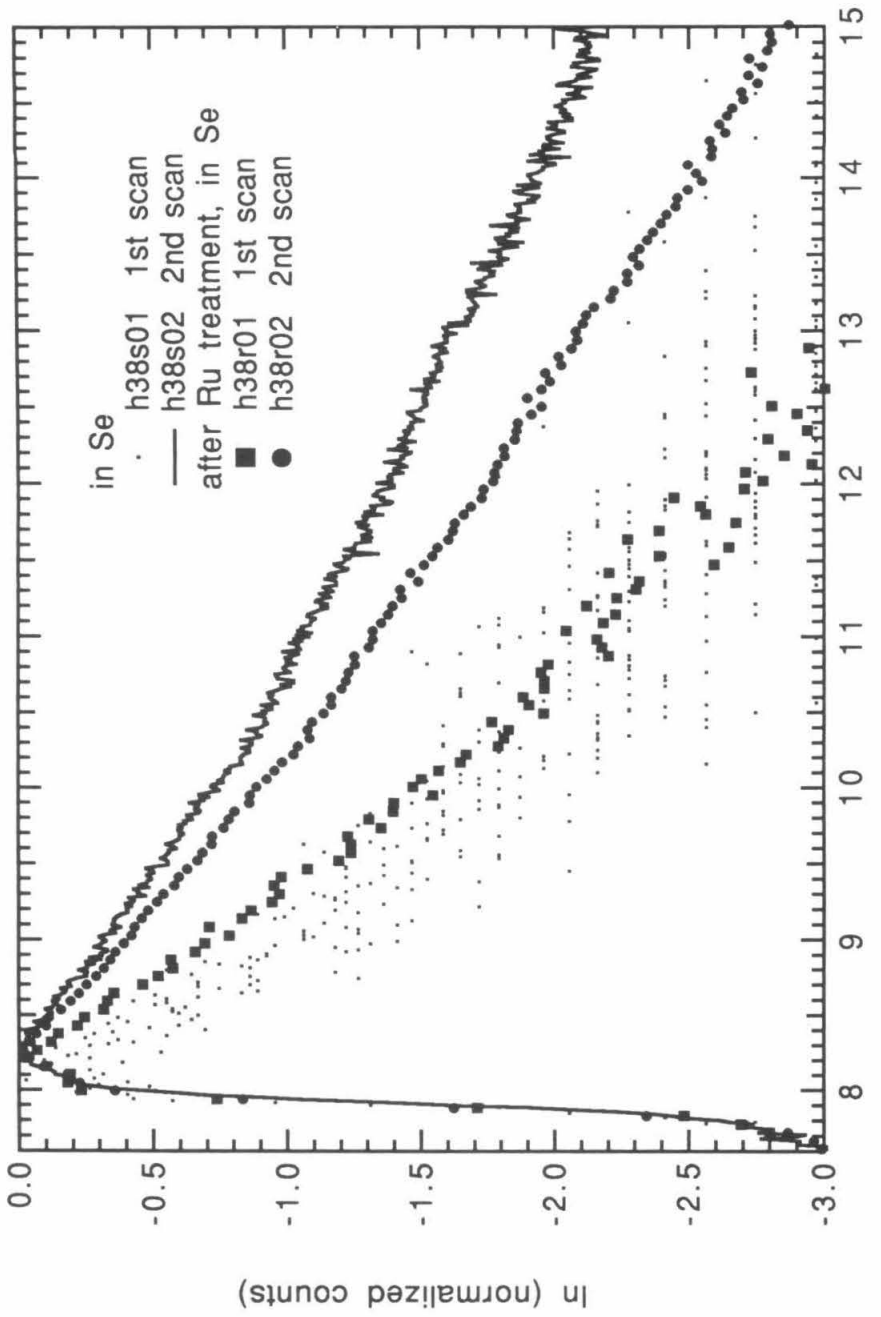
in Se
h38s01 1st scan
h38s02 2nd scan
after Ru treatment, in Se
h38r01 1st scan
h38r02 2nd scan
0.0
-0.5
-1.0
-1.5
-2.0
-2.5
-3.0
8
9
10
11
12
13
14
15
time (ns)
ln (normalized counts)

Figure 5-14(a).

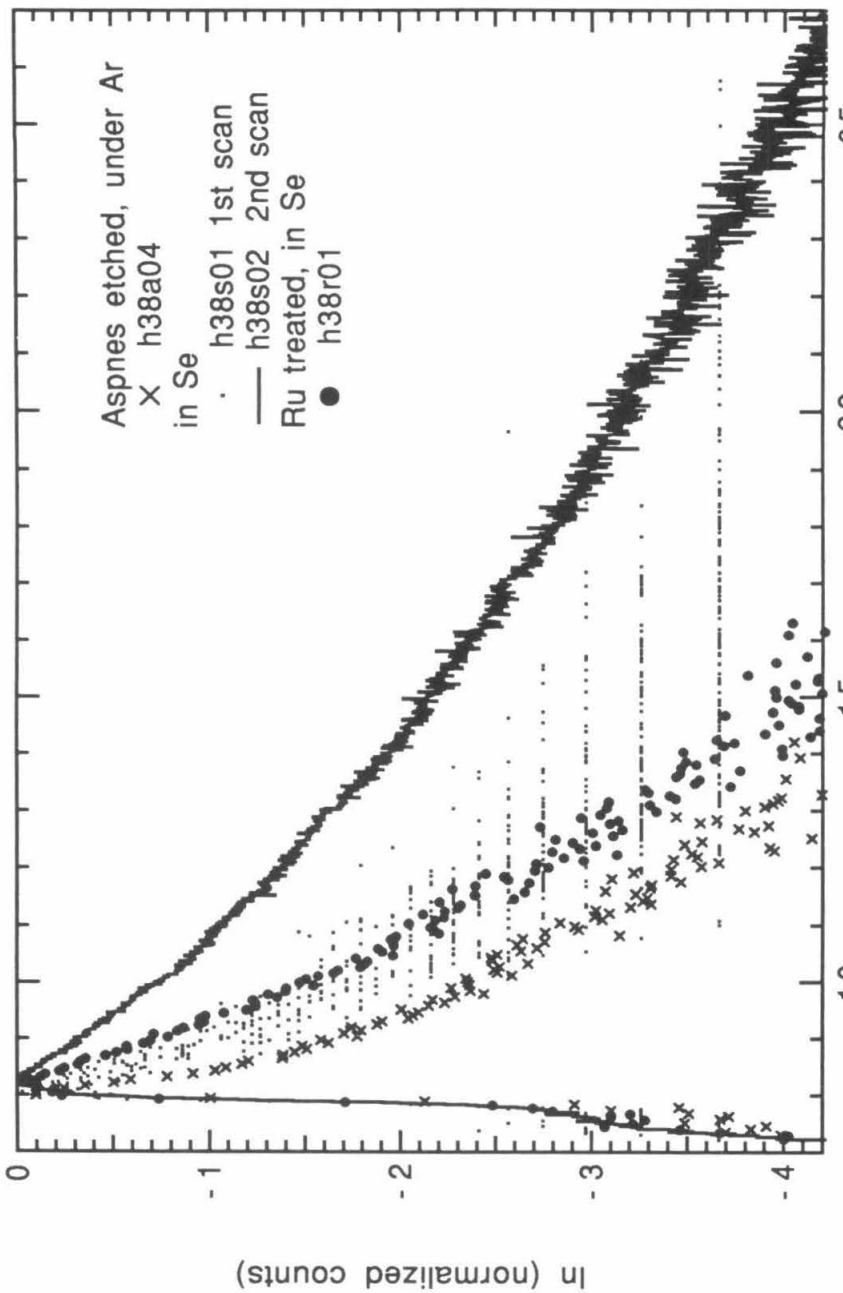
Aspnes etched, under Ar
X h38a04
in Se
h38s01 1st scan
h38s02 2nd scan
Ru treated, in Se
h38r01
ln (normalized counts)
time (ns)
0
-1
-2
-3
-4
10
15
20
25

Figure 5-14(b).

Figure 5-15(a). Lifetimes for both the Aspnes-etched sample under argon and in KOH - Se_2^{2-} - Se^{2-} lengthened during illumination .

h33a01: (152 sec) Aspnes etched, under argon, first data set. The 1/e lifetime was 0.98 ns.

h33a02: (257 sec) Aspnes etched, under argon, second data set.The 1/e lifetime is 1.65 ns.

h33s01: (28 sec) GaAs in KOH - Se_2^{2-} - Se^{2-}, first data set. The 1/e lifetime is 2.23 ns.

h33s02: (1700 sec) GaAs in KOH - Se_2^{2-} - Se^{2-}, second data set. The 1/e lifetime is 5.33 ns.

h33s03: The data collection for this file was appended to the counts in h33s02. Additional counts were collected for 3987 seconds. The final lifetime was still 5.33 ns.

Figure 5-15(b). After lengthening initially, the decays for untreated GaAs in KOH - Se_2^{2-} - Se^{2-} stayed constant during the last three data sets. The ruthenium-treated sample had a fixed lifetime that did not change under illumination.

h33s03: (2692 sec) Further data collection at same point as for data set h33s02 on sample immersed in KOH - Se_2^{2-} - Se^{2-} . The 1/e lifetime is 5.65 ns.

h33s05: (2773 sec) Further data collection at same point as for data set h33s03 on sample immersed in KOH - Se_2^{2-} - Se^{2-} . Same lifetime as h33s03.

h33s06: (6987 sec) Further data collection at same point as for data set h33s03 on sample immersed in KOH - Se_2^{2-} - Se^{2-} . Same lifetime as h33s03.

h33r01: (13 sec) After ruthenium treatment, first data set. 1/e lifetime is 1.96 ns.

h33r02: (58 sec) After ruthenium treatment, second data set. 1/e lifetime is 2.22 ns.

h33r03: (101 sec) After ruthenium treatment, third data set. 1/e lifetime is 2.39 ns.

Figure 5-15(c). Over the course of 30 minutes, the lifetime for the ruthenium-treated sample changed slowly from 1.96 ns as measured from the first data set to 3.05 ns as measured on the last data set.

h33r03: (101 sec) After ruthenium treatment, third data set. 1/e lifetime is 2.39 ns.

h33r04: (1351 sec) After ruthenium treatment, fourth data set. 1/e lifetime 2.96 ns.

h33r07: (4176 sec) After ruthenium treatment, sixth data set. 1/e lifetime 3.05 ns.

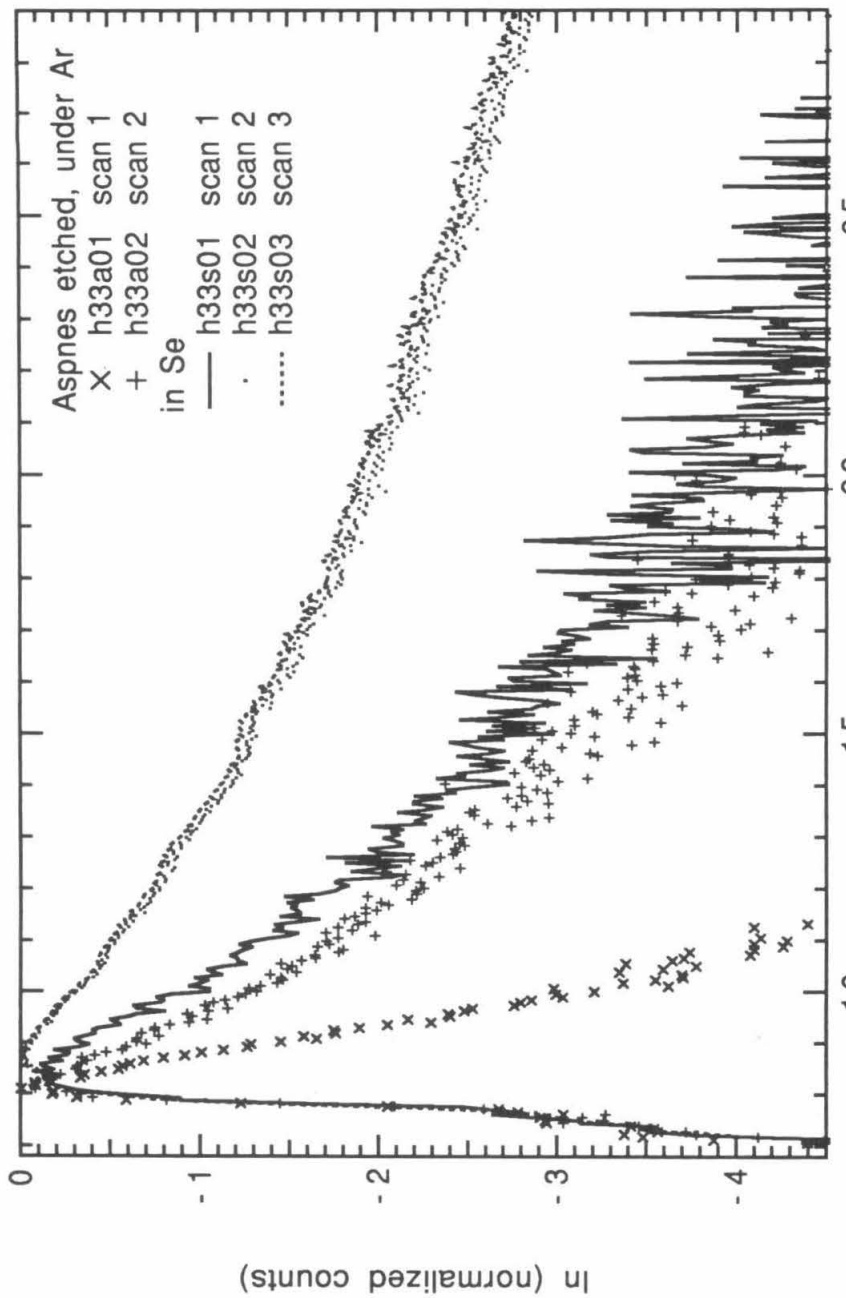
Aspnes etched, under Ar
X h33a01 scan 1
+ h33a02 scan 2
in Se
h33s01 scan 1
h33s02 scan 2
h33s03 scan 3
ln (normalized counts)
0
-1
-2
-3
-4
10
15
20
25
time (ns)

Figure 5-15(a).

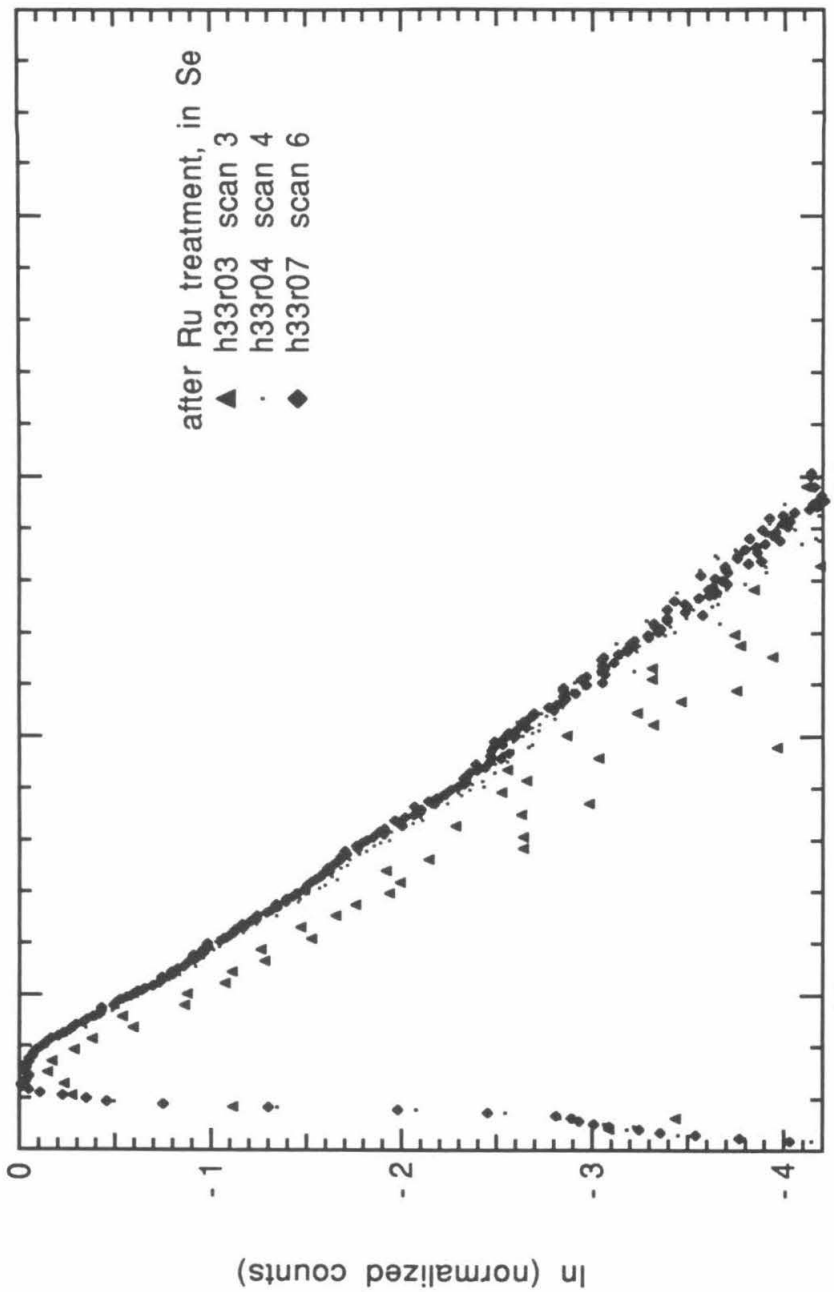
after Ru treatment, in Se
h33r03 scan 3
h33r04 scan 4
h33r07 scan 6
0
-1
-2
-3
-4
10
15
20
25
time (ns)
ln (normalized counts)

Figure 5-15(c).

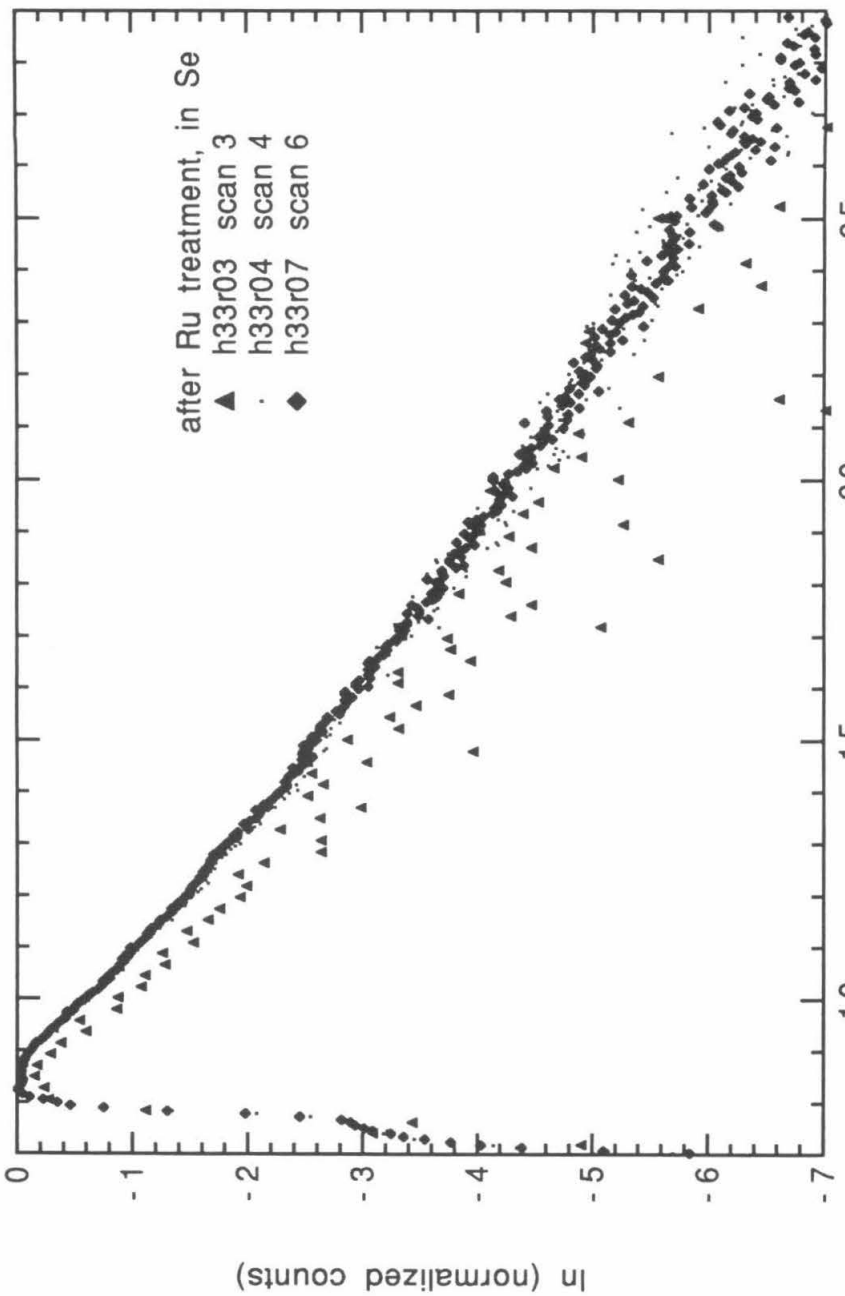
after Ru treatment, in Se
h33r03 scan 3
h33r04 scan 4
h33r07 scan 6
ln (normalized counts)
time (ns)
0
-1
-2
-3
-4
-5
-6
-7
10
15
20
25

Figure 5-15(c).

Figure 5-16. Low-injection PL decays for ruthenium-treated GaAs in KOH - Se_2^{2-} - Se^{2-} . The ruthenium-treated surface had a constant lifetime during 20 minutes of illumination.

h1323s01: (768 sec) GaAs in KOH - Se_2^{2-} - Se^{2-} . 1/e lifetime is 1.44 ns.

h1323r01: (99 sec) After ruthenium treatment, first data set. 1/e lifetime is 0.67 ns.

h1323r02: (1182 sec) After ruthenium treatment, second data set. 1/e lifetime is 0.7 ns.

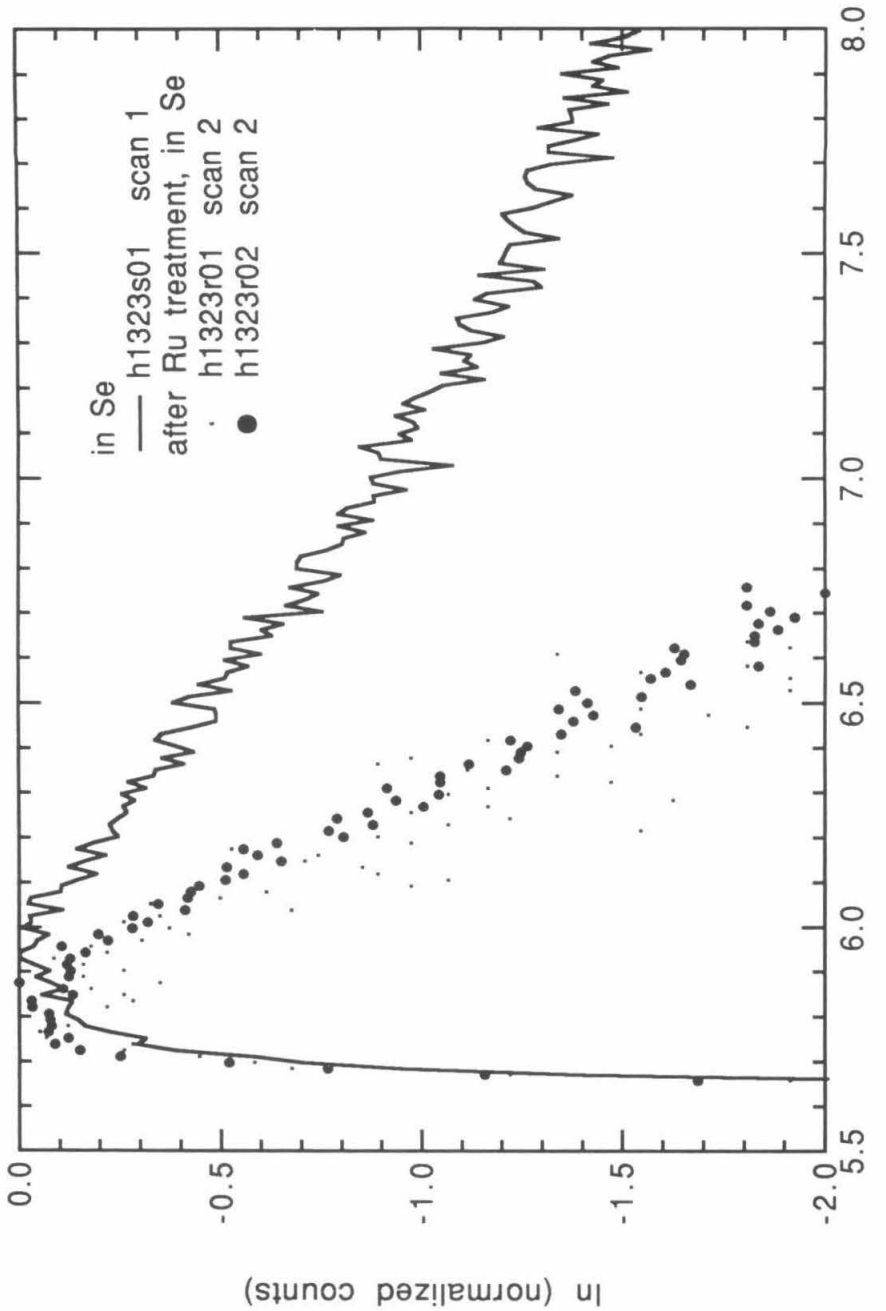
in Se
h1323s01 scan 1
after Ru treatment, in Se
h1323r01 scan 2
h1323r02 scan 2
ln (normalized counts)
time (ns)
0.0
-0.5
-1.0
-1.5
-2.0
5.5
6.0
6.5
7.0
7.5
8.0

Figure 5-16.

c. Osmium

Osmium also caused an initial shortening of the lifetime which rapidly returned to a long lifetime, more characteristic of lifetimes in KOH - Se^{2-} - Se_2^{2-} solutions prior to metal ion treatment. Overall, the lifetimes measured from decays collected for less than one minute are very similar to those collected for ruthenium for less than one minute. They appear to have returned to long decays more quickly than the ruthenium treated surfaces did, however.

Sample h32

Starting from an Aspnes etched surface with a 1/e lifetime in air of 0.38 ns, sample h32 had an initial lifetime in selenide solution of 3.39 ns, after 1750 seconds of counting. After osmium treatment the counts started at 1800 and climbed to 220 during 26 seconds of counting, and the lifetime measured from the recorded curve is 2.18 ns. The counts continued to climb, and the second curve, stopped after 401 seconds of illumination had a lifetime of 3.74 ns. A further 3000 seconds of counting raised it negligibly to 3.9 ns, which was shorter than the initial 5.1 ns lifetime for the capped sample, but longer than the original decay recorded in KOH - Se^{2-} - Se_2^{2-} solution. The selenide solution curve and the three traces recorded after osmium treatment are shown in Figure 5-17.

Sample h37

For sample h37, the lifetimes are different, but the pattern is the same. As depicted in Figure 5-18, the final selenide solution lifetime was 3.55 ns after 839 seconds of counting. The 1/e lifetime for the first recorded osmium decay was 1.20 ns, although the counting statistics for the 5 seconds of data collection cannot be assumed to be highly accurate. The measured lifetime climbed to 2.83 ns after 1764 seconds of illumination. Figure 5-18(a) shows the luminescence decay from the final Aspnes etched surface under argon (h37a08), the two data sets taken for the sample immersed in KOH - Se^{2-} - Se_2^{2-}

solution, and the first data set recorded after osmium treatment. Figure 5-18(b) shows the ever-increasing lifetime for the sample after osmium treatment.

Sample h41

Finally, in Figure 5-19, the final data set in KOH - Se^{2-} - Se_2^{2-} solution, followed by two data sets after osmium treatment are shown for sample h41. The lifetime for the pre-treatment data set is 2.35 ns after 288 seconds of illumination; the two osmium data sets are very similar in shape to the selenide solution data set, although the 1/e values measured from the linear plots are 1.90 and 2.36 ns respectively. The decay from the final Aspnes etched surface is also shown for comparison.

Table 5-VI Summary of experiments for osmium surface treatment.

Sample	h32	h37	h41	h21	h17
Date	5/11/91	5/11/91	5/11/91	11/6/90	10/24/90
Initial Power	76 mW		84 mW		end at 35 mW
Comments					
	Lifetimes	in ns			
Unetched	5.09	5.31	4.5	7.18	14.0
Bromine (#min etched)	(3:30) .59	(6:00)	(5:15)	(7:15)	(5:30) 1.33
Aspnes (cumulative #sec collected)	.38 (701)	1.35 (77)	3.92 (28)	3.19 (86)	1.83 (114)
		.64 (69)			
		1.02 (214)			
		.47 (108)			
		.87 (~150)			
Bromine		(0:45) 1.02	(1:00) 1.5-3.2?	(1:20) 1.65	
		.83	1:00 1.23	1.34	
Aspnes		.82 (45)	.73 (56)	1.34 (51)	

			.63 (469)[a]	break .97 (63)	
				1.24 (545)[e]	
Se (1)	2.84 (2187)	3.26 (635)	1.77 (30)	Counts climb ↓	1.22 (136)
(2)	3.00 (3050)	3.55 (839)	1.85 (147)	2.28 (14)	2.53 (747)
(3)	3.39 (1750)[b]		2.33 (351)	2.48 (59)	
			1.52[a],1.62	1.63 (152)	
			2.35 (288)	2.48 (177)	
				2.33 (228)	
				2.87 (507)	
Os	2.18 (26)	1.20 (5)	1.90 (145)[c,d]	1.54 (8)	1.22 (36)
	3.74 (401)	1.68 (88)	2.36 (32)	1.74 (35)	2.07 (275)
	3.74 (1011)	2.48 (706)		~1.9 (65)	3.24 (647)
	3.90 (4243)[g]	2.83 (1764)		~2.0 (100)	1.22 (34)[a]
				2.94 (332)	
				1.41 (7)[a]	
Aspnes					1.24 (23)
					1.63 (82)
					.79[f]

a) Illumination spot moved.
b) Laser adjusted to 111 mW.
c) 84 mW measured.
d) Laser spike in data removed.
e) 1/2 Aspnes only.
f) Data taken 10/28/90
g) 90 mW at end

Figure 5-17. PL decays for osmium-treated GaAs. After the osmium treatment, the decays get longer, and the final decay for the osmium-treated sample is longer than longest decay prior to osmium treatment.

h32s05: (1750 sec) GaAs in KOH - Se_2^{2-} - Se^{2-} . 1/e lifetime is 3.44 ns.

h32o01: (26 sec) After osmium treatment, first data set. 1/e lifetime is 2.18 ns.

h32o02: (401 sec) After osmium treatment, second data set. 1/e lifetime is 3.74 ns.

h32o04: Concatenated counts onto h32o03 (not shown). Total collection for 3190 seconds. 1/e lifetime is 3.90 ns.

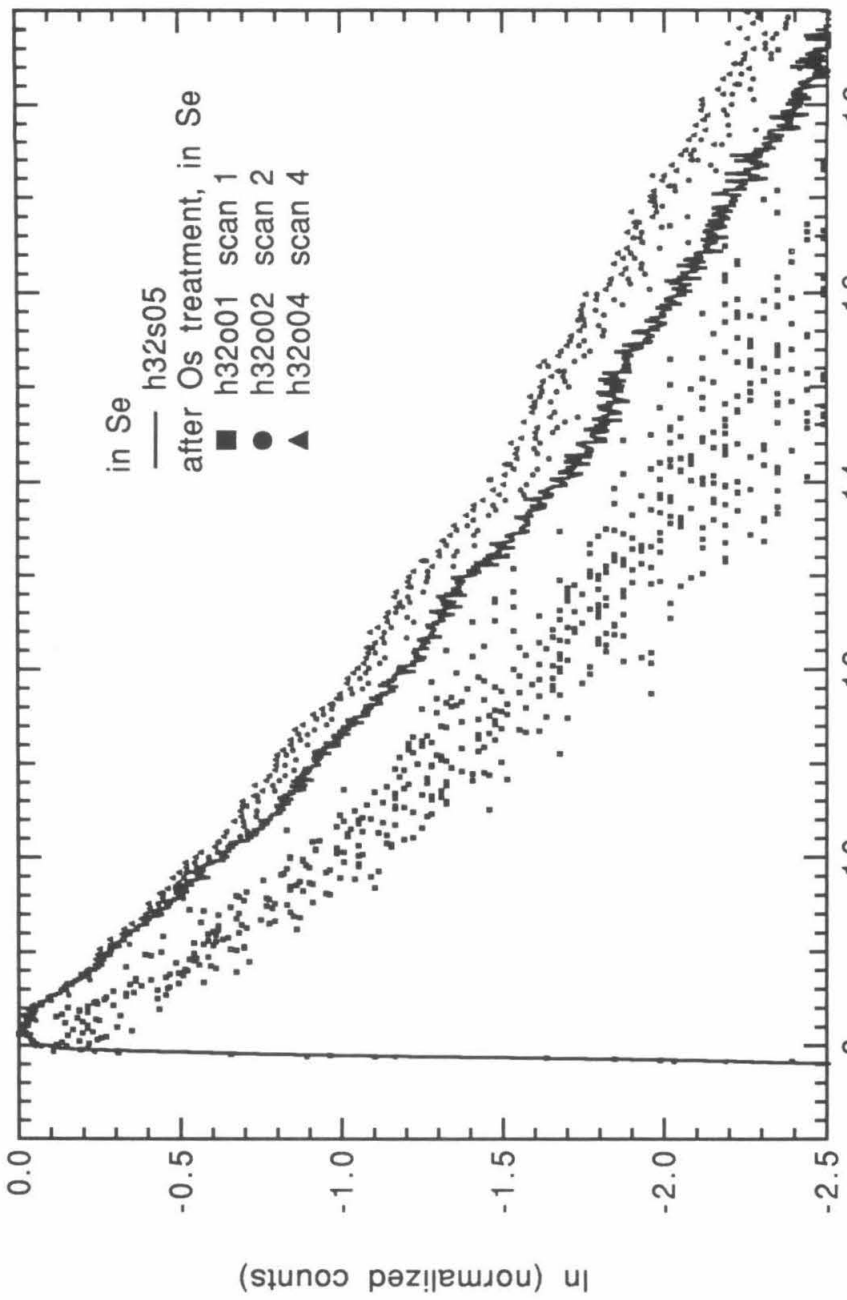
in Se
h32s05
after Os treatment, in Se
h32o01 scan 1
h32o02 scan 2
h32o04 scan 4
0.0
-0.5
-1.0
-1.5
-2.0
-2.5
8
10
12
14
16
18
ln (normalized counts)
time (ns)

Figure 5-17.

Figure 5-18(a). PL decays for osmium-treated GaAs. The etched and osmium-treated samples have similar lifetimes, and the untreated sample in KOH - Se_2^{2-} - Se^{2-} is long.

h37a08: (45 sec) New data set for an Aspnes-etched sample under argon. 1/e lifetime is 0.82 ns which is the same as the data set prior to the Aspnes etch.

h37s01: (635 sec) GaAs in KOH - Se_2^{2-} - Se^{2-} , first data set. 1/e lifetime is 3.26 ns.

h37s02: (839 sec) GaAs in KOH - Se_2^{2-} - Se^{2-} , second data set. 1/e lifetime is 3.55 ns.

h37o01: (5 sec) After osmium treatment, first data set. 1/e lifetime is 1.20 ns.

Figure 18(b). After osmium treatment, the GaAs PL decay becomes increasingly longer under illumination.

h37o01: (5 sec) After osmium treatment, first data set. 1/e lifetime is 1.20 ns.

h37o02: (88 sec) After osmium treatment, second data set. 1/e lifetime is 1.68 ns.

h37o03: (706 sec) After osmium treatment, third data set. 1/e lifetime is 2.48 ns.

h37o04: Concatenated onto h37o03. Counted for an additional 1654 seconds. 1/e lifetime is 2.83 ns.

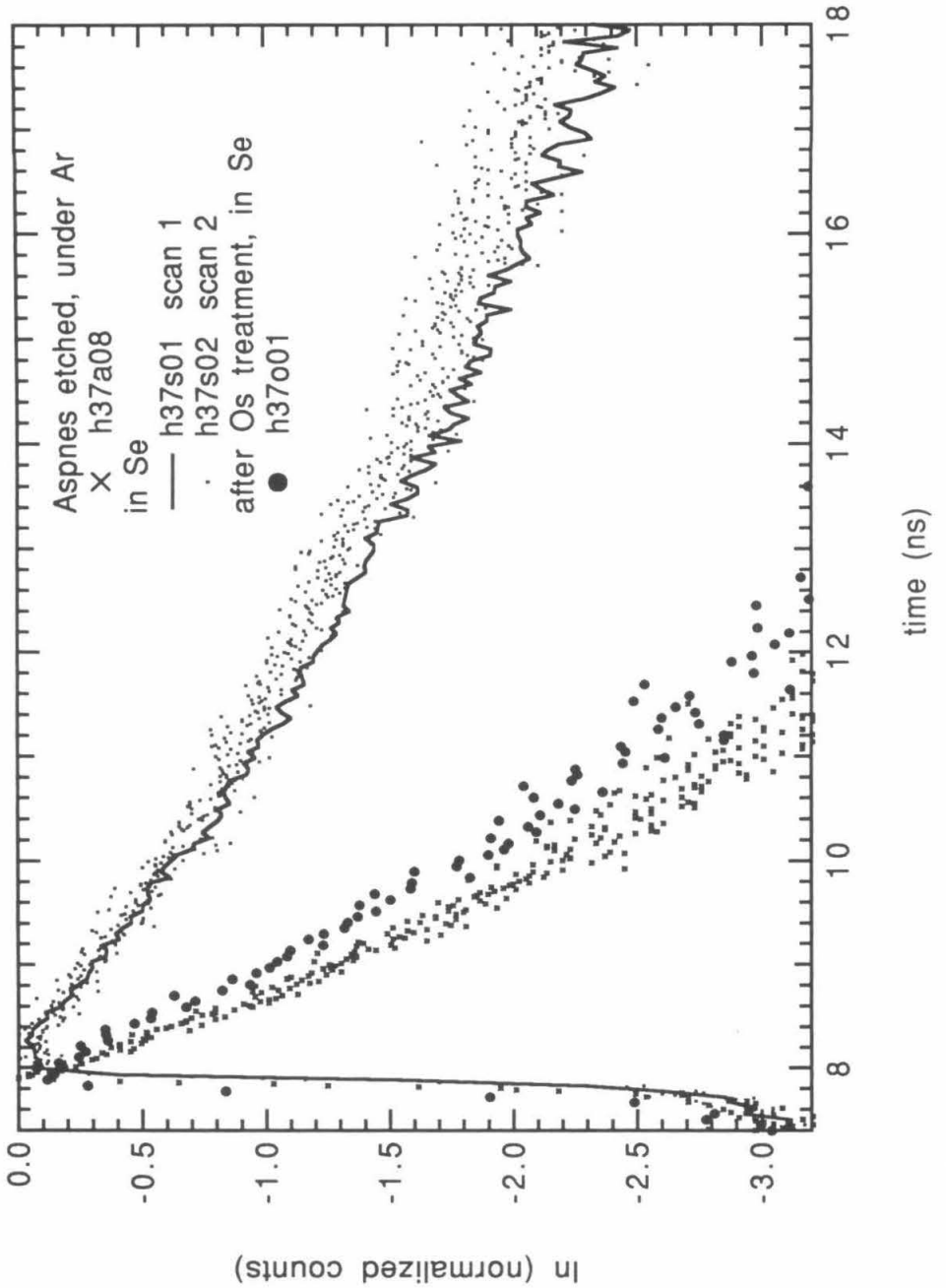
Aspnes etched, under Ar
X h37a08
in Se
h37s01 scan 1
h37s02 scan 2
after Os treatment, in Se
h37o01
ln (normalized counts)
0.0
-0.5
-1.0
-1.5
-2.0
-2.5
-3.0
8
10
12
14
16
18
time (ns)

Figure 5-18(a).

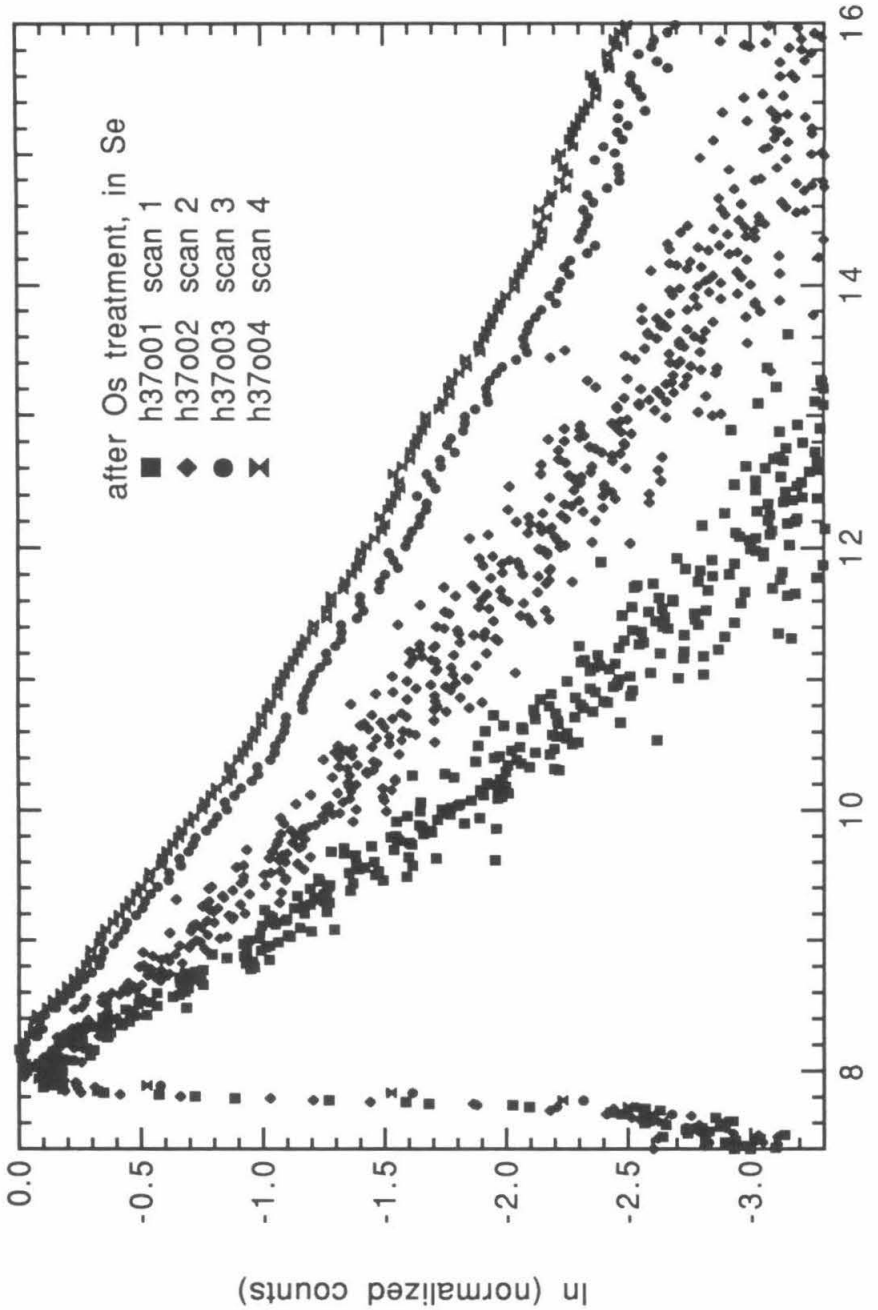
after Os treatment, in Se
h37o01 scan 1
h37o02 scan 2
h37o03 scan 3
h37o04 scan 4
0.0
-0.5
-1.0
-1.5
-2.0
-2.5
-3.0
8
10
12
14
16
time (ns)
ln (normalized counts)

Figure 5-18(b).

Figure 5-19. PL decays for osmium-treated GaAs. After osmium treatment, the observed lifetime was similar to that observed prior to osmium treatment.

h41a05: (469 sec) After repeated Aspnes' etches, under argon 1/e lifetime is 0.63 ns.

h41s08: (288 sec) GaAs in KOH - Se_2^{2-} - Se^{2-} , first data set for this spot of illumination. 1/e lifetime is 2.35 ns.

h41o01: (145 sec) After osmium treatment, first data set. 1/e lifetime is 1.91 ns.

h41o02: (32 sec) After osmium treatment, first data set at a new spot. 1/e lifetime is 2.36 ns.

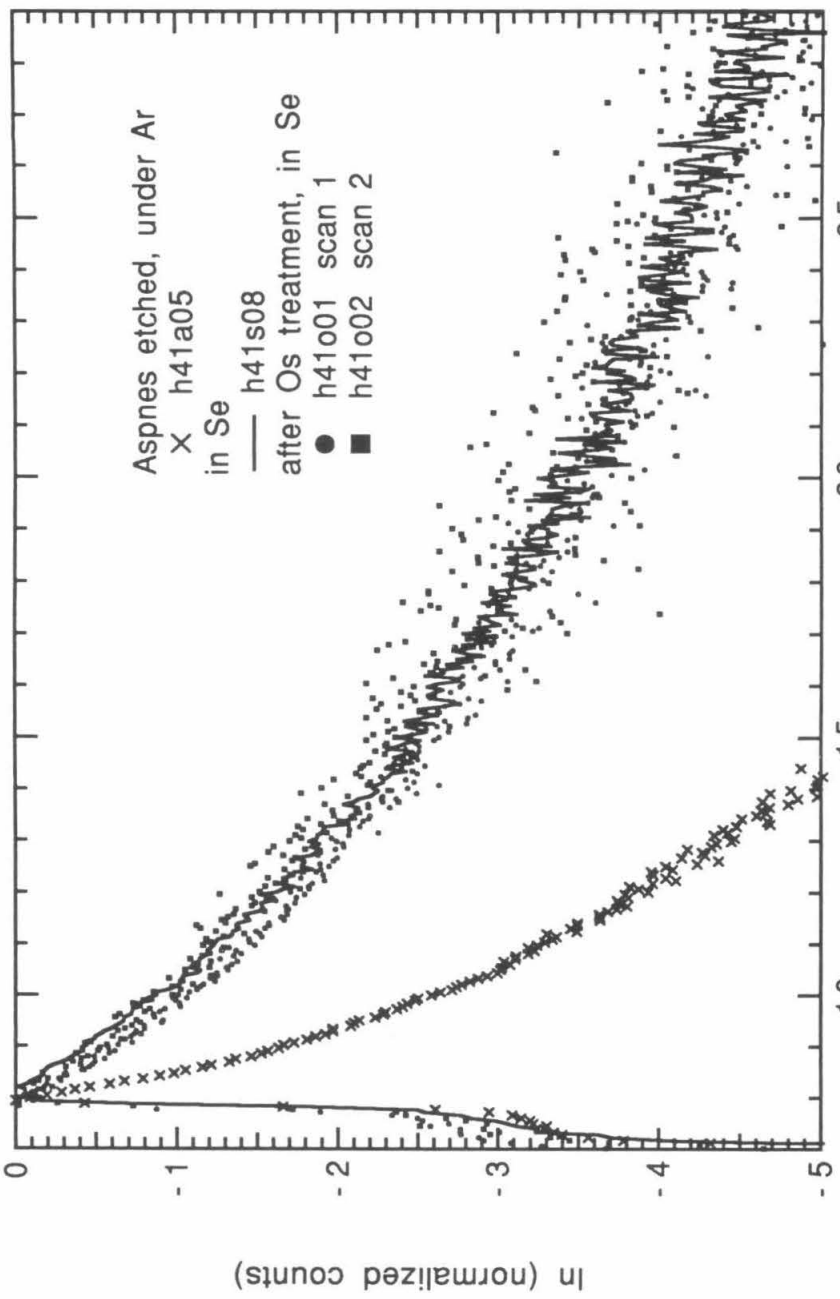
Aspnes etched, under Ar
X h41a05
in Se
h41s08
after Os treatment, in Se
h41o01 scan 1
h41o02 scan 2
0
-1
-2
-3
-4
-5
10
15
20
25
time (ns)
ln (normalized counts)

Figure 5-19.

2. GaAs in Ferrocene/Acetonitrile Solutions

Finally, in the interest of determining whether this technique is sensitive to the effects of a redox couple such as ferrocene in a nonaqueous solvent where GaAs is not subject to photocorrosion, preliminary experiments were performed for GaAs in a dimethylferrocene-acetonitrile solution without electrolyte. The results are presented in Table 5-VII and Figures 5-20 and Figure 5-21. After 6 minutes of etching with bromine and 3 Aspnes etches, the curve designated h42e03 in Figure 5-20 was taken, and found to have a 1/e time of 1.48 ns, which is significantly longer than had been previous recorded for any etched surface. This suggests that the point where this decay was measured was not completely AlGaAs free. However, a decay was then recorded for a sample in dry acetonitrile in a cell prepared in the nitrogen glove box. The lifetime shortened to that shown in the curve labelled h42ac01, which has a 1/e time of 0.60 ns. The cell was returned to the glove box, and several grains of ferrocene and ferrocenium (in about a 10 to 1 ratio) were added to the solution. The count rate for the initial data set, h42f01, started at 800 counts/sec and climbed rapidly to 2600 counts/sec. Each of two successive data sets continued to climb, although they appear to have plateaued with about the same decay as seen in the acetonitrile solution originally. However, the curve shapes in solutions with and without the redox couple are significantly different.

In work performed in January 1990, an experiment was performed to test whether the effects of metal ions on the decays in the ferrocene/acetonitrile systems could be discerned. In steady-state current voltage experiments, no catalytic effects have been observed for this redox system,[4] but it was thought that if it does affect the hole transfer rate in this system, the perturbations to the carrier concentration might be detectable in the photoluminescence decay. The decay was first measured after Aspnes etching is shown in Figure 21(b), curve g5j29a7. It was taken into a nitrogen glove box and inserted in a cell containing a CH_3CN-0.7 **M** $LiClO_4$ -1 **mM** - dimethylferrocenium - 0.1 **M**

dimethylferrocene solution, and several decays having very low count rates were recorded. The count rate climbed slightly during data collection. The last data set, collected for 1410 seconds is shown in Figure 5-21(a), Curve g5j29f5. The electrode was soaked in the Ru(III) solution for 30 seconds and reinserted into the cell, and the data sets g5j29r1, g5j29r2, and g5j29r4 of Figures 5-21(a) and (b) were recorded at one spot. Although the data has a great deal of scatter, the counts clearly climbed higher, and the lifetimes got longer. At a new spot, shown in g5j19r5, data was collected for 34 seconds, and has a slightly shorter lifetime, which proceeds to lengthen again, until the third data set, g5j29r7, at which point the illumination time was 297 seconds. The sample was removed from solution and reetched using the Aspnes procedure. The final decay for the sample, in air, was very similar to the last couple of data sets taken in solution. A system response taken at this time, lj29n5, is shown for comparison in Figure 5-21(a). The experiment was repeated on the same sample in June 1990, at a lower intensity, except only dimethylferrocenium was added to the acetonitrile. It was only possible to conclude that samples in acetonitrile decay almost, if not, as fast, as those immersed in a solution of dimethylferrocenium, with or without ruthenium ions. The resolution of these experiments was poor, so it is not possible to state with assurance that the ruthenium resulted in a faster surface capture velocity. It is believed, however, that further investigations using the more highly optimized TCPC system currently available are warranted.

Table 5-VII. Summary of experiments for GaAs in dimethylferrocene/ acetonitrile solutions.

Sample	h42	g5	more g5	
Date	5/13/91	1/29/90	5/31/90	
Initial Power				
Comments		Yariv sample PMT detection	Low Injection	Continued from previous column
Unetched	5.44	6.01		
Bromine (#min etched)	(4:00)	(40 sec HF)[a] 1.13		
Aspnes (cumulative #sec collected)		1.87	1.56	
Bromine	(2:00)			
Aspnes				
2nd Aspnes	3.92 (27)			
	4.13			
	(1:00 Br) 1.87 2.18			
	1.48			
ACN	.60 (417)		1.05	
Fc		1.4	1.05	
Fc/Fc^+	.43 (35)		1.05	
	.68 (76)			
	.75 (526)			
Ru		1.04	1.70	.37
		1.39		
		1.89		
		2.02		
		1.56		
		1.83		Aspnes 2.0
		1.96 2.02		

a) Cap on Yariv material is etched by HF.

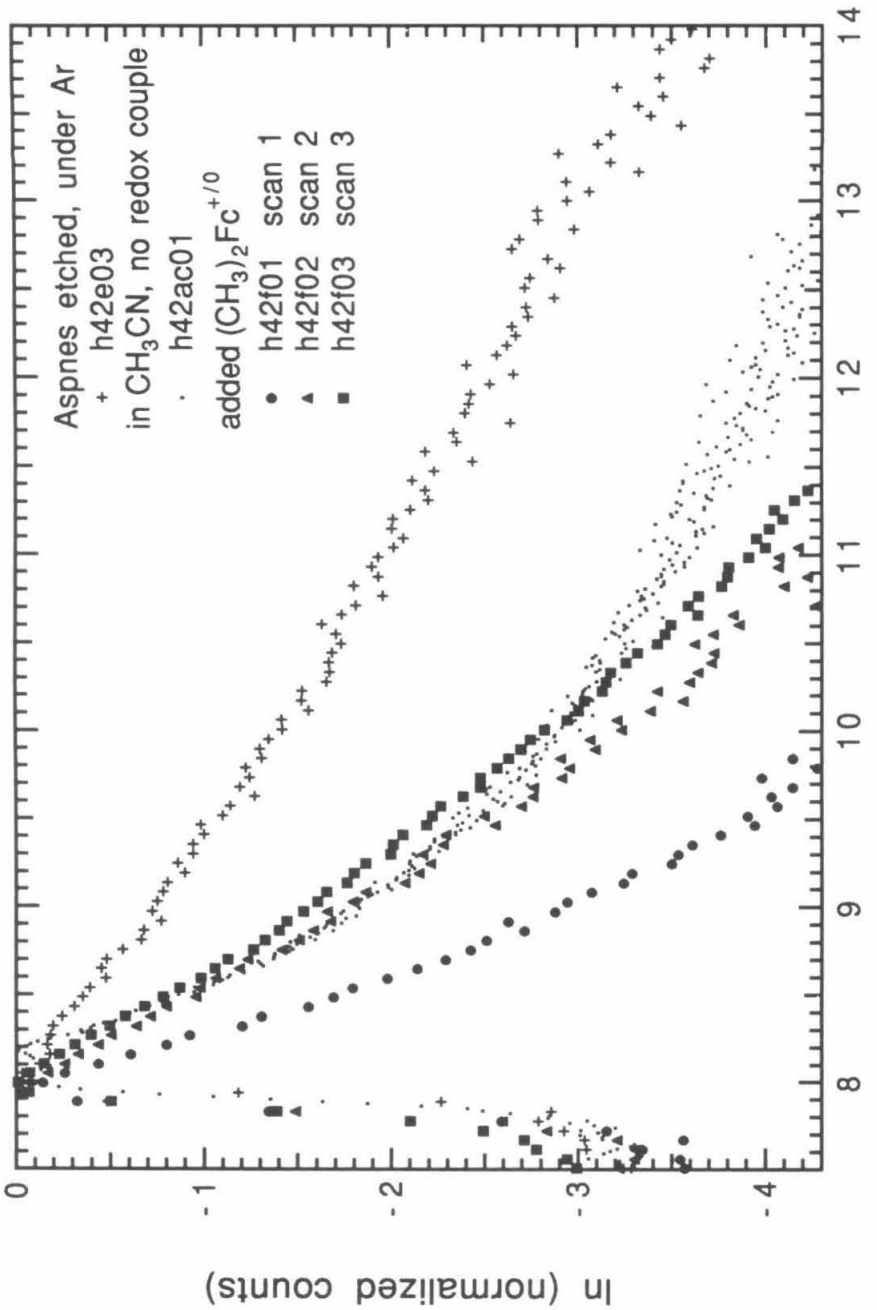

Figure 5-20. PL decays for GaAs in dimethylferrocene/acetonitrile solutions.

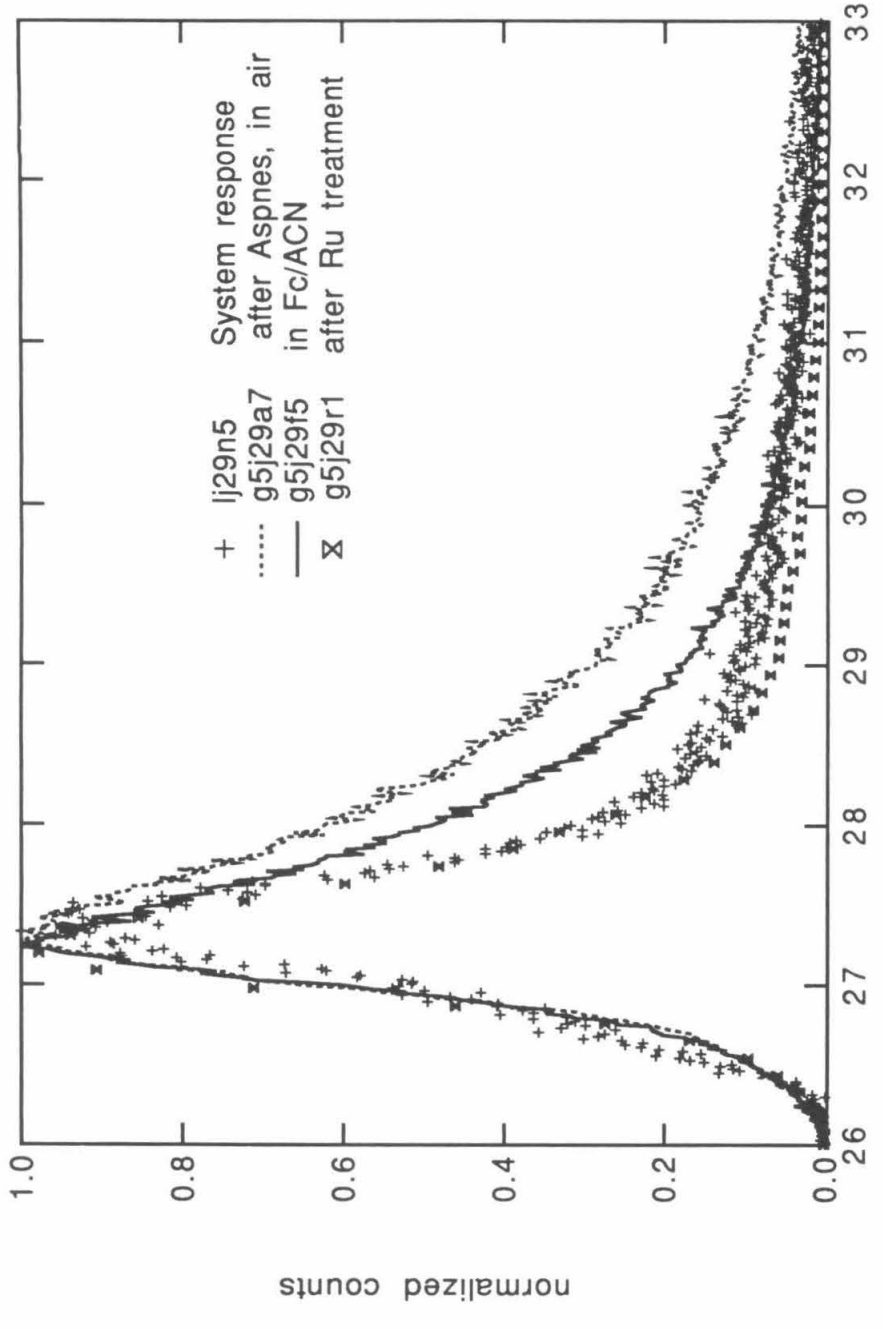

Figure 5-21(a). PL decays of etched GaAs in air, and in dimethylferrocene/CH_3CN before and after Ru(III) ion treatment.

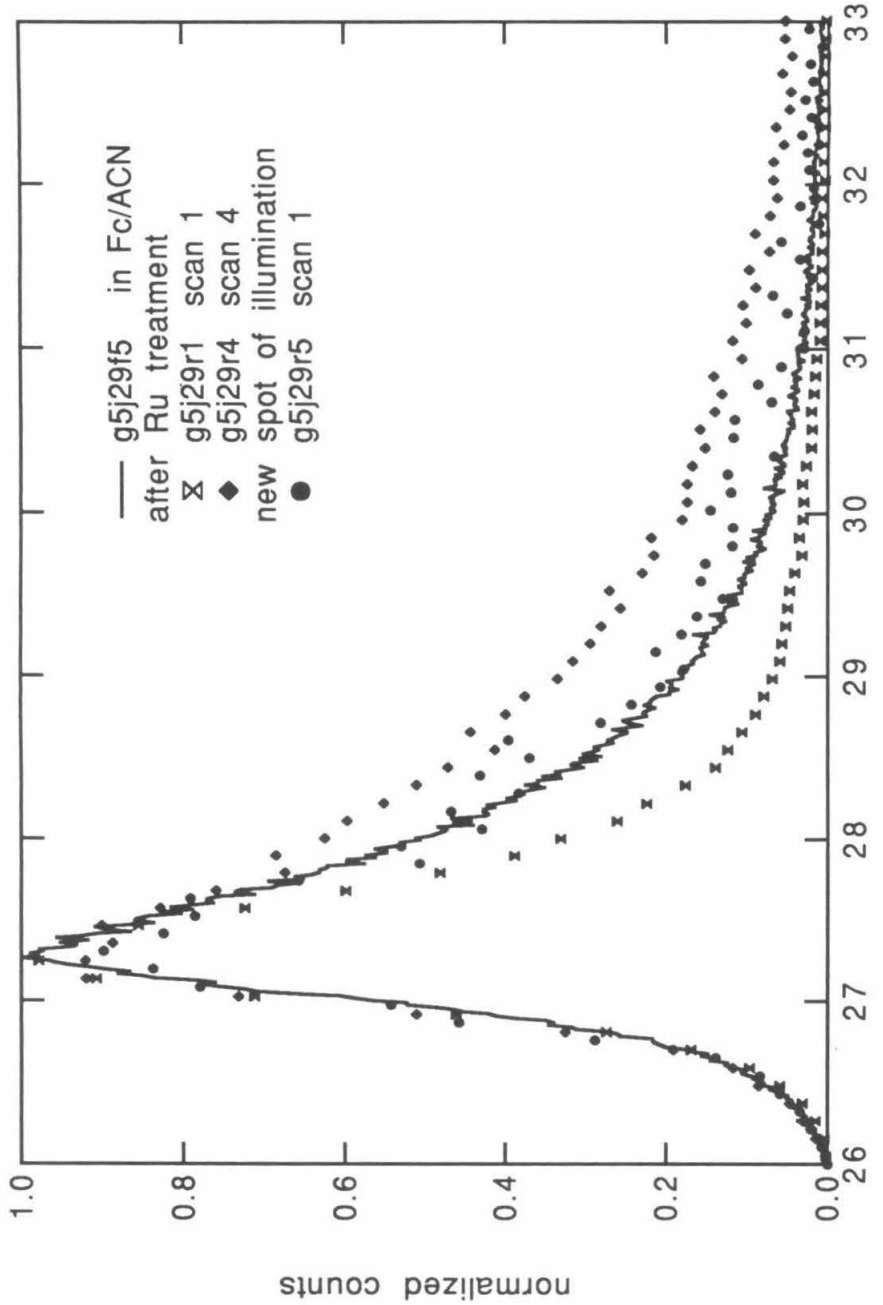

Figure 5-21(b). PL decays of etched GaAs in dimethylferrocene/CH_3CN before and after Ru(III) ion treatment.

D. Discussion and Modelling Results

Using the program discussed in Chapter 3, fits to the data sets were attempted. As shown in Figure 5-5 above, the capped samples were almost purely bimolecular decays, and very good fits of the model to the data could be obtained, assuming a value for $k_{radiative}$, and letting the intensity vary, as well as the x-axis offset, and the amplitude of the simulated decay. From these fits, a value for the incident light intensity, izero, was obtained for use in modelling the subsequent decays in KOH - Se^{2-} - Se_2^{2-} solution before and after metal ion treatment. Although the model does not account for the ever-changing surface under illumination, fits to the decays for the prototypical experiment detailed under the cobalt section above (sample h34) are presented in Figures 5-22 to 5-25. The parameters in the model are recorded directly on the plot. For the experiments in which surface rates were varied, the parameters of interest are the density of surface states (ntf) and the hole transfer rate constant (kht). The surface rate due to trapping can be converted to an equivalent surface recombination velocity (SRV) by multiplying by the trapping rate constant, $1x10^{-8}$ cm^3/sec, which was fixed in the calculation. Likewise, the SRV due to hole transfer can be obtained by multiplying the hole transfer rate constant by the concentration of acceptors, $1x10^{20}$ cm^{-3}, which was also fixed in the calculation and is an approximation to the concentration of a 1**M** solution.

Figure 5-22 shows the computer-generated fit to PL decays of unetched sample h34 used in cobalt experiment (File h34u01). The variables in the fit were the incident intensity (izero), the offset, and the amplitude. A good fit was found for izero equal to $7.5x10^{13}$ photons/cm^2. Figure 5-23(a) and (b) show the computer-generated fits to PL decays of samples under argon etched using Br_2/CH_3OH and the Aspnes etch, respectively. Using the incident intensity that was obtained from the fit shown in Figure 5-22, the best fit values of the trap density were found to correspond to a surface recombination velocity of $2x10^5$ cm/sec and $1.1x10^5$ cm/sec, respectively. The quality of fit for the Br_2/CH_3OH

etched surface was better, most likely due to the fact that there had been less change in the surface during illumination.

In Figure 5-24(a) - (c) the computer-generated fits to PL decays successively recorded for samples immersed in KOH - Se_2^{2-} - Se^{2-} are shown. The electron transfer rate constant was fixed at $1x10^{-18}$ cm^4/sec and the concentration of donors and acceptors was set to $1x10^{20}$ cm^{-3}. Both the density of traps and the rate constant for holes were allowed to vary, although the effective surface rate is the larger of the two, and experimentally it was not possible to distinguish between them. For the first data set, before significant lengthening of the decay, the effective SRV was found to be $3.7x10^4$ cm/sec. At the conclusion of the second data set in KOH - Se_2^{2-} - Se^{2-} the sample had been irradiated for 96 seconds, and the best-fit SRV was $2.2x10^4$ cm/sec. The third data set, during which the count rate was still climbing, had a best-fit SRV of $5.1x10^3$ cm/sec.

The computer-generated fits to PL decays for cobalt-treated samples immersed in KOH - Se_2^{2-} - Se^{2-} are shown in Figure 5-25. Both the surface trap density and the rate constant for hole transfer were allowed to vary. For the first data set recorded, the best-fit SRV was $2.2x10^5$ cm/sec. For the second data set, the lifetime increased slightly, and the best fit was obtained for an SRV of $1.4x10^5$ cm/sec.

A consistent value for the surface loss rates of the etched surfaces under argon was found and is comparable to that reported by others. In the fits to the decays of sample h41 (Figure 5-10), which were relatively constant during two sets of data collection, the etched surface SRV is found to fit most closely to $S=1.8x10^5$ cm/sec. The fits for the etched surfaces shown in Figure 5-23 (a) and (b), etched with Br_2/CH_3OH and the Aspnes etch, respectively have values of $2.0x10^5$ and $1.1\ x10^5$ cm/sec. These are similar to the values reported by Gmitter and co-workers[5] who used rf conductivity to measure the decay of carriers and determined that the surface recombination velocity of the etched surface in air (etched using 1:8:500 H_2SO_4:H_2O_2:H_2O) is $\geq$ 20000 cm/sec.

Figure 5-22. Computer-generated fit to PL decays of unetched sample h34 used in cobalt experiment (File h34u01). The variables in the fit were the incident intensity (izero), the offset, and the amplitude. A good fit was found for izero = 7.5×10^{13} photons/cm^2. **(I)** The linear fit superimposed on the data. **(II)** The residuals for the linear fit (*i.e.*, the difference between the fit and the linear data for each point).

Figure 5-23. Computer-generated fits to PL decays of etched samples under argon, prior to immersion in KOH - Se_2^{2-} - Se^{2-} or metal ion treatment. I, II and III for each plot are linear, log and residuals plots, as in Figure 5-22. **(a)** The decay for the Br_2/CH_3OH etched surface. The incident intensity was that obtained from the fit shown in Figure 5-22. The variables were the number of traps at the surface (ntf), the offset and the amplitude. The trapping rate constants for both electrons and holes were fixed at 1×10^{-8} cm^3/sec. ntf was found to be 2.0×10^{13} cm^{-2} **(b)** The PL decay after the final Aspnes etch, during which the count rate changed slightly. The variables were ntf, offset and amplitude. The best fit was obtained for ntf = 1.1×10^{13} cm^{-2} (SRV = 1.1×10^5 cm/sec).

Figure 5-24. Computer-generated fits to PL decays for etched samples immersed in KOH - Se_2^{2-} - Se^{2-} prior to metal ion treatment. The electron transfer rate constant was fixed at 1×10^{-18} cm^4/sec and the concentration of donors and acceptors was set to 1×10^{20} cm^{-3}. Both the density of traps and the rate constant for holes were allowed to vary. I, and II for each plot are linear and residuals plots, as in Figure 5-22. **(a)** The first data set in KOH - Se_2^{2-} - Se^{2-} recorded for 15 seconds. For the first data set, before significant lengthening of the decay, the effective SRV was found to be 3.7×10^4 cm/sec. **(b)** The second data set in KOH - Se_2^{2-} - Se^{2-}; the sample had been irradiated for 96 seconds. Best fit of SRV was 2.2×10^4 cm/sec. **(c)** The third data set, during which the count rate was still climbing. Best fit of SRV was 5.1×10^3 cm/sec.

Figure 5-25. Computer-generated fits to PL decays for cobalt-treated samples immersed in KOH - Se_2^{2-} - Se^{2-}. Both the trap density and the rate constant for holes were allowed to vary. I, II and III for each plot are linear, log and residuals plots, as in Figure 5-22.**(a)** The first data set recorded during 51 seconds of illumination had a best-fit SRV of 2.2×10^5 cm/sec. **(b)** The second data set, recorded for a sample illuminated for 292 seconds, had a best-fit SRV value of 1.4×10^5 cm/sec.

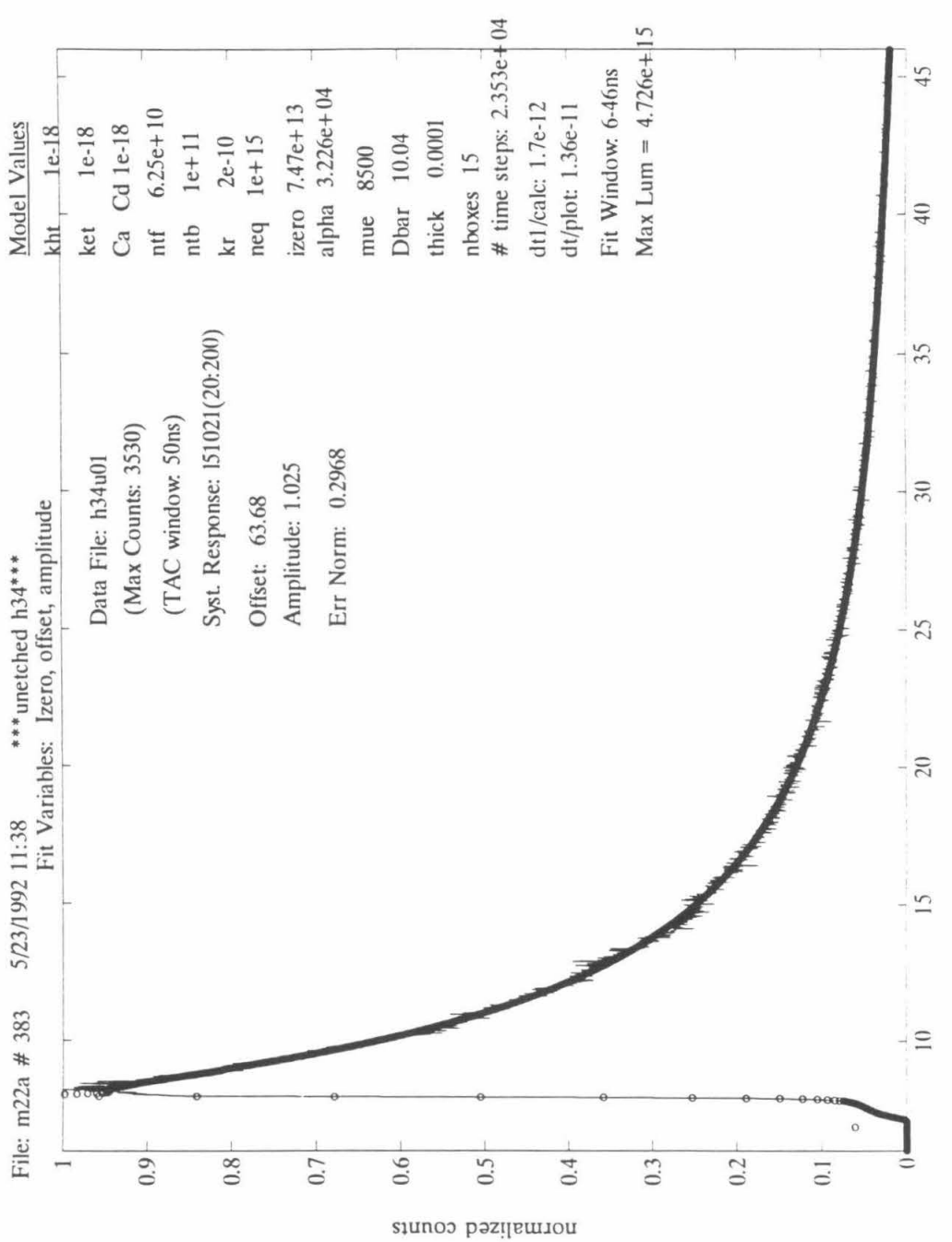
File: m22a # 383 5/23/1992 11:38 ***unetched h34***
Fit Variables: Izero, offset, amplitude
Data File: h34u01
(Max Counts: 3530)
(TAC window: 50ns)
Syst. Response: l51021(20:200)
Offset: 63.68
Amplitude: 1.025
Err Norm: 0.2968
Model Values
ket 1e-18
Ca Cd 1e-18
ntf 6.25e+10
ntb 1e+11
kr 2e-10
neq 1e+15
izero 7.47e+13
alpha 3.226e+04
mue 8500
Dbar 10.04
thick 0.0001
nboxes 15
time steps: 2.353e+04
dt1/calc: 1.7e-12
dt/plot: 1.36e-11
Fit Window: 6-46ns
Max Lum = 4.726e+15
kht 1e-18
normalized counts
time (ns)

Figure 22 - I

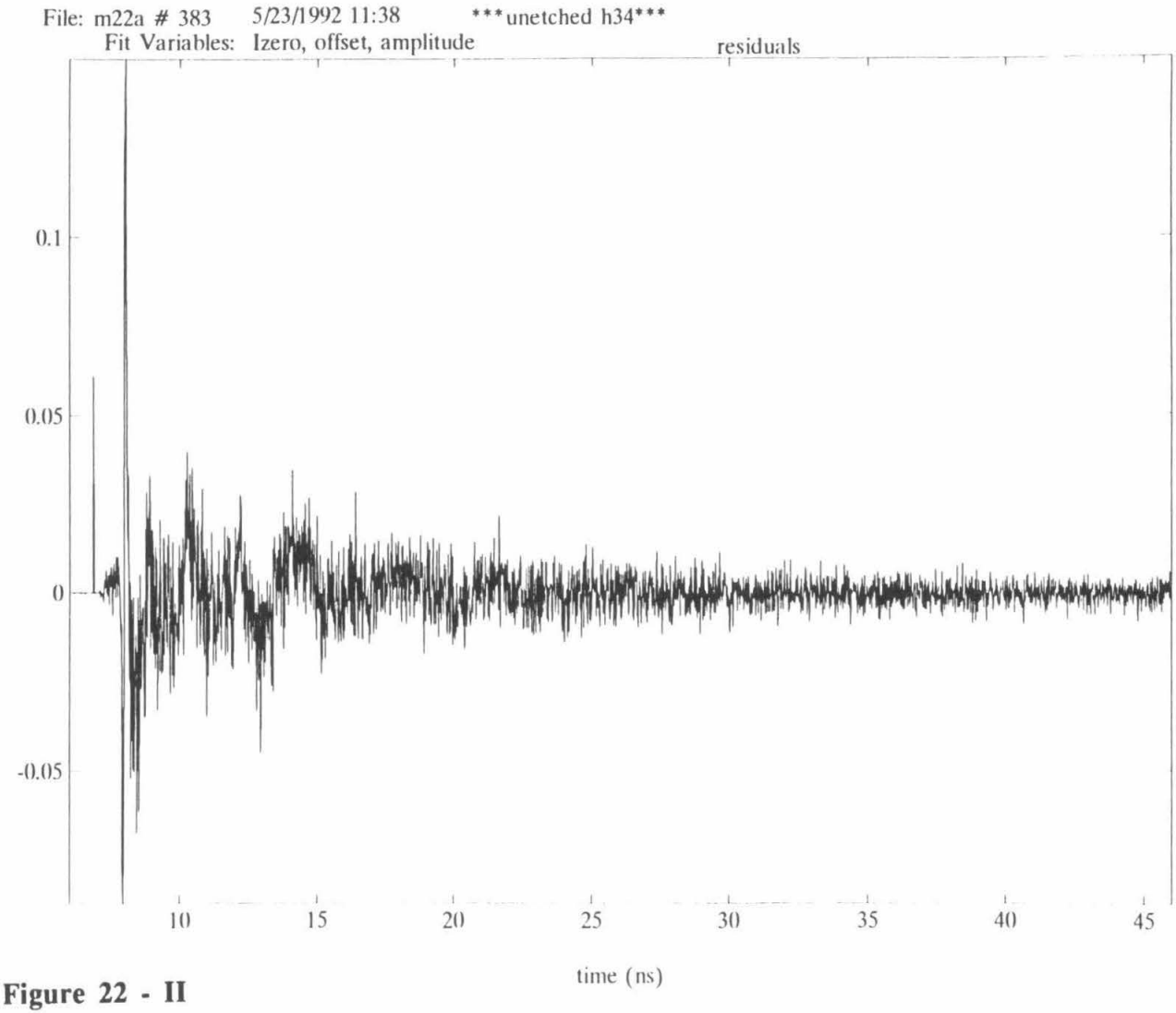
File: m22a # 383 5/23/1992 11:38 ***unetched h34***
Fit Variables: Izero, offset, amplitude
residuals
0.1
0.05
0
-0.05
10
15
20
25
30
35
40
45
time (ns)

Figure 22 - II

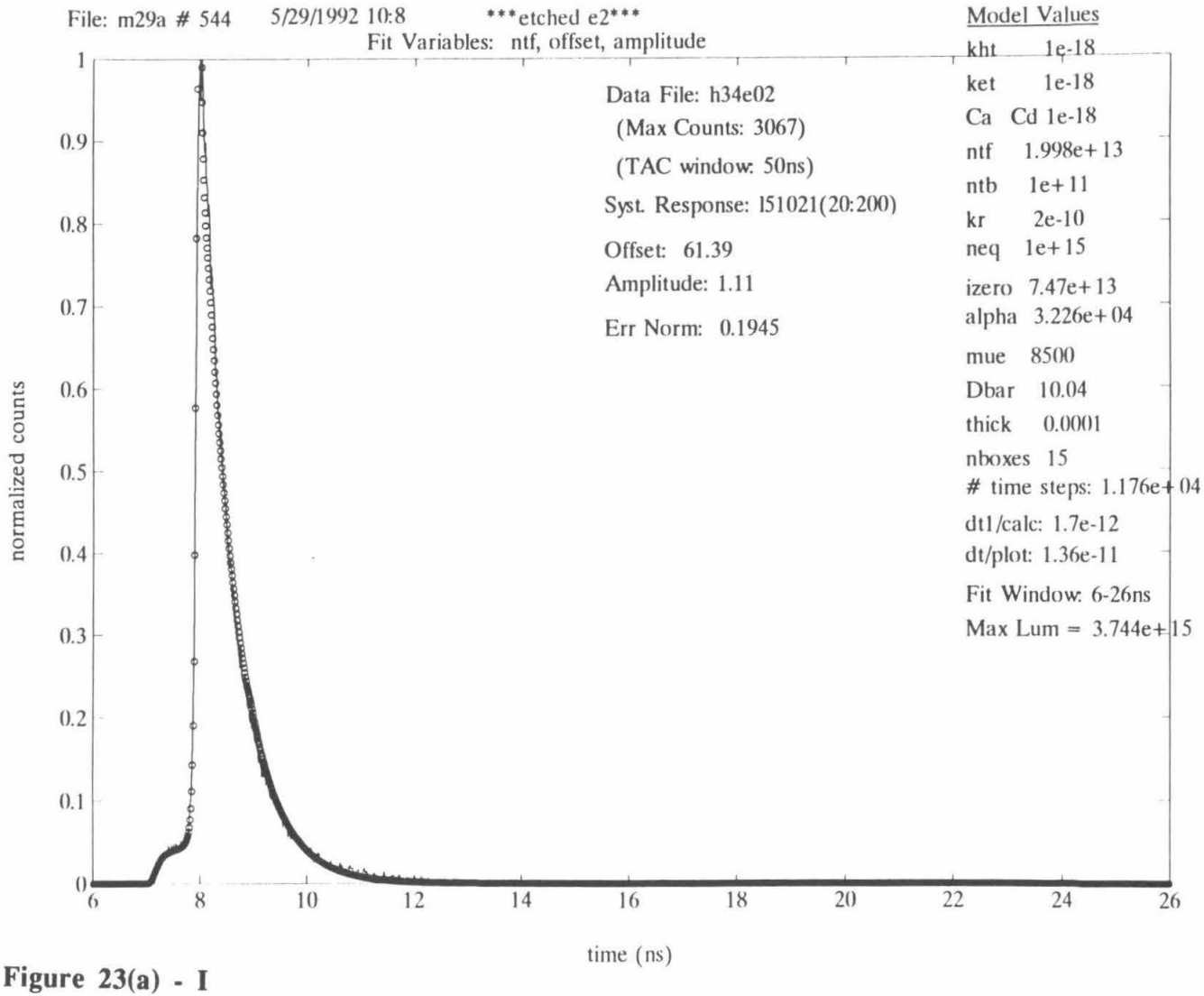
File: m29a # 544 5/29/1992 10:8 ***etched e2***
Fit Variables: ntf, offset, amplitude
Data File: h34e02
(Max Counts: 3067)
(TAC window: 50ns)
Syst. Response: l51021(20:200)
Offset: 61.39
Amplitude: 1.11
Err Norm: 0.1945
Model Values
kht 1e-18
ket 1e-18
Ca Cd 1e-18
ntf 1.998e+13
ntb 1e+11
kr 2e-10
neq 1e+15
izero 7.47e+13
alpha 3.226e+04
mue 8500
Dbar 10.04
thick 0.0001
nboxes 15
time steps: 1.176e+04
dt1/calc: 1.7e-12
dt/plot: 1.36e-11
Fit Window: 6-26ns
Max Lum = 3.744e+15
normalized counts
time (ns)
0
0.1
0.2
0.3
0.4
0.5
0.6
0.7
0.8
0.9
1
6
8
10
12
14
16
18
20
22
24
26

Figure 23(a) - I

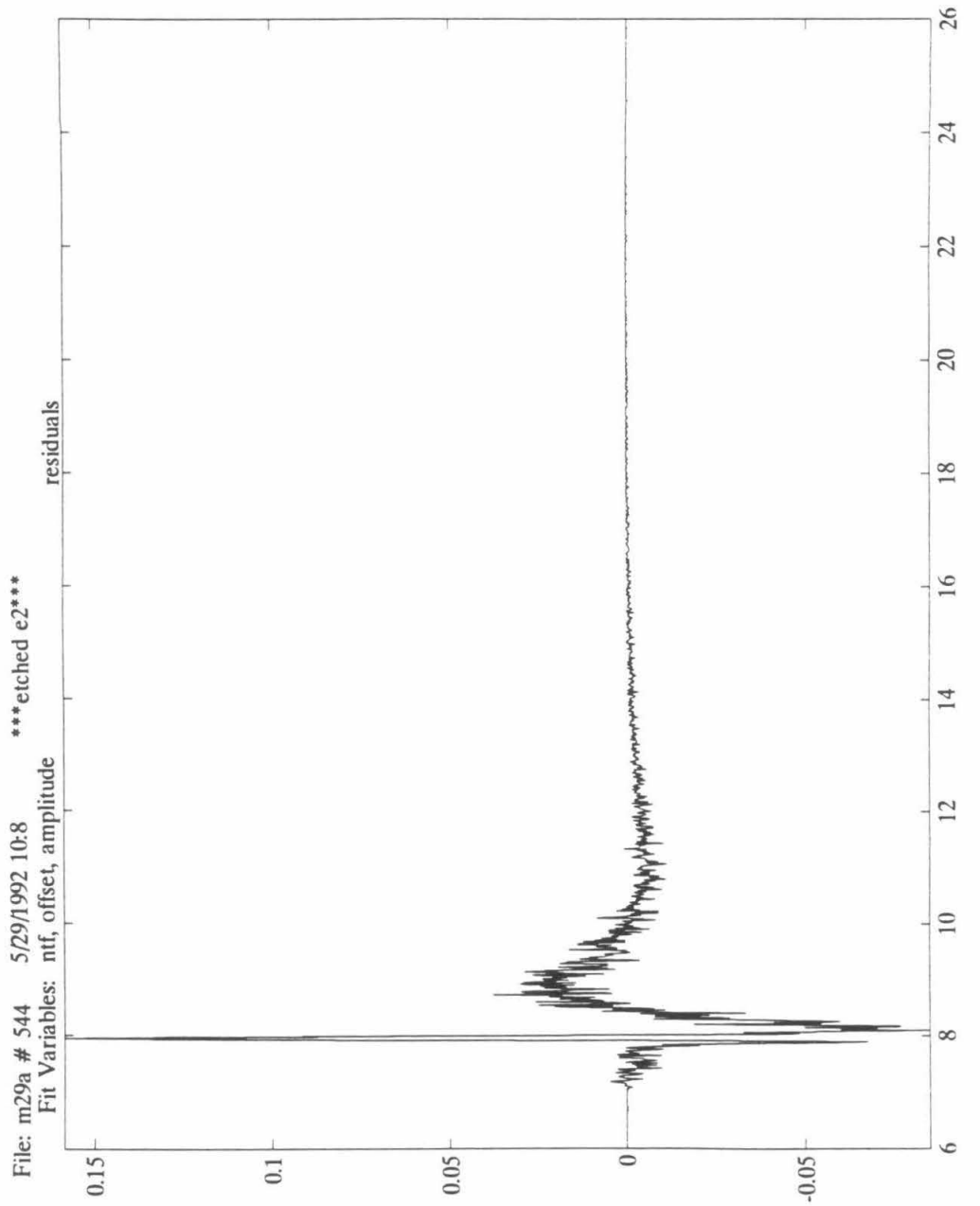

Figure 23(a) - II

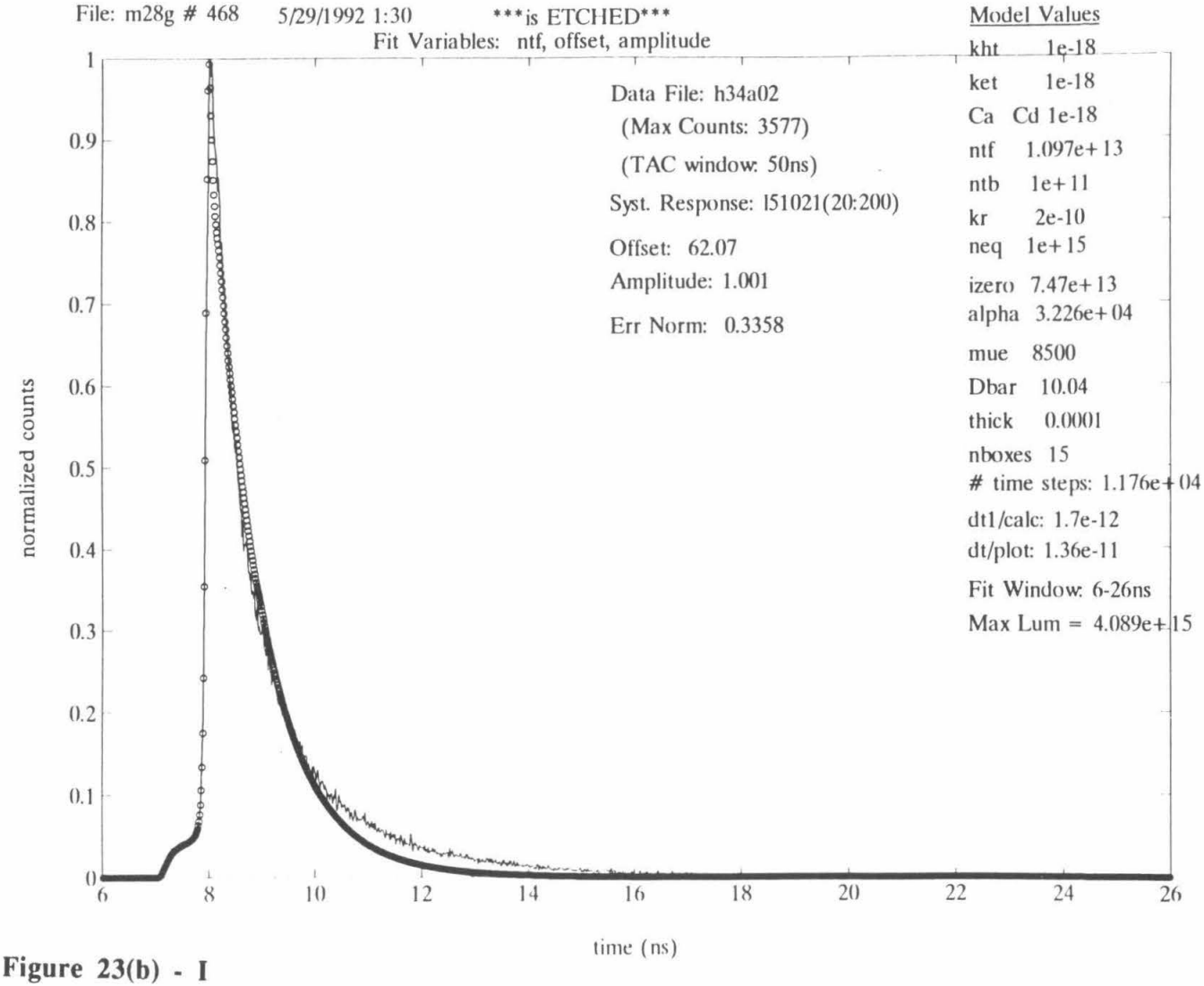
File: m28g # 468 5/29/1992 1:30 ***is ETCHED***
Fit Variables: ntf, offset, amplitude
Data File: h34a02
(Max Counts: 3577)
(TAC window: 50ns)
Syst. Response: l51021(20:200)
Offset: 62.07
Amplitude: 1.001
Err Norm: 0.3358
Model Values
kht 1e-18
ket 1e-18
Ca Cd 1e-18
ntf 1.097e+13
ntb 1e+11
kr 2e-10
neq 1e+15
izero 7.47e+13
alpha 3.226e+04
mue 8500
Dbar 10.04
thick 0.0001
nboxes 15
time steps: 1.176e+04
dt1/calc: 1.7e-12
dt/plot: 1.36e-11
Fit Window: 6-26ns
Max Lum = 4.089e+15
normalized counts
time (ns)
0
0.1
0.2
0.3
0.4
0.5
0.6
0.7
0.8
0.9
1
6
8
10
12
14
16
18
20
22
24
26

Figure 23(b) - I

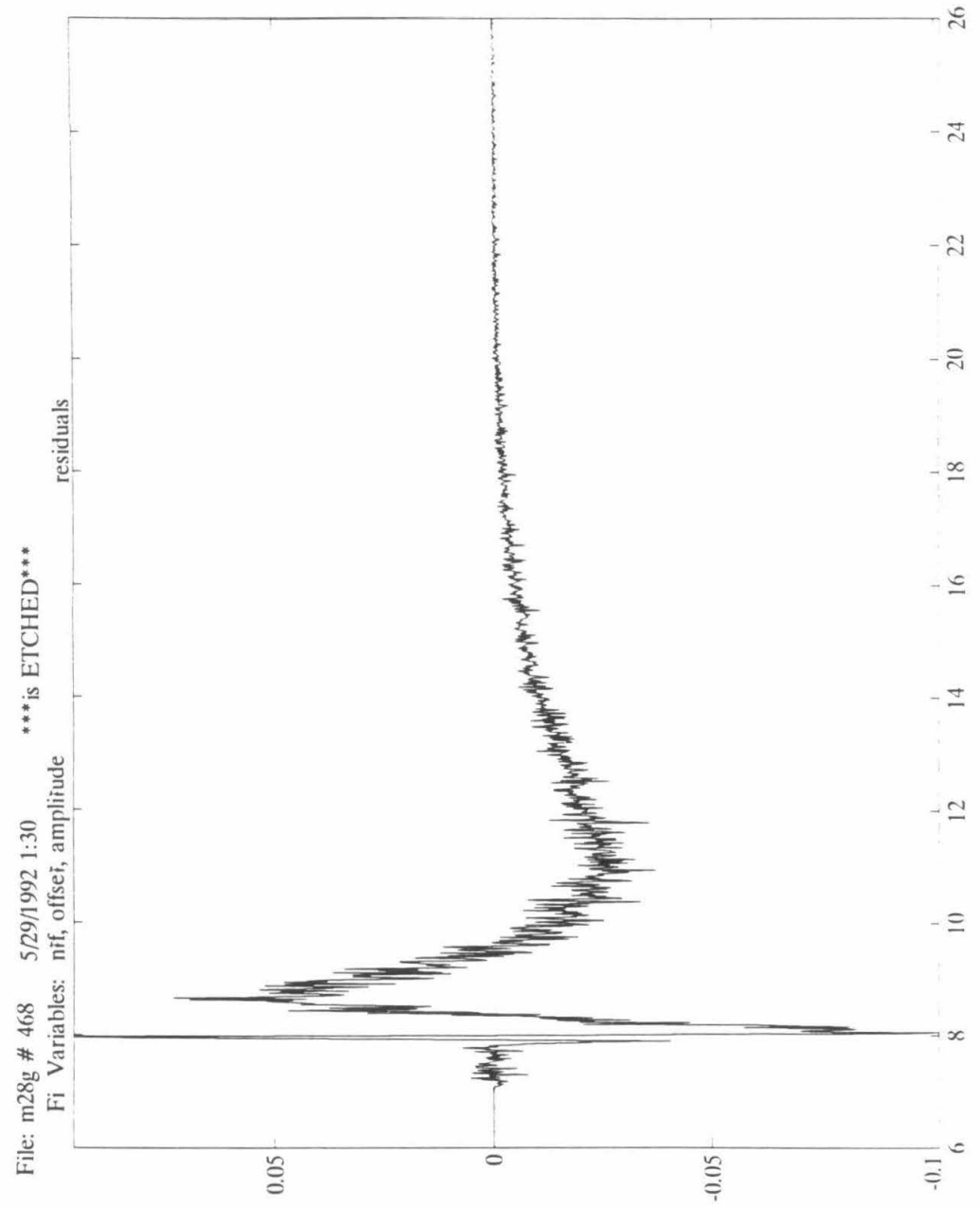

Figure 23(b) - II

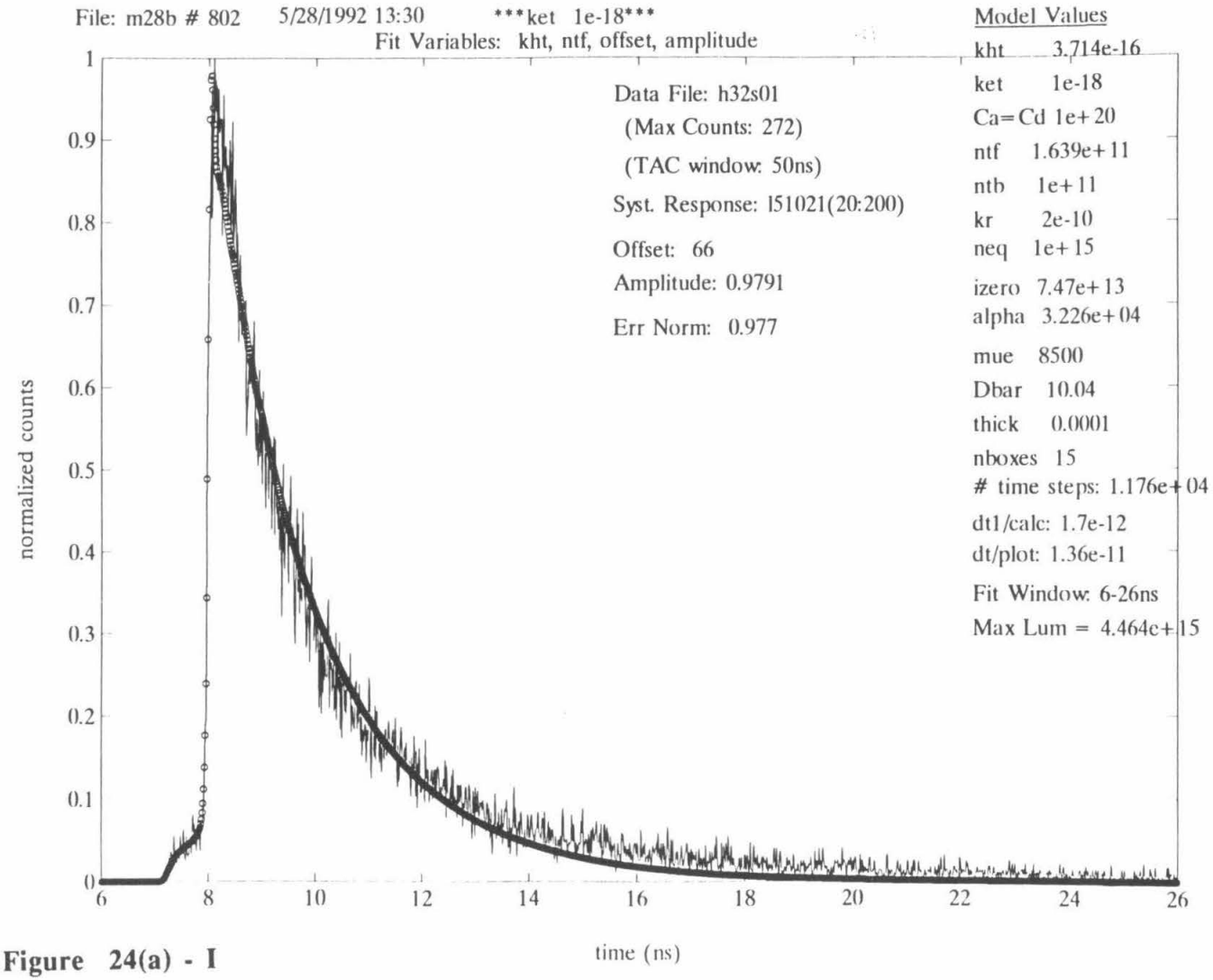
File: m28b # 802 5/28/1992 13:30 ***ket 1e-18***
Fit Variables: kht, ntf, offset, amplitude
Data File: h32s01
(Max Counts: 272)
(TAC window: 50ns)
Syst. Response: l51021(20:200)
Offset: 66
Amplitude: 0.9791
Err Norm: 0.977
Model Values
kht 3.714e-16
ket 1e-18
Ca=Cd 1e+20
ntf 1.639e+11
ntb 1e+11
kr 2e-10
neq 1e+15
izero 7.47e+13
alpha 3.226e+04
mue 8500
Dbar 10.04
thick 0.0001
nboxes 15
time steps: 1.176e+04
dt1/calc: 1.7e-12
dt/plot: 1.36e-11
Fit Window: 6-26ns
Max Lum = 4.464e+15
normalized counts
time (ns)
0
0.1
0.2
0.3
0.4
0.5
0.6
0.7
0.8
0.9
1
6
8
10
12
14
16
18
20
22
24
26

Figure 24(a) - I

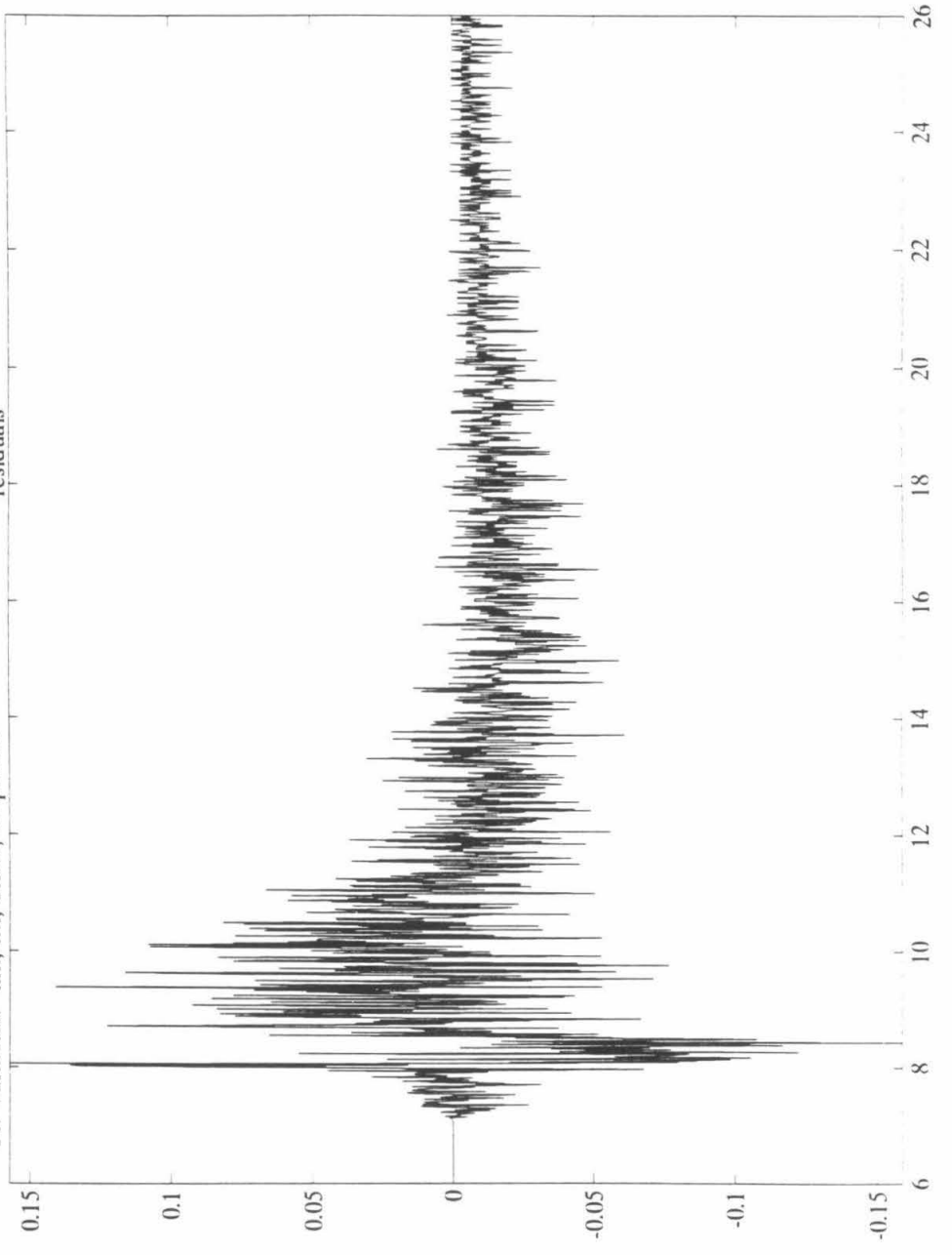

Figure 24(a) - II

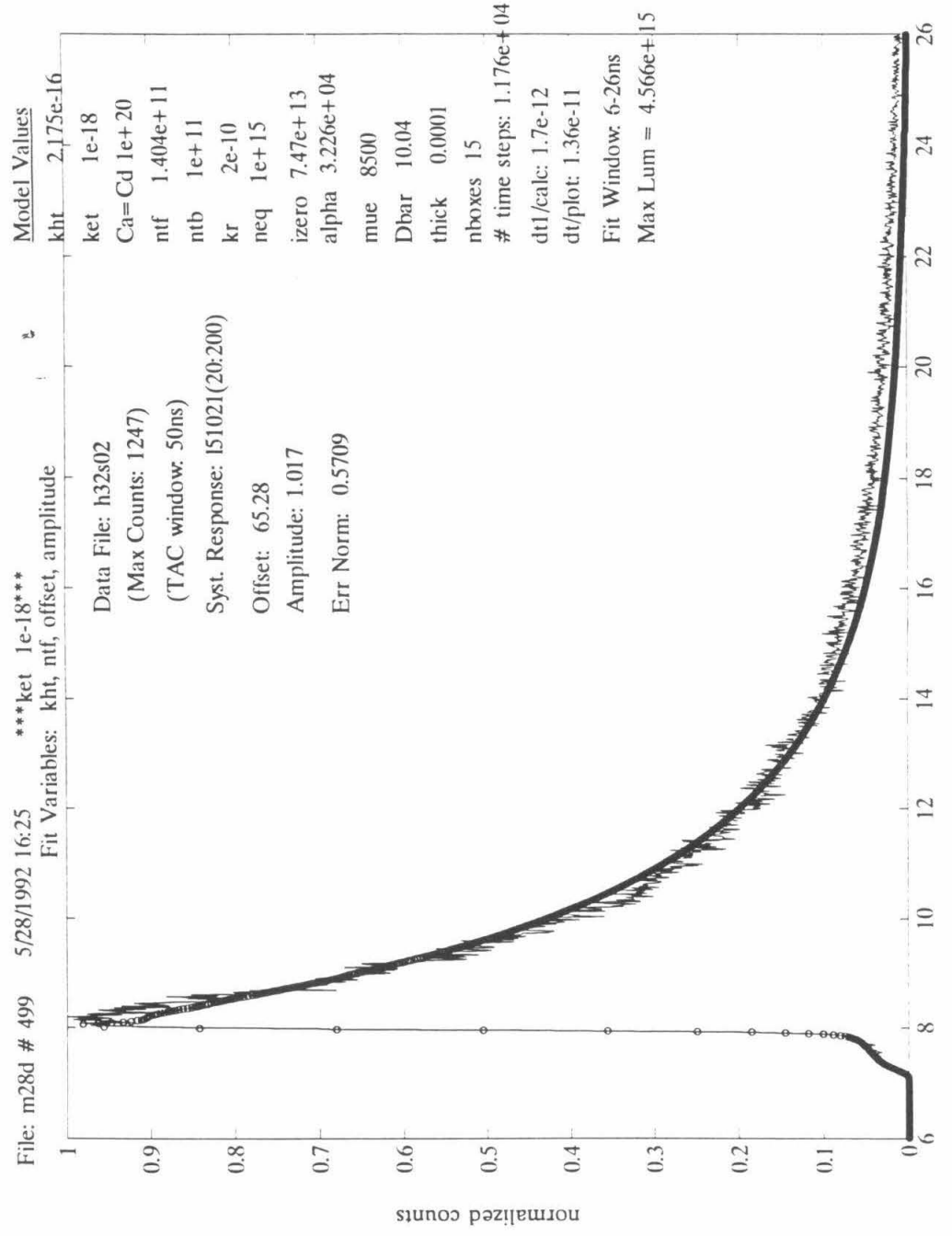
File: m28d # 499 5/28/1992 16:25 ***ket 1e-18***
Fit Variables: kht, ntf, offset, amplitude
Data File: h32s02
(Max Counts: 1247)
(TAC window: 50ns)
Syst. Response: l51021(20:200)
Offset: 65.28
Amplitude: 1.017
Err Norm: 0.5709
Model Values
kht 2.175e-16
ket 1e-18
Ca=Cd 1e+20
ntf 1.404e+11
ntb 1e+11
kr 2e-10
neq 1e+15
izero 7.47e+13
alpha 3.226e+04
mue 8500
Dbar 10.04
thick 0.0001
nboxes 15
time steps: 1.176e+04
dt1/calc: 1.7e-12
dt/plot: 1.36e-11
Fit Window: 6-26ns
Max Lum = 4.566e+15
normalized counts
time (ns)

Figure 24(b) - I

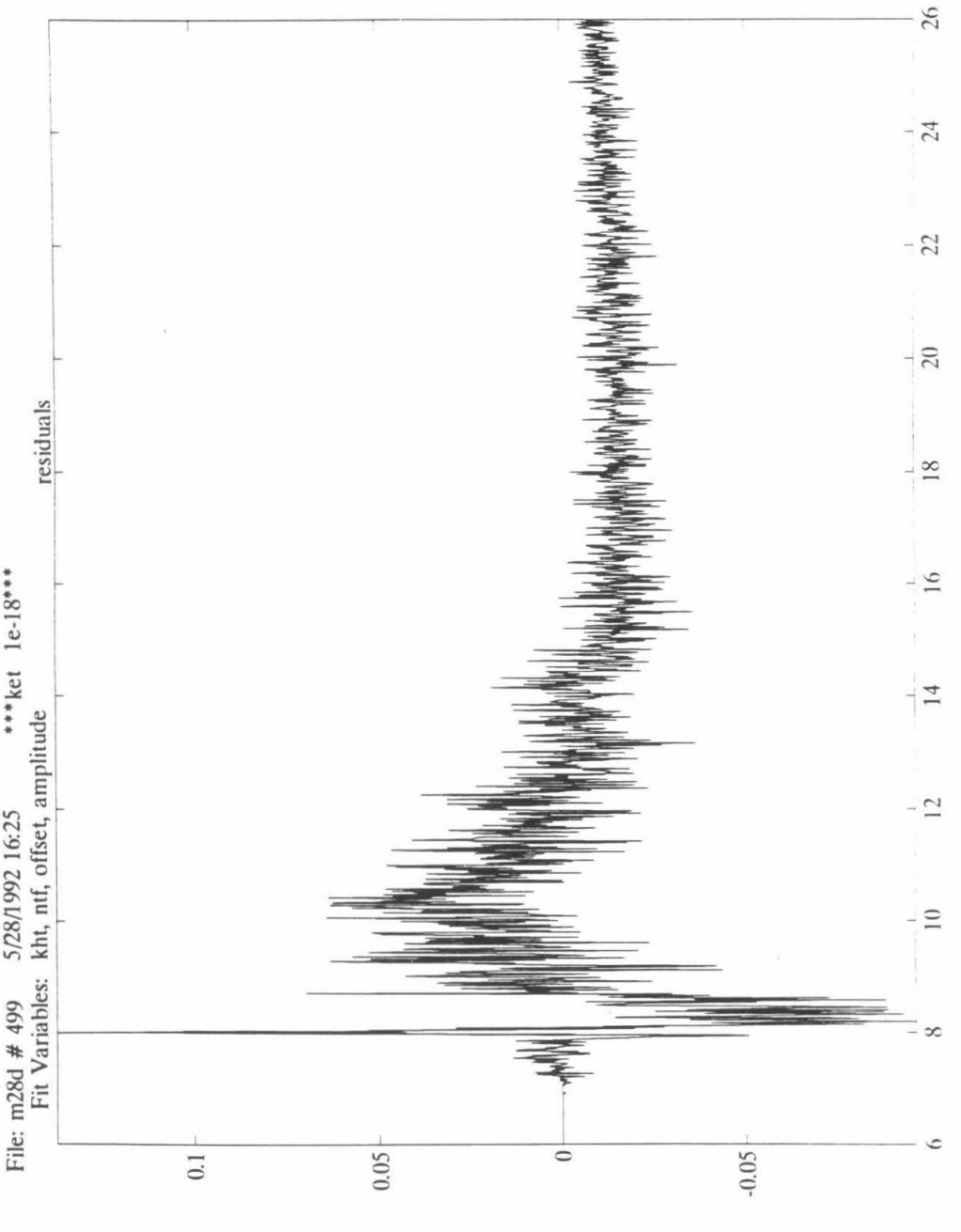

Figure 24(b) - II

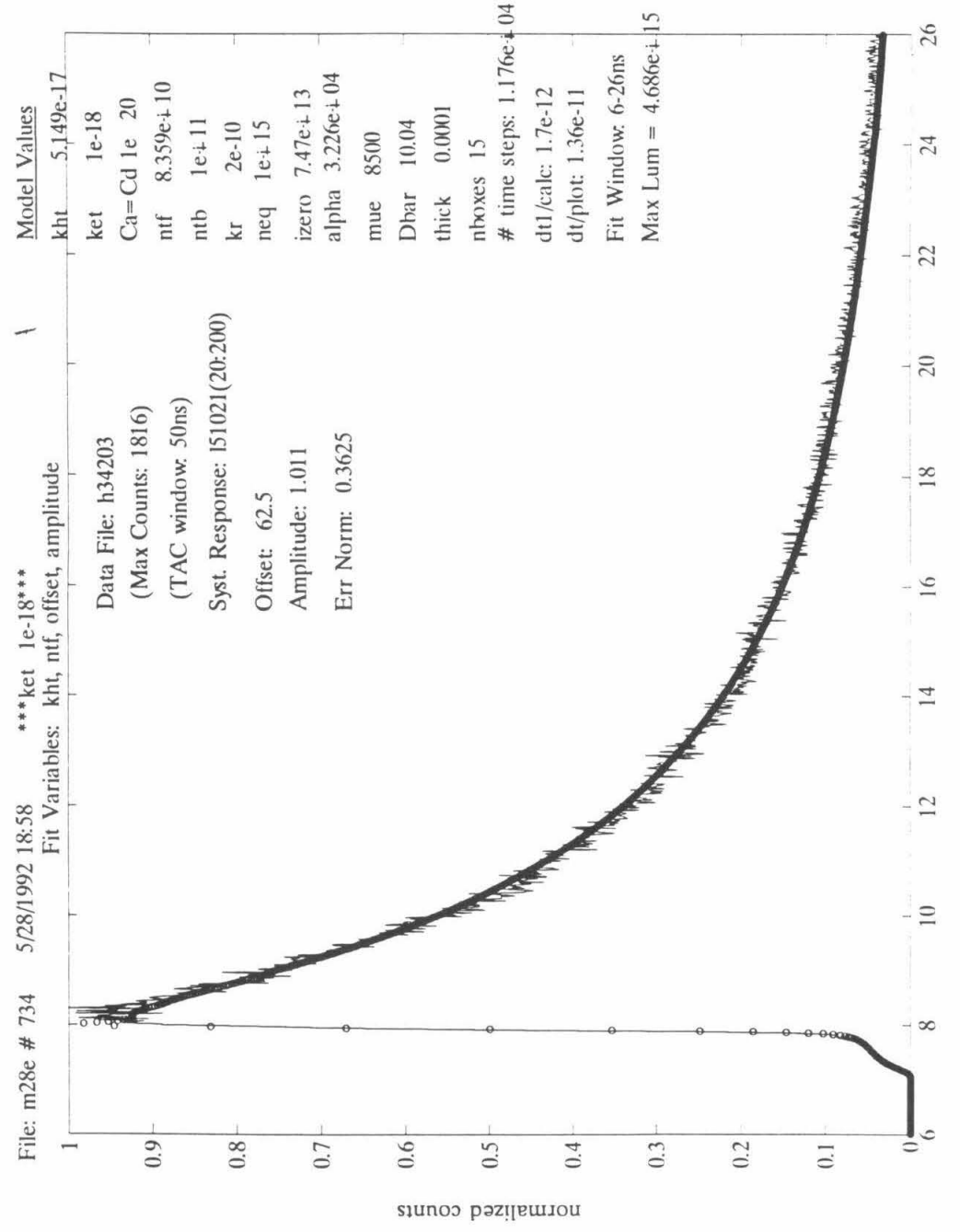
File: m28e # 734 5/28/1992 18:58 ***ket 1e-18***
Fit Variables: kht, ntf, offset, amplitude
Data File: h34203
(Max Counts: 1816)
(TAC window: 50ns)
Syst. Response: 151021(20:200)
Offset: 62.5
Amplitude: 1.011
Err Norm: 0.3625
Model Values
kht 5.149e-17
ket 1e-18
Ca=Cd 1e 20
ntf 8.359e+10
ntb 1e+11
kr 2e-10
neq 1e+15
izero 7.47e+13
alpha 3.226e+04
mue 8500
Dbar 10.04
thick 0.0001
nboxes 15
time steps: 1.176e+04
dt1/calc: 1.7e-12
dt/plot: 1.36e-11
Fit Window: 6-26ns
Max Lum = 4.686e+15
normalized counts
time (ns)

Figure 24(c) - I

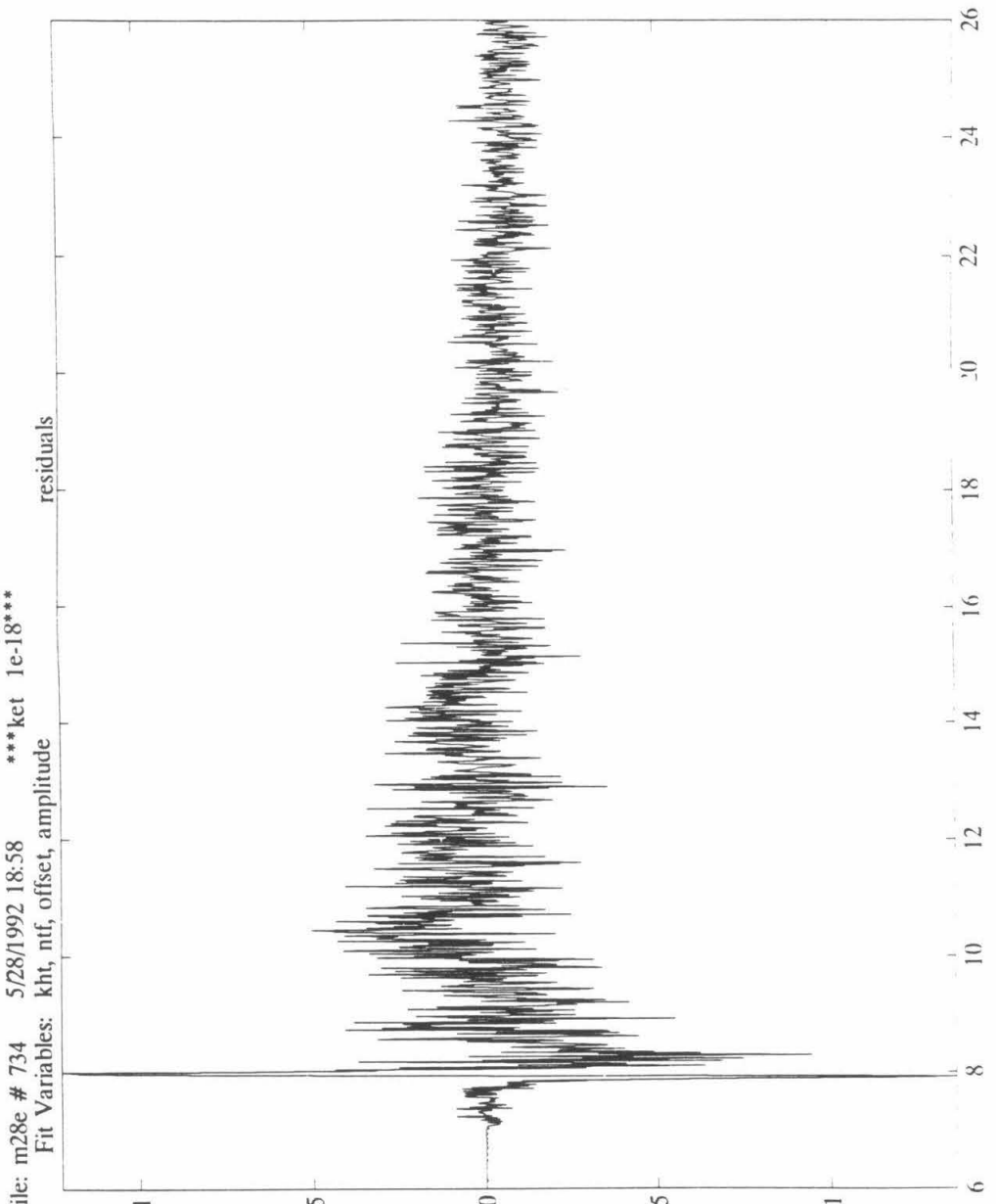

Figure 24(c) - II

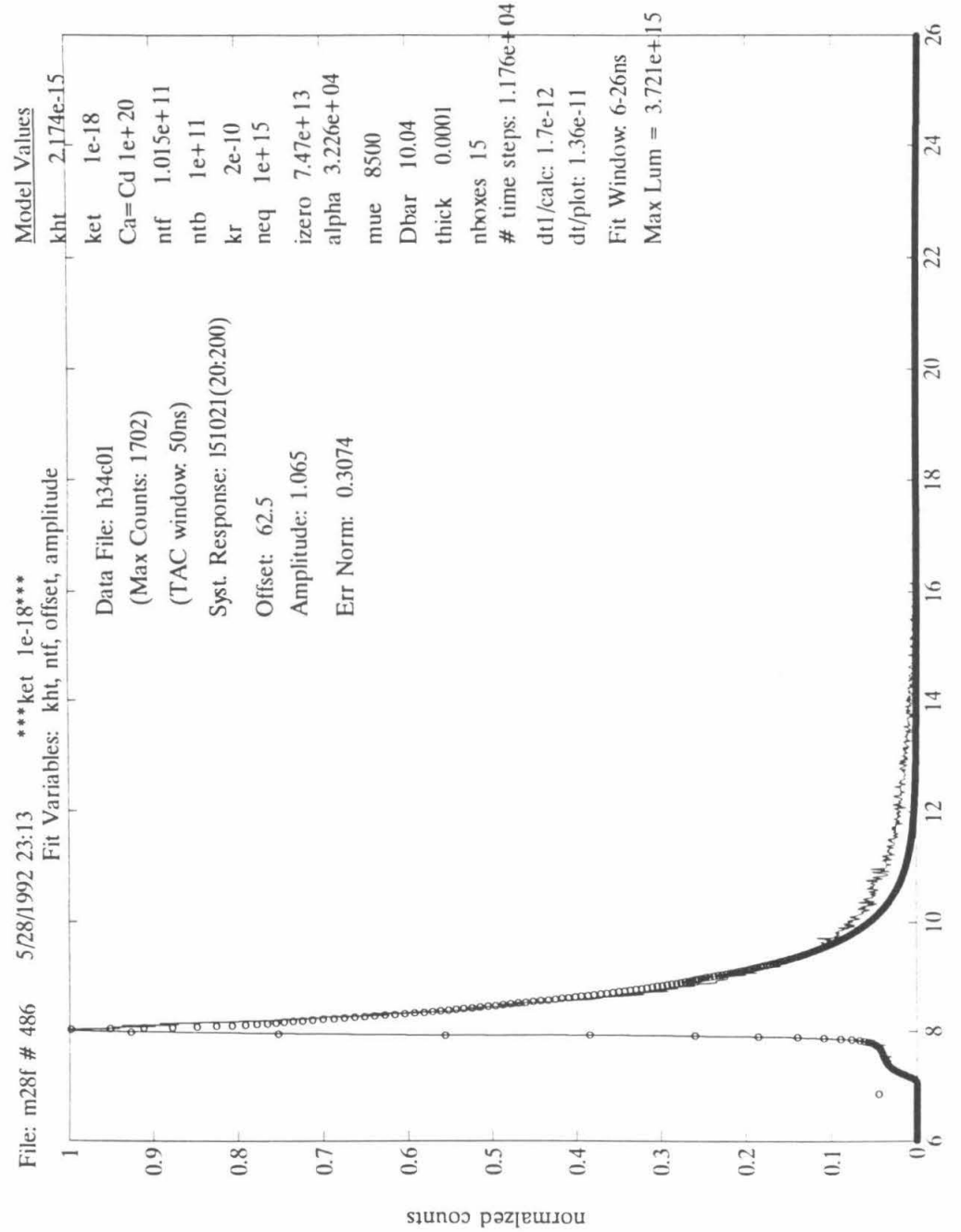
File: m28f # 486 5/28/1992 23:13 ***ket 1e-18***
Fit Variables: kht, ntf, offset, amplitude
Model Values
kht 2.174e-15
ket 1e-18
Ca=Cd 1e+20
ntf 1.015e+11
ntb 1e+11
kr 2e-10
neq 1e+15
izero 7.47e+13
alpha 3.226e+04
mue 8500
Dbar 10.04
thick 0.0001
nboxes 15
time steps: 1.176e+04
dt1/calc: 1.7e-12
dt/plot: 1.36e-11
Fit Window: 6-26ns
Max Lum = 3.721e+15
Data File: h34e01
(Max Counts: 1702)
(TAC window: 50ns)
Syst. Response: I51021(20:200)
Offset: 62.5
Amplitude: 1.065
Err Norm: 0.3074
normalized counts
time (ns)

Figure 25(a) - I

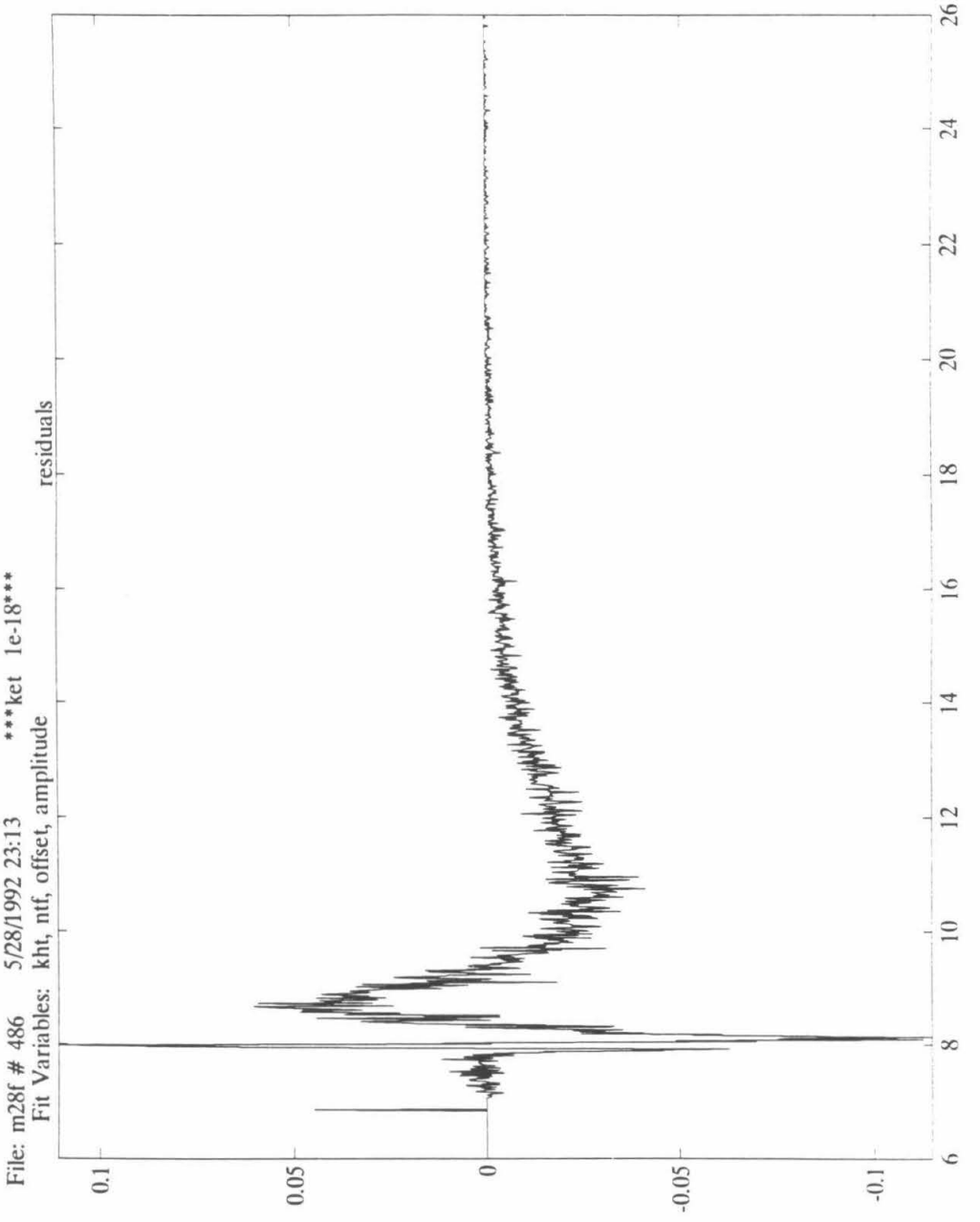

Figure 25(a) - II

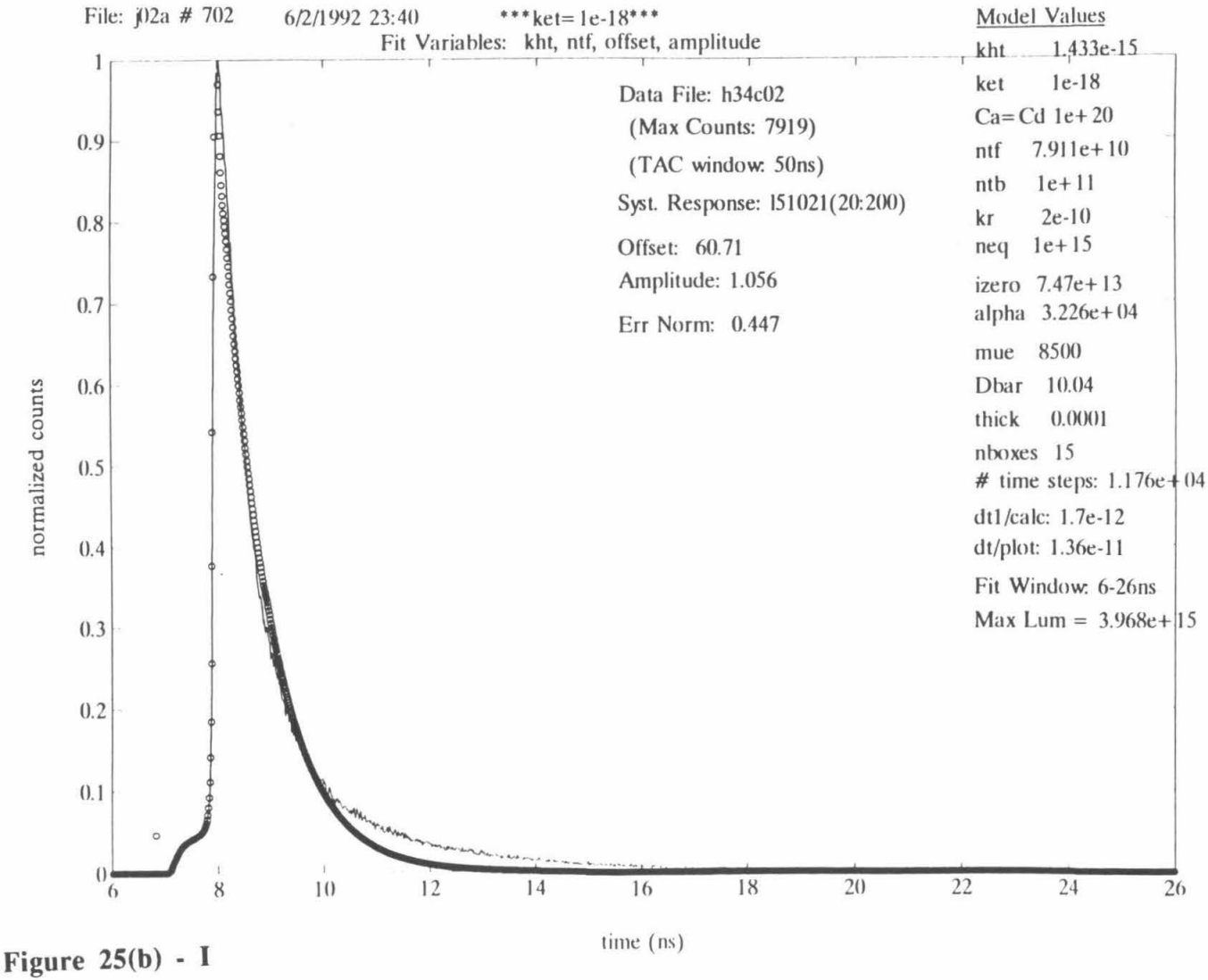
File: j02a # 702 6/2/1992 23:40 ***ket= 1e-18***
Fit Variables: kht, ntf, offset, amplitude
Data File: h34c02
(Max Counts: 7919)
(TAC window: 50ns)
Syst. Response: l51021(20:200)
Offset: 60.71
Amplitude: 1.056
Err Norm: 0.447
Model Values
kht 1.433e-15
ket 1e-18
Ca=Cd 1e+20
ntf 7.911e+10
ntb 1e+11
kr 2e-10
neq 1e+15
izero 7.47e+13
alpha 3.226e+04
mue 8500
Dbar 10.04
thick 0.0001
nboxes 15
time steps: 1.176e+04
dt1/calc: 1.7e-12
dt/plot: 1.36e-11
Fit Window: 6-26ns
Max Lum = 3.968e+15
normalized counts
time (ns)
0
0.1
0.2
0.3
0.4
0.5
0.6
0.7
0.8
0.9
1
6
8
10
12
14
16
18
20
22
24
26

Figure 25(b) - I

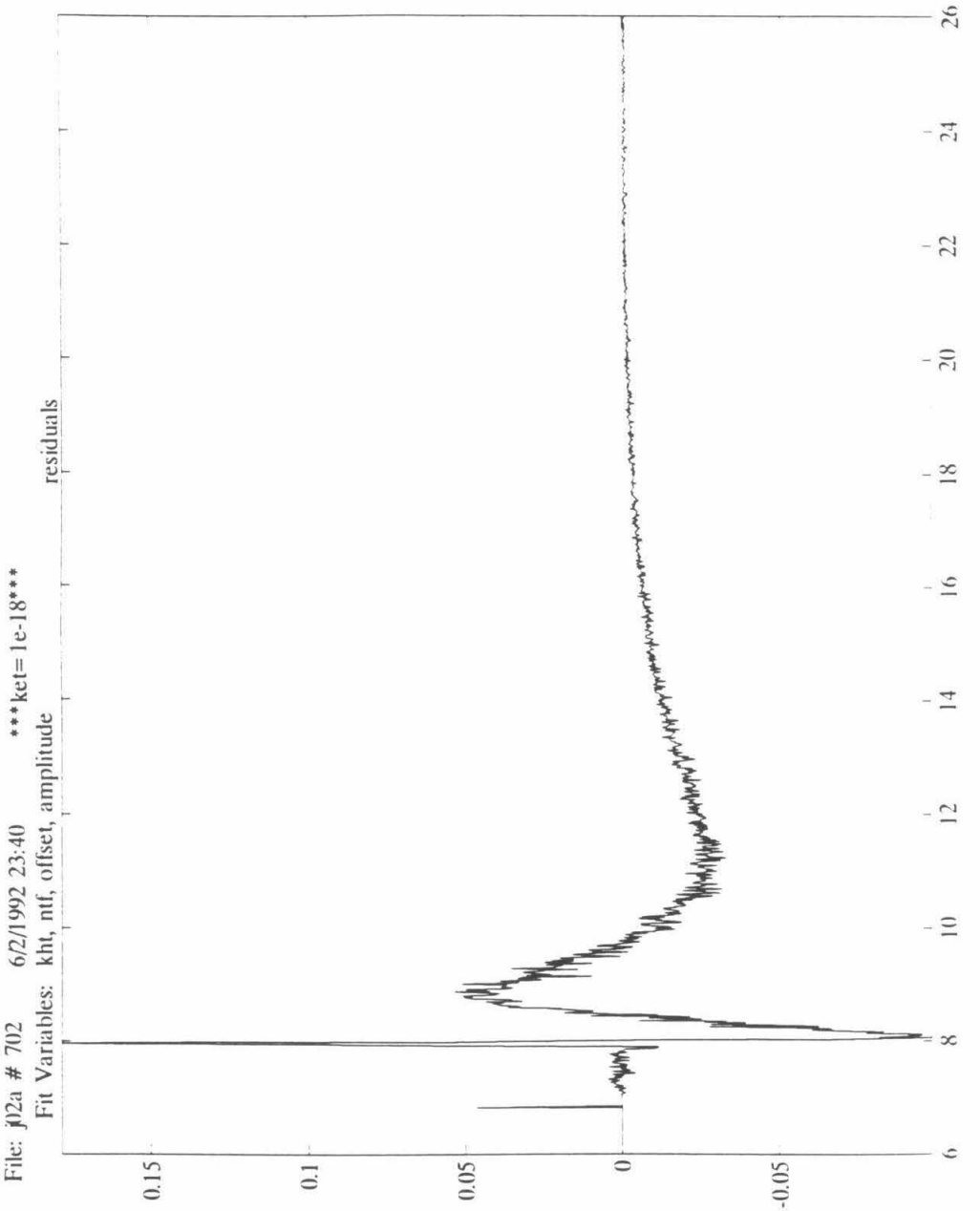

Figure 25(b) - II

Although the lifetimes measured in KOH - Se^{2-} - Se_2^{2-} solutions increased with time, the data sets taken after several minutes of illumination remained nearly constant; the third data set for the sample in KOH - Se^{2-} - Se_2^{2-} solution prior to metal ion treatment, shown in Figure 5-23(c), is well fit by the model and yields an SRV of 5.1×10^3 cm/sec. The decay after cobalt treatment for the curve recorded in 51 seconds is best fit with an SRV of 2.2×10^5 cm/sec, while that recorded later is slightly slower, with an SRV of 1.4×10^5 cm/sec. These are in accord with the results of Gmitter and co-workers who obtained S~1700 cm/sec in 0.6 **M** K_2Se/1.0 **M** KOH solution. After immersion in a 0.01 **M** $RuCl_3$/0.1 **M** HCl solution, they observed a much faster decay for which they reported S~13,000 cm/sec.

Gmitter *et al.*[4] attributed the reduction of carrier loss in KOH - Se^{2-} - Se_2^{2-} solutions to a reduction in the number of elemental arsenic surface states where recombination can occur. They claim that the KOH - Se_2^{2-} - Se^{2-} solution dissolves the deleterious arsenic and arsenic oxides. In the work of Tufts *et al.*[6] correlations between surface arsenic and arsenic oxides measured using XPS have been made with current-voltage properties in KOH - Se_2^{2-} - Se^{2-} solution. It has been found that independent of whether the GaAs surface is initially covered with oxides or elemental arsenic or is a stoichiometric GaAs surface, the final surface after illumination in electrochemical experiments is a stoichiometric GaAs surface, both when cycled and when held at the maximum cell power point. It is consistent, therefore, to suppose that the observed increase in lifetime during illumination in the TCPC experiments corresponds to a similar conversion of the surface from oxide-rich to oxide-free.

The decays in solution after metal ion treatment change slightly less, on an absolute scale, than the decays measured under argon do. The 1/e lifetime for the cobalt-treated surface in solution was 0.12 ns longer for the data set stopped after 300 seconds of illumination than it was for the data set collected in the first 50 seconds. Under argon,

there was an increase of 0.23 ns between data sets recorded after 90 and 300 seconds of illumination. It is possible that a similar change occurs at each surface, in which case it must be independent of the KOH - Se_2^{2-} - Se^{2-} solution which purportedly causes this change in the untreated samples. The data sets in KOH - Se^{2-} - Se_2^{2-} solution, without metal ions increase from 1.70 ns measured after 15 seconds, to 2.20 ns, measured after 96 seconds of illumination. Larger absolute changes in the lifetime are consistently observed for the untreated samples relative to treated samples immersed in KOH - Se^{2-} - Se_2^{2-} solution. Because losses at the surface are so much higher for the metal ion treated samples, it may be that comparable absolute decreases in surface loss are occurring in the the treated and untreated cases, but that it affects proportionately less of the losses for the metal treated surfaces.

Limited surface studies of the effects of metal ions have also been made and are consistent with the trends observed in this work. Of the three metal ions studied, the TCPC decays obtained for cobalt were the least affected by illumination. Using XPS and EXAFS it has been previously determined that the cobalt ion treatment in the photoelectrochemical cells causes the growth of a Co(II)-oxo overlayer, nearly 100 monolayers thick, on the GaAs surface. Moreover, the Co-GaAs surfaces develop a $CoSe_x$ surface phase, where x is approximately 1.8.[7] On the other hand, it has been found that less than a third of a monolayer of ruthenium deposits on the surface, and the Ru^{II} species does not appear to persist at the surface of GaAs electrodes held at open circuit.[8] No studies regarding the perseverance of osmium are available for comparison. One explanation for the rapid change in the lifetime properties of the ruthenium and osmium treated surfaces is that the high intensity illumination results in their oxidation or reduction, at which point they do not bind to the surface. In the electrochemical experiments, the electrode is repeatedly cycled to cathodic potentials, and the photon fluxes are not as high, so it may be that the loss of metal ions does not occur in those experiments.

In an attempt to ascertain whether the deviations observed in the fits was attributable to the changing lifetime a simple model calculation made by summing several curves with parameters that reflect the decreasing surface loss was performed. The sum of simulated decays with k_{ht} values of 1,2,3,4,and $5x10^{-15}$ cm^4/sec which are in the range of the value found to best fit the cobalt treated curve discussed above (h34c01) is shown in Figure 5-26(a). Taking the sum of these curves yields a curve in which the later portion of the decay deviates away from the fixed k_{ht} value, in a manner similar to that of the data. In other words, the later times are more heavily affected by the decreasing rate of surface loss, while the early times are fit equally well with the sum, or with a fixed value. The sum is shown relative to three of the constituent curves, along with the experimental data in Figure 5-26(b).

The magnitude of this effect is more noticeable for the shorter decays. Performing the same summing operation on five curves with k_{ht} values in different ranges is shown in Figures 5-26(c) and 5-26(d). For k_{ht} =17,13,9, 5, and $1x10^{-15}$ the sum and individual curves are shown in Figure 5-26(c), along with the h34c01 data set to reiterate the point made with Figure 5-26(a). For k_{ht} =17,13,9, 5, and $1x10^{-16}$ the sum and individual curves are shown in Figure 5-26(d), where it can be seen that the sum is again weighted towards the slower curves, which have the larger magnitudes.

No accurate measure of the contribution of each individual lifetime can be made using this sort of analysis, and no absolute measure of the rates of electron and hole transfer are attempted. It is suggested, however, that experiments which measure fresh surfaces after every laser pulse be made. This may possibly be done either by moving the sample on a continuous basis or using a detection technique requiring many fewer laser shots, such as a streak camera. Alternatively, it is possible that if the sample were illuminated from the back side, the surface affects might be avoided. In the original photoluminescence measurements of Nelson *et al.*[9] discussed above, as well as in the work

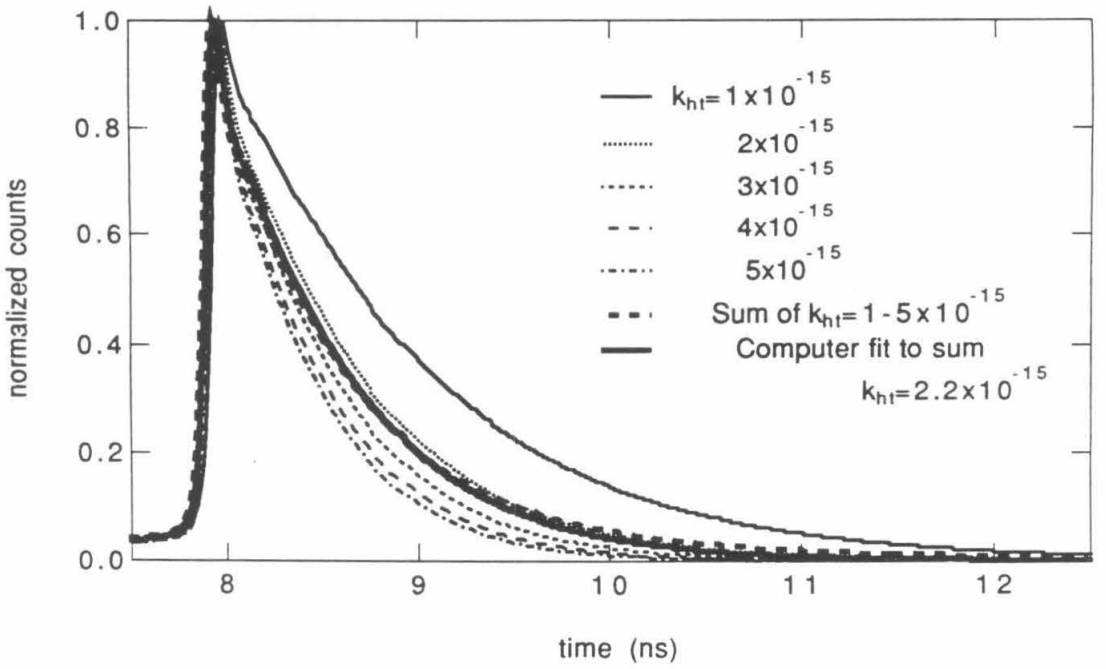

Figure 5-26(a). Simulation of sum of decays for five rate constants.

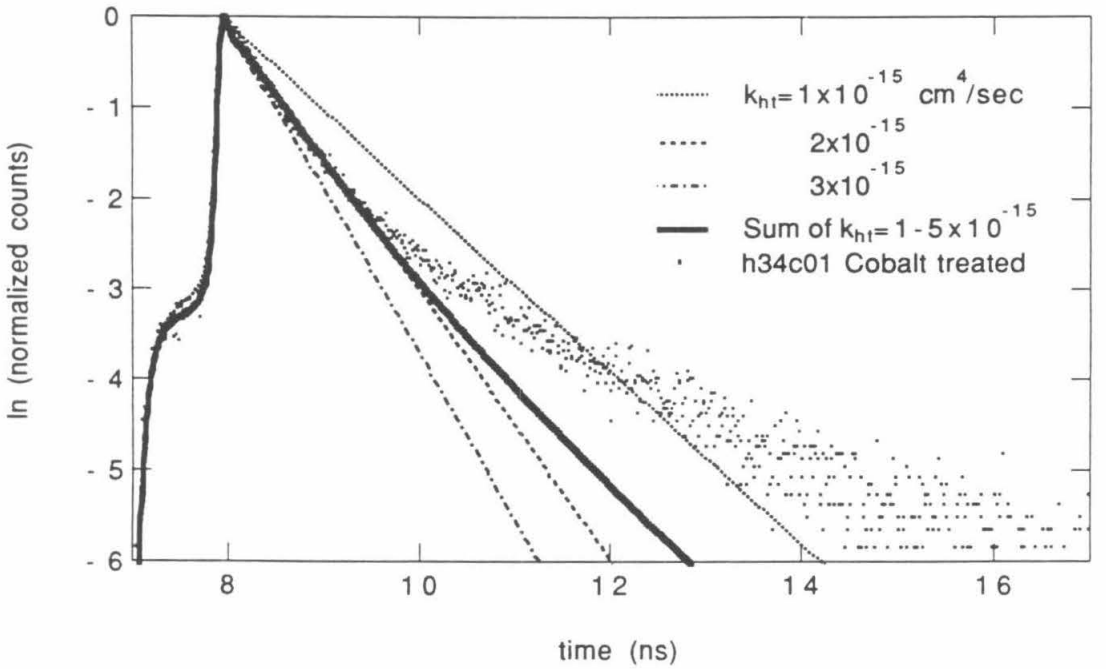

Figure 5-26(b). Simulation of sum of decays for five rate constants compared to data.

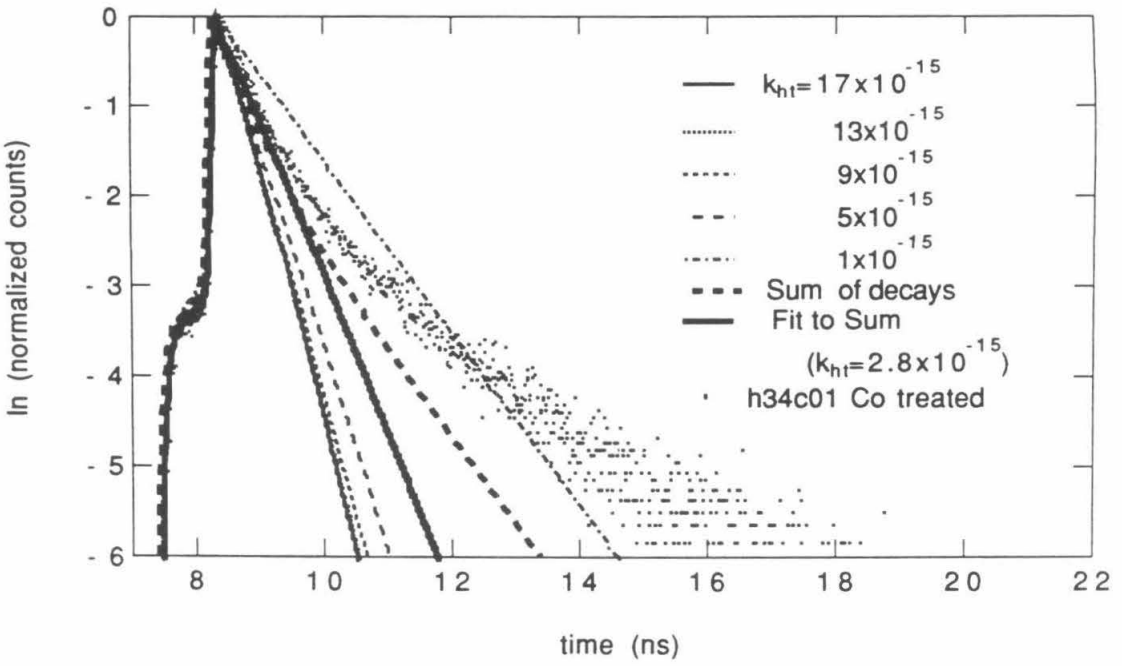

Figure 5-26(c). Simulation of sum of decays for five rate constants.

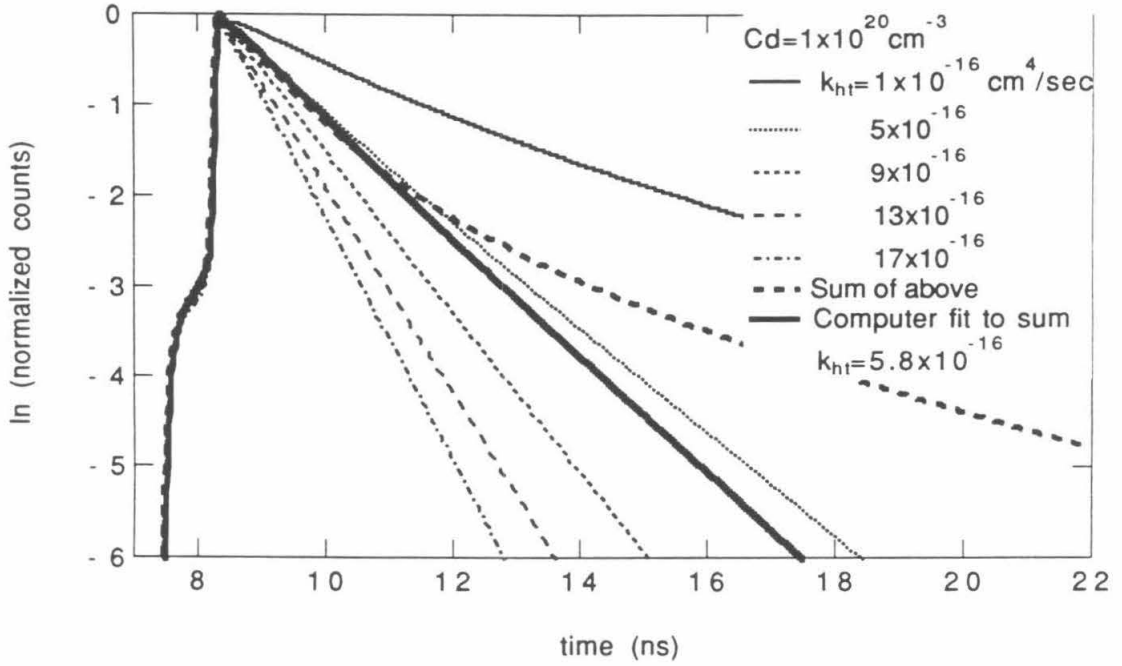

Figure 5-26(d). Simulation of sum of decays for five rate constants.

of Sell and Casey[10] the GaAs heterostructures were selectively etched from the back side so that incident and emitted radiation could pass through a hole in the substrate, and the metal ion treatment was performed on the front side.

Effects due to high intensity illumination have been noted by other workers. Under one kilowatt of steady-state illumination, Suzuki and Ogawa[11] have observed a *degradation* in photoluminescence which they attributed to excitation-enhanced oxidation of GaAs surfaces, but they noted that in contrast to GaAs, $Al_{0.3}Ga_{0.7}As$ and InP showed no or slow degradations under the same excitation. Although it is believed that the opposite effect occurred in the present experiments in KOH - Se^{2-} - Se_2^{2-} solutions, (i.e., that oxides were removed), the greater stability of these surfaces under illumination recommends them as candidates for further work. The surface recombination velocity of InP is known to be much lower than that for GaAs.

An additional source of uncertainty in the fits is that several values for model parameters were chosen from values reported in the literature and no experimental verification was obtained in this work. Confirmation of the radiative rate constant could be made by measurements which accurately determine the photon flux at the surface, which may be feasible using a calibrated photodiode at the focus of the laser beam. The diffusion constant varies due to the high carrier densities at the surface. From transient grating experiments, Gomez-Jahn and Miller[12] report a value of about 6 cm^2/sec for the ambipolar diffusion constant which would predict that the flattening of the profile should occur in 600 ps instead of 400 ps as it does for the value of 10 cm^2/sec used in our results. The use of several sample widths and laser wavelengths which should affect the diffusion components in particular would be helpful. At only slightly higher resolution than was available here, it may be possible to resolve the early time components, especially for the capped samples. The effect of the diffusion component is visible in the model generated curves; a point of

inflection shortly after the peak corresponds to the time at which diffusion has flattened the initial exponential absorption profile, and other loss mechanisms take over.

E. Conclusion

It is clear that the transition metal ions studied in this work increase the rate of loss of carriers at the GaAs/KOH - Se_2^{2-} - Se^{2-} interface. Moreover, cobalt was significantly more robust as a surface modification agent than either ruthenium or osmium were. However, several difficulties in quantifying the results were encountered. Much of the effort described in this thesis was aimed at obtaining reproducible decays for one series of experiments, which was hindered by the effects of long term illumination. Approximations for a net surface hole capture velocity can be made, but elucidation of the separate mechanisms of surface trapping, electron transfer and hole transfer processes could not be made. A suitably stable system must be found, and experiments in which the concentrations of the redox species and energies are varied should be performed. If these dependencies can be observed, it is expected that highly informative conclusions about the kinetics can be made.

In conclusion, it should be noted that the mere fact that changes in the surface charge transfer rates are detectable in experiments as was demonstrated in this thesis leaves open the hope that the difficulties will be addressed and that kinetics and identities of species at semiconductor/liquid junctions will be further elucidated.

APPENDIX

Computer Code for Finite Difference Calculations and Data-Fitting

The C program "nlc.c" was written by me and encodes the algorithm for the finite difference calculation. It is compiled with the header file "lumparm2.h" and invoked by a command line call from the MATLAB program (The MathWorks, Inc., Natick MA). The interactively-run MATLAB program passes variables to the compiled code by writing the arrays "misc_var" and "kht_offv" to disk in the files "miscvar.dat" and "khtoffv.dat", respectively, which are read by nlc.c. The "nlc.c" code, in turn, performs the calculation and writes a file to disk called "lum.dat" that contains the array *lum* which it has calculated. The MATLAB program loads this array for further manipulation and plotting. The "savemat.c" and "loadmat.c" subroutines for reading and writing data accessible to the MATLAB program are supplied with the MATLAB software.

The calculation runs as a DO loop which is performed for the number of time iterations required by the user. The changes in concentration in each box are calculated for each of the processes described in the text.

The MATLAB macros "RSgfit.m" and "RSnl.m" were written by me. "RSgfit.m" is run from the MATLAB command line and inputs the users requirements for the calculation, including the file names. It calls the MATLAB subroutine "fmins" to perform the minimization of the function "RSnl.m" "RSnl.m" calls the compiled code "nlc.c" and performs the convolution and plotting functions applied to the data.

The BASIC program "nllum12.bas" is the finite-difference program written primarily by N. S. Lewis. Concentration profiles and simulated conductivity and luminescence decays are stored according to the user's specifications. Parameters can be input either using a batch file or from the computer keyboard at runtime.

nlc.c

```
#include <math.h>
#include <stdio.h>
#include <errno.h>
#include "lumparm2.h"        /*misc parameters which may sometimes need to be changed*/

double lum[80000];                    /*array calculated, passed to MATLAB*/
char FilenameSuffix[3];
int lngthlum;
void nllum(float[10],float[30],double *);        /*my function with finite difference*/
void getparms(char [15],float *mv);
void WriteConcentrations(int IterationNumber,float *pold,float *nold,int nboxes,int ntimes,float dt);
main()
{ int i, k2=0;

          FILE *fp, *fopen();
          char name[20];
          int type, mrows, ncols, imagf,misc18;
          double *xr, *xi;

 float kht_offv[10],misc_var[30];  /*kht_offv will contain the variables  chosen in MATLAB to be varied.
                                     misc_var contains things like how many times to save data files, etc.*/
 /*fp2=fopen("miscvar.mat","r");
  printf("opened miscvar.mat");
  loadmat(fp2,1000,"misc_var",1,15,0,misc_var,(double *)0);
  fclose(fp2);*/
 getparms("miscvar.dat",misc_var);
 misc18=misc_var[18];
 printf("PASS : %d\n",misc18);
 if(misc18==1)
  { printf("\n START!!! \nRead miscvar.dat \n");
    printf("misc18 = %d \n",misc18);
   }
 if(misc18%10==0||misc18==1)
  {printf("PASS = %f \nCheck on miscvar variables\n",misc_var[18]);
   printf("   ns in calc: %f  ",misc_var[2]);
   printf("nboxes: %f\n",misc_var[8]);
   }
 getparms("khtoffv.dat",kht_offv);
 if(misc18%10==0||misc18==1)
  {printf("Check on khtoffv variables: \n");
   printf("   kht_offv(1): %e  ",kht_offv[0]);
   printf("2: %e ",kht_offv[1]);
   printf("3: %e\n ",kht_offv[2]);
   }
 nllum(kht_offv, misc_var, lum);
/* from testls.c we'll get assignments from a file saved by MATLAB*/
          if ((fp = fopen("foo.mat","r")) == NULL)
          {
                    printf ("Can't Open foo.mat\n");
                    exit (1);
          }
```

```
        if (loadmat(fp, &type, name, &mrows, &ncols, &imagf, &xr, &xi)) {
                printf("\nRead error\n");
        }
        fclose(fp);
fp=fopen("lum.mat","w");
 if(misc18==1)
  printf("lngthlum  = %d\n ",lngthlum);
  savemat(fp, type, "lum", lngthlum, 1, 0, lum,(double *)0); /* not sure
                                                        if second param should be
                                                        1000.  See savemat.c
                                                header.*/
 if(misc18==1)
  printf("successfully saved\n");
 fclose(fp);
}

void nllum(float *kht_offv,float *misc_var,double *lum)
{
 int nboxes,ntimes,nn,i,k,l,misc18,PassNumber,StoreConcProfiles,NumFilesToStore;
 float Simulation_dt_Multiplier;
 float kht,ntf,izero,ket,Ca,Cd,kr,ntb;
 float De,Dp,D,Dbar,thick,dx,Dstar,alpha;
 float peq,nisqkrdt,ftbulk,ftbulk_mt,krdt;
 float twoD;
 float khtCddt,ketCadt,krdx,NtCn,NtCp,ftfCh,ftfCe,ftbCe,ftbCh;
 float in_pulse[10],ftfss,ftfss_mt,ftbss,ftbss_mt;
 float hbsurftr,ebsurftr,hsurftrp,esurftrp,dsurftrp;
 float dt,dt1,delta;
 float pold[10],nold[10],ftb[10],ftb_mt[10];
 float pp[10],pm[10],np[10],nm[10],dp[10],dn[10],n1[10],p1[10];
 float drad[10],htrapped[10],etrapped[10],dtrapped;
 float sum=0;
 misc18          =misc_var[18];
 PassNumber      =misc_var[18];
 StoreConcProfiles=misc_var[21];
 printf("StoreConcprofiles = %d ",StoreConcProfiles);
 kht     =kht_offv[0];
 ket     =kht_offv[1];
 ntf     =kht_offv[2];
 izero   =kht_offv[3];
 Ca      =kht_offv[5];
 Cd      =kht_offv[6];
 kr      =kht_offv[7];
 ntb     =kht_offv[8];
                /* will be changed frequently */
 /*  Initialize parameters  */
 De =.0257*mue;
 Dp =.0257*mup;
 D=2*De*Dp/(De+Dp);
 Dbar=D;
 nboxes=0;
 Simulation_dt_Multiplier=2;
```

```
thick=.0001;
if (misc18==1)
 printf("In nllum body, misc_var[8] = %f \n",misc_var[8]);
if(misc18==1)
 printf("nboxes %d ",nboxes);
while (nboxes <misc_var[8])    /* calculate number of boxes
                                   based on answer in MATLAB calling
                                   routine.*/
  {
   Simulation_dt_Multiplier=Simulation_dt_Multiplier/2 ;
   dt=Simulation_dt_Multiplier*.0136e-9;
   dt1=dt;                          /*hold value of dt so it doesn't
                                     get changed later.*/
   delta=dt*D/.4;
   dx=sqrt(delta);
   nboxes = floor(thick/dx) ;
   printf("nboxes %d ",nboxes);
  }

dx=thick/nboxes;                    /*recalculate dx based on noboxes*/
D=D*dt/(dx*dx);
Dstar=D;
alpha=1.0/invalpha;
peq=ni*ni/neq;
nisqkrdt=ni*ni*kr*dt;
ntimes=floor((misc_var[2]*1e-9)/dt) ;
printf("in nlc.c dt = %e ",dt);
if(misc_var[18]==1)
 {printf("\n ntimes = %d \n",ntimes);
  /*printf("dt = %e \n",dt);*/
  printf("misc_var(2) = %f \n",misc_var[2]);
  }
ftbulk=1/(1+ni/neq);                /*  %bulk trap - initialization
                                      of fraction full: */
ftbulk_mt=1/(1+neq/ni);
krdt=kr*dt;
/*  consolidate constants:*/
twoD=2*D;
khtCddt=kht*Cd*dt;
ketCadt=ket*Ca*dt;
krdx=kr*dx;
NtCn=ntb*knblk*dt;
NtCp=ntb*kpblk*dt;
ftfCh=ntf*kpss*dt;
ftfCe=ntf*knss*dt;
ftbCh=ntbck*kpss*dt;
ftbCe=ntbck*knss*dt;
/* Calculate concentrations before calculation begins*/
for (i=1;i<=nboxes; ++i)
 {in_pulse[i]=(izero/dx)*(exp(-alpha*(i-1)*dx)-exp(-alpha*(i)*dx));
   if(misc_var[18]==1)
     printf("i, in_pulse[i] %d %e \n",i,in_pulse[i]);
```

```
  }
/*  surface traps:  For now surface traps same as bulk. */
ftfss=ftbulk;
ftfss_mt=ftbulk_mt;
ftbss=ftfss;
ftbss_mt=ftfss_mt;
 /*use row vectors to parallel boxes along x axis - easy to visualize?
   row 1 will be old values, row 2 will be new values */

for (i=1; i<=nboxes; ++i)
  {       pold[i]=peq + in_pulse[i];
          nold[i]=neq + in_pulse[i];
  }
/* nn=length(n)  SHOULD BE NBOXES, RIGHT? */
for (i=1; i<=nboxes; ++i)
  { ftb[i]   =ftbulk;
    ftb_mt[i]=ftbulk_mt;
  }

/*  **********TOP OF time LOOP in k *********
   Basically changes due to each process in the model are
   calculated and stored as "dp" or "dn", then they are
   added to pold or nold at the end.*/

for (k=1;k<=ntimes;++k)          /* ntimes = 1000 */
  {
                              /* First Process:  Diffusion: */
   dp[1]=D*(pold[2]-pold[1]);
   dn[1]=D*(nold[2]-nold[1]);

    for(i=2;i<=nboxes-1;++i)
          { dp[i]=-twoD*pold[i]+D*(pold[i+1]+pold[i-1]);
            dn[i]=-twoD*nold[i]+D*(nold[i+1]+nold[i-1]);
          }
   dp[nboxes]=D*(pold[nboxes-1]-pold[nboxes]);
   dn[nboxes]=D*(nold[nboxes-1]-nold[nboxes]);

                                  /* update Diffusion
                                  before everything else: */
    for (i=1; i<=nboxes; ++i)
          { pold[i]=pold[i]+dp[i];
            nold[i]=nold[i]+dn[i];
          }
                                  /* substract off eq
                                  values before next part: */
    for (i=1; i<=nboxes; ++i)
          { p1[i]=pold[i]-peq;
            n1[i]=nold[i]-neq;
          }
     for (i=1; i<=nboxes; ++i)
          {
                                  /* 2nd Process: bulk
```

```
                                radiative recomb:*/
        drad[i]=krdt*pold[i]*nold[i]-nisqkrdt;
                                /* 3rd Process: bulk trapping:        */
        htrapped[i]=((ftb[i]*pold[i])-(p1blk*ftb_mt[i]))*NtCp;
        etrapped[i]=((ftb_mt[i]*nold[i])-(n1blk*ftb[i]))*NtCn;
                                /* update trap filling:*/
        dtrapped=(etrapped-htrapped)/ntb;
        ftb[i]=ftb[i]+dtrapped;
        ftb_mt[i]=ftb_mt[i]-dtrapped;
       }

                                /* 4th Process: surface trapping*/
hsurftrp=(pold[1]*ftfss-ftfss_mt*p1ss)*ftfCh;
esurftrp=(nold[1]*ftfss_mt-ftfss*n1ss)*ftfCe;
dsurftrp=(esurftrp-hsurftrp)/ntf;
ftfss=ftfss+dsurftrp;
ftfss_mt=ftfss_mt-dsurftrp;
                                /* Calculate total change */
                                /* First box */
dp[1]=-p1[1]*khtCddt/dx-htrapped[1]-hsurftrp/dx-drad[1];
dn[1]=-n1[1]*ketCadt/dx-etrapped[1]-esurftrp/dx-drad[1];
                                /*  boxes 2:penultimate  */
 for (i=2;i<=nboxes-1;++i)
       {
        dp[i]=-htrapped[i]-drad[i];
        dn[i]=-etrapped[i]-drad[i];
       }
                                /*  last box */
hbsurftr=(pold[nboxes]*ftbss-ftbss_mt*p1ss)*ftbCh;
ebsurftr=(nold[nboxes]*ftbss_mt-ftbss*n1ss)*ftbCe;
dsurftrp=(ebsurftr-hbsurftr)/ntbck;
 ftbss=ftbss+dsurftrp;
 ftbss_mt=ftbss_mt-dsurftrp;
dp[nboxes]=-htrapped[nboxes]-hbsurftr/dx-drad[nboxes];
dn[nboxes]=-etrapped[nboxes]-ebsurftr/dx-drad[nboxes];
                                /*update pold, nold*/
 for (i=1; i<=nboxes; ++i)
       {
        pold[i] = pold[i]+dp[i];
        nold[i] = nold[i]+dn[i];
    if(misc18%10==0||misc18==1)
      if (k==100)
       if(i==1)
       printf("nold[1]:  k: %d: %e ",k,nold[1]);
         if (k==(ntimes/2))
       if(i==1)
        printf("  %d: %e ",k,nold[1]);
         if (k==ntimes)
       if(i==1)
        printf("  %d: %e \n",k,nold[1]);
       }
 if(StoreConcProfiles==1 & PassNumber==1)
```

```
        {
        if(k==1)
       { printf("input suffix ");
          scanf("%s",FilenameSuffix);
        printf("FilenameSuffix is %s\n",FilenameSuffix);
          printf("How many files do you want to save at start? ");
          scanf("%d",&NumFilesToStore);
        printf("Numfiles toStore %d ",NumFilesToStore);
       }
      if(k<NumFilesToStore||fmod(k,100)==0)
        WriteConcentrations(k,pold,nold,nboxes,ntimes,dt);
        }
                                  /*calculate total luminescenc*/
    for (i=1;i<=nboxes;++i)
        sum=sum+(nold[i]*pold[i]-ni*ni);

    lum[k-1]=krdx*sum*dt;         /*multiply sum by constants
                          and store point in lum[]*/
     sum=0;
     lngthlum=k;
   }
  if (misc18==1)
   printf("Got to the end of nllum\n");
}

void getparms(char fname[12],float *Parms)
{
 FILE *fopen(),*sourcefile;
 float Val;
 char Input[255];
  int i;
 sourcefile=fopen(fname,"r");
 i=0;
 while(!feof(sourcefile))
 {
  fgets(Input,254,sourcefile);
  sscanf(Input,"%g",Parms+i);
   i=i+1;
  }
}

void WriteConcentrations(int IterationNumber,float *pold,float *nold,int nboxes, int ntimes,float dt)

{
 FILE *fopen(),*ConcFile;
 char fnm[3];
 char IterationString[2];
  int i,k;

 k=IterationNumber;
 sprintf(fnm,"p%d",IterationNumber);
 strcat(fnm,FilenameSuffix);
```

```
 if(k==100||k==(ntimes/2)||k==ntimes)
   printf("fnm  %s\n ",fnm);
 ConcFile=fopen(fnm,"w");
 fprintf(ConcFile,"%d\n",k);
 fprintf(ConcFile,"%e\n",dt);
 for (i=1; i<=nboxes; ++i)
  fprintf(ConcFile,"%e\n",pold[i]);
 fclose(ConcFile);
/* now for n*/
  sprintf(fnm,"n%d",IterationNumber);
 strcat(fnm,FilenameSuffix);
 if(k==100||k==(ntimes/2)||k==ntimes)
   printf("fnm  %s\n ",fnm);
 ConcFile=fopen(fnm,"w");
  fprintf(ConcFile,"%d\n",k);
  fprintf(ConcFile,"%e\n",dt);
 for (i=1; i<=nboxes; ++i)
  fprintf(ConcFile,"%e\n",nold[i]);
 fclose(ConcFile);
}
```

lumparm2.h

```
#define ni          1.8e6
#define neq           1.0e15
#define invalpha    .000031
#define mue         8500
#define mup         200
#define p1blk       ni
#define n1blk       ni
#define p1ss        ni
#define n1ss        ni
#define kpblk       1e-8
#define knblk       1e-8
#define knss        1e-8
#define kpss        1e-8
#define ntbck       6.25e10
```

RSgfit.m

```
echo off
clc
clear
format compact
countg=0;
nfile=0;
clear str_var; %str_var(8,5)=' '; %initialize a string matrix 5x5.
misc_var(13)=5;  %Value which determines which machine this is running on.
misc_var(14)=input('input 1 for unetched, 2 for selenide, 3 for entering fixed kht ');
TypeOfCalculation=misc_var(14);
if misc_var(14)~=1
 fprintf('MAKE SURE AND CHANGE NLLUMS FIXED PARAMETERS TO CORRECT VALUES!!!
');
end
```

```
misc_var(15)=1;  %not in use yet 1 for setting back surface trapping = front, 2 for
                 % setting it equal to 6.25e10;
TitleString=input('Input description for Plot Title: ','s')
str_var(1,:)=input(' Input a 5 character string variable for suffix used in naming files to store parameters and
plots: ','s')
misc_var(8)=input('number of variables being changed?  izero,offv, ntf, kr, ntb, Amp ' );
 for in=2:(1+misc_var(8))
  str_var(in,:)=input(' 5 character string of name of var ','s');
 end
str_var(:,:)
misc_var(2)        =input('At what interval should plots be stored? ');
 PlotInterval      =misc_var(2);
misc_var(3)        =input('How many ns do you want to calculate for? ');
 CalcTime          =misc_var(3);
misc_var(4)        =input('Where on x axis should data fitting start? (IN NS) ');
 StartFitTime      =misc_var(4);
misc_var(5)        =input('How many ns should I display? ');
 PlotTimeWindow =misc_var(5);
misc_var(9)        =input('What is minimum number of boxes desired in calculation ? 5? ');
 MinNumBoxes   =misc_var(9);
misc_var(10)       =input('Do you want to print ln plots? 0 for no, 1 for yes');  %controls printing of ln
plots.  Set to 1 for plots.
misc_var(11)       =1;  %multiple at which resids are plotted
 ResidPlotScaler=misc_var(11);
misc_var(19)       =countg;
 LastPlot          =0;
misc_var(18)       =LastPlot;
misc_var(22)       =input('Do you want to store conc and fraction profiles? 1 for yes, 0 for no');
misc_var(25)   =input('Store unconvoluted Data on Last Plot? 1 for yes');
StoreUnconvoluted=misc_var(25);
mydata  = input('name of file in /work/gnr/src/data (must end in .mat) ','s')
eval(['load /work/gnr/src/data/',mydata]);


Data     = (eval(mydata))';            %DATA IS ONE row
fprintf('First three points of Data are \n');
Data(1:3)
excit     =input('name of syst resp (must end in .mat) ','s')
eval(['load /work/gnr/src/data/',excit]);

ExcitDin=(eval(excit))';     % EXCITDATA IS ONE ROW
fprintf('First three points of Response Function are: \n');
ExcitDin(1:3)
misc_var(12)       =Data(1:1);          %time scale for Data set
misc_var(1)        =Data(1:1)/ExcitDin(1:1)  %first point should be the time window from rbgen
DataVsSystRespRes=misc_var(1);   %Resolution of Data compared to SystemResponse
SystRespTimeScale_ns=.0136*ExcitDin(1:1)/50
misc_var(20)=SystRespTimeScale_ns;
TimePerPtForData=DataVsSystRespRes*SystRespTimeScale_ns
EndWindowPt     =round((StartFitTime+CalcTime)/(TimePerPtForData));  % npts to keep
StartWindowPt   =round(StartFitTime/(TimePerPtForData));
Data=Data(StartWindowPt:EndWindowPt);
```

```
misc_var(21)=StartWindowPt-1;
fprintf(['After cutting out the window for fit,the length of Data is ' num2str(length(Data)) '\n']);
pause(1)
Data(1,1)=Data(1,2);                    %gets rid of that first time point

% Figures out where max of data set is.
maxd=max(Data);
for i=1:length(Data)
 if Data(i)==maxd
   PtOfMax_inData=i
 end
end
%Figures out where max of syst response is:
maxed=max(ExcitDin);
l_ED=length(ExcitDin);
for i=1:l_ED
 if ExcitDin(i)==maxed
   EDmaxpt=i
 end
end
if l_ED >=4000
 ExcitData=ExcitDin(EDmaxpt-100:EDmaxpt+299);
else
 ExcitData=ExcitDin;
end
axis([1 2 3 4]); axis;
plot(ExcitData),pause(1)
chooseED='y';
leftptn=0;
rightptn=0;
while chooseED=='y'
 leftpt=input('What point of syst resp data shall I start with? ')
 rightpt=input('What point to end with? ')
 ExcitData(1:1+rightpt-leftpt)=ExcitData(leftpt:rightpt);
 ExcitData(2+rightpt-leftpt:4097)=[];
 rightptn=leftptn+rightpt;
 leftptn=leftptn+leftpt;
 axis([1 2 3 4]);axis;
 plot(ExcitData,'o'),pause(1)
 chooseED=input('Do you want to choose again? y/n ','s')
end
title(['System Response file ' excit])
text(.5,.9,' points chosen for system response: ','sc')
text(.6,.85,[num2str(leftptn) ': ' num2str(rightptn)],'sc');
 t1(1:6)=fix(clock);
 text(.5,.8,[num2str(t1(2)) '/' num2str(t1(3)) '/' num2str(t1(1)) ' ' num2str(t1(4))  ':'num2str(t1(5))],'sc')
%print
%   Let's plot this data.
misc_var(6)=leftptn;
misc_var(7)=rightptn;
y = Data(:);
lengthy= length(y)
```

```
t = 1:length(Data);
lengtht=length(t);
edtime=1:length(ExcitData);
axis([1 2 3 4]);axis;
plot(t,y/max(y),edtime,ExcitData/maxed,'o')
 title('Input data'), pause(1)
clc;
lengthED=length(ExcitData);
fprintf(['The number of points in the excitation files is: ' num2str(lengthED) '\n']);
fprintf(['The point where maximum occurs in the data is ' num2str(PtOfMax_inData) '\n']);
%The necessary offset will be the distance from the peak of the
%simulated data to the peak of the real data. The simulated data should peak at about
%half the width of the response function that it is convoluted with, since it starts
% at zero, and the only offset from x=0 is that introduced by the response function
%that it is convoluted with. Thus, if we subtract this amount from the point
%where the Data is max, we should have a first approximation guess.

OffsetGuess=PtOfMax_inData*DataVsSystRespRes-.5*lengthED;

global Data ExcitData lum nfile countg mydata excit misc_var str_var kht_offv TitleString
% Data must be stored in kht_offv in following order
%  : kht,ket,ntf,izero,offv,Ca,Cd

if misc_var(14)==1   %unetched
  'Unetched varies offv and izero '
  val1=input('guess for izero ?');
  val2_answer=input('guess for offv (enter #) or OffsetGuess (enter 0)');
  if val2_answer==0
   val2=OffsetGuess;
  else
   val2=val2_answer;
  end
  Amplitude=1;
  ko = fmins('RSnl',[val1 val2])
elseif misc_var(14)==2  %selenide  or metals
  fprintf('5/6/92 varies kht, ket and offv ');
  %misc_var(16)=input('value for izero? ');
  %misc_var(17)=input('value for offv? ');
  val1=input('guess for kht ?');
  val2=input('guess for ket ?');
  val3=input('guess for offv? ');
  %val3=input('guess for ntf ? (6.25e10) ');
  ko= fmins('RSnl',[val1 val2 val3 1])
 elseif misc_var(14)==3
 RedoManyTimes=1;
 while RedoManyTimes==1
   misc_var(23)=input('Enter a value for kht (izero) ');
   misc_var(24)=input('Enter a value for ket (nada) ');
   str_var(1,:)=input('Enter file suffix to name expt (e.g. 04a): ','s')
   countg=0;
   LastPlot=1;
   misc_var(18)=LastPlot;
```

```
  RSnl
  fprintf('\nResult from RSnl is number above:')
  RedoManyTimes=input('Do you want to enter new values and run again? yes=1');
  fprintf(['Last file stored was ' str_var(1,:) ]);
  fprintf([' Variables were kht = ' num2str(misc_var(23)) ' ket = ' num2str(misc_var(24))]);
end
elseif misc_var(14)==4
 ko =fmins('rnllumx',[1])
else
'unetched, se or metal not selected'
end

%   And the above are the nonlinear parameters.
save finallum.dat lum /ascii
save finalkht.dat ko /ascii

%Make last call to RSnl with final params and plot it.
PlotInterval=1;
misc_var(2)=PlotInterval;
if (LastPlot==0)  %if LastPlot=1 hasn't already been done.
 LastPlot=1;
 misc_var(18)=LastPlot;
 RSnl
 fprintf('\nResult from RSnl is number above.\n')
end
fprintf(['Total of ' num2str(countg) ' runs were made.  Thus, data is stored as follows:\n']);
fprintf(['In directory plotfiles:\n']);
fprintf([' Final linear plot is:  p' num2str(countg) str_var(1,1:4) '.jet\n']);
fprintf(['       ln     plot   : pl  " \n']);
fprintf(['       Resid  plot   : pr  " \n']);
fprintf(['In directory lumfiles:\n']);
if(StoreUnconvoluted==1)
 fprintf([' Unconvoluted data: lr' num2str(countg) str_var(1,1:4) '.mat\n']);
else
 fprintf(['Uncovoluted not stored.']);
end
fprintf(['Convoluted and offset fit     lc' num2str(countg)  str_var(1,1:4) '\n']);
```

RSnl.m

```
function q=nllum12(var_pass)

countg=countg+1;                    %Starts at 0 in RSgfit, passed globally
misc_var(19)=countg;
LastPlot=misc_var(18);
TypeOfCalculation=misc_var(14);
StoreUnconvoluted=misc_var(25);
if TypeOfCalculation==3     %Fixed, one time run.
  kht_offv(1)=1e-18; %misc_var(23);          %kht
  kht_offv(2)=1e-18; %misc_var(24);          %ket
  kht_offv(3)= 6.25e10;    %ntf var_pass(3);            %
  kht_offv(4)=misc_var(23); %7.449e13;  %misc_var(16);       % izero 7.449e13;
  kht_offv(5)=146;                    %(for 7 boxes) 77
```

```
  kht_offv(6)=1e-20;                    % Ca
  kht_offv(7)=1e-20;                    % Cd
  kht_offv(8)=2e-11;                    % kr
  kht_offv(9)=1e11;                     % ntb
  kht_offv(10)=1;             %amplitude
end
if LastPlot==0                          %Iterative types of run
 if TypeOfCalculation==1          % Unetched (capped) case
  kht_offv(1)=1e-18;                    % kht
  kht_offv(2)=1e-18;                    % ket
  kht_offv(3)=6.25e10;                  % ntf
  kht_offv(4)=var_pass(1);              % izero
  kht_offv(5)=var_pass(2);              % offv
  kht_offv(6)=1e-18;                    % Ca
  kht_offv(7)=1e-18;                    % Cd
  kht_offv(8)=2e-11;        % kr
  kht_offv(9)=1e11;                     % ntb
  kht_offv(10)=1; %var_pass(3);    %amplitude
 elseif TypeOfCalculation==2      %Selenide (surface rates) case
  kht_offv(1)=var_pass(1);              %kht
  kht_offv(2)=var_pass(2);              %ket
  kht_offv(3)= 6.25e10;    %ntf var_pass(3);              %
  kht_offv(4)=7.445e12;  %misc_var(16);    % izero 7.449e13;
  kht_offv(5)=var_pass(3);              %misc_var(17);   % offv 293.137(for 7 boxes) 77
  kht_offv(6)=1e20;                     % Ca
  kht_offv(7)=1e20;                     % Cd
  kht_offv(8)=2e-10;                    % kr
  kht_offv(9)=1e11;                     % ntb
  kht_offv(10)=var_pass(4);             %amplitude
 end
end

kht       =kht_offv(1);
ket       =kht_offv(2);
ntf       =kht_offv(3);
izero     =kht_offv(4);
offv      =kht_offv(5);
Ca        =kht_offv(6);
Cd        =kht_offv(7);
kr        =kht_offv(8);       %2e-10
ntb       =kht_offv(9);       %1e11;  %kht_offv(5);
Amplitude=kht_offv(10);
DataVsSystRespRes=misc_var(1);
PlotInterval      =misc_var(2);
CalcTime          =misc_var(3);
MinNumBoxes       =misc_var(9);
StartFitTime      =misc_var(4);
PlotTimeWindow    =misc_var(5);
ResidPlotScaler =misc_var(11);
SystRespTimeScale_ns=misc_var(20);
StartingDataPtMinus1=misc_var(21);
% An memory write error occurs if the khtoffv and miscvar data
```

```
%is written onto prior existing files.
!rm khtoffv.dat
!rm miscvar.dat

for j=1:10
fprintf('khtoffv.dat','%g \n', kht_offv(j))
end
for j=1:22
fprintf('miscvar.dat','%g \n', misc_var(j))
end

%khbt   =1e-6;  %This prog doesn't have et at back surface, just trapping
%kebt   =1e-6;

ntbck   =6.25e10;
mue     =8000;  %kht_offv(5);
mup     =200;
De      =.0257*mue;
Dp      =.0257*mup;
D       =2*De*Dp/(De+Dp);
Dbar    =D;
nboxes  =0;

Simulation_dt_Multiplier=2;
thick   =.0001;
while nboxes < MinNumBoxes
 Simulation_dt_Multiplier=Simulation_dt_Multiplier/2;
 dt      =Simulation_dt_Multiplier*.0136e-9;        %Usually, for MNB=5,Simulation_dt_Multiplier=1
 dt1     =dt;                            %dt1 stores value of dt that calc uses
 delta   =dt*D/.4;
 dx      =sqrt(delta);
 nboxes = fix(thick/dx);
end
if countg==1
  fprintf(['dt in RSnl = %g' dt 'seconds\n'])
end
dx      =thick/nboxes;  %Recalculates dx based on nboxes.
D       =D*dt/(dx*dx);
Dstar   =D;
invalpha=.000031;
alpha   =1.0/invalpha;
ni      =1.8e6;
neq     =1e15;
peq     =ni*ni/neq;
nisqkrdt=ni*ni*kr*dt;

ntimes=round((CalcTime*1e-9)/dt);
%bulk trap - initialization of fraction full:
ftbulk  =1/(1+ni/neq);
ftbulk_mt=1/(1+neq/ni);
krdt    =kr*dt;
%trap variables:
```

```
 %number density:
p1blk   =ni;
n1blk   =ni;
p1ss    =ni;
n1ss    =ni;
kpblk   =1e-8;
knblk   =1e-8;
knss    =1e-8;
kpss    =1e-8;

%consolidate constants:
twoD    =2*D;
khtCddt =kht*Cd*dt;
ketCadt =ket*Ca*dt;
krdx    =kr*dx;
NtCn    =ntb*knblk*dt;
NtCp    =ntb*kpblk*dt;
ftfCh   =ntf*kpss*dt;
ftfCe   =ntf*knss*dt;
ftbCh   =ntbck*kpss*dt;
ftbCe   =ntbck*knss*dt;

for i=1:nboxes              %Initialize boxes with injection pulse.
 in_pulse(1,i)=(izero/dx)*(exp(-alpha*(i-1)*dx)-exp(-alpha*(i)*dx));  % a row vector end
end

if countg==1
 fprintf('See if in_pulse matches nlc in RSnl.m ')
 in_pulse(1,:)
end

%surface traps:
ftfss=ftbulk;
ftfss_mt=ftbulk_mt;
  %front:
    %holes:
    %electrons:
  %back:
ftbss=ftfss;
ftbss_mt=ftfss_mt;
    %holes
    %electrons:

% use row vectors to parallel boxes along x axis - easy to visualize?
% row 1 will be old values, row 2 will be new values
p(1,:)=peq + in_pulse(1,:);
n(1,:)=neq + in_pulse(1,:);
nn=length(n);

ftb(1,1:nboxes)=zeros(1:nboxes)+ftbulk;
ftb_mt(1,1:nboxes)=zeros(1:nboxes)+ftbulk_mt;
if size(p) ~= size(ftb)
```

```
'after ftb(1,1:nboxes)'
'iteration ',k,'fit  # ', countg
'D ',D, 'Dstar ',Dstar,'Dbar ',Dbar
'size(p) ',size(p),'size(ftb) ',size(ftb)
end
!rm lum.mat
%Call compiled C code with finite difference algorithm:
!nlc
%Load simulated data file written by nlc.c
load lum    % lum is read in as a single column.
lum=lum';   % Converts lum to single row matrix.

%excitation function and simulated luminescence should be at .0136 ns/pt
% if not, lum needs to be put on ExcitData time scale.
SystRespToLumRatio=round(SystRespTimeScale_ns*(1.0e-9)/dt)
if (SystRespToLumRatio ~= 1)
 if(countg==1)
   fprintf('Now changing time scale in simulation to match SystRespTimeScale\n');
 end
  LumLength=length(lum)
        %Make matrix whose values are the columns we wish to keep.  The
        %first point to cut is 2 or whatever the ratio is, the increment is the ratio,
        %and do this all the way to the end of the lum matrix:
   CullMatrix=1:SystRespToLumRatio:LumLength;
   length(CullMatrix)
  % Set these columns to null.
   lum=lum(:,CullMatrix);
 dt        = dt*SystRespToLumRatio
end

%Save raw simulation for special events:
if(StoreUnconvoluted==1 & LastPlot==1)
  fnm2=['lr' num2str(countg) str_var(1,1:4) '.mat'];
  lumstore2=lum';
  fprintf(['STORING ASCII FILE OF UNCONVOLUTED LUM DATA IN lumfiles/' fnm2 '\n']);
  eval(['save lumfiles/' fnm2 ' lumstore2 -ascii']); %save lum column
end
max(lum)
lum=conv(ExcitData,lum);    %still one ROW
NptsConvolutedLum=length(lum)
NptsData=length(Data);
max(lum)
% set up for offset
%to calculate offset
if offv < 1
  fprintf('Trying to make offv<1, set it to 1')
  offv=1
end
lum(offv+1:NptsConvolutedLum+offv)=lum(1:NptsConvolutedLum);
lum(1:offv)=zeros(1:offv);
NptsOffsetLum=NptsConvolutedLum+offv;
```

```
 % The convoluted simulation data is now at .0136ns/pt (or more strictly, at
 % the time scale of the system response), so if real data is at lower
 % resolution, we need to select out points from lum at the same time interval
 % before we subtract simulation from real:
NptsCorrectedResLum=fix((NptsOffsetLum)/DataVsSystRespRes);
for i=1:NptsCorrectedResLum  % take simulated lum data at same interval is real data
 lum(i)=lum(1+DataVsSystRespRes*(i-1));
end
lum(NptsCorrectedResLum+1:NptsOffsetLum)=[];
MaxLum=max(lum)
lum=Amplitude*lum/max(lum);
Data=Data/max(Data);

%save lum for future ref.  misc_var(21) has the number of pts chopped
% off the front of data for fit.  Need to put these back on for accurate
% overlay in external program.
if (rem(countg,PlotInterval)==0|LastPlot==1)
 fnm2=['lc' num2str(countg) str_var(1,1:4)];
 StartingZeroes(1:StartingDataPtMinus1)=zeros(1:StartingDataPtMinus1);
 lumstore=[StartingZeroes lum];
 lumstore=lumstore';
 fprintf(['STORING ASCII FILE OF SIMULATED DATA IN lumfiles/' fnm2 '\n']);
 eval(['save lumfiles/' fnm2 ' lumstore -ascii']); %save lum column
end
smsize=min(NptsCorrectedResLum,NptsData);
lum=lum(1:smsize);
Data=Data(1:smsize);

q1=lum-Data(1:smsize);
q=sum(q1.^2);
%to plot progress:
 time=(1:smsize)*dt*1e9*DataVsSystRespRes+StartFitTime;

 txt_vars(1,30)=' ';
 for it=2:(1+misc_var(8))
   txt_vars(1,1+5*(it-2):5+5*(it-2))=str_var(it,1:5);
 end

 MachineStr='RS6000/520  ';
 if TypeOfCalculation==1
   code_str='  RSnl unetched ';
 elseif TypeOfCalculation==2
   code_str='  RSnl Se ';
 elseif TypeOfCalculation==3
   code_str='  Fixed Parameters - Run one Pass, Only.';
 elseif TypeOfCalculation==4
   code_str=' nllumx';
 end

 %Residuals plot:
 if (rem(countg,ResidPlotScaler*PlotInterval)==0|LastPlot==1)
   axis([StartFitTime StartFitTime+PlotTimeWindow min(q1) max(q1)]);
```

```
 plot(time,q1(1:smsize))
 text(.05,.98,['# ' num2str(countg)],'sc')
 text(.3,.98,[TitleString],'sc')
 text(.6,.95,'residuals ','sc')
 text(.1,.95,[str_var(1,:) code_str '/' MachineStr 'vary: ' txt_vars(1,:)],'sc')
 t1(1:6)=fix(clock);
 text(.15,.98,[num2str(t1(2)) '/' num2str(t1(3)) '/' num2str(t1(1)) ' ' num2str(t1(4))  ':'num2str(t1(5))],'sc')
 xlabel('time (ns)')
 filename=['pr' num2str(countg) str_var(1,1:4)];
 fnmResidPlot=filename;
 eval(['meta plotfiles/' filename]);
 if (LastPlot==1)
  eval(['!gpp plotfiles/' filename ' -djet -ol '])
 end
end
%Plot of Data with Fit
if (rem(countg,5)==0|rem(countg,5)==3|rem(countg,PlotInterval)==0|countg==1|LastPlot==1)
 if(rem(countg,5)==0|countg==1|LastPlot==1)
  axis([StartFitTime StartFitTime+PlotTimeWindow 0 1]);
  plot(time,Data(1:smsize),time,lum,'o')
  ylabel('normalized counts');
 end

  %alternate ln with linear plots, if ln plots requested
  if(misc_var(10)==1 & rem(countg,5)==3 & LastPlot~=1)
   axis([StartFitTime StartFitTime+PlotTimeWindow -8 0]);
   plot(time,log(Data(1:smsize)),time,log(lum),'o')
   ylabel('ln(normalized counts)')
  end
 xlabel('time (ns)');
 text(.05,.98,['# ' num2str(countg)],'sc')
 xt =.5;
 yt = .9;
 sep=.05;
 text(xt,yt,['offv = ' num2str(offv)],'sc')
 text(xt,yt-1*sep,['Amplitude = ' num2str(Amplitude)],'sc')
 text(xt,yt-2*sep,['err norm = ' num2str(q)],'sc')
 text(xt-.05,yt-3*sep,['Data File: ' mydata],'sc')
 text(xt-.04,yt-4*sep,['MCA window: ' num2str(misc_var(12)) 'ns'],'sc')
 strt=misc_var(6);
 stp=misc_var(7);
 text(xt-.05,yt-5*sep,['Syst. Response: ' excit '(' num2str(strt) ':' num2str(stp) ')'],'sc')
 t1(1:6)=fix(clock);
 text(.15,.98,[num2str(t1(2)) '/' num2str(t1(3)) '/' num2str(t1(1)) ' ' num2str(t1(4))  ':'num2str(t1(5))],'sc')
 text(.3,.98,[TitleString],'sc')
 xt=.8;
 yt=.98;
 sep2=.035;
 text(xt,yt-sep2,['kht 'num2str(kht)],'sc')
 text(xt,yt-2*sep2,['ket 'num2str(ket)],'sc')
 text(xt,yt-3*sep2,['Ca=Cd ' num2str(Ca)],'sc')
 text(xt,yt-4*sep2,['# time steps ' num2str(ntimes)],'sc')
```

```
text(xt,yt-5*sep2,['nboxes ' num2str(nboxes)],'sc')
text(xt,yt-6*sep2,['ntf 'num2str(ntf)],'sc')
text(xt,yt-7*sep2,['ntb 'num2str(ntb)],'sc')
text(xt,yt-8*sep2,['kr ' num2str(kr)],'sc')
text(xt,yt-9*sep2,['neq 'num2str(neq)],'sc')
text(xt,yt-10*sep2,['izero 'num2str(izero)],'sc')
text(xt,yt-11*sep2,['alpha 'num2str(alpha)],'sc')
text(xt,yt-12*sep2,['mue 'num2str(mue)],'sc')
text(xt,yt-13*sep2,['Dbar 'num2str(Dbar)],'sc')
text(xt,yt-14*sep2,['thick ',num2str(thick)],'sc')
text(xt,yt-15*sep2,['dt1 in calc'],'sc')
text(xt,yt-16*sep2,['    ' num2str(dt1)],'sc')
text(xt,yt-17*sep2,['dt on plot'],'sc')
text(xt,yt-18*sep2,['    ' num2str(dt)],'sc')
text(xt,yt-19*sep2,['tmax=ntimes*dt1'],'sc')
text(xt,yt-20*sep2,['    ' num2str(ntimes*dt1*1e9) 'ns'],'sc')
text(xt,yt-21*sep2,['Max Lum = 'num2str(MaxLum)],'sc')

text(.1,.95,[str_var(1,:) code_str '/' MachineStr 'vary ' txt_vars(1,:)],'sc')

% Will now store whatever is on the screen - designed to store linear plot
 if rem(countg,PlotInterval)==0
    nfile=nfile+1;
    nstr =int2str(nfile);
    filename=['p' num2str(countg) str_var(1,1:4)];
    fnmLinearPlot=filename;
    fprintf(['Files where Linear Plot is stored:  ' filename '.met\n'])
    eval(['meta plotfiles/' filename]);
  if (LastPlot==1)
    eval(['!gpp plotfiles/' filename ' -djet -ol ']);
  end

 end
end
pause(1)
% Now supposed to bring ln plot to screen and then store ln plot.
%Ln plots
 if (misc_var(10)==1 & rem(countg,PlotInterval)==0 |LastPlot==1)
   axis([StartFitTime StartFitTime+PlotTimeWindow -8 0]);
   nstr=int2str(nfile);
   plot(time,log(Data(1:smsize)),time,log(lum),'o')
   text(.1,.95,[str_var(1,:) code_str '/' MachineStr 'vary: ' txt_vars(1,:)],'sc')

   ylabel('ln (normalized counts) ')
   xlabel(' time (ns)')
    xt =.5;
    yt = .9;
    sep=.05;
   text(xt,yt,['offv = ' num2str(offv)],'sc')
   text(xt,yt-1*sep,['Amplitude = ' num2str(Amplitude)],'sc')
   text(xt,yt-2*sep,['err norm = ' num2str(q)],'sc')
   text(xt-.05,yt-3*sep,['Data File: ' mydata],'sc')
```

```
 text(xt-.04,yt-4*sep,['MCA window: ' num2str(misc_var(12)) 'ns'],'sc')
 text(xt-.05,yt-5*sep,['Syst. Response: ' excit '(' num2str(strt) ':' num2str(stp) ')'],'sc')
 t1(1:6)=fix(clock);
 text(.15,.98,[num2str(t1(2)) '/' num2str(t1(3)) '/' num2str(t1(1)) ' ' num2str(t1(4))  ':'num2str(t1(5))],'sc')
 text(.05,1,['# ' num2str(countg) ' ln'],'sc')
 text(.3,.98,[TitleString],'sc')
 filename=['pl' num2str(countg) str_var(1,1:4)];
 fnmLnPlot=filename;
 fprintf(['Files where Ln Plot is stored:  ' filename '\n'])
 eval(['meta plotfiles/' filename]);
 if (LastPlot==1)
   eval(['!gpp plotfiles/' filename ' -djet -ol ']);
 end

end
if (LastPlot==1)
 fprintf(' THE FOLLOWING FILENAMES ARE READY TO BE FTPd TO BILRC0 \n');
 fprintf(' AND PLOTTED BY TYPING "lp" filename AFTER LOGGING ON TO BILRC0 \n ');
 fprintf(['plotfiles \n'fnmLinearPlot '.jet \n'])
 fprintf([fnmResidPlot '.jet \n'])
 fprintf([fnmLnPlot '.jet \n']);
end
%save iteration, err norm, value of variables
fnm=['mp' mydata '.' str_var(1,1:4)];
 if countg==1
 fprintf(['File name for storage of parameters is: ' fnm ' \n'])
 fprintf(fnm, fnm)
 fprintf(fnm,[ '  ' num2str(t1(2)) '/' num2str(t1(3)) '/' num2str(t1(1)) ' ' num2str(t1(4))  ':'num2str(t1(5))
\n'])
 fprintf(fnm, ' First, the parameters that should not be changing\n ')
 fprintf(fnm, 'dt (on plot)  dt1 (in calc)     dx  \n ')
 fprintf(fnm, '%4.3e ',dt)
 fprintf(fnm, '%4.3e ',dt1)
 fprintf(fnm, '%4.3e \n',dx)
 fprintf(fnm, ' ntbck      Ca        Cd        ni        neq       peq\n')
 fprintf(fnm, '%4.3e ',ntbck)
 fprintf(fnm,'%4.3e ',Ca)
 fprintf(fnm, '%4.3e ',Cd)
 fprintf(fnm, '%4.3e ',ni)
 fprintf(fnm,'%4.3e ',neq)
 fprintf(fnm,'%4.3e\n',peq)
 fprintf(fnm,' alpha       n1blk       p1blk       n1ss       p1ss \n')
 fprintf(fnm,'%4.3e ',alpha)
 fprintf(fnm, '%4.3e ',n1blk)
 fprintf(fnm,'%4.3e ',p1blk)
 fprintf(fnm,'%4.3e ',n1ss)
 fprintf(fnm,'%4.3e\n',p1ss)
 fprintf(fnm, 'kpblk       knblk       kpss       knss\n')
 fprintf(fnm,'%4.3e ',kpblk)
 fprintf(fnm,'%4.3e ',knblk)
 fprintf(fnm,'%4.3e ',kpss)
 fprintf(fnm,'%4.3e\n\n',knss)
```

```
 fprintf(fnm, ' #,  ERR NORM,  nboxes,  offv,   Amplitude,  izero \n')
 fprintf(fnm, 'kht        ket        ntf        ntb        mue        kr     thick     offset \n\n')
end
fprintf(fnm, '%3.0f',countg)
fprintf(fnm,',   %4.3f ',q)
fprintf(fnm,',     %1.0f ',nboxes)
fprintf(fnm,',    %4.3f',offv)
fprintf(fnm,',    %4.3f',Amplitude)
fprintf(fnm,',  %4.3e  \n',izero)
fprintf(fnm,'%4.3e ',kht)
fprintf(fnm,'%4.3e ',ket)
fprintf(fnm,'%4.3e ',ntf)
fprintf(fnm,'%4.3e ',ntb)
fprintf(fnm,'%4.1f ',mue)
fprintf(fnm,'%4.3e ',kr)
fprintf(fnm,'%3.2e ',thick)
fprintf(fnm,'%4.2e\n\n',offv)
```

nllum12.bas

```
10 REM This program will calculate carrier concentrations vs time
20 REM for photoinjected carriers and will plot lum. vs time also
49 DEFSNG A, C-Z
50 DEFINT B
55 B.AUTOCOUNT = 0
57 AUTO.FLAG = 0
58 BFILE.COUNT = 0
90 INPUT "Enter batch job (0) or manual inputs (1)"; AUTO.FLAG
92 IF AUTO.FLAG = 1 GOTO 5000
93 INPUT "Enter number of files to be read"; NUMINPUT
95 DIM IN.FILNAME$(NUMINPUT)
96 FOR NUMBER = 1 TO NUMINPUT
98 INPUT "Enter filename for input (5 chars)"; IN.FIL$
100 IN.FILNAME$(NUMBER) = IN.FIL$ + ".inp"
105 NEXT NUMBER
110 BFILE.COUNT = BFILE.COUNT + 1
120 IF (BFILE.COUNT = NUMINPUT + 1) GOTO 1999
125 OPEN IN.FILNAME$(BFILE.COUNT) FOR INPUT AS #1
130 INPUT #1, KET, KHT, COX, CRED, NTF, NTB, KR, NI, NEQ, IZERO, PULSETIME
135 INPUT #1, INVALPHA, INVALPHA.LUM, MUE, MUP, BACK.FLAG, SBACK, TMAX, THICK
140 INPUT #1, B.ITER, B.NUMFILES, B1LUM, B2LUM, LUMTIME, OUT.FL$
149 CLOSE #1
150 REM This section calculated or sets other needed parameters
152 B.COUNT = 1
155 FTFSS = 1 / (1 + (NI / NEQ)): FTBSS = FTFSS
157 FTFSS.MT = 1 / (1 + (NEQ / NI)): FTBSS.MT = FTFSS.MT
160 KNSS = 1E-08
170 KPSS = 1E-08
190 KNB = 1E-08
200 KPB = 1E-08
205 FTBULK = 1 / (1 + (NI / NEQ))
207 FTBULK.MT = 1 / (1 + (NEQ / NI))
210 NI.SQR = NI ^ 2
```

```
230 P1SS = NI
240 N1SS = NI
250 P1B = NI
260 N1B = NI
267 PEQ = NI.SQR / NEQ
304 ALPHA = 1 / INVALPHA: ALPHA.LUM = 1 / INVALPHA.LUM
305 DE = .0257 * MUE
315 DP = .0257 * MUP
320 D = 2! * DE * DP / (DE + DP)
411 DT = TMAX / B.ITER
412 DELTA = DT * D / .4
413 DX = SQR(DELTA)
414 BOXES = INT(THICK / DX)
415 IF AUTO.FLAG = 0 GOTO 421
416 PRINT "This yields "; BOXES; "boxes."
417 INPUT "If this is unacceptable, enter 1, otherwise enter 0"; BOX.FLAG
418 IF BOX.FLAG = 1 THEN INPUT "Enter new # of iter"; B.ITER: GOTO 411
421 B.STORE = B.ITER \ B.NUMFILES
422 B.COUNTER = B.STORE: REM initializing the file count index now to store the first file
423 BVSAVE = 0: REM this is the real index that I need for the arrays..
425 BLUM.COUNTER = 1: REM this is the real index that I need to save lum and conc
428 BLUMSAVE = 1: REM initializing the count for lum and conc arrays
440 REM really I will need a back trap density someday, but not for now..
450 REM here is where the flag goes for solution species to diffuse
500 WDTH = THICK / BOXES
505 REM lets make sure our boxes are at equilibrium before filling them
506 REM ALSO LETS INITIALIZE THE TRAP LEVELS AT 0.5 FRACTION FILLED
507 B.AUTOCOUNT = B.AUTOCOUNT + 1
508 IF (AUTO.FLAG = 0 AND B.AUTOCOUNT > 1) GOTO 520
510 DIM NNEW(BOXES), NOLD(BOXES), PNEW(BOXES), POLD(BOXES), FTB(BOXES),
FTB.MT(BOXES)
512 DIM LUM(6000), EFSURFREC(100), HFSURFREC(100), EBULKREC(100)
513 DIM HBULKREC(100), EINTREC(100), HINTREC(100), EBSURFREC(100), HBSURFREC(100)
514 DIM COND(6000), ETOTAL(100), PTOTAL(100)
520 FOR B.INDEX = 1 TO BOXES
530 NNEW(B.INDEX) = NEQ
531 NOLD(B.INDEX) = NEQ
532 POLD(B.INDEX) = PEQ
533 PNEW(B.INDEX) = PEQ
535 FTB(B.INDEX) = FTBULK
538 FTB.MT(B.INDEX) = FTBULK.MT
540 NEXT B.INDEX
590 TIME = 0
600 REM this section initializes the boxes with concentrations
601 REM we will ultimately have to scale these to make them convenient..
603 IF B.COUNT >= (B.ITER + 1) GOTO 1800
605 IF B.COUNTER = B.STORE THEN BVSAVE = BVSAVE + 1: B.COUNTER = 0: BSAV.FLAG = 1
ELSE BSAV.FLAG = 0
612 TIME = TIME + DT
613 IF (TIME <= LUMTIME) THEN BLUMSTORE = B1LUM ELSE BLUMSTORE = B2LUM
620 REM we need to assign nold values based on the generation rates...
621 REM also assign pold these values...
```

```
622 REM NOTE:  this is where we return to reinject more carriers with light
630 IF PULSETIME < DT THEN INJECT = IZERO ELSE INJECT = IZERO * DT
635 IF (TIME > PULSETIME) AND (B.COUNT > 1) GOTO 750
650 FOR BOX = 1 TO BOXES
660 CONC = (INJECT / WDTH) * (EXP(-1! * ALPHA * (BOX - 1) * WDTH) - EXP(-1! * ALPHA *
BOX * WDTH))
665 NNEW(BOX) = NOLD(BOX) + CONC
670 PNEW(BOX) = POLD(BOX) + CONC
680 POLD(BOX) = PNEW(BOX): NOLD(BOX) = NNEW(BOX)
682 IF (PNEW(BOX) <= PEQ) AND (NNEW(BOX) <= NEQ) GOTO 750
690 NEXT BOX
750 REM   NOW, let them diffuse...
780 GOSUB 2000
800 REM NOW, we turn on interfacial transfer in first (and maybe last) box
810 GOSUB 2400
900 REM NOW, let them recombine in all boxes
910 GOSUB 2600
950 REM NOW, let them recombine with traps at the surface(s)
960 GOSUB 2800
1000 REM now let them luminesce
1010 GOSUB 3000
1080 REM now lets reset nold=nnew and pold=pnew
1085 GOSUB 3400
1100 REM now calculate the conductivity and total survived carriers
1107 COND(BLUMSAVE) = 0: DC.TOT = 0: ETOTAL(BVSAVE) = 0: PTOTAL(BVSAVE) = 0
1110 FOR BOXH = 1 TO BOXES
1112 REM this used to goto 1145 if n and p <=eq values
1115 DC = ((MUE * (NOLD(BOXH) - NEQ)) + (MUP * (POLD(BOXH) - PEQ))) * WDTH
1120 DC.TOT = DC.TOT + DC
1130 ETOTAL(BVSAVE) = ETOTAL(BVSAVE) + ((NOLD(BOXH) - NEQ) * WDTH)
1133 PTOTAL(BVSAVE) = PTOTAL(BVSAVE) + ((POLD(BOXH) - PEQ) * WDTH)
1145 NEXT BOXH
1150 COND(BLUMSAVE) = DC.TOT * 1.602E-19 / THICK
1200 REM THE KEY IS BSAV.FLAG AND bvsave ..IF BSAV.FLAG =1 THEN STORE..
1210 IF BSAV.FLAG = 0 GOTO 1400
1214 MDDLE$ = STR$(BVSAVE)
1215 B.LNTH = LEN(MDDLE$)
1216 ND$ = RIGHT$(MDDLE$, B.LNTH - 1)
1220 OUT.FILE$ = OUT.FL$ + ND$ + ".con"
1230 OPEN OUT.FILE$ FOR OUTPUT AS #1
1232 WRITE #1, BVSAVE, B.COUNT, B.COUNT * DT, BOXES, WDTH
1235 WRITE #1, ETOTAL(BVSAVE), PTOTAL(BVSAVE), EBULKREC(BVSAVE),
HBULKREC(BVSAVE), EINTREC(BVSAVE), HINTREC(BVSAVE), EFSURFREC(BVSAVE),
HFSURFREC(BVSAVE)
1240 WRITE #1, EBSURFREC(BVSAVE), HBSURFREC(BVSAVE), FTB(BOXES \ 2),
LUM(BLUMSAVE), COND(BLUMSAVE)
1250 FOR BOXI = 1 TO BOXES
1255 WRITE #1, NOLD(BOXI), POLD(BOXI)
1260 NEXT BOXI
1290 CLOSE #1
1399 PRINT "Just wrote file "; OUT.FILE$; " on iteration "; B.COUNT; " .  Crunching away!"
1400 REM this is where we put anything else we need to do
```

```
1500 REM lets increment the counters now...
1507 IF (BLUM.COUNTER >= BLUMSTORE) THEN BLUMSAVE = BLUMSAVE + 1:
BLUM.COUNTER = 0
1510 B.COUNT = B.COUNT + 1
1515 B.COUNTER = B.COUNTER + 1: BLUM.COUNTER = BLUM.COUNTER + 1
1585 REM return again to re-inject (if necessary) for the next iteration..
1590 GOTO 600
1800 REM end the program now..done with iterations
1805 LUM.FILE$ = OUT.FL$ + ".lum"
1815 OPEN LUM.FILE$ FOR OUTPUT AS #2
1817 IF AUTO.FLAG = 0 THEN WRITE #2, IN.FILNAME$(BFILE.COUNT), BLUMSAVE, DT,
B1LUM, B2LUM, LUMTIME: GOTO 1830
1820 WRITE #2, IN.FIL$, BLUMSAVE, DT, B1LUM, B2LUM, LUMTIME
1830 FOR B.LOOP = 1 TO BLUMSAVE
1840 WRITE #2, LUM(B.LOOP)
1850 NEXT B.LOOP
1860 CLOSE #2
1865 COND.FILE$ = OUT.FL$ + ".cnd"
1870 OPEN COND.FILE$ FOR OUTPUT AS #3
1872 IF AUTO.FLAG = 0 THEN WRITE #3, IN.FILNAME$(BFILE.COUNT), BLUMSAVE, DT,
B1LUM, B2LUM, LUMTIME: GOTO 1880
1875 WRITE #3, IN.FIL$, BLUMSAVE, DT, B1LUM, B2LUM, LUMTIME
1880 FOR B.LOOP2 = 1 TO BLUMSAVE
1885 WRITE #3, COND(B.LOOP2)
1890 NEXT B.LOOP2
1895 CLOSE #3
1900 REM now lets see if another input file is waiting to be read and recycle
1910 IF AUTO.FLAG = 0 THEN GOTO 110
1999 END
2000 REM this is the diffusion sub-routine for all boxes but first and last
2001 REM better Do the first box first..
2005 NNEW(1) = (D * DT / (WDTH ^ 2)) * (NOLD(2) - NOLD(1)) + NOLD(1)
2010 PNEW(1) = (D * DT / (WDTH ^ 2)) * (POLD(2) - POLD(1)) + POLD(1)
2015 FOR BOXB = 2 TO BOXES - 1
2020 NNEW(BOXB) = ((D * DT / (WDTH ^ 2)) * (NOLD(BOXB + 1) - (2 * NOLD(BOXB)) +
NOLD(BOXB - 1))) + NOLD(BOXB)
2030 PNEW(BOXB) = ((D * DT / (WDTH ^ 2)) * (POLD(BOXB + 1) - (2 * POLD(BOXB)) +
POLD(BOXB - 1))) + POLD(BOXB)
2040 NEXT BOXB
2060 REM now let's do the last box
2075 NNEW(BOXES) = (D * DT / (WDTH ^ 2)) * (NOLD(BOXES - 1) - NOLD(BOXES)) +
NOLD(BOXES)
2080 PNEW(BOXES) = (D * DT / (WDTH ^ 2)) * (POLD(BOXES - 1) - POLD(BOXES)) +
POLD(BOXES)
2085 FOR BOXC = 1 TO BOXES
2090 POLD(BOXC) = PNEW(BOXC): NOLD(BOXC) = NNEW(BOXC)
2095 NEXT BOXC
2099 RETURN
2400 REM This routine takes care of reactions at the ends of the system
2405 KETB.FLUX = 0: KHTB.FLUX = 0: KETF.FLUX = 0: KHTF.FLUX = 0
2408 REM this used to goto 2415 if nold(1)<=neq
2410 KETF.FLUX = ((NOLD(1) - NEQ) * KET) * (COX * DT)
```

```
2415 REM this used to goto 2440 if pold(1)<=peq
2420 KHTF.FLUX = ((POLD(1) - PEQ) * KHT) * (CRED * DT)
2440 IF BACK.FLAG = 1 GOTO 2451
2443 REM this used to goto 2447 if nold(boxes)<=neq
2445 KETB.FLUX = ((NOLD(BOXES) - NEQ) * KET) * (COX * DT)
2447 REM this used to goto 2451 if pold(boxes)<=peq
2450 KHTB.FLUX = ((POLD(BOXES) - PEQ) * KHT) * (CRED * DT)
2451 REM this is where a bsav.flag if statement might go..
2455 EINTREC(BVSAVE) = KETF.FLUX + KETB.FLUX
2458 HINTREC(BVSAVE) = KHTF.FLUX + KHTB.FLUX
2499 REM now let's put these fluxes back in terms of concentrations and update
2500 PNEW(1) = POLD(1) - (KHTF.FLUX / WDTH)
2502 IF PNEW(1) < (.5 * POLD(1)) THEN PRINT "h surf ct too fast. Decrease dt!"
2505 NNEW(1) = NOLD(1) - (KETF.FLUX / WDTH)
2507 IF NNEW(1) < (.5 * NOLD(1)) THEN PRINT "n surf ct too fast.  Decrease dt!"
2510 PNEW(BOXES) = POLD(BOXES) - (KHTB.FLUX / WDTH)
2515 NNEW(BOXES) = NOLD(BOXES) - (KETB.FLUX / WDTH)
2519 IF PNEW(BOXES) < (.5 * POLD(BOXES)) THEN PRINT "h back ct too fast. Decrease dt!"
2520 IF NNEW(BOXES) < (.5 * NOLD(BOXES)) THEN PRINT "e back ct too fast. Decrease dt!"
2522 REM this used to reset pold(boxes)=pnew(boxes)
2525 REM same as 2522 but for nold(boxes)
2530 REM same as 2522 but for pold(1)
2535 REM same as 2522 but for nold(1)
2590 RETURN
2600 REM Now let's turn on the recombination pathways nonradiatively
2602 EBULKREC(BVSAVE) = 0: HBULKREC(BVSAVE) = 0
2610 FOR BOXD = 1 TO BOXES
2615 REM this used to goto 2625 and set htrapped=0 if pold(boxd)<=peq
2620 HTRAPPED = ((FTB(BOXD) * POLD(BOXD)) - (P1B * FTB.MT(BOXD))) * DT * (NTB * KPB)
2625 PNEW(BOXD) = PNEW(BOXD) - HTRAPPED
2627 REM this used to goto 2635 if nold(boxd)<=neq and set etrapped=0
2630 ETRAPPED = ((FTB.MT(BOXD) * NOLD(BOXD)) - (N1B * FTB(BOXD))) * DT * (NTB * KNB)
2635 NNEW(BOXD) = NNEW(BOXD) - ETRAPPED
2640 REM now update trap fraction that is occupied, ftb(boxd)
2645 FTB(BOXD) = ((NTB * FTB(BOXD)) + ETRAPPED - HTRAPPED) / NTB
2647 FTB.MT(BOXD) = ((NTB * FTB.MT(BOXD)) + HTRAPPED - ETRAPPED) / NTB
2650 IF FTB(BOXD) > 1! THEN PRINT "Bulk trap fraction >1 in iter"; B.COUNT; "and box"; BOXD
2655 IF FTB.MT(BOXD) < 0! THEN PRINT "Bulk trap fraction <0 in iter"; B.COUNT; "and box";
BOXD
2670 REM this used to reset pold= pnew
2675 REM this used to reset nold=nnew
2680 REM now lets make sure to keep track of all the trapped carriers
2681 REM this is where an if bsav.flag statement might go..
2690 EBULKREC(BVSAVE) = EBULKREC(BVSAVE) + (ETRAPPED * WDTH)
2695 HBULKREC(BVSAVE) = HBULKREC(BVSAVE) + (HTRAPPED * WDTH)
2697 REM this used to branch out of loop (goto 2710) if pold<peq and nold<neq
2700 NEXT BOXD
2710 REM now lets turn these concentrations into the real rec. fluxes
2720 REM already done this above in 2690,2695
2750 REM now we are done with the recombination loop
2790 RETURN
2800 REM Now lets do the same thing with surface rec. pathways: front first..
```

```
2802 EFSURFREC(BVSAVE) = 0: HFSURFREC(BVSAVE) = 0: EBSURFREC(BVSAVE) = 0:
HBSURFREC(BVSAVE) = 0
2810 REM this used to goto 2825 if pold(1)<=peq and set hfstrapped=0
2820 HFSTRAPPED = ((FTFSS * POLD(1)) - (FTFSS.MT * P1SS)) * (NTF * KPSS) * DT
2825 PNEW(1) = PNEW(1) - (HFSTRAPPED / WDTH)
2827 IF PNEW(1) < (.5 * POLD(1)) THEN PRINT "h fr. ss rate too fast. Decrease dt!"
2829 REM this used to goto 2835 if nold(1)<=neq and set efstrapped=0
2830 EFSTRAPPED = ((FTFSS.MT * NOLD(1)) - (FTFSS * N1SS)) * (NTF * KNSS) * DT
2835 NNEW(1) = NNEW(1) - (EFSTRAPPED / WDTH)
2837 IF NNEW(1) < (.5 * NOLD(1)) THEN PRINT "e fr. ss rate too fast. Decrease dt!"
2840 REM now update trap fraction that is occupied, ftfss
2845 FTFSS = ((NTF * FTFSS) + EFSTRAPPED - HFSTRAPPED) / NTF
2847 FTFSS.MT = ((NTF * FTFSS.MT) + HFSTRAPPED - EFSTRAPPED) / NTF
2850 IF FTFSS > 1! THEN PRINT "FSurf trap fraction >1 in iter"; B.COUNT; "and box 1"
2855 IF FTFSS.MT < 0! THEN PRINT "FSurf trap fraction <0 in iter"; B.COUNT; "and box 1"
2870 REM this used to reset pold(1)=pnew(1)
2875 REM this used to reset nold(1)=nnew(1)
2878 IF BACK.FLAG = 1 GOTO 2940
2880 REM now lets take care of the back surface
2882 REM this used to goto 2890 if pold(boxes)<=peq and set hbstrapped=0
2885 HBSTRAPPED = ((FTBSS * POLD(BOXES)) - (FTBSS.MT * P1SS)) * (NTF * KPSS) * DT
2890 PNEW(BOXES) = PNEW(BOXES) - (HBSTRAPPED / WDTH)
2892 IF PNEW(BOXES) < (.5 * POLD(BOXES)) THEN PRINT "h bk. ss rate too fast. Decrease dt!"
2894 REM this used to goto 2897 if nold(boxes)<=neq and set ebstrapped=0
2895 EBSTRAPPED = ((FTBSS.MT * NOLD(BOXES)) - (FTBSS * N1SS)) * (NTF * KNSS) * DT
2897 NNEW(BOXES) = NNEW(BOXES) - (EBSTRAPPED / WDTH)
2900 IF NNEW(BOXES) < (.5 * NOLD(BOXES)) THEN PRINT "e bk. ss rate too fast.  Decrease dt!"
2905 REM now update trap fraction that is occupied, ftbss
2910 FTBSS = ((NTF * FTBSS) + EBSTRAPPED - HBSTRAPPED) / NTF
2912 FTBSS.MT = ((NTF * FTBSS.MT) + HBSTRAPPED - EBSTRAPPED) / NTF
2915 IF FTBSS > 1! THEN PRINT "BSurf trap fraction >1 in iter"; B.COUNT; "and box 1"
2920 IF FTBSS.MT < 0! THEN PRINT "BSurf trap fraction <0 in iter"; B.COUNT; "and box 1"
2925 REM this used to reset pold(boxes)=pnew
2930 REM this used to reset nold(boxes)=nnew
2935 GOTO 2985
2937 REM put in back surf vel. calc here...
2940 REM for now, lets set the back surf. rec. vel. to zero...
2950 REM nonsense goes here
2960 REM nonsense was here too
2985 REM remember to count up the back recombination flux too...
2987 EFSURFREC(BVSAVE) = EFSTRAPPED: EBSURFREC(BVSAVE) = EBSTRAPPED
2988 HFSURFREC(BVSAVE) = HFSTRAPPED: HBSURFREC(BVSAVE) = HBSTRAPPED
2990 REM now we are done with the recombination loop
2999 RETURN
3000 REM This is a calculation of the luminescence and then conductivity too
3005 LUM(BLUMSAVE) = 0
3010 FOR BOXG = 1 TO BOXES
3018 REM this used to goto 3025 and set r.conc=0 if both nold and pold were <eq
3020 R.CONC = (((NOLD(BOXG) * KR) * POLD(BOXG)) - (NI.SQR * KR)) * DT
3025 LUM(BLUMSAVE) = LUM(BLUMSAVE) + (R.CONC * WDTH)
3030 NNEW(BOXG) = NNEW(BOXG) - R.CONC
3032 IF NNEW(BOXG) < (.5 * NOLD(BOXG)) THEN PRINT "e. lum rate too fast.  Decrease dt!"
```

```
3040 PNEW(BOXG) = PNEW(BOXG) - R.CONC
3042 IF PNEW(BOXG) < (.5 * POLD(BOXG)) THEN PRINT "h lum rate too fast.  Decrease dt!"
3050 REM this used to reset nold(boxg)=nnew
3055 REM this used to reset pold(boxg)=pnew
3056 REM this used to goto 3085 (out of loop) if n and p <=eq values
3060 REM this is where diff. cond. went but now its in 1100 section
3080 NEXT BOXG
3085 REM
3199 RETURN
3200 REM this is where Auger routine might eventually go...
3400 REM this is where we will reset old=new because all recomb. is over..
3410 FOR BOXK = 1 TO BOXES
3420 NOLD(BOXK) = NNEW(BOXK)
3430 POLD(BOXK) = PNEW(BOXK)
3440 NEXT BOXK
3499 RETURN
5000 REM this section inputs the data manually
5010 INPUT "Enter name for this input file (<6 chars)"; IN.FIL$
5110 INPUT "Enter value for ket, cm4/s"; KET
5120 INPUT "Enter value for kht, cm4/s"; KHT
5130 INPUT "Enter value for cox, molec/cm3"; COX
5140 INPUT "Enter value for cred, molec/cm3"; CRED
5150 INPUT "Enter value for front surface trap density, Ntf, cm-2"; NTF
5180 INPUT "Enter value for bulk trap density, Ntb, cm-3"; NTB
5210 INPUT "Enter value for radiative recombination coefficient, kr, cm3/s"; KR
5220 INPUT "Enter intrinsic carrier density, ni, cm-3"; NI
5265 INPUT "Enter equilibrium dopant density"; NEQ
5270 INPUT "Enter photon intensity, phot/cm2-sec"; IZERO
5275 INPUT "Enter pulse width, sec (zero for delta pulse)"; PULSETIME
5280 INPUT "Enter photon penetration depth, cm-1"; INVALPHA
5290 INPUT "Enter band gap photon penetration depth, cm-1"; INVALPHA.LUM
5300 INPUT "Enter electron mobility, cm2/v-s"; MUE
5310 INPUT "Enter hole mobility, cm2/v-s"; MUP
5320 INPUT "Is back surface boundary condition the same as front (Y=0, N=1)"; BACK.FLAG
5325 IF BACK.FLAG = 1 THEN INPUT "Enter back surface rec. vel., cm/s"; SBACK
5390 INPUT "Enter end time for simulation, sec"; TMAX
5400 INPUT "Enter wafer thickness, cm"; THICK
5405 INPUT "Enter number of iterations desired"; B.ITER
5420 INPUT "Enter how many concentration profiles do you want to store (<100)"; B.NUMFILES
5425 INPUT "Enter initial frequency for lum data storage"; B1LUM
5427 INPUT "Enter second frequency for lum data storage"; B2LUM
5430 INPUT "Enter time to switch from 1st to second frequency"; LUMTIME
5431 DT = TMAX / B.ITER
5432 IF (((TMAX - LUMTIME) / (DT * B2LUM) + (LUMTIME) / (DT * B1LUM)) > 5900) THEN
PRINT "Too many points taken: adjust collection frequencies": GOTO 5425
5440 PRINT "Filename is family for output.  Can include drive and dir if desired"
5450 INPUT "Enter data output filename (no more than 5 chars!)"; OUT.FL$
5999 GOTO 150
```